LONG-TERM PERFORMANCE OF RADON BARRIERS IN LIMITING RADON FLUX FROM FOUR URANIUM MILL TAILINGS CONTAINMENT FACILITIES

by

Alex M. Michaud

A Thesis submitted in partial fulfillment of

the requirements for the degree of

Master of Science

(Civil & Environmental Engineering)

at the

UNIVERSITY OF WISCONSIN-MADISON

2018

MASTER OF SCIENCE

(Civil & Environmental Engineering)

At the

UNIVERSITY OF WISCONSIN-MADISON

2018

Approved by:

William J. Likos, Ph. D

ABSTRACT

Compacted clay covers have traditionally been constructed to contain Uranium mill tailings (UMT) at disposal sites throughout the United States. These clay covers, typically referred to as Radon (Rn) barriers, are designed to limit water percolation into and gaseous Radon flux out of Uranium mill tailings piles in accordance with the Uranium Mill Tailings Radiation Control Act of 1978 (UMTRCA), which was enacted to require the safe disposal and long-term containment of Uranium mill tailings. Uranium mill tailings are the by-product of the Uranium mining process and contain low levels of Uranium and its daughters. One of the main requirements stipulated by UMTRCA is to limit the amount of Radon flux from the waste into the atmosphere. Radon (Rn-222), a daughter progeny of Uranium, is a colorless, odorless, radioactive gas (half-life = 3.8 d) that is known to cause lung cancer. UMTRCA requires these barriers to reduce Rn flux emanations from the cover system to a maximum of 20 pCi/m^2s (0.74 Bq/m^2s).

The Rn barriers used at UMTRCA disposal facilities are designed to be a thick, dense, saturated layer with both low permeability and low gaseous diffusivity. The low permeability limits the amount of water flux into the waste from precipitation, while the low gaseous diffusivity allows Radon to attenuate significantly while traveling from the waste towards the surface through the process of diffusion. Because Rn barriers are designed to be very dense and saturated, they create a barrier that is penetrable for Rn, but travel times are very long. Thus, it takes many half-lives for the Rn to travel to the surface, significantly reducing the concentration of the Rn along the way. These Rn barriers are typically covered with one or more protective layers.

Many of these Rn barriers were constructed 20 – 30 years ago and show signs that significant change has taken place since their construction. It is well understood that the effects of exposure to many environmental factors will change the engineering properties of these types of covers relative to their design properties. More specifically, the effects of soil desiccation,

freezing, thawing, and animal and plant intrusion are known to deteriorate compacted clay covers over time. While significant research has been performed to observe how hydraulic conductivity may be affected by these environmental factors, very little research has been conducted to evaluate similar effects on Rn diffusivity.

The main focus of this study is to assess the Rn flux limiting performance of Rn barriers at four UMTRCA disposal sites after two to three decades of service. Fieldwork was performed in 2016 at the Falls City, TX and Bluewater, NM sites and in 2017 at the Shirley Basin South, WY and Lakeview, OR sites. Rn flux measurements were obtained at each of the four sites from the surface of the Rn barrier at multiple test pit locations. Rn flux measurements were obtained using accumulation chamber methods and continuous alpha Rn detectors, which provide a near real-time concentration buildup curve at intervals specified by the user. Small activated carbon (AC) canisters were used in tandem with the continuous monitors. Test pits were excavated at various locations so that the effects of vegetation, seasonal ponding, animal burrowing, cover protection type/thickness, and Rn barrier thickness could be isolated.

In general, greater Rn fluxes were measured at locations where deep-rooting vegetation was found relative to locations without vegetation. Additionally, Rn flux was found to be lower where the Rn barrier remained at levels of water content and saturation near as-built conditions. Rn fluxes measured in 2016 and 2017 were also compared with flux measurements taken immediately after construction of the Rn barrier at three of the sites. The fluxes measured in 2016 and 2017 were found to be greater than those measured immediately after construction at two sites and were relatively unchanged at one site. The barriers at the two sites that showed increases in Rn flux were found to be drier than as-built conditions, which is believed to significantly contribute to the observed increase in Rn flux. Similar magnitudes of Rn flux were measured from the Shirley Basin South site relative to flux measurements taken immediately after

construction. The water content and saturation levels of the Rn barrier at this site were found to have increased slightly compared to as-built measurements.

A laboratory apparatus was assembled and used to test the Rn diffusion coefficient of thin-walled, 70 mm diameter soil samples taken from the Shirley Basin South, WY site. Rn diffusion coefficients measured with the apparatus were in good agreement with values found in literature.

The two methods of Rn flux measurement (continuous monitor and AC canister) were compared to assess the viability of each for flux measurement. The findings show that the two methods were in good agreement when considering the measurement of Rn concentration only. The AC canister method was found to lack reliability and consistency for determining flux when used with accumulation chambers due to the nonlinear concentration buildup of Rn in accumulation chambers and the lack of consistency in the multiple factors that affect this trend.

ACKNOWLEDGEMENTS

I would like to acknowledge and thank the many individuals without whom this research would not have been possible. First, I would like to acknowledge and thank my advisor, Dr. William Likos, for allowing me to be involved in this research and for the support, advice, and guidance I received from him throughout my time at UW-Madison. I would also like to thank my committee member Dr. Craig Benson for continually challenging me in our weekly meetings and inspiring me through his impressive research. I also would like to acknowledge Dr. James Tinjum, for graciously agreeing to provide his expertise and feedback as my third committee member.

I would also like to acknowledge Mr. Xiaodong "Buff" Wang for his significant help throughout my research. Buff was always available to lend a listening ear or to provide some level-headed advice when performing lab tests or preparing for fieldwork. Buff also helped fabricate nearly all the parts that make up the diffusion testing apparatus that we designed.

I would like to thank those who helped with the fieldwork portions of my research. Chris Enos, Simon Hensen, Todd Chojnowski, Brandon Pahl and Ross Koderl provided substantial aid during our time in the field and their hard work is deeply appreciated. I would also like to acknowledge the additional individuals with whom I was able to work during our fieldwork. It was a pleasure to work with Mark Fuhrmann, Jody Waugh, Bill Albright, Morgan Williams, Aaron Tigar, and Kuo Tian in the field and I feel that I gained a wealth of knowledge in the process.

Finally, I would like to thank my friends and fellow graduate students in the GLE program at UW-Madison for making this such a memorable experience. You all made moving to a new city much more comfortable and quickly made Madison feel like home. I feel lucky to have made such great friends in these two years. Thank you also to my beautiful fiancée, Ani, who provided an unmatched amount of moral support throughout this entire process.

Financial support for this research was provided by the University of Wisconsin-Madison, The Legacy Management Office of the United States Department of Energy, and the United States Nuclear Regulatory Commission. The findings, recommendations, and opinions presented in this paper are solely those of the author, and do not necessarily represent the policies or opinions of the sponsors.

TABLE OF CONTENTS

LIST OF FIGURES

LIST OF TABLES

1 INTRODUCTION

Over the past 30 years, many uranium mines and processing sites have been decommissioned, primarily in the western United States. The byproduct of decades of uranium processing at these sites is hundreds of thousands (often tens of millions) of tons of “spent” uranium ore, known as uranium mill tailings. Although much of the useful uranium has been extracted from the ore, the tailings still contain significant amounts of low-level radiation. One of the decay progenies of uranium (and the focus of this research) is Radon gas. Radon is an odorless, invisible, radioactive gas that has been known to be harmful to humans and cause lung cancer. The Uranium Mill Tailings Radiation Control Act (UMTRCA) of 1978 is a federal act that was established to provide standards for the safe, long-term disposal of uranium mill tailings in the United States. UMTRCA requires that the tailings be contained to limit infiltration of water into the waste, limit the emission of Radon (Rn) gas from the tailings into the atmosphere to a maximum flux of 0.74 Bq/m^2s, and be effective in physically containing the tailings for 1000 years, but not less than 200 years.

Compacted clay covers have typically been used at UMTRCA disposal sites due to their low water permeability and low gaseous diffusivity and are typically referred to as Rn barriers. In theory, their low gas diffusivity significantly impedes the diffusion of Rn through the Rn barrier, which allows the Rn to decay to “safe” levels at the surface, due to the relatively short half-life of Rn (3.8 d). A typical UMTRCA disposal cell cover profile consists of a Rn Barrier placed and compacted directly over the uranium tailings and is typically overlain by various protective and/or erosion control layers. These protective layers can consist of drainage materials, riprap, growth media or some combination of the three. The protective layers are also intended to limit the effects that numerous environmental and biological factors can have on the Rn barrier including erosion, freeze-thaw cycles, drying/desiccation, and biota intrusion. It is expected that these factors may have negative impacts on the hydraulic conductivity and diffusivity of the Rn barrier.

The aim of this research is to evaluate UMTRCA uranium mill tailings disposal cells with respect to their long-term effectiveness in limiting Rn flux into the atmosphere. Four disposal sites were studied in 2016 and 2017; Falls City, TX, Bluewater, NM, Shirley Basin South, WY, and Lakeview, OR. The four sites (average of 23 years of service at the time of fieldwork) were visited and measurements of Rn flux emanating from the surface of the cover were obtained. Rn fluxes were measured at test pits chosen at specific locations within the disposal cells to investigate how natural soil forming processes (pedogenisis) might affect the engineering properties of these compacted clay cover systems. A deeper understanding of how these covers change within a short-time period (20 - 30 years) will lead to a better-informed design process for future disposal sites in the long-term (1000 years).

Flux measurements were made using accumulation chambers fitted with continuous alpha-track RAD7 Rn monitors. An adaptation of traditional activated carbon methods of flux measurement using inexpensive, commercially available activated carbon canisters was also used and the results were compared.

2 BACKGROUND

The Uranium Mill Tailings Radiation Control Act (UMTRCA) of 1978 requires that disposal cells be effective in containing Uranium mill tailings for up to one thousand years, or for at least two hundred years (40 C.F.R. § 192.02). Historically, compacted clay covers have been used as the covers for containing the tailings. UMTRCA requires that the cover have low permeability and low diffusivity to limit percolation of water into the waste and to limit gaseous flux from the waste into the atmosphere, respectively. The maximum Rn flux allowed by UMTRCA is 20 pCi/m^2s or 0.74 Bq/m^2s, averaged over the entire area the disposal cell (40 C.F.R. § 192.02).

While not necessarily directly correlated with Rn diffusion coefficients, studies have shown that the hydraulic conductivity of similar cover systems can be significantly increased by

environmental factors such as desiccation, freezing conditions, vegetation and animal burrowing. Multiple field-scale studies on compacted clay covers have shown that freezing conditions can have adverse effects on these covers. Some studies have shown that freeze-thaw cycling can cause the hydraulic conductivity of compacted clay covers to increase by 70 – 300 times in the zone of frost penetration (Benson et al., 1995). Significant Increases in hydraulic conductivity have also been observed close to the surface due to the desiccation of compacted clay covers at the field scale in as little as two to four years of service (W. H. Albright et al., 2006, C. H. Benson et al., 2007). Desiccation cracks can form due to drying of covers containing expansive clays and can create “soil structure” (cracks) that can create preferential flow conduits for water to permeate.

In early disposal cell designs, UMTRCA cover profiles consisted of (from bottom to top) a low-permeability Rn barrier, a drainage layer, and a surface layer of riprap or other durable rock to prevent erosion. However, soon after construction of these early barriers, plants began to grow within the riprap. While vegetation can have beneficial effects and serve to reduce the amount of water percolation through the protective layers through transpiration If the roots of these plants extend into the underlying uranium tailings, it is possible that contaminants within the tailings can more easily be transported into the atmosphere through transpiration. The water uptake from the roots can also dry out the barrier significantly and increase the corresponding diffusion coefficient of the barrier. Furthermore, as these roots degrade, pathways can be left behind that may act as conduits for Rn flow (DOE 1999, GJO). A study done by the Department of Energy, for example, showed that the saturated hydraulic conductivity of a Rn barrier at the Burrell Disposal cell increased an average of 2 orders of magnitude at locations where plant roots had penetrated the barrier. A common question that arises at disposal cells on which native vegetation has begun to grow is whether or not it is worth the investment to remove the growth.

While less research has been performed to study how pedogenisis can change the gaseous diffusivity of engineered clay cover systems, some studies have shown that a similar

degradation effect can be expected. In theory, the same cracks that are created from desiccation, freeze-thaw cycling, and biointrusion and have been shown to cause increases in hydraulic conductivity can act as pathways for Rn to more easily escape into the environment. Hinton & Whicker (1985) performed a field scale study to observe how overburden depth and vegetation above a clay cover constructed over uranium tailings might affect Rn flux after two years. The study found that average Rn flux from the vegetated portion of the cover was typically one order of magnitude greater than that of the bare overburden, indicating that the roots of the planted grasses had compromised the Rn barrier after only two years. Lab studies have also shown that grasses can cause increases in Rn flux when compared to bare covers (Overmeyer et al., 1980).

A typical UMTRCA cover profile is shown in **Figure 2.1**. In its simplest form, an UMTRCA cover profile consists of (bottom to top) a low permeability Rn barrier, a protective/drainage layer, and either a rip-rap layer or vegetated topsoil layer for erosion protection at the surface. The dense, highly saturated Rn barrier is designed to have a low Rn diffusion coefficient. This makes it very difficult for Rn to pass through the barrier, resulting in a long, tortuous path for Rn to travel before making it to the atmosphere. Because Rn has a half-life of only 3.8 days, it should take many half-lives for the Rn to travel through the barrier allowing the concentration to attenuate significantly before reaching the soil surface. Therefore, the Rn flux at the surface should be much less than the Rn flux emanating from the tailings.

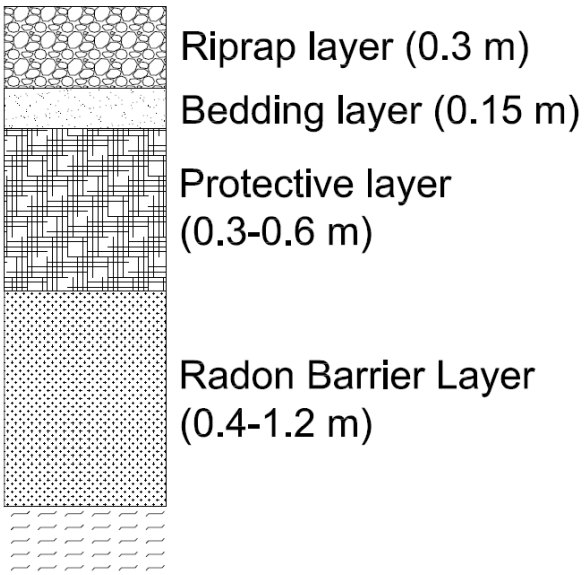

Figure 2.1 - Typical UMTRCA Cover Profile

It is very important for the Rn barrier clay to remain highly saturated in order to maintain a low diffusion coefficient during its service life. Studies have shown that the Rn diffusion coefficient of soil is highly dependent on the saturation level (Rogers & Nielson, 1991). As the void spaces between soil particles become saturated with water, it becomes more difficult for Rn gas to pass through, resulting in a highly tortuous pathway for Rn gas to permeate to the surface. Thus, when Rn barriers are designed, the long-term moisture content must be carefully determined based on precipitation averages and various other hydraulic properties of the barrier soil.

The standard for measuring Rn flux from the covered surface of a Uranium mill tailings pile is described by Method 115 of 40 CFR and Appendix A of Hartley et al. (1986) and involves the use of activated charcoal (AC). The method of measuring Rn flux from the soil surface using activated charcoal was originally proposed by Countess (1976). Countess proposed the use of military-grade activated charcoal canisters taken from gas masks. In this method, the small

canister (area = 87 cm^2) is pushed into the ground surface or sealed with wet clay and Rn is allowed to diffuse through the canister for up to 24-hours. Then, the Rn is analyzed using gamma spectroscopy. The current method for Rn flux determination is very similar to that originally published by Countess, however, a larger chamber is used (Hartley et al. 1986). In this method, a circular PVC cap with a 10-inch diameter (Area = 507 cm^2) and dimensions as shown in **Figure 2.2**, containing activated carbon granules spread evenly on a mesh, is positioned on a flat soil surface. The chamber also includes a small, 1/4" diameter hole at the top to minimize the effects of atmospheric pressure changes (Hartley et al. 1986).

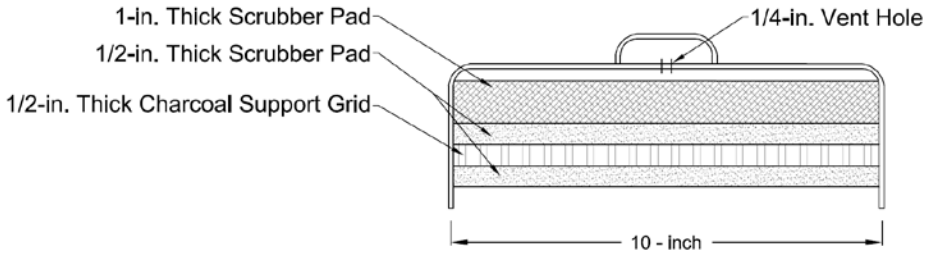

Figure 2.2 – Large-Area Activated Charcoal Canister (LAACC) as described in EPA, 1986.

Once the chamber is deployed, Rn is allowed to adsorb onto the activated carbon in the chamberfor approximately 24-hours. After the test has been completed, the charcoal is transferred to a small container and allowed to equilibrate for four hours. Then, a sodium iodide scintillation crystal (NaI) is used to measure the peaks of Bismuth-214. The number of counts, as well as the exposure time and chamber area can then be used to calculate Rn flux. Rn flux is determined using the following equation (Hartley et al. 1986):

$$J = \frac{c\lambda^2}{KAE(1 - e^{-\lambda t_e})(e^{-\lambda(t_w)} - e^{-\lambda(t_c)})}$$

Where J is Radon flux (pCi/m^2s), C is the net counts under the Bismuth-214 peak, λ is the Rn decay constant ($2.097x10^{-6}$ s^{-1}), A is the area of the chamber (m^2), E is the efficiency of the

detector (counts/degradation), K is the conversion factor from degradation/s to pCi (0.037 degradation/s/pCi), t_e is the exposure time (s), t_w is the time from the end of exposure to the start of counting (s), and t_c is the counting time (s).

In order to calculate a flux using the passive AC flux chamber method, two assumptions must be made and are typically made in practice (Hartley et al. 1986). The first is that 100% of the Rn within the chamber is adsorbed onto the activated carbon. The second assumption is that the Rn flux from the soil surface is constant throughout the flux test. Both of these assumptions are known to be unrealistic; however, the uncertainty has previously been shown to be insignificant (Hartley et al. 1986).

The first assumption may not be valid for a number of reasons. First, it is well known that water molecules in humid environments will compete to fill activation sites in the activated carbon (Hartley et al. 1986, IAEA PUBLICATIONS, 2013). This means that as absolute humidity increases, the efficiency of AC in adsorbing Rn gas decreases. If the efficiency of the AC decreases significantly, Rn may begin to build in concentration within the open airspace of the chamber, which may affect the concentration gradient, and thus make the second assumption invalid. It is also well known that temperature influences the efficiency of AC in adsorbing Rn gas. This is due to the fact that as temperature decreases, the activity of Rn molecules also decreases and thus less Rn is adsorbed onto the particles. In most applications, correction factors are used to adjust for moisture gained in the carbon as well as the temperature at which the measurement was taken.

The second assumption is based on the validity of the first assumption. If the volume of void space is minimized between the ground surface and the AC, and it is assumed that the AC adsorbs 100% of the Rn, then it can be assumed that the Rn concentration gradient between the Rn in the soil voids and the open volume within the chamber is constant throughout the test. This

means that if the Rn flux is purely diffusive, the flux should remain constant throughout the exposure time. This has been shown to be true for short exposure times (<36 hours) (Hartley et al. 1986). If the efficiency of the AC in adsorbing Rn begins to diminish, Rn will likely begin to build in concentration within the void space of the chamber.

Typically, flux tests using activated carbon are required to determine the average Rn flux emanating from the surface of a Uranium mill tailings pile once a cover has been installed (40 CFR – Method 115). These measurements are taken to confirm that the presence of the Rn barrier is allowing for significant attenuation of Rn to occur within it and that the average, area-weighted surface flux is below the UMTRCA limit of 0.74 Bq/m^2s. 40 CFR Appendix B also includes details on the number of flux measurements required from a disposal cell after completion of cover construction. In most instances, one hundred flux measurements are required from each distinct region of the disposal facility.

In addition to the AC adsorption method, there exist additional methods for Rn flux determination. The measurement of Rn concentrations can be performed with passive or active methods. For passive measurement of Rn concentration, no electricity is required to power the instrument at the time of measurement. Instead, the Rn is adsorbed via diffusive mechanisms to some surface or material and the material is later analyzed for Rn concentration. In active measurement systems, an electrical power source is required to power flow pumps or scintillation detectors to collect and/or determine the Rn concentration.

The above described Rn concentration measurement methods can then be used with flux methods to determine flux from the surface of Uranium mill tailings piles. Rn flux can be determined using accumulation, flow-through, or adsorption methods. Accumulation chambers involve placing a closed flux chamber (with its open end down) onto the surface of the Rn barrier and allowing the concentration of Rn to build within. This method is typically used with a Rn

measurement system that can give real-time reports of concentration, so that the non-linear buildup curve can be observed. Flow-through chambers rely on a flow-pump to force the Rn containing air through a detection system such as AC or a scintillation cell. The flow rate must be sufficient that Rn does not build up within the chamber, but not so great that the AC cannot adsorb the Rn. Adsorption methods typically involve the use of AC spread evenly within a chamber that is pressed onto the ground so that the space between the AC and the ground surface is minimized. Minimizing this volume promotes the diffusion of Rn onto the AC and also makes it more difficult for Rn concentration to build within the chamber. Traditionally, when measuring Rn flux from the surface of Uranium tailings piles, passive, adsorption methods are employed due to their low-cost, ruggedness, and ease of deployment of tens of tests in a short time period (IAEA, 1992). In this research, the accumulation chamber method was used, and continuous Rn concentrations were measured using a RAD7, electronic Rn monitor. Small, commercially available activated carbon canisters were also used within each accumulation chamber to determine the Rn concentration within each chamber at the end of the exposure time.

3 MATERIALS

3.1 Flux Chambers

Flux chambers of various geometries were used to measure Rn flux **(summarized in Table 3.1 and Figure 3.3)**. Circular Polyvinyl Chloride (PVC) end caps were used for the small and extra small flux chambers with diameters of 0.30 m and 0.15 m, respectively. Three different medium chambers were used in the field. The first set of medium chambers were constructed of rectangular HDPE, the second set of rectangular rigid fiberglass, and the final set were constructed from the bottoms of circular HDPE barrels which were cut to size. The final medium chamber geometry/material was chosen because it was rigid and also the same circular shape as the small and extra small chambers. The large flux chambers were made from the inner rings of a sealed double ring infiltrometer most typically used to measure hydraulic conductivity in the

field (ASTM D5093). The small flux chambers used in this research (0.30 m diameter) were similar in geometry and size to the conventional flux chambers typically used for as-built flux measurements (0.25 m diameter) at UMTRCA sites.

Table 3.1 – Summary of flux chamber sizes used in this study.

Flux Chamber Designation	Area (m^2)	Volume (m^3)
Large	2.323	0.352
Medium (1)	0.590	0.204
Medium (2)	0.282	0.056
Medium (3)	0.257	0.035
Small	0.071	0.011
Extra Small	0.020	0.002

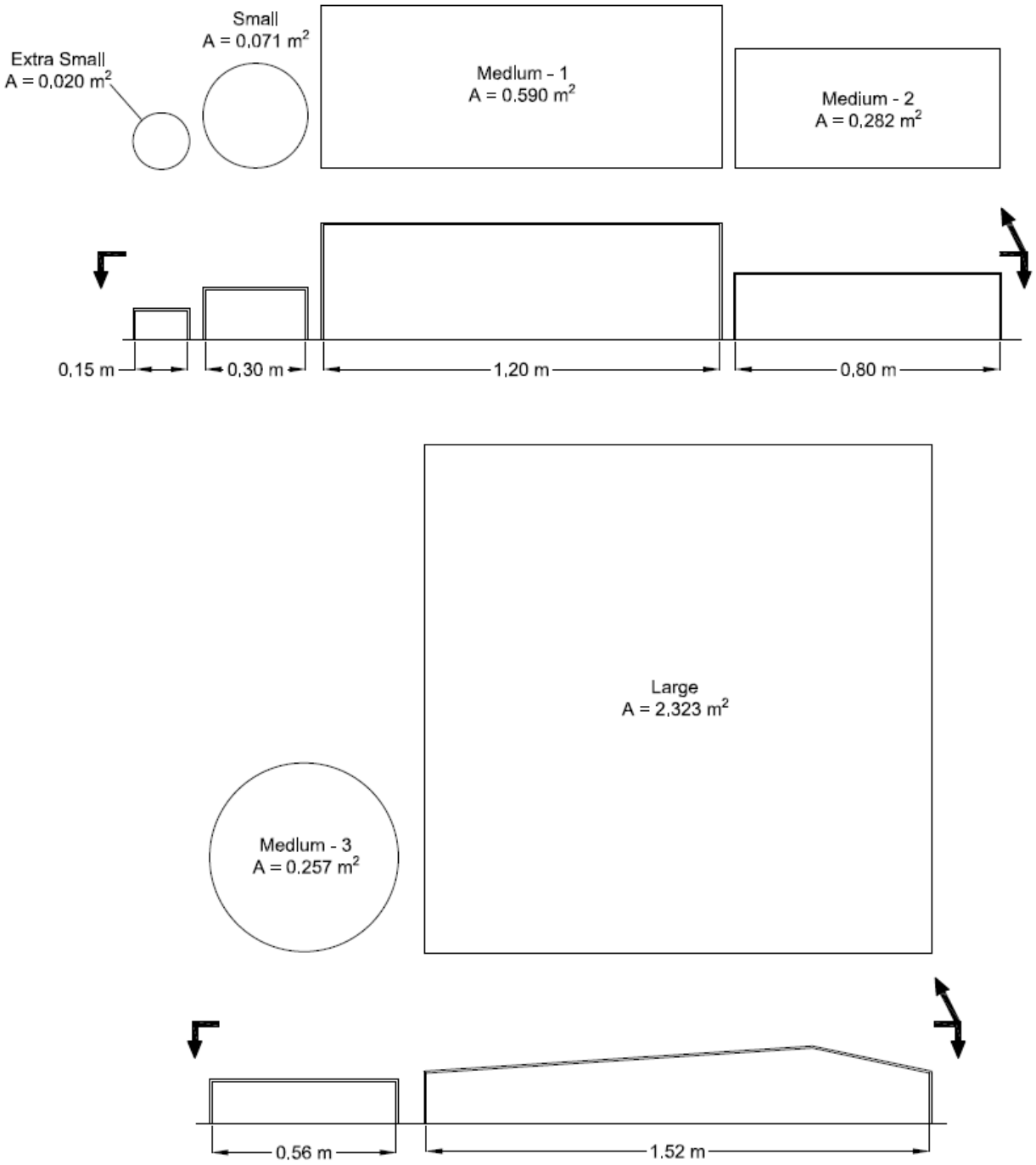

Figure 3.3 – Section and plan views of the different flux chambers used in this research.

3.2 Activated Carbon Canisters

100-mm diameter canisters containing 90 g of granulated activated carbon (AC) were used in this study to measure Rn concentrations within each flux chamber. The canisters were supplied by the Radon Testing Corporation of America (Elmsford, NY). Activated carbon (or charcoal) granules are typically made from wood or coconut shells and have a very high specific surface area due to the high micro porosity properties (Canoba, López, & Oliveira, 1999). This high surface area makes the material highly adsorbent when exposed to gases through the phenomenon known as Van der Waals forces (Canoba et al., 1999). The canisters are perforated on one side and are initially sealed. The seals are removed immediately prior to testing and the canisters are placed directly on the soil surface inside the flux chambers (perforated side facing upward) to expose the granules to the air within the chamber. Upon completion of the test, new seals are placed on the perforated end of the canister to assure that Rn is only allowed to sorb onto the AC during the desired testing period. The AC canisters are then sent to a lab (The Radon Testing Corporation of America, RTCA, Elmsford, NY) for lab analysis of Rn concentration using gamma spectroscopy using a sodium iodide detector. Samples were typically tested by the lab within three to four days after the flux test was completed.

The Rn concentration, *C*, reported by the lab takes into account the Rn decay that takes place during the exposure time and between the end of the flux test and the time of gamma ray spectroscopy analysis in the lab. The concentration is also adjusted for moisture adsorbed onto the granules and the temperature at which the canisters were exposed, both of which are known to affect the efficiency of the AC in adsorbing Rn gas

3.3 Continuous Electronic Radon Monitors

In addition to activated carbon, continuous electronic Radon monitors were used to measure the increase of Rn concentration within each flux chamber. RAD7 alpha detectors (Durridge Company, Inc. Billerica, MA) were attached to each flux chamber with flexible tubing to

form a closed loop with the chamber volume. The RAD7 is an electronic monitor that contains a solid-state detector that senses alpha radiation (in the form of an electrical signal) emitted from the decay of Radon and the various, alpha particle emitting daughter progeny of Radon (including Polonium-218, Polonium-214, and Polonium-210) within the air that is pumped through the detector. The RAD7 then converts this recorded electronic signal to a Rn concentration at a sampling interval specified by the user (Chao et al. 1997). During most flux tests obtained for this research, a sampling interval of 0.25 hours was used. For some flux tests when small and extra small chambers were used, sampling intervals of 0.083 hr (5 min) were used to more effectively capture the early portion of Rn concentration buildup. Desiccation columns were also used in line with the system to reduce the relative humidity of the air passing through the RAD7. This is important, as humidity in the air reduces the accuracy of the RAD7. At high humidity, water molecules attach to the various molecules and slow them down within the RAD7 before they can reach the alpha detector. Even if the radioactive particle decays and produces an electrical charge, the RAD7 will not detect it if it has not reached the sensor (Durridge Company, Inc. RAD7 Manual).

3.4 Thin-Wall Tube Diffusion Testing Apparatus

A testing apparatus was modified from a flexible wall permeameter (ASTM 5084-3), similar to the apparatus used by Stefani (2016) to measure the Rn diffusion coefficient of 70 mm diameter thin-wall tube samples. **Figure 3.4**, below, shows the components of the apparatus. The apparatus features two hollow chambers, one below the sample and one above, both constructed of sections of 70 mm diameter PVC pipe. The bottom chamber is referred to as the accumulation chamber, while the top is referred to as the detection chamber. Flexible tubing is connected to both chambers. The accumulation chamber is connected to a desiccant column, then to a RAD7, followed by a Rn source and an air gas bubbler (to humidify the air so as not to dry the sample).

The detection chamber is also connected to a desiccant column and a RAD7. A clear, outer plexiglass cylinder surrounds the sample and hollow chambers. The annulus space between the outer cylinder and the sample is filled with water and connected with tubing to a burette so that hydrostatic pressure can be applied to the sample. A flexible membrane is used with rubber O-rings to create an impermeable boundary around the sample and hollow chambers.

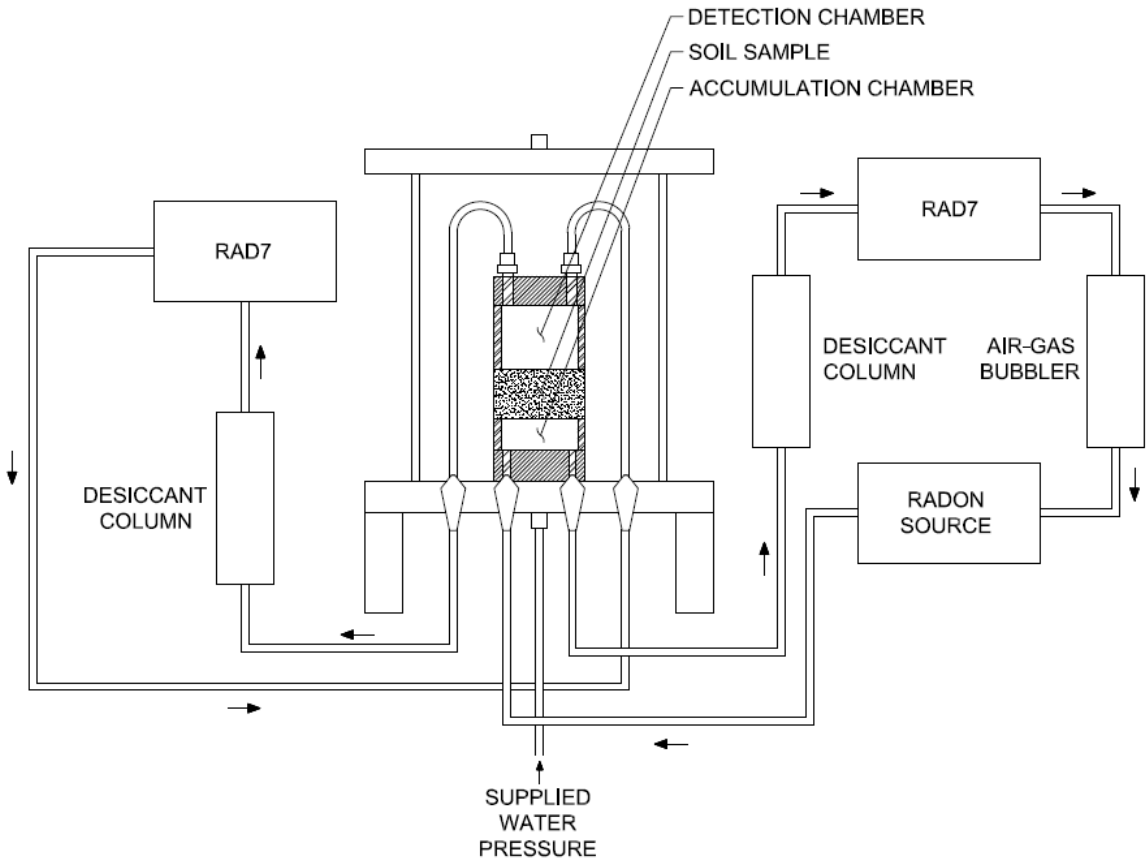

Figure 3.4 – Schematic of thin-wall tube diffusion testing apparatus.

3.5 Radon Sources

In the lab, Rn Barrier soil from previous research at the Falls City, TX UMTRCA site was used as a Rn source. Because this soil was used to construct the Rn barrier and was sourced

from a local borrow pit, it contains levels of Ra-226 that are greater than most typical soils found on earth. Approximately 35 kg of wet Rn barrier soil was gathered from the trimmings of multiple 350 mm diameter samples from the Falls City site and were placed inside an airtight, HDPE, 114 L drum. Tubing was then connected to the drum so that a closed loop could be created. The concentration of the Rn gas within the drum was constantly monitored with a RAD7 detector. The mass of Uranium containing soil generated a concentration of Rn that typically remained within the range of 3,000 +/- 400 Bq/m^3.

4 METHODS

4.1 Lab Methods

4.1.1 Determination of Flux from Activated Carbon

Rn flux was calculated using the single-point Rn concentration from the gamma-ray spectroscopy lab results of the AC tests. Two assumptions were made when using this single point Rn concentration from AC methods to determine flux. The first was that the Rn concentration within the chamber is in equilibrium with the Rn adsorbed onto the AC. The second was that the Rn concentration increases in a linear fashion within the closed flux chamber during the accumulation period. Rn flux is calculated using the following equation:

$$J = \left(\frac{C}{t}\right)\left(\frac{V}{A}\right)$$

Where, *J* is Radon flux (Bq/m^2-h), *C* is Rn concentration at the end of the flux test (reported by the lab) (Bq/m^3), *t* is the duration of the flux test (hour), *V* is the volume of the flux chamber (m^3), and *A* is the area of the flux chamber (m^2).

4.1.2 Determination of Flux from Continuous Electronic Radon Monitor (RAD7)

The RAD7 electronic Radon monitor measures and reports a Rn concentration at an interval specified by the user (0.25 hours for most flux measurements in this study) creating a

nearly “real-time” buildup curve of Radon concentration versus time within the closed flux chamber. In order to calculate flux from the Rn concentration buildup curve, a theoretical equation is fit to the data. A typical Rn buildup curve obtained using the RAD7 is shown in **Figure 4.5**. The concentration of Rn initially builds linearly, then the rate of increase begins to diminish, until eventually, some “plateau” of maximum concentration is reached. The diminishing slope of the buildup curve is caused by the reduction of concentration gradient, Rn decay, and sometimes leakage. Rn flux (J_o) is determined by fitting the theoretical equation for Rn buildup to the measured data. The theoretical equation used from Chao et al., 1997 is:

$$C(t) = \left(C_i - \frac{J_o A + qC_o}{V\left(\lambda + D + \frac{q}{V}\right)} \right) e^{-\left(\lambda + D + (q/V)\right)t} + \frac{J_o A + qC_o}{V\left(\lambda + D + \frac{q}{V}\right)} \qquad \text{(Eq. 1)}$$

Where *C(t)* is the Rn concentration (Bq/m^3) inside the chamber at time *t* (hr), C_i is the initial Rn concentration inside the chamber (Bq/m^3), J_o is the initial Rn flux rate of the material (Bq/m^{2}s), *A* is the chamber area (m^2), *q* is the chamber leakage rate (m^3/hr) (assumed to be zero), C_o is the background mean Rn concentration in the ambient air (Bq/m^3), *V* is the volume of the chamber (m^3), λ is the Rn-222 decay constant (hr^{-1}), and *D* is the “back diffusion” rate of the material (hr^{-1}). The equation simplifies to the following when the leakage rate, *q*, is assumed to be zero:

$$C(t) = \left(C_i - \frac{E_o A}{V(\lambda + D)} \right) e^{-(\lambda + D)t} + \frac{J_o A}{V(\lambda + D)} \qquad \text{(Eq. 2)}$$

Using the method of least-squares regression, the Rn flux, J_o is determined (see **Figure 4.5** for curve fit example from field data). The initial flux emanating from a material or surface can also be calculated considering only the initial, linear portion of the Rn buildup curve. In this initial region of Rn buildup, flux is independent of back diffusion and decay and so can easily be

determined (C. Y. H. Chao et al., 1997). Rn fluxes using only the initial portion of the buildup curves were calculated using the following equation:

$$J_o = (M_e)\left(\frac{V}{A}\right) \quad \text{(Eq. 3)}$$

Where J_o is equal to the Rn flux (Bq/m^{2}hr), M_e is the slope of the initial, linear portion of the curve(Bq/m^{3}hr), V is the volume of the flux chamber (m^3), and A is the area of the flux chamber (m^2). All Rn fluxes reported in this study using the RAD7 were averages of the two methods described above (Stefani, 2016). In some cases, the early portion of the buildup curves had the expected shape but dropped significantly after a few hours which was likely caused by a leak due to desiccation of the bentonite seal around the edge of the flux chamber in contact with the top surface of the Rn barrier. In these cases, only the early linear portion of the Rn buildup curve was used to calculate Rn flux.

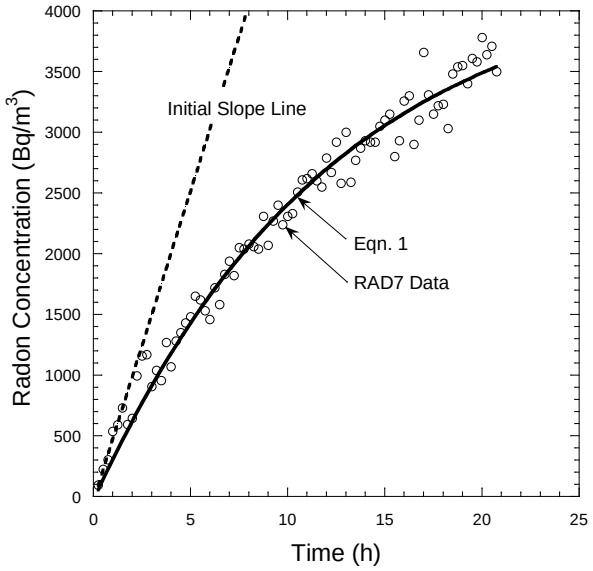

Figure 4.5 – Example of a Rn buildup curve from RAD7 data, fit with Eqn. 1.

4.1.3 Rn Diffusion Coefficient Determination on 70 mm Diameter Samples

Diffusion testing was performed on 70 mm diameter (thin-wall tube) samples using steady-state methods similar to those described in Jiranek (2000) and using the apparatus described above and shown in **Figure 3.4**. Samples of soil were extruded in lengths of approximately 40 - 50 mm and dimensions and mass were carefully measured. The samples were then placed in the testing apparatus between the accumulation and detection chambers. A flexible membrane was then placed over the sample and hollow chambers before the full apparatus was assembled and the annulus space filled with water. The pressure of the water was then increased to 2.5 kPa. Next, the bottom, accumulation chamber was connected via tubing to an external source of Rn gas (see Radon sources section 3.5) to create a closed loop of constant Rn concentration. While the bottom of the sample was exposed to the constant concentration of Rn, the detection chamber was constantly flushed with fresh air. This is performed so that the two initial boundary conditions for steady state diffusion are met: 1 – a constant Rn concentration on one end of the sample, and

2 – a Rn concentration equal to zero exists on the opposite end of the sample. This method is continued for a period of time much greater than what is known as the “relaxation time” (Jiranek, 2000). The relaxation time is calculated as the following:

$$t_{rel} = \frac{1}{D\left(\frac{1}{l^2} + \pi^2\left(\frac{1}{d^2}\right)\right)} \quad \text{(Eqn. 4)}$$

Where t_{rel} is the relaxation time of the tested material (s), D is the Rn diffusion coefficient (m^2/s), l is the diffusion length ($l = (D/\lambda)^{1/2}$) (m), λ is the Rn decay constant ($2.1 \times 10^{-6}\ s^{-1}$) and d is the thickness of the sample (m). Because the diffusion coefficient is not known until after the test has been run, a common empirical equation is used to determine an approximate diffusion coefficient and ultimately the relaxation time required. The following equation was proposed by (Rogers & Nielson, 1990) for estimating the diffusion coefficient of soil:

$$D = D_{ao} * n * e^{-6Sn - 6S^{14n}} \quad \text{(Eqn. 5)}$$

Where D is the diffusion coefficient of the material (m^2/s), D_{ao} is the Rn diffusion coefficient in air (m^2/s), n is the porosity (%), and S is the degree of saturation (%).

Once a time much greater than the relaxation time has been reached, purging with fresh air in the detection chamber is stopped and the detection chamber is connected to a second RAD7 and a closed loop is created. The concentration buildup curve within the chamber is then measured for approximately four to eight hours. During the period shortly after the closure of the detection chamber, the effects of back diffusion are typically small enough to be ignored, and the buildup of Rn within the chamber is linear(C. Y. Chao & Tung, 1999). Therefore, the following

approximate equation can be used to quantify the increase of Rn in the detection chamber (a version of equation 3, solved for *C(t)*) (Jiranek, 2000):

$$C(t) = \frac{JA}{V}t \qquad \text{(Eqn. 6)}$$

Where *C(t)* is the concentration of Rn in the chamber at time *t* (s), *J* is the Rn flux from the surface of the soil sample (Bq/m^{2}s), A is the area of the soil sample (m^2) and *V* is the volume of the detection chamber (m^3). The Rn flux from the sample surface can be determined by optimizing the fit between the theoretical and measured Rn concentration buildup in the detection chamber using least-squares regression. Once this flux is determined, the diffusion coefficient can then be calculated by iterating D (which is buried within the diffusion length, *l*, term), until the measured flux determined from equation 6 matches the theoretical flux in the following equation 7:

$$J(d) = \frac{2\,C_o\,l\,\lambda}{e^{d/l} - e^{-d/l}} \qquad \text{(Eqn. 7)}$$

Where *J(d)* is the Rn flux (Bq/m^{2}s) from the top surface of the sample at a distance *d* (m) from the bottom of the sample, C_o is the constant Rn concentration within the accumulation chamber (Bq/m^3), *l* is the diffusion length($l = (D/\lambda)^{1/2}$) (m), λ is the Rn decay constant (2.1 x 10^{-6} s^{-1}) and *d* is the thickness of the sample (m).

4.1.4 Water Content Profiles

Each of the 70 mm diameter thin walled tube samples obtained from the Rn barrier at each of the test pits were cut in the lab into sections approximately 40 - 50 mm in length to obtain continuous profiles of water content versus depth. The gravimetric water content was measured in accordance with ASTM D2216, *Standard Test Methods for Laboratory Determination of Water*

(Moisture) Content of Soil and Rock by Mass. Additionally, the dimensions and mass of each section were measured so that dry unit weight, volumetric water content, and saturation profiles could be created. The gravimetric water content, dry unit weight and saturation of each of the 350 mm diameter samples were also measured in the laboratory.

4.1.5 Large Scale Saturated Hydraulic Conductivity

The 350 mm diameter block samples obtained at each of the field sites were trimmed to a testing diameter of approximately 305 mm using the procedures described in Benson et al. (2011) and the saturated hydraulic conductivity of each was measured in accordance with ASTM D 5084, *Standard Test Methods for Measurement of Hydraulic Conductivity of Saturated Porous Materials Using a Flexible Wall Permeameter*. The apparatus used to conduct the saturated hydraulic conductivity tests was the same apparatus described in Benson et al. (2011).

4.1.6 Soil Water Characteristic Curves (SWCC)

Soil water characteristic curves were obtained in the lab from select samples following ASTM D 6836 – 02 (Method A and D) *Standard Test Methods for Determination of the Soil Water Characteristic Curve for Desorption Using a Hanging Column, Pressure Extractor, Chilled Mirror Hygrometer, and/or Centrifuge.*

4.1.7 Characterization of Radon Barrier Soil

Soil from either the 350 mm or 70 mm diameter samples was used to perform tests to classify the soil in accordance with the Unified Soil Classification System (USCS). The grain size distribution of each of the soil samples was determined using mechanical sieving and hydrometer analysis in accordance with *ASTM D 422 Standard Test Method for Particle-Size Analysis of Soils*. The Atterberg limits of select samples were also measured in accordance with ASTM D 4318 – 17, *Standard Test Methods for Liquid Limit, Plastic Limit, and Plasticity Index of Soils.* The

specific gravity of select samples was measured in accordance with ASTM D 854 – 14, *Standard Test Methods for Specific Gravity of Soil Solids by Water Pycnometer.*

4.2 Field Methods

4.2.1 Test Pits

Test pits were excavated using small excavators at each disposal site so that Rn flux could be measured directly from the Rn barrier surface (**Figure 4.6**). Test pits were typically chosen to be adjacent to a surface feature that was hypothesized to affect the Rn flux at that location. In most cases, control test pits were also chosen adjacent to these test pits but were devoid of the surface feature. At each test pit location, an excavation through the top protective layers was made to expose the top surface of the Rn barrier. Test pit dimensions varied at each excavation but were approximately 3 m x 4 m. Soils from protective layers were stockpiled and later replaced and compacted to as-built conditions after flux measurements were taken.

Figure 4.6 – Removal of the protective layers of soil to expose the Rn barrier.

4.2.2 Surface Flux Measurements

At each test pit location, four Rn flux measurements were taken from the surface of the exposed Rn barrier (**Figures 4.7 & 4.8**). Typically, all four flux chamber sizes (large, medium, small, and extra small, **Table 3.1**) were used at each test pit to observe scale-dependent phenomena. Prior to beginning each flux measurement, moistened bentonite paste was placed by hand around the edges of each flux chamber to create a seal. This was done to minimize the effects of Rn gas leakage during each flux measurement.

When schedule and test pit excavation size allowed, additional flux measurements were taken from the Rn barrier surface at each location to increase the size of the dataset. Typically, these duplicate measurements were taken immediately adjacent to the initial set of flux measurements to minimize any potential differences in tailings activity, Rn barrier thickness, and barrier conditions. Rn concentrations were measured, and fluxes were calculated following the procedures previously described in sections 4.1.1 and 4.1.2, above.

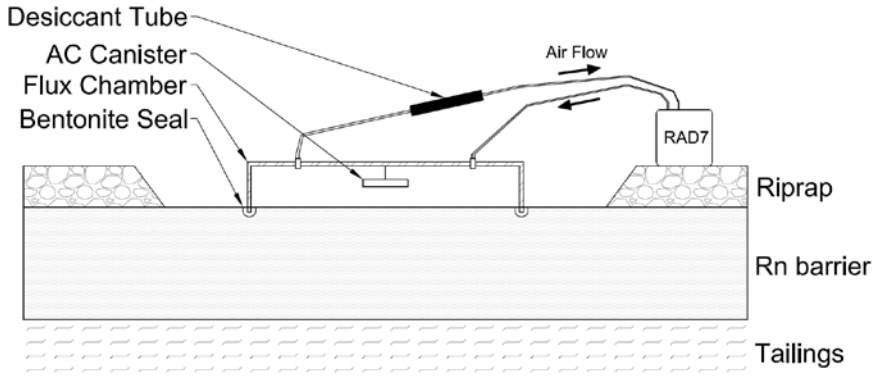

Figure 4.7 Schematic of flux test on Rn barrier surface.

Figure 4.8 – Installation of flux chambers on the Rn barrier surface.

4.2.3 Waste Flux Measurements

At each test pit location, Rn flux was measured using a small flux chamber placed directly on the tailings (**Figures 4.9 & 4.10**). Bentonite paste was again used to create a seal between the soil and the edges of the chamber to minimize gas leakage from the chamber. Rn concentrations were measured, and fluxes were calculated following the same procedures previously described in sections 4.1.1 and 4.1.2.

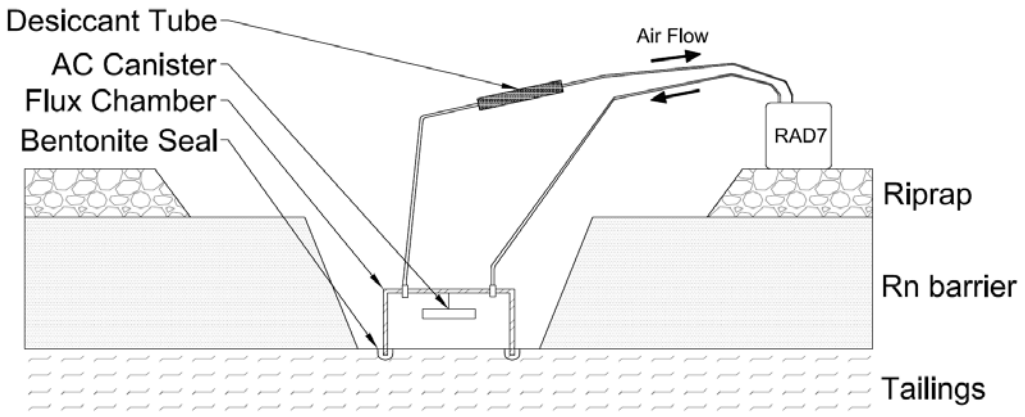

Figure 4.9 – Schematic of a flux test taken directly on the tailings.

Figure 4.10 – A small flux chamber installed directly on the tailings.

4.2.4 Soil Sampling

4.2.4.1 70 mm Diameter Thin Wall Tubes

After surface flux measurements were made at each of the test pits, thin-walled 70 mm diameter tubes were pushed through the Rn Barrier soil using the bucket of a small excavator using a procedure similar to that described in ASTM D1587, Standard Practice for Thin-Walled

Tube Sampling of Fine-Grained Soils for Geotechnical Purposes. At some test pit locations, the Rn Barrier was thicker than the length of a single thin-walled tube and so the soil was benched, and tubes were pushed from the lower elevation for the full barrier profile to be sampled. These samples were collected so that continuous profiles of in-situ water content, dry unit weight, and saturation could be created (see section 4.1.4).

4.2.4.2 350 mm Diameter Block Samples

Intact, large-scale (350 mm diameter) "block" samples were also collected from each test pit to measure hydraulic properties in the laboratory. Blocks samples were excavated following the procedure described in Benson et al. (2011) and in accordance with ASTM D D7015-13, *Standard Practices for Obtaining Intact Block (Cubical and Cylindrical) Samples of Soils*. At locations where the Rn Barrier was thick enough, multiple block samples were collected in a stacked arrangement so that depth-dependent hydraulic properties could be observed. Blocks were excavated using hand and power tools and contained within PVC pipes with inside diameters of 355 mm and heights of 254 mm. Upon extraction of each block sample from the test pit, the ends were sealed with plastic sheeting and then secured with wooden boards. All block samples were transported by truck to the University of Wisconsin-Madison where they were stored in a 100% humidity room prior to testing to prevent drying out of the sample.

4.2.4.3 Pb-210

Small soil samples of Rn barrier material were collected for lab analysis of Pb-210 from each test pit at two sites, Shirley Basin South, WY and Lakeview, OR. Five to seven samples were collected from the exposed sidewall at each test pit from increasing distances from the tailings. This was done so that profiles of Pb-210 versus distance from tailings could be created. Samples were extracted using hand tools and typically consisted of approximately 150 g of soil. Each sample was stored in a separate, labeled 250 mL food container and shipped to the University of Wisconsin for later analysis.

5 RESULTS

The following results sections refer data shown in **Appendices I through IV**. Each of these appendices provide detailed summaries of all measured data and includes test pit locations, Rn fluxes, field samples, lab test results, soil classification, as well as profiles of water content, saturation, and dry density versus depth.

5.1 Radon Flux: Surface Feature versus Control

Rn flux measurements were measured at the surface of Rn barriers at four sites. Test pits were excavated as pairs so that the fluxes measured from beneath a surface feature hypothesized to affect the performance of the barrier could be compared to a control location that lacked that surface feature. Each paired test pit was chosen to be within relatively close proximity to the other so that variability in Rn barrier thickness and tailings activity would be minimized and only the effects of the surface feature would be measured. A total of eight test pit pairs were compared at three of the four sites visited in 2016 and 2017. The descriptions of each of the pairs can be found in **Table 5.1.1**.

Table 5.1.1 – Description of Test Pit Pairs.

Site	Test Pit ID	Description
Falls City, TX	TP-2	Control
	TP-1	Mesquite Tree
	TP-4	Control
	TP-3	Mesquite Tree
Bluewater, NM	TP-1	Seasonal Ponding
	TP-2	No Ponding
	TP-4	Control
	TP-5	Salt Brush Colony
	TP-6	Ant Mound
	TP-8	Control
	TP-7	Small Salt Brush
Lakeview, OR	DC-4A	Control
	DC-4B	Grass
	DC-10	Control
	DC-11	Bitterbrush
	DC-13	Control
	DC-12	Bitterbrush

Rn flux was measured from the surface of additional test pits as well, however, this section will only refer to measurements obtained from test pit pairs. **Table 5.1.2** summarizes the Rn fluxes measured from the surface of each of the paired pits as well as the tailings flux, barrier thickness, average water content and average saturation measured at each of the pits. **Figure 5.1.1**, below, also summarizes the fluxes measured from each pair of pits.

Table 5.1.2 – Comparison of findings from test pit pairs from three sites.

Site	Test Pit ID	Surface Feature/Condition	Feature/Control	Geometric Mean Surface Flux (Bq/m^2s)	% Difference From Control Pit Flux	Rn Barrier Thickness (m)	Tailings Flux (Bq/m^2s)	Average Water Content*	Average % Saturation
Falls City, TX	TP-2	Mesquite Tree	Control	0.248	-	0.52	2.058	0.38	93
	TP-1		Mesquite Tree	0.309	25%	0.58	1.928	0.34	79
	TP-4	Mesquite Tree	Control	0.069	-	0.46	0.26 - 1.54	0.32	91
	TP-3		Mesquite Tree	0.589	754%	0.56	5.151	0.37	NM
	TP-6	5:1 Rip-Rap Slope	Top Edge of Slope	0.009	-	0.56	42.479	0.41	88
	TP-5		Middle of Slope	0.011	22%	0.71	0.097	0.38	94
Bluewater, NM	TP-1	Seasonal Ponding	Ponding	0.003	-	0.65	0.009	0.12	86
	TP-2		No Ponding	0.031	933%	0.61	0.109	0.11	60
	TP-4	Salt Brush/Ant Mound	Control	0.013	-	0.69	11.985	0.09	69
	TP-5		Salt Brush Colony	0.849	6431%	0.62	1.854	0.06	NM
	TP-6		Ant Mound	0.244	1777%	0.64	5.954	0.07	41
	TP-8	Salt Brush	Control	0.010	-	1.06	NM	0.11	65
	TP-7		Small Salt Brush	0.007	-30%	2.35	NM	0.09	59
	TP-3	Sparse Vegetation	-	0.032	-	0.63	4.508	0.08	77
	TP-9	Vegetated Topsoil	-	0.240	-	0.41	1.025	-	-
Shirley Basin South, WY	DC-2	Top Deck	High As-Built Flux	0.047	-	0.68	8.38	0.25	88
	DC-3	Lower Deck		0.008	-	0.65	370.26	0.24	92
	DC-4			0.040	-	NM	NM	0.23	90
	DC-5			0.130	-	0.56	0.24	0.32	97
	DC-6	5:1 Rip-Rap Slope	Wind-Blown Fines	0.159	-	0.49	69.93	0.26	97
Lakeview, OR	DC-4A	5:1 Rip-Rap Slope w/ Vegetation	Control	0.009	-	0.38	NM	0.42	92
	DC-4B		Grass	0.005	-44%	0.38	NM	0.42	92
	DC-10	Bitterbrush	Control	0.004	-	0.41	NM	0.38	87
	DC-11		Bitterbrush	0.022	450%	0.43	0.048	0.33	NM
	DC-13	Rabbitbrush	Control	0.011	-	0.66	NM	0.26	NM
	DC-12		Rabbitbrush	0.006	-45%	0.61	0.368	0.36	NM
	DC-2	Bitterbrush	Bitterbrush	0.005	-	0.43	0.086	0.30	84
	DC-5	Animal Burrow	Animal Burrow	0.011	-	0.46	0.07	0.29	81

* Gravimetric Water Content and Saturation Determined from 70 mm diameter Shelby tube samples.

NM = Not Measured

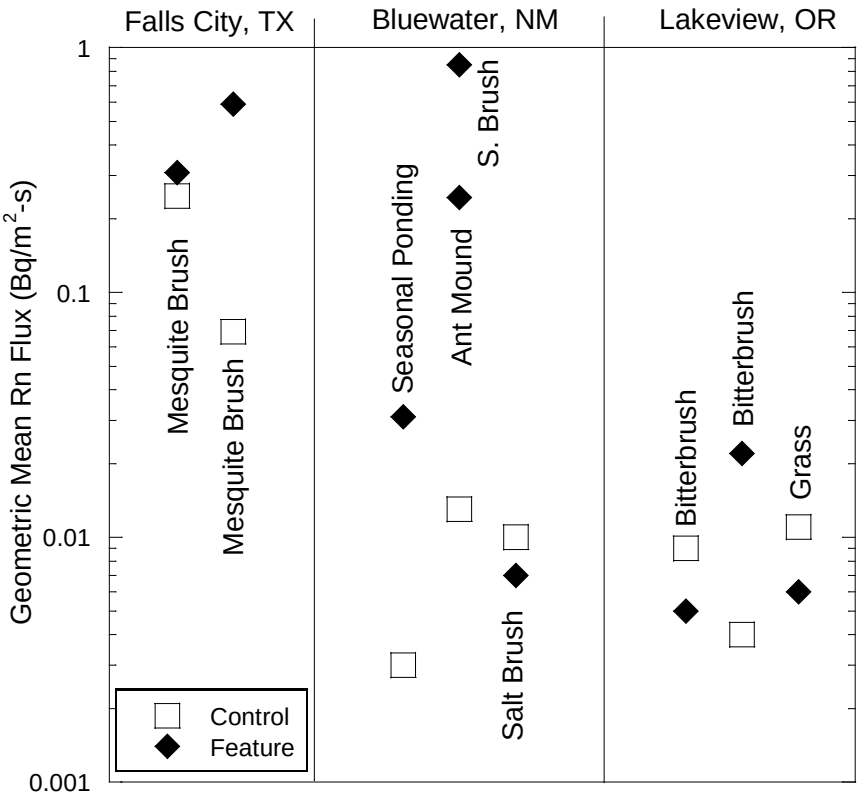

Figure 5.1.1 - Comparison of fluxes measured from test pit pairs from three sites.

5.1.1 Effects of Woody Vegetation on Rn Flux

In general, Rn fluxes measured at test pits that contained woody, deep-rooting vegetation were much greater when compared to fluxes measured from control pits, suggesting that the vegetation may have affected the performance of the barrier in these locations. At the Falls City, TX site, two pairs of test pits were investigated, both of which focused on the effects of mesquite tree(s) and subsurface root structure on Rn flux emanating from the barrier surface. It was

hypothesized that the presence of the mesquite tree would result in larger fluxes compared to locations without this vegetation for two main reasons. It was hypothesized that the mesquite tree roots would extend into the Rn barrier and dry it out and that the presence and water transpiration activity of roots within the Rn barrier would create macrostructure in the soil, create pathways for Rn to short-circuit the barrier, and more easily escape to the surface.

The average flux measured from test pit 3 (Mesquite Brush) was more than seven times greater than the adjacent test pit 4 (control) and was very close to the UMTRCA limit of 0.74 Bq/m^2s, which is consistent with the hypothesis. Furthermore, the thicknesses of the two pits were comparable. However, the flux measured from the tailings beneath the mesquite pit was greater than that measured beneath the control pit, which may have contributed to the elevated fluxes measured from the mesquite pit. The water content did not appear to be lowered in test pit 3 due to the presence of the Mesquite Tree and was found to have a greater water content compared to the control. The elevated fluxes measured at the surface at test pit 3 may also be due to the pathways created from the root structure. **Figure 5.1.2** (below) shows an example of a large root found in the thin-wall Shelby tube during lab sampling.

Figure 5.1.11 – A large root protruding from a thin-walled Shelby tube sample from TP-3 from Falls City, TX.

A similar comparison can be made between test pits 1 (Mesquite Tree) and test pit 2 (control). Greater average flux was measured from beneath the mesquite tree in test pit 1 than from the control pit, however, the increase in mean flux was small (~25% increase). Both the thickness and tailings flux at each of the test pits were very close in magnitude. In this case, the water content and saturation both seem to have been affected by the Mesquite Tree. The water content and saturation were found to be 11% and 15% lower beneath the Mesquite Tree than at the control pit, however, this did not seem to affect the Rn attenuating performance of the barrier.

At the Bluewater, NM site, two pairs of test pits were excavated to study the effects of the presence of saltbush colonies on Rn flux. Similar to the effects due to the presence of the Mesquite Trees at Falls City, it was hypothesized that the roots of the Saltbush would reduce the saturation of the barrier soil, create structure (cracking) and create pathways for Rn flow, leading to increases surface Rn flux.

The average flux measured from test pit 5 (saltbush colony) was greater than sixty times the average flux measured from test pit 4 (control). The average water content in test pit 5 was approximately 33% lower than the control test pit and multiple roots were observed in 70 mm diameter Shelby tube samples obtained from test pit 5 (**Figures 5.1.3 and 5.1.4**). Both of these characteristics likely served to increase the Rn diffusion coefficient of the Rn barrier beneath test pit 5 and are likely the main reasons why elevated fluxes were measured. The thickness of the barrier at each of the test pits was comparable. Furthermore, the flux from the tailings beneath test pit 5 (saltbush colony) were much less than the tailings flux measured from test pit 4 (control), strengthening the hypothesis that the saltbush colony was the main cause of the elevated flux measurements.

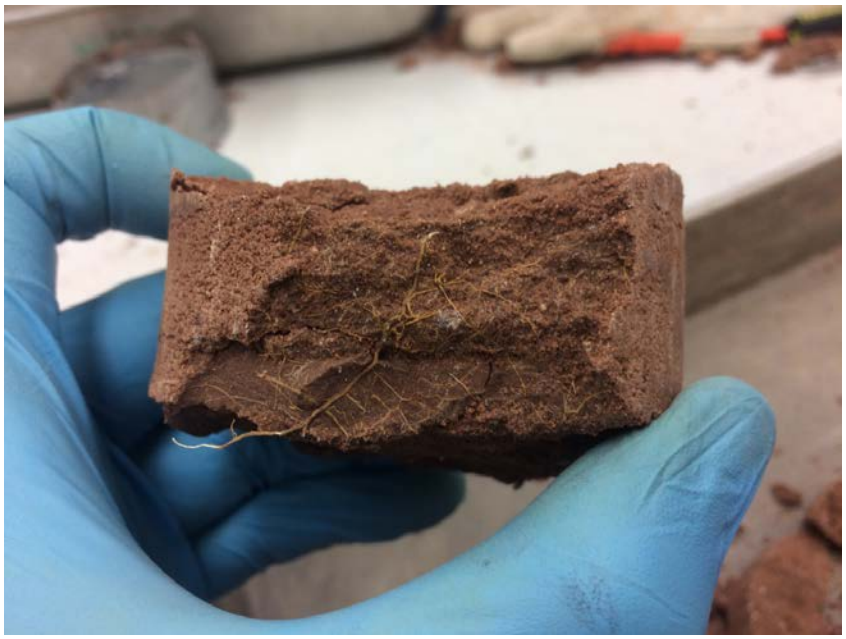

Figure 5.1.12 - Root structure in 70 mm diameter Shelby tube sample from Bluewater, NM test pit 5.

Figure 5.1.13 – Large root in 70 mm diameter Shelby tube sample from Bluewater, NM test pit 5.

An additional pair of test pits was excavated from the carbonate tailings pile at the Bluewater site to observe the effects of a saltbush colony on Rn flux, however, the expected trend was not observed. The average flux measured from test pit 7 (small saltbush) was slightly lower

than that measured at test pit 8 (control), the opposite of what was expected. However, it is likely that the greater thickness of the Rn barrier beneath the saltbush caused this discrepancy. The Rn barrier beneath the saltbush colony was approximately 120% thicker than at the control pit. It is possible that any soil structure formation caused due to the presence of the saltbush colony may have been limited to the surface of the barrier. Due to the increased thickness of the Rn barrier at this location, it is likely that most of the Rn attenuation occurred at the relatively unaffected, wetter portion of the barrier closest to the tailings.

Two pairs of test pits were excavated at the Lakeview, OR site to observe the effects of bitterbrush and rabbitbrush on Rn flux. The same prediction was made regarding elevated Rn flux beneath the bitterbrush due to the presence of the root structure.

The average flux measured from test pit 11 (bitterbrush) was greater than four times the average flux measured from test pit 10 (control). The thickness of the Rn barrier at both test pit locations were within 2 cm of each other. The average water content of the Rn barrier soil beneath the bitterbrush was also found to be approximately 13% lower than the soil in the control test pit. It is believed that the presence of the bitterbrush contributed to the greater surface Rn flux measured due to the drying effect of the root structure as well as the pathways created by the roots. Unfortunately, Rn flux measurements obtained directly from the tailings beneath the control pit were unsuccessful and thus the effect of tailings flux beneath the control location remains unknown.

Surface flux measurements were also obtained from an additional pair of test pits excavated above a rabbitbrush (DC-12) and a control location (DC-13), however, the expected trend was not observed. The flux from beneath the rabbitbrush at DC-12 was approximately 45% less than that measured at the control location. The water content beneath the rabbitbrush in test pit DC-12 was found to be approximately 38% greater than the control pit, which also was not

expected. This greater saturation level of the barrier soil likely offset any degradation within the Rn barrier that may have been caused by the root structure, resulting in very similar surface fluxes.

5.1.2 Effects of Seasonal Ponding on Rn Flux

Test pit 2 was chosen at the Bluewater, NM site due to the presence of seasonal ponding at that location. A control test pit (TP-2) without seasonal ponding was chosen in the vicinity of TP-2 so that the effects of the ponding on the Rn flux could be observed. It was hypothesized that the seasonal ponding would result in an area of the Rn barrier with higher levels of saturation, which would lower the diffusion coefficient, and result in lower surface flux measurements compared to the pit without ponding. As predicted, the Rn barrier soil at the ponding location had average water contents and saturations 9% and 43% greater than the location without ponding, respectively. As a result, the average Rn flux measured from the location without ponding was approximately 9.3 times larger than the location with ponding. The thickness of the Rn Barrier at each of the test pits was comparable, however, the fluxes measured from the tailings were significantly different. The flux measured from the tailings beneath the location with seasonal ponding was approximately 12 times lower than the flux measured from the tailings beneath the location without ponding. This likely contributed to the difference in surface flux measurements between the two test pits.

5.1.3 Effects of Animal Burrowing

At the Bluewater, NM site, test pit 6 was excavated at the location of a large ant mound and was compared to the control test pit 4 to observe the effects that an ant mound might have on Rn flux. It was hypothesized that the burrowing of the ants might reduce the saturation and density of the barrier material if they extended into it. Furthermore, it was predicted that the burrows might act as pathways for Rn to flow and short-circuit the barrier.

The average flux measured from TP-6 was found to be approximately 17 times greater than that measured at the control test pit. The average water content of the barrier beneath the ant mound was found to be approximately 22% less than that of the control pit. The thickness of the barrier at each location was very similar, and the tailings flux from beneath the ant mound was approximately 50% of that measured from the tailings beneath the control pit. Both of these characteristics strengthen the hypothesis that the ant mound was the main contributing factor to the elevated Rn flux at this location.

5.1.4 Effects of Grass Growth in Rip-Rap

Test pits 4A (bare rip-rap) and 4B (rip-rap w/grass) were chosen at the Lakeview, OR site to analyze the potential effects of grass growth within the 5:1 rip-rap slope. It was hypothesized that the presence of the grass would remove moisture from the barrier, reduce the saturation of the barrier and thus result in elevated fluxes from the area. This prediction was not observed, however, and the flux from beneath the grass was actually about 45% less than that measured beneath the pit with bare rip-rap. Additionally, no significant differences in water content were observed between the two pits. The possibility exists that the root structure of the grass did not penetrate into (or deeply into) the Rn barrier and thus did not affect the engineering properties of the barrier.

It must be noted that the Rn fluxes measured from most locations at the Lakeview, OR site were so low that they were believed to be background levels and not actually linked to the tailings. It is very likely that the Rn fluxes measured from the surface were actually measurements of the Rn emanating from the barrier soil itself, which has measurable levels of Radium-226 within it. Therefore, the variability of the Rn flux measurements between test pits and associated control pits may be solely due to the spatial variability of the Ra-226 content of the barrier soil and not directly related to the presence (or lack thereof) of a surface feature.

5.2 2016 / 2017 Rn Flux versus As-Built Rn Flux

It is required by CFR 40 C.F.R. § 192.02 that at the end of the construction of an Rn barrier at UMTRCA sites, flux measurements must be taken from the surface to prove that the barrier is effectively reducing Rn flux rates to below the regulatory standard of 0.74 Bq/m^2s. These measurements are obtained using adsorption methods using activated carbon (AC) and small flux chambers (see section 2 for additional discussion of methods). The post-construction Rn flux measurements (hereon referred to as as-built fluxes), as well as additional information regarding construction of the disposal site, are summarized in completion reports and are available to the public. The as-built flux measurements from Falls City, TX, Bluewater, NM, and Shirley Basin South, WY are summarized in **Table 5.2.1 & 5.2.2**, below. Also summarized in **Table 5.2.1 & 5.2.2** are the averages of all flux measurements obtained during fieldwork performed in 2016 and 2017.

Table 5.2.1 – Summary of Rn fluxes measured for this research and post-construction (as-built).

Site	Geometric Mean As-Built Flux (Bq/m^2s)	Geometric Mean '16 / '17 Flux (Bq/m^2s)
Falls City, TX	0.018	0.074
Bluewater, NM	0.032	0.040
Shirley Basin South, WY	0.033	0.027
Lakeview, OR	N/A	0.008

Table 5.2.2 - Summary of Rn fluxes measured for this research and post-construction (as-built), differentiated by location.

Site	Location on Disposal Cell	Geometric Mean As-Built Flux (Bq/m^2s)	AVG As-Built Water Content	Geometric Mean '16/'17 Flux (Bq/m^2s)	AVG '16/'17 Water Content
Falls City, TX	Top Deck	0.018	42.2	0.231	35.9
	5:1 Rip Rap Slope	0.018	42.2	0.010	39.8
Bluewater, NM	Main Tailings Pile	0.032	12.3	0.033	9.6
	Acid Tailings	0.120	10.4	0.240	N/A
	Carbonate Pile	0.027	12.4	0.009	10.7
Shirley Basin South, WY	Top Deck	0.032	23.4	0.008	24.4
	Bottom Deck	0.034	23.4	0.034	26.3
Lakeview, OR	Top Deck	N/A	N/A	0.008	32.3
	5:1 Rip-Rap Slope	N/A	N/A	0.006	41.8

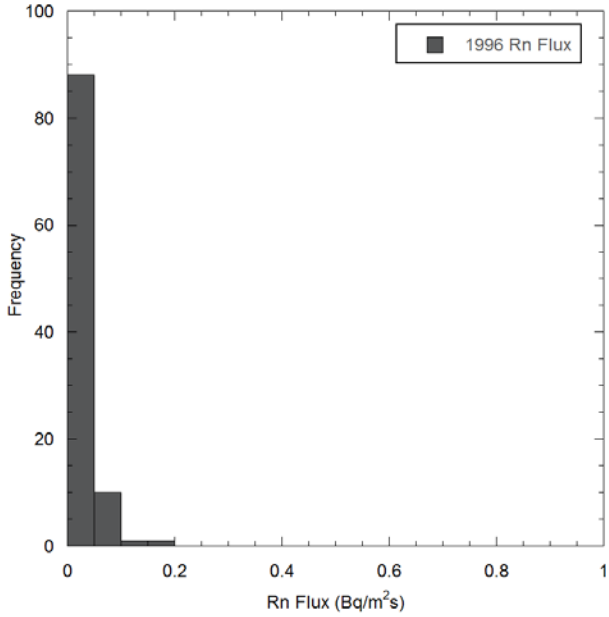

Figure 5.2.14 – As-built flux measurements from Falls City, TX.

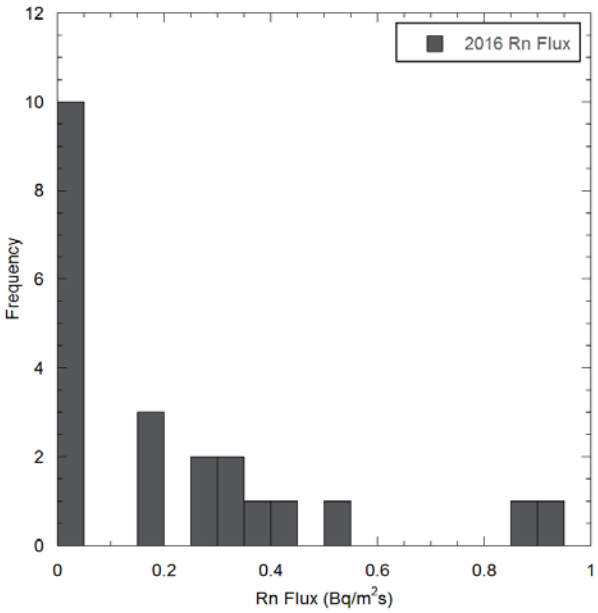

Figure 5.2.215 – Flux measurements from this research from Falls City, TX.

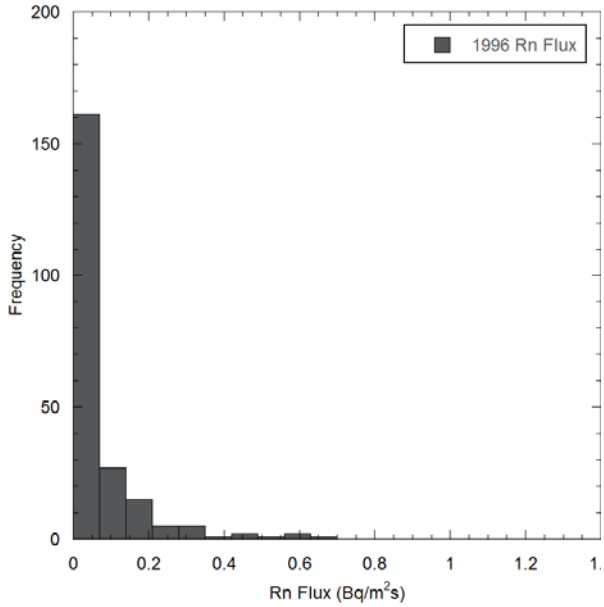

Figure 5.2.3 – As-built flux measurements from Bluewater, NM.

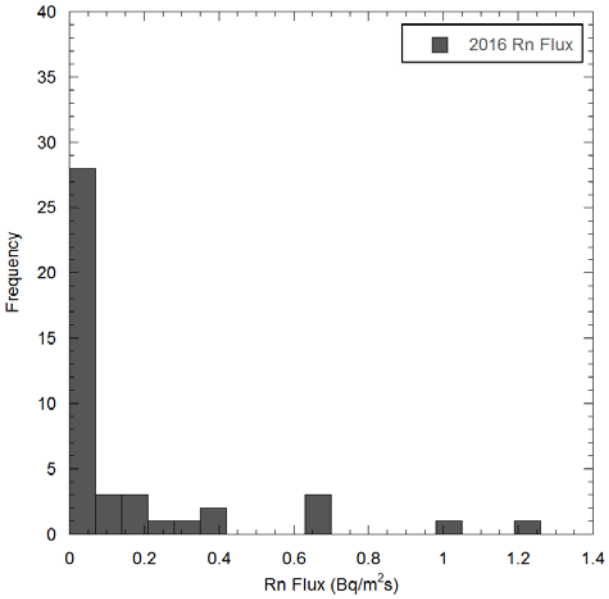

Figure 5.2.4 – Flux measurements from this research from Bluewater, NM.

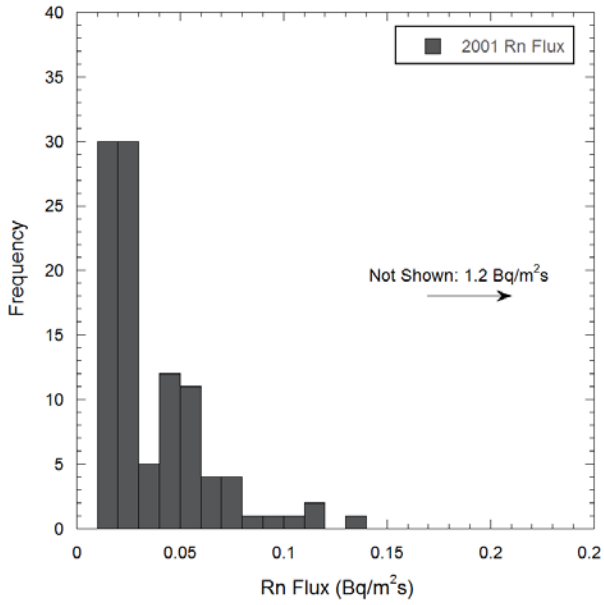

Figure 5.2.5 - As-built flux measurements from Shirley Basin South, WY.

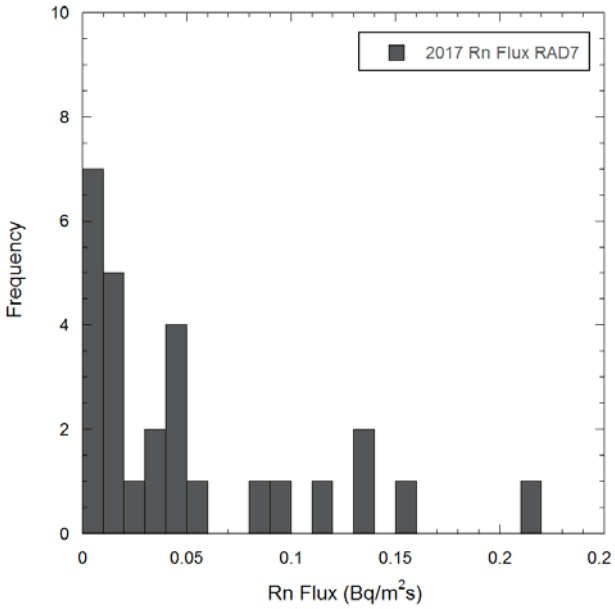

Figure 5.2.6 - Flux measurements from this research from Shirley Basin South, WY.

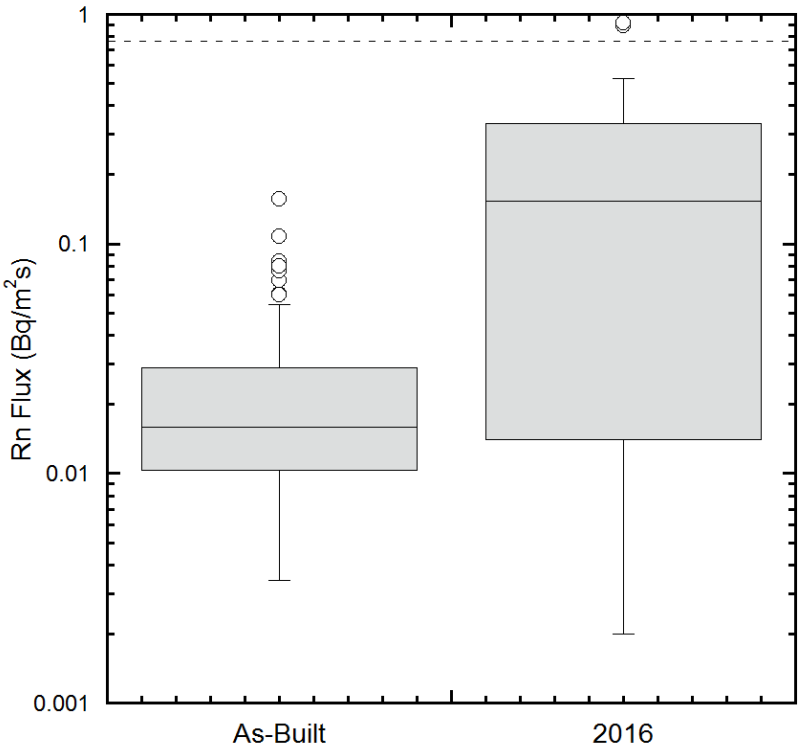

Figure 5.2.7 – Box plot showing as-built and 2016 measurements of Rn flux from Falls City, TX.

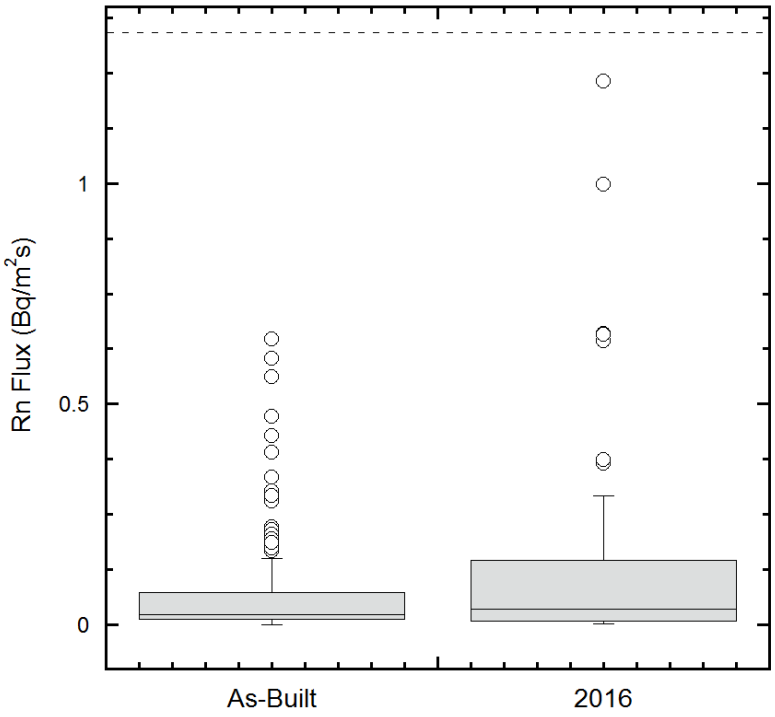

Figure 5.2.8 - Box plot showing as-built and 2016 measurements of Rn flux from Bluewater, NM.

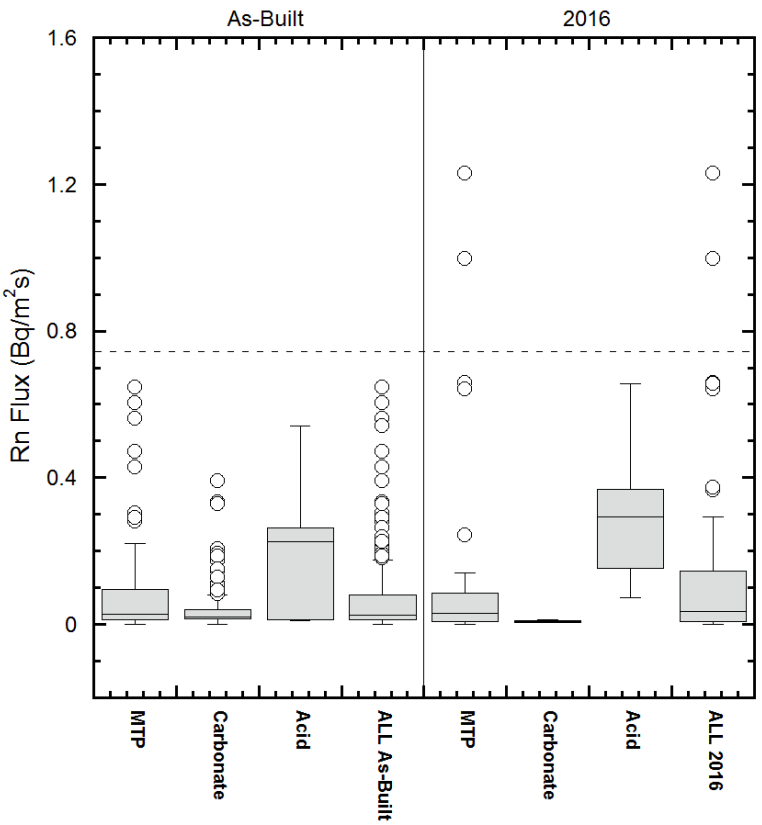

Figure 5.2.9 - Box plot showing as-built and 2016 measurements of Rn flux from Bluewater, NM, separated by location.

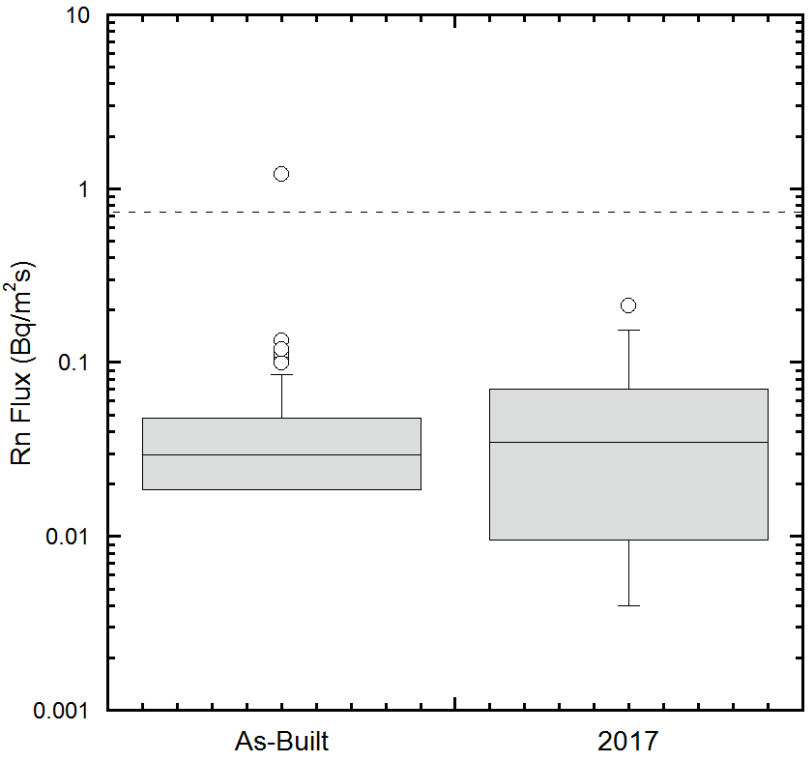

Figure 5.2.10 - Box plot showing as-built and 2016 measurements of Rn flux from Shirley Basin South, WY.

Figures 5.2.7 – 5.2.10 use the box plot method to show the distribution of the flux measurements from this research and as-built conditions. The horizontal line represents the median flux value from each dataset. The top (UQ) and bottom (LQ) of the boxes represent the +/- 25% limits of the dataset and the distance between the top and bottom represent the interquartile distance (IQD). The whiskers represent the maximum and minimum values that fall within an “acceptable range”. The individual points represent outliers which are either greater than the UQ + 1.5*IQD or less than LQ – 1.5*IQD.

At the Falls City site, the geometric mean of all Rn fluxes measured in 2016 was approximately four times the magnitude of the geometric mean as-built flux. The fluxes measured from the upper deck area of the disposal cell in 2016 are the main contributor to the higher geometric mean relative to as-built. If only the fluxes from the top deck are considered, the

geometric mean flux was approximately 13 times the magnitude of the as-built mean. Alternatively, the geometric mean flux value from the 5:1 slope in 2016 was only about 60% of the as-built mean. The findings suggest that the main contributing factors to the elevated flux measurements from the top deck in 2016 are likely the dryer Rn barrier relative to the as-built values, as well as the effect of the mesquite on the Rn barrier.

At the Bluewater site, a similar trend was observed. If all flux measurements obtained in 2016 are considered, the geometric mean flux value was approximately 1.25 times the magnitude of the as-built geometric mean flux. Flux measurements were separated by location and compared to the as-built fluxes from that corresponding location (see Table 5.2.2). While the flux measurements obtained from the main tailings pile and acid tailings pile in 2016 showed increases relative to as-built (1.03 and 2.0 times, respectively), the geometric mean flux from the carbonate pile was actually found to be lower than as-built (0.33 times) although sample size was small for both 2016 and as-built fluxes at this location. One can notice in Figure 5.2.8 that while the box plots for the main tailings pile show a relatively similar distribution, a number of outliers exist in the 2016 measurements that exceed all as-built values. These outliers represent the fluxes measured from the test pit with a saltbush colony and a very dry barrier and were above the UMTRCA flux limit of 0.74 Bq/m^2s.

The water content profiles measured at Bluewater in 2016 also suggest that the Rn barrier soil was significantly drier than when as-built flux measurements were obtained. The main tailings pile and carbonate tailings piles were found to have water contents lower than as-built measurements by 22% and 14%, respectively.

Both the Falls City and Bluewater sites exhibited decreases in Rn barrier water content compared to as-built conditions. This is likely due to the fact that as-built measurements of water content were obtained during compaction of the barrier, when high, optimum water contents were

required to meet compactions standards. The as-built flux measurements also likely represent a “best-case” scenario as the Rn barrier was highly saturated, relatively free of defects and likely had the lowest diffusion coefficient it will ever have had at the time of measurement.

The fluxes measured at the Shirley Basin South site did not show a statistically significant difference compared to as-built measurements. This site was relatively free of surface features that were expected to cause increases in Rn fluxes. Rather, test pit locations were chosen to be in the vicinity of locations where high as-built fluxes were measured. Regardless of this, the geometric mean Rn flux measured in 2017 was found to be about 0.8 times the magnitude of geometric mean flux determined from as-built measurements. The water content measured in 2017, averaged across all test pits, was also found to have increased slightly relative to as-built measurements. It appears that very little change had occurred to affect the Rn diffusion coefficient of the Rn barrier soil at the time of these measurements.

When comparing the 2016/2017 flux values with as-built fluxes at each of the three locations, the distinction must be made that fieldwork was purposely performed during the time of year that was expected to yield the driest conditions. The diffusion coefficient of the soil in these Rn barriers, is inversely proportional to the saturation level. Thus, if the barrier was very dry, it would result in a larger diffusion coefficient (and potentially a higher surface flux) than would a saturated barrier (as-built conditions). Therefore, there exists some bias in the average surface flux measurements obtained in 2016/2017 and reported in this study.

In addition to this, the majority of test pits were excavated in pairs to observe the effects of various surface features on Rn flux. This means that roughly half of the test pits excavated were at locations that were expected to cause elevated surface fluxes. Generally, test pits were also excavated in close proximity to locations where high as-built fluxes were measured. Conversely, the as-built fluxes were instead placed in locations based on a grid pattern at regular

intervals. Thus, the comparison of fluxes measured in 2016 and 2017 to as-built fluxes is not necessarily statistically ideal and the biases must not be ignored.

5.3 Activated Carbon versus RAD7 Methods for Rn Flux Determination

As previously introduced, a new, inexpensive method for Rn flux determination was used in combination with an accepted method to determine the plausibility of the method for Rn flux measurement (section 4.1.1). The new method involved the use of a commercially available activated charcoal/carbon canister (section 3.2) placed inside the open volume of an accumulation chamber sealed to the Rn barrier surface for a known time period. The canisters were sent to a lab and a single Rn concentration was reported.

5.3.1 Comparison of Rn Concentrations Measured Using AC vs RAD7

First, the two methods were compared in their ability to determine the Rn concentration reached within the accumulation chamber. **Figures 5.3.3 through 5.3.5** below, show a comparison of the two methods for concentration determination by plotting x-y pairs of RAD7 – AC concentration, respectively. For the RAD7 values, the average concentration of the last hour of measurement was used (see **Figure 5.3.1** for example). It must be noted that in some cases the concentration buildup curves determined using the RAD7 were not typical. That is, they did not exhibit the shape of the expected Rn buildup curve and instead showed a decrease in Rn concentration after reaching a peak value (example shown in **Figure 5.3.2**). In this instance, the flux between the two methods could still be compared using the initial, linear portion of the buildup curve, however, the concentrations could not confidently be compared. **Figure 5.3.3** shows all field data points on a log-log scale so that extreme values can be shown. **Figures 5.3.4 and 5** show data points below concentrations of 10,000 Bq/m^3 and 2,000 Bq/m^3, respectively, plotted on an arithmetic scale so that the trend can be observed for concentrations of lower magnitudes.

A line was fit to the data points using a best-fit linear-regression for each dataset. A line with a 1:1 slope was also shown in each plot as a reference. If the two methods were in perfect agreement for each test, the points would fall on this 1:1 line.

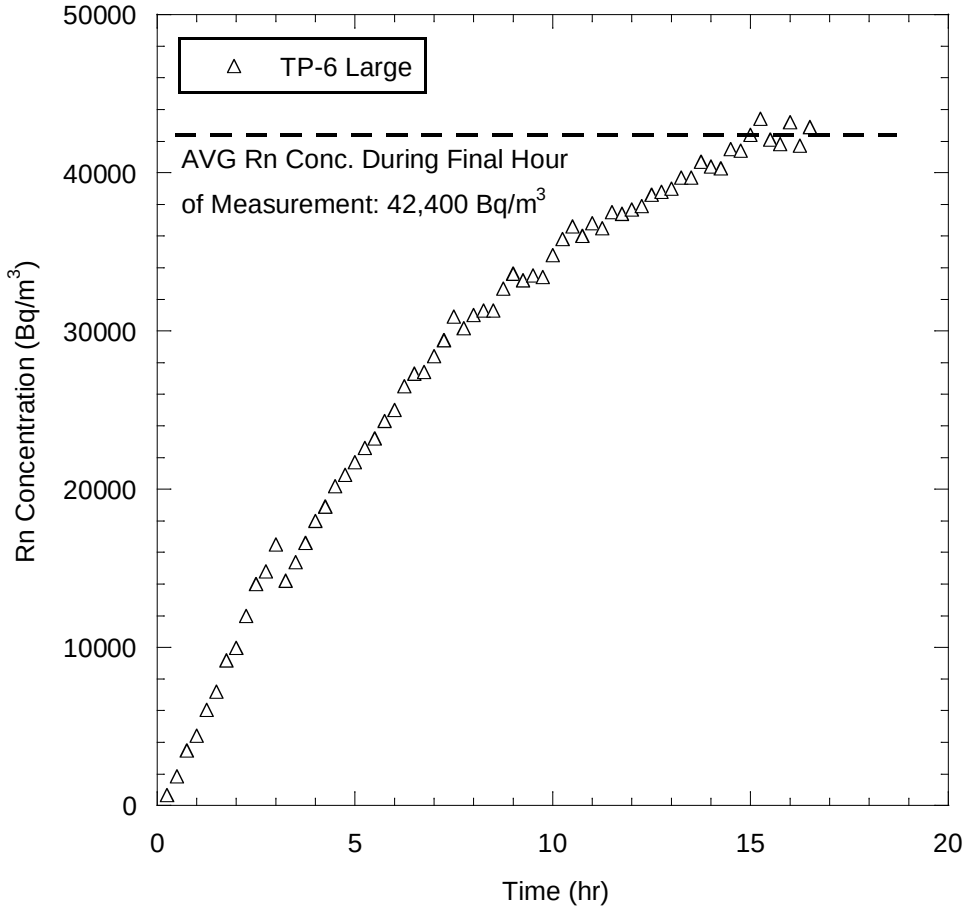

Figure 5.3.1 – Example of average concentration used from RAD7 data (Bluewater, NM 2016)

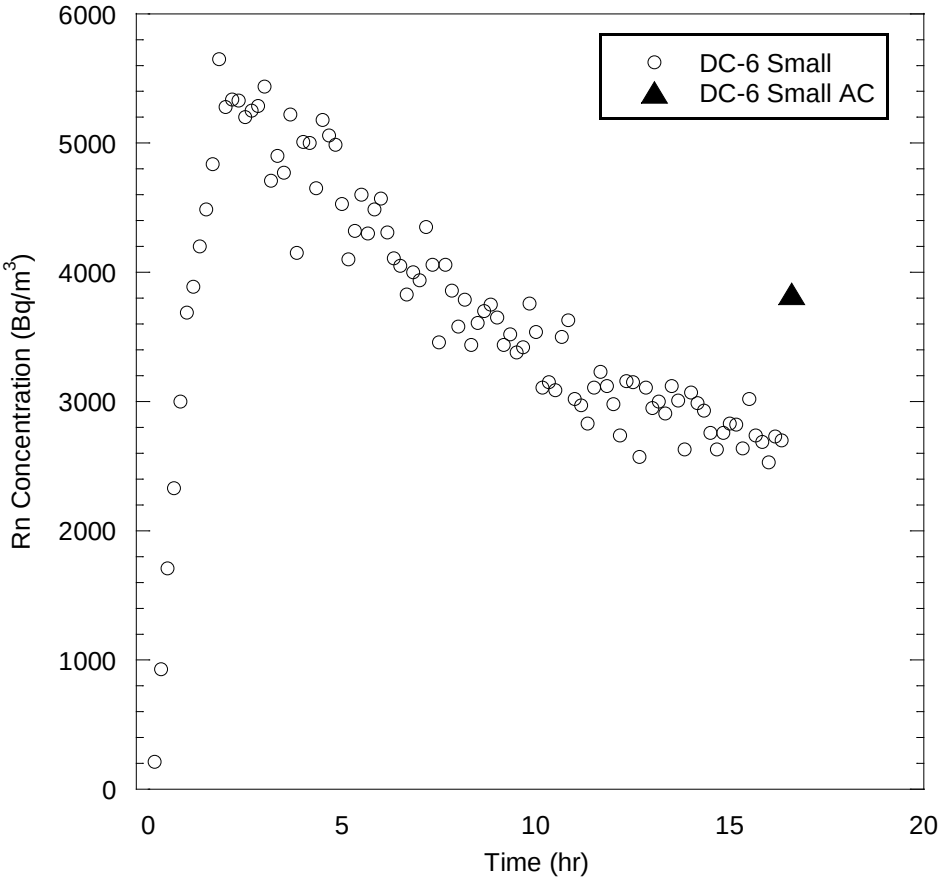

Figure 5.3.16 – Example of Rn buildup curve with sharp decrease in concentration (Shirley Basin South, WY 2017).

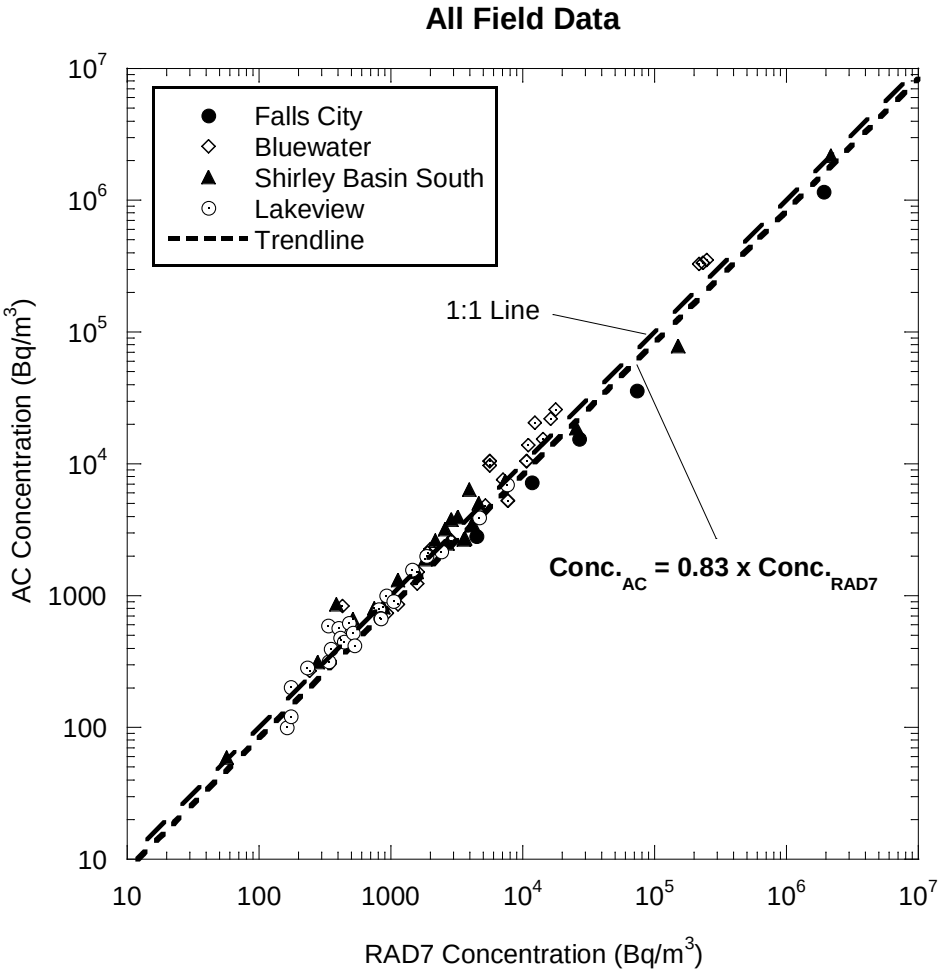

Figure 5.3.3 – Comparison of the AC and RAD7 methods in determining Rn concentration (all field data points included). n = 76, R^2 = 0.94

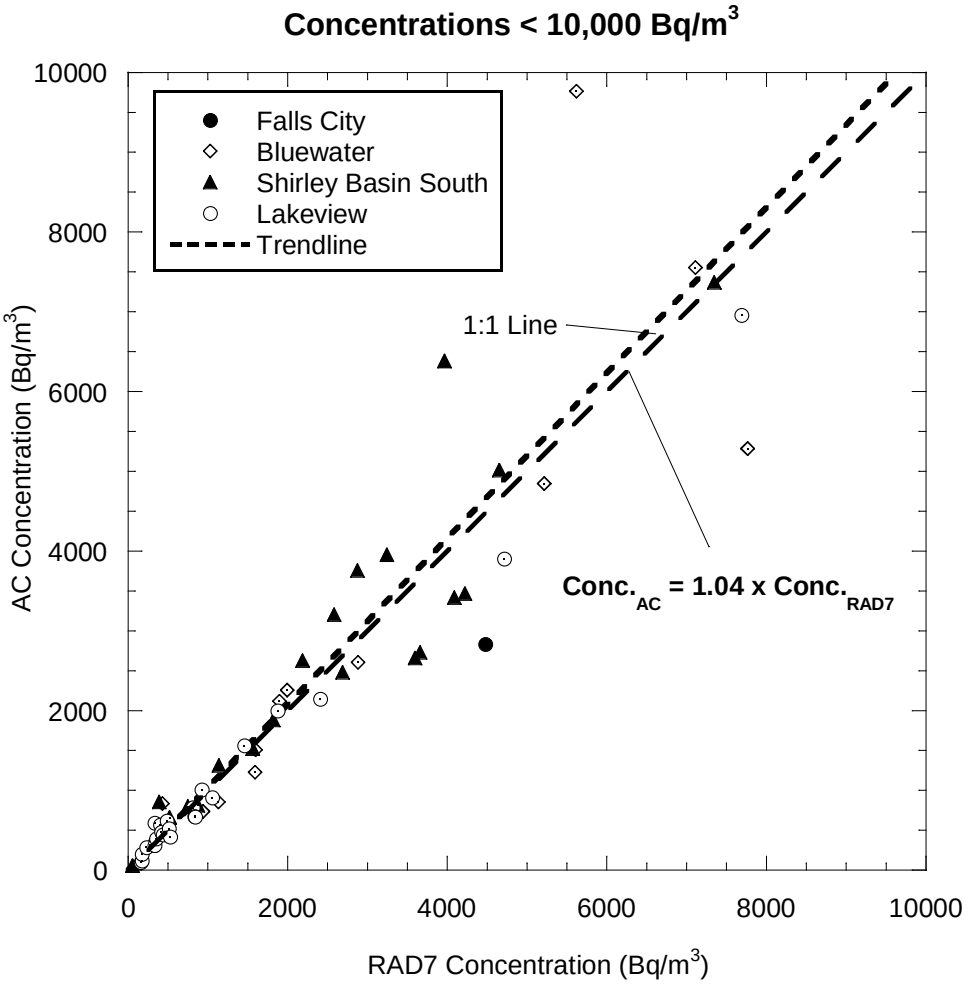

Figure 5.3.4 - Comparison of the AC and RAD7 methods in determining Rn concentration (Rn concentrations below 10,000 Bq/m^3). n = 60, R^2 = 0.82

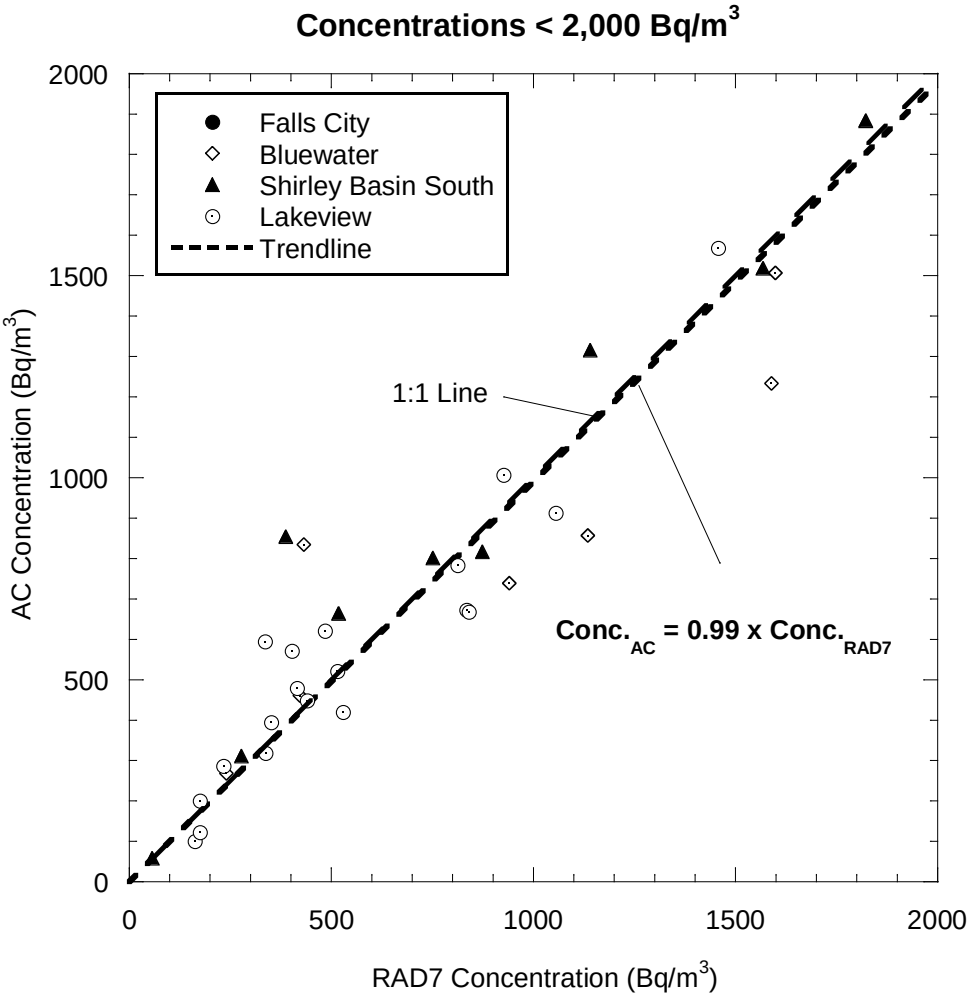

Figure 5.3.5 - Comparison of the AC and RAD7 methods in determining Rn concentration (Rn concentrations below 2,000 Bq/m^3). n = 35, R^2 = 0.86

Figures 5.3.3 – 5.3.5 show that the AC and RAD7 methods agree very well in determining the maximum Rn concentration reached within each chamber. When considering all data points, the line fit to the data points has a slope of 0.83, indicating that the concentration determined from the AC method is typically about 83% of the concentration determined by RAD7 methods. However, a few extreme values had a large influence on this trend. When only the values below 10,000 Bq/m^3 and 2,000 Bq/m^3 are considered, the lines fit to the datasets show much better agreement with slopes of 1.04 and 0.99, respectively. The latter two trendlines also fit the data very well, indicated by the R-squared values of 0.82 and 0.86, respectively.

5.3.2 Comparison of Fluxes Measured Using AC Canisters vs RAD7

The same method was used to analyze the agreement of RAD7 and AC methods in determining Rn flux. **Figures 5.3.6 through 5.3.8** show fluxes calculated using RAD7 on the x-axis versus the corresponding fluxes calculated using the AC method on the y-axis. **Figure 5.3.6** shows all field data points on a log-log scale so that extreme values can be shown. **Figures 5.3.7 and 5.3.8** show data points below concentrations of 1.0 Bq/m^2s and 0.1 Bq/m^2s, respectively, so that this relationship could be observed for all data points. The majority of flux magnitudes for field measurements taken from the surface of the Rn barrier were below the UMTRCA limit of 0.74 Bq/m^2s and so particular emphasis is placed on **Figure 5.3.7** with values below 1.0 Bq/m^2s.

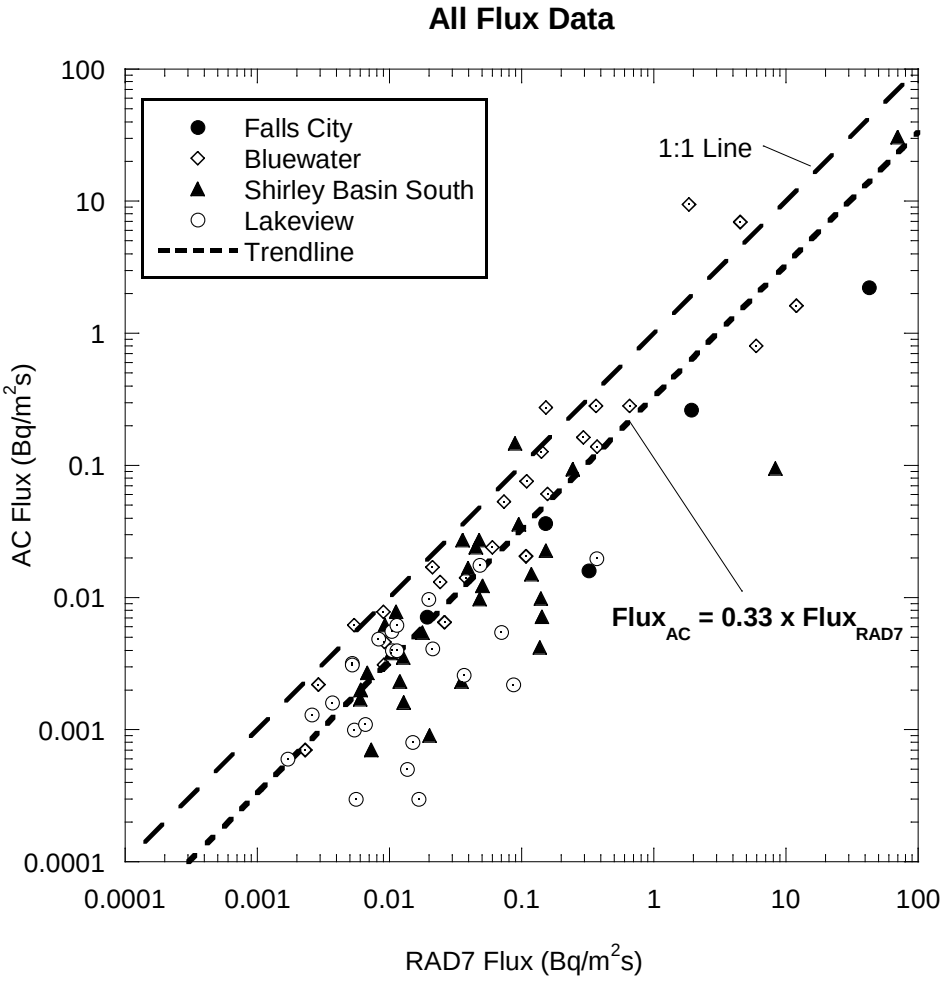

Figure 5.3.6 - Comparison of the AC and RAD7 methods in determining Rn flux (All Rn flux data included). n = 81, R^2 = 0.75

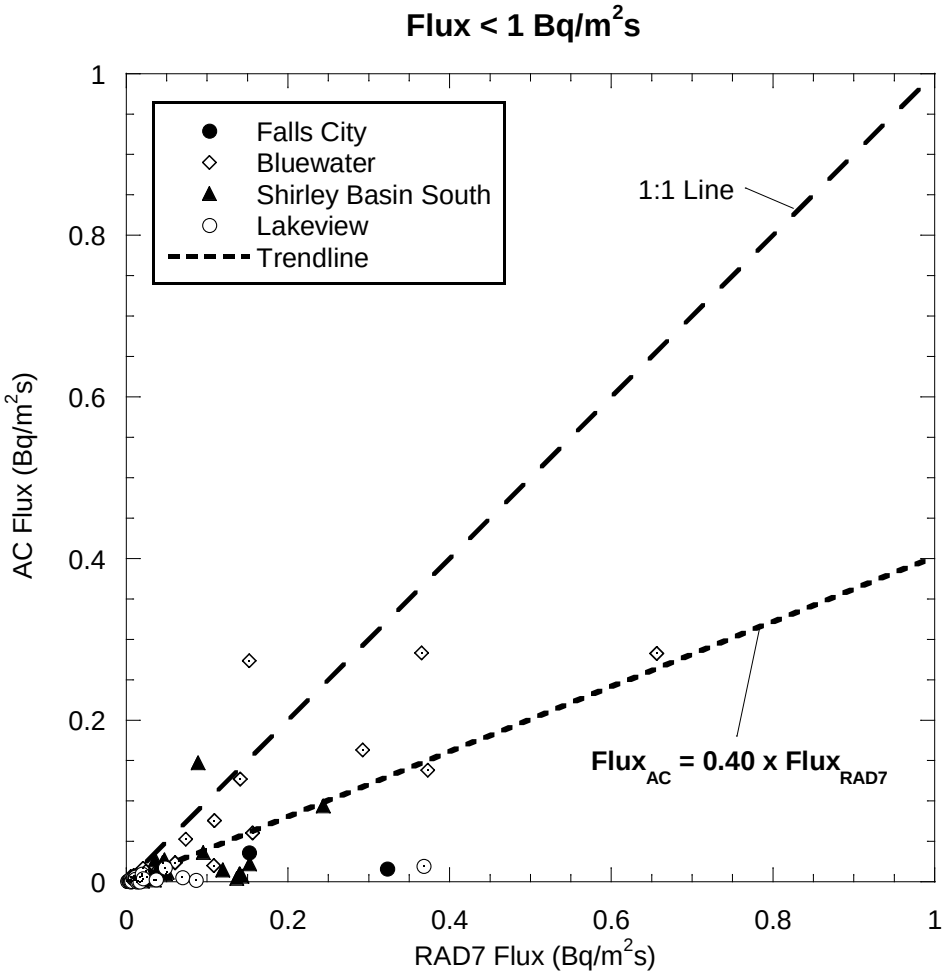

Figure 5.3.7 - Comparison of the AC and RAD7 methods in determining Rn flux (Rn fluxes below 1 Bq/m^2s). n = 74, R^2 = 0.54

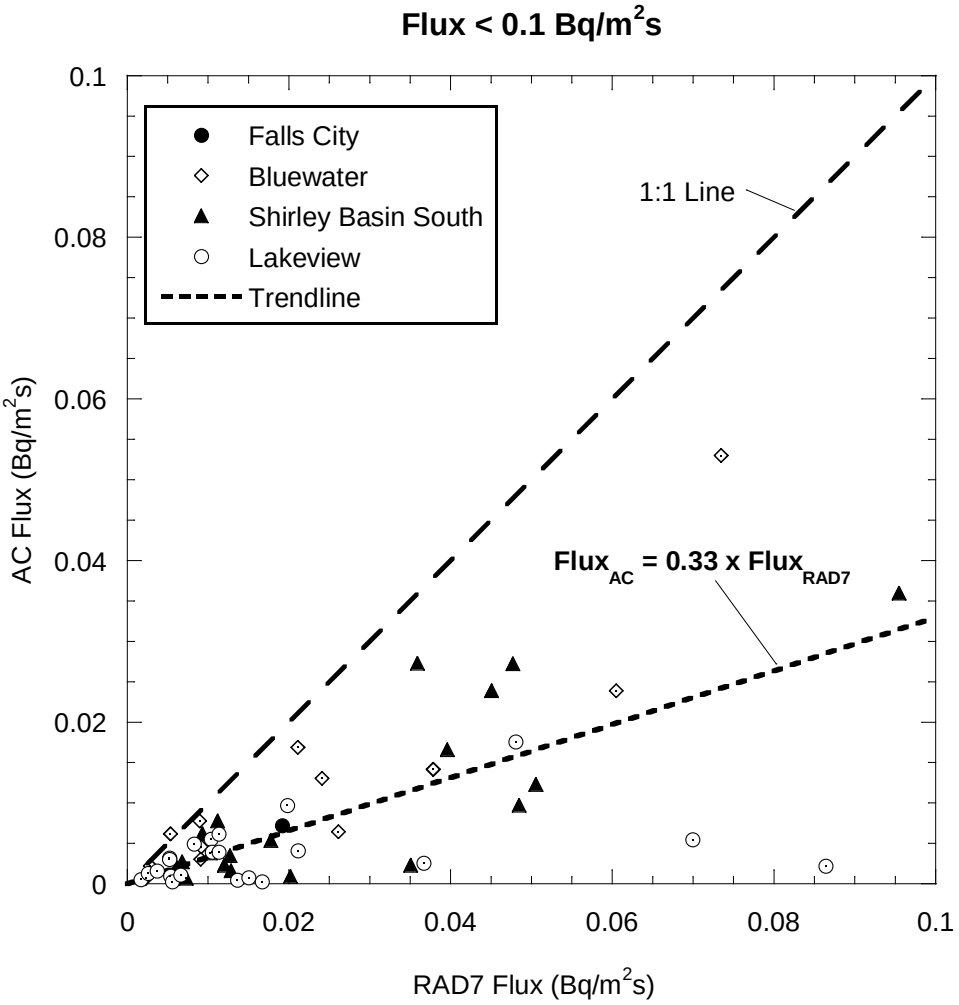

Figure 5.3.8 - Comparison of the AC and RAD7 methods in determining Rn flux (Rn fluxes below 1 Bq/m^{2}s). n = 54, R^2 = 0.39

The slope of the line fit to all of the field data points in **Figure 5.3.6** indicates that the flux determined from the AC method is typically 33% of that determined using the RAD7 method, however, this slope is heavily influenced by extreme values, both large and small. Similar ratios between the two methods are shown in **Figures 5.3.7 and 5.3.8** where the slopes of the lines are 0.40 and 0.33, respectively. In all cases, a significant amount of scatter exists within the dataset (R-squared values of 0.75, 0.54 and 0.39 in Figures 6, 7 and 8, respectively). The reason for this scatter is likely because the Rn concentration buildup with time in an accumulation chamber is nonlinear and the single point AC method assumes a linear buildup. Two variables are believed to affect the accuracy of flux calculations using single concentration points in accumulation chambers with non-linear concentration buildups: chamber volume and AC exposure time.

As previously discussed, Rn concentration in a closed chamber placed over a Rn emanating surface will initially increase in a linear fashion, as the effects of back diffusion, diminishing gradient, and decay will be minimal. However, as time progresses, the Rn concentration within the chamber will build at a decreasing rate and will eventually level off completely. This leveling off typically occurs more quickly in chambers of small volumes. Therefore, the Rn concentration within a flux chamber will remain within or close to the linear portion of the buildup curve longer in larger chambers as it takes longer for a maximum equilibrium to be reached.

Even if the assumption that the AC concentration is in equilibrium with the Rn in the chamber at all times is true, this still indicates that using a single point concentration value to determine flux may severely underestimate the maximum Rn flux, depending on the chamber size and exposure time used. For example, if the flux test is stopped within the linear portion of the buildup curve (typical in larger chamber volumes), the assumption that Rn concentration build linearly is likely true, as the Rn has increased at a constant rate to that point and this slope will be very close to the maximum slope. However, if the test is stopped at a much later time, it is likely

that the concentration within the chamber will have reached a maximum, steady value (typical of smaller chambers). The slope of the Rn buildup to that single concentration point will be less than the maximum slope of Rn buildup in the initial concentration buildup portion of the curve. **Figure 5.3.9**, below, depicts this phenomenon under idealized conditions.

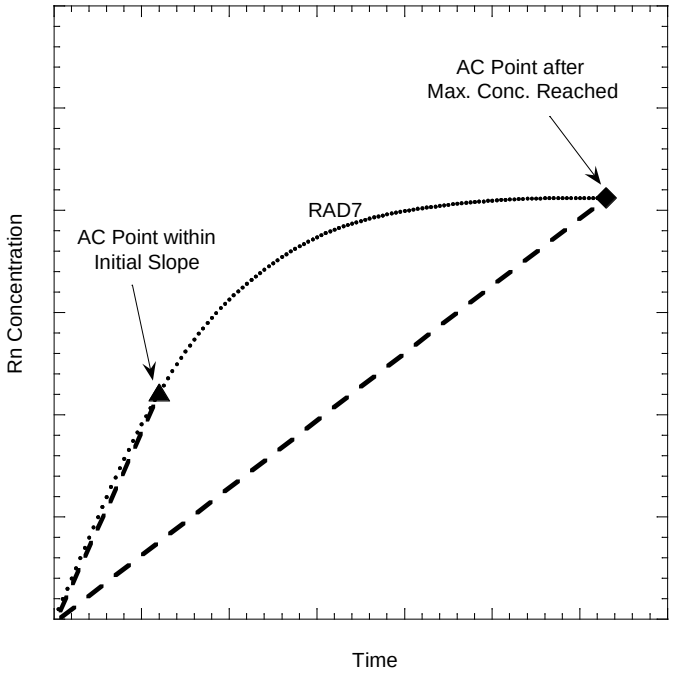

Figure 5.3.9 – An idealized depiction of Rn concentration buildup within a flux chamber.

A similar trend was also observed in many of the fluxes measured in the field. **Figures 5.3.10a – 5.3.10c** show side-by-side comparisons of Rn buildup curves determined with RAD7 monitors in addition to the AC measurements for flux measurements from three chamber sizes taken at the same test pit. As previously discussed, a comparison of the three buildup curves indicates that a maximum, steady state concentration is reached within the small chamber much sooner than the medium and large sized chambers. This results in a slope value significantly

smaller than the initial slope in the small chamber. As the chamber size gets larger, the discrepancy between the two slopes diminishes significantly and the methods agree more closely in flux determination.

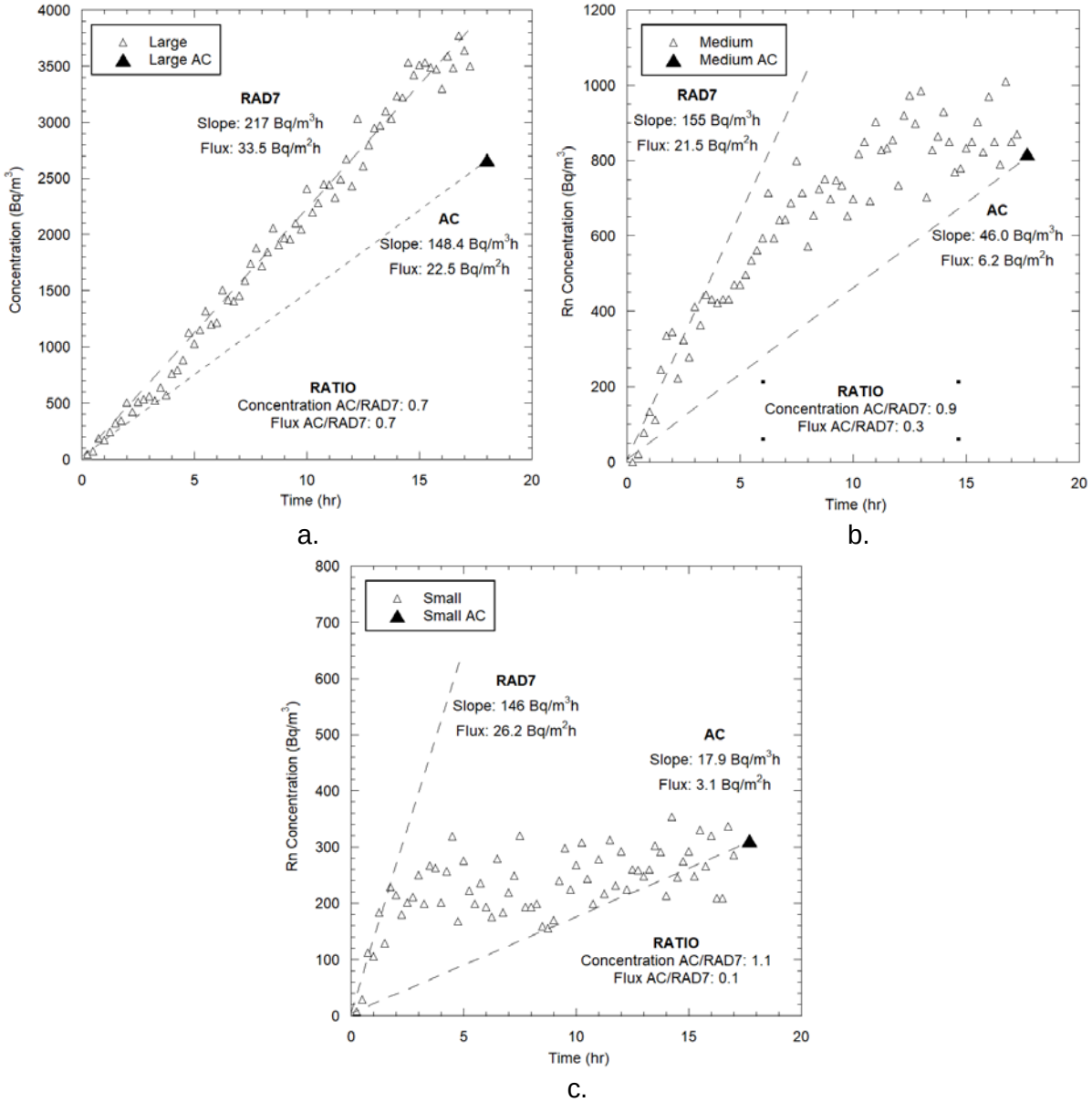

Figure 5.3.10 a - 5.3.10c – Rn buildup curves measured using the RAD7 plotted with the corresponding AC value for three chamber sizes obtained from DC-3 at Shirley Basin South, WY in 2017.

This trend was investigated further by separating both chamber size and exposure time and comparing the flux determined using the two methods. In addition to separating the datasets by chamber size, the exposure times were separated into two groups. “Short” exposure times were described as 3.5 – 8.4 hours (AVG = 4.4) while “long” exposure time was considered to be between 14.5 and 22.3 hours (AVG = 17.6). **Figures 5.3.11 – 5.3.13** show fluxes calculated with RAD7 on the x-axis versus AC on the y-axis for each condition. As done previously, a linear regression was performed on each dataset to develop a linear relationship between the two methods. A summary of the slope, R-squared values, and number of tandem measurements can be found in **Table 5.3.1**, below.

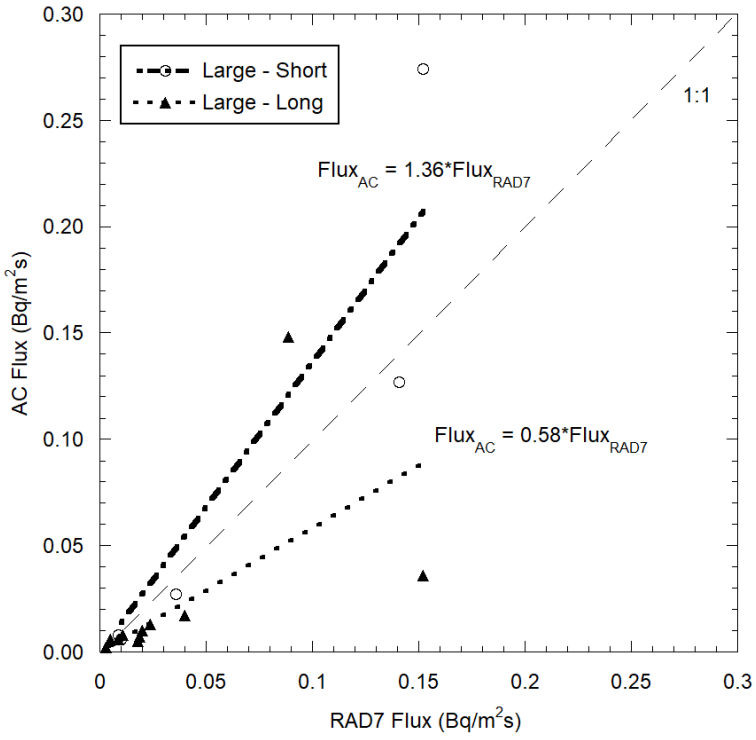

Figure 5.3.11 – Comparison of the two methods in determining flux in Large chambers.

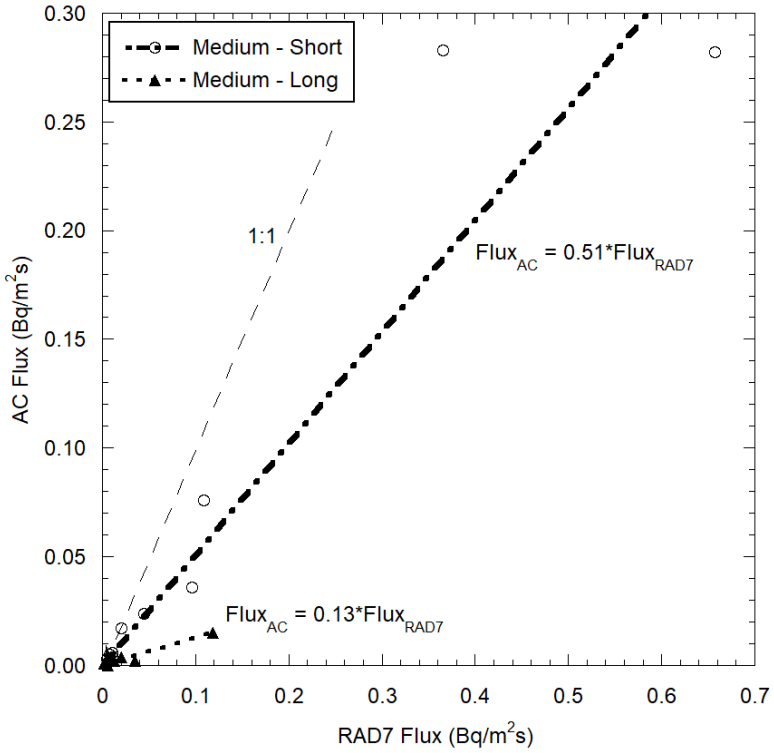

Figure 5.3.12 - Comparison of the two methods in determining flux in Medium chambers.

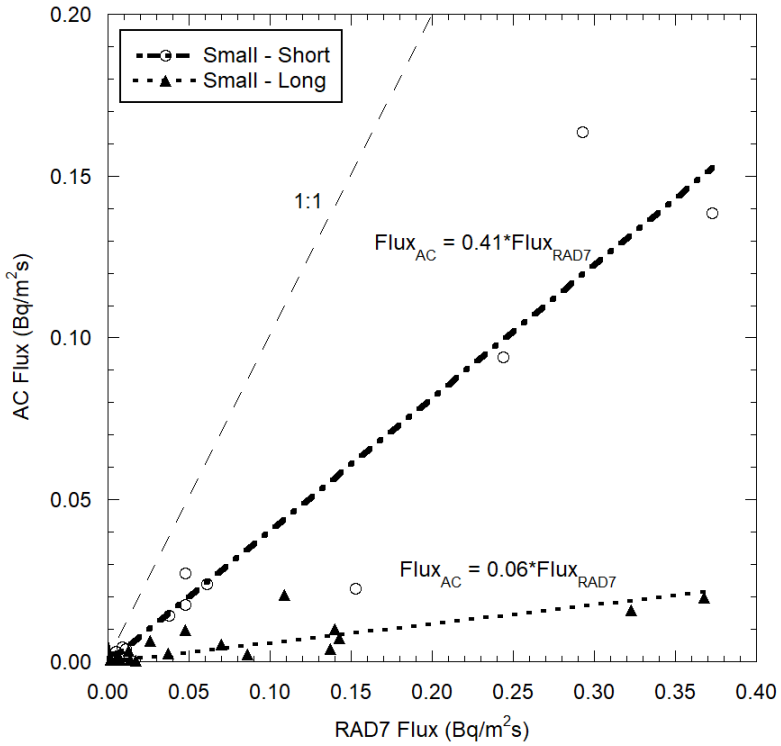

Figure 5.3.13 - Comparison of the two methods in determining flux in Small chambers.

Table 5.3.1 – Summary of linear regression values for comparison of AC and RAD7 methods in flux determination (see Figures 5.3.11 – 5.3.13).

Chamber Size	Exposure Time	$Flux_{AC}$ / $Flux_{RAD7}$	R^2	n
Large	Short	1.36	0.83	5
	Long	0.59	0.33	11
Medium	Short	0.51	0.89	10
	Long	0.13	0.89	13
Small	Short	0.41	0.70	11
	Long	0.06	0.55	18

As predicted, two general trends can be observed with the data presented in Table 5.3.5. First, it is apparent that as flux chamber volume is increased, the ratio of fluxes determined using AC versus RAD7 monitors becomes closer to one. Secondly, a general trend can be observed which shows that the two methods are in better agreement when a short exposure time (3.4 – 8.4 hours) is used versus a prolonged exposure time (14.5 – 22.3 hours).

While this new method is inexpensive, requires very little field equipment, and agrees quite well in measurements of Rn concentration, due to the non-linearity of the buildup of Rn within accumulation chambers, this new method is not recommended for Rn flux measurement. The lack of agreement of flux values using the new method compared to an accepted method (RAD7) indicates that the methods used are not the intended purpose of these canisters. Furthermore, the ratio of the fluxes determined from the two methods from tandem tests does not indicate that a conversion factor could confidently be applied to flux values to adjust for underestimated Rn flux.

It should be noted, however, that the two methods for flux determination agreed somewhat well when large flux chambers were used. On average, when short time periods were used, the flux determined using the AC canisters were only about 36% greater than fluxes determined using the RAD7 monitors. Thus, this method may prove to be an inexpensive alternative if only an

estimate of Rn flux is required and field equipment is limited. However, in order to further prove that this can be a reliable alternative, further testing should be performed.

5.4 Effects of Scale on Rn Flux Measurements

The effects of flux chamber area on Rn flux measurements was investigated using the flux measurements acquired at each of the four UMTRCA sites. It was hypothesized that if too small an area is used to measure Rn flux, the measurement may not actually be representative. For example, if the majority of Rn flux emanating through the Rn barrier is through cracks spaced far apart from one another, there is a chance that a small area flux chamber may not be placed on an area that has cracks representative of the larger area. It may be placed directly on the crack or may not incorporate the crack at all. In theory, if the driving factor controlling the property in question (Rn flux in this case) is very small in scale, a small area chamber should suffice and provide the same result as would a chamber with a greater area. The discrepancy exists when the structure within the soil controlling the Rn flux is larger in scale. Figure **5.4.1**, below provides a simple example of how measurements may be affected by flux chamber area at different scale of soil structure.

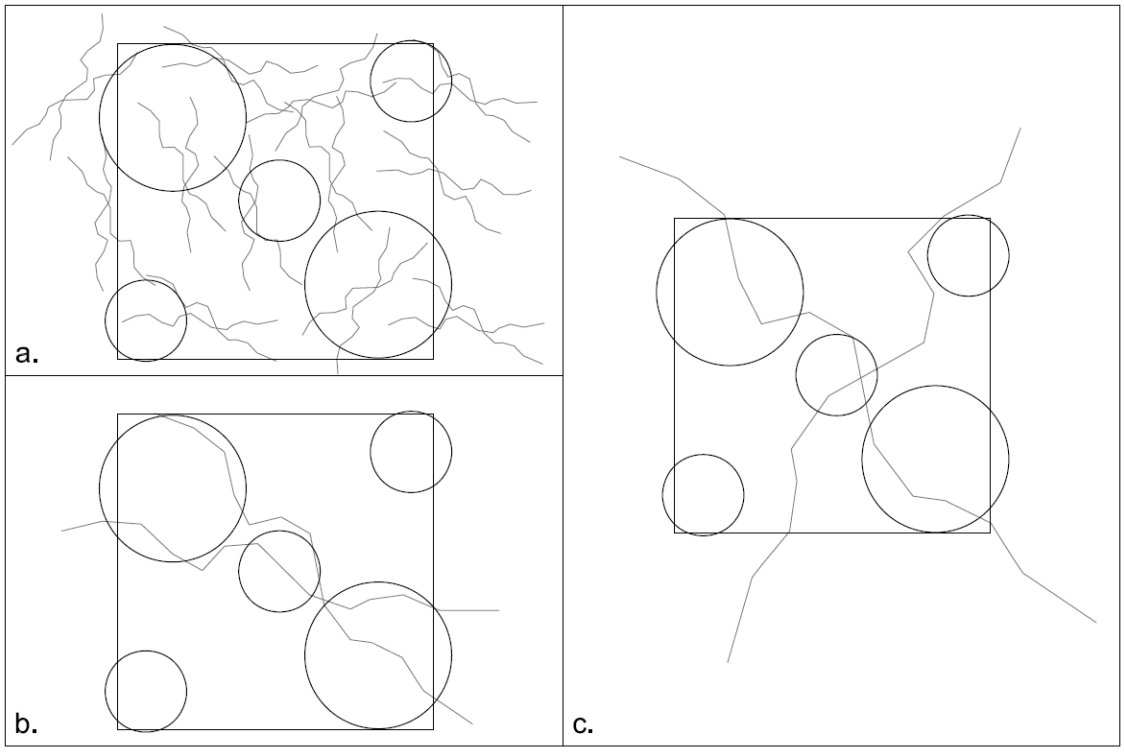

Figure 5.4.1 – Simple example of how scale of soil structure and sampling area may affect measurements. The dark lines represent flux chambers and the light lines represent cracks in the Rn barrier. Crack spacing a < b < c.

A simple analysis of the Rn flux data collected at the four UMTRCA sites was used to investigate whether or not the area of the flux chamber used to measure Rn flux in the field significantly affected measurements. For each test pit, a geometric mean flux value was calculated from the combined measurements from that pit (typically from flux chambers with different areas). Then, each individual flux value was divided by the geometric mean flux of that test pit. If the result was equal to one, then the value was equivalent to the mean. If all flux measurements obtained from a test pit were the same, then the value will be one for each of them. It was hypothesized that this ratio would have significant scatter for extra small chambers and would have less scatter as chamber size is increased. **Figure 5.4.2** and **Table 5.4.1**, below, show this ratio for flux measurements from all four UMTRCA sites.

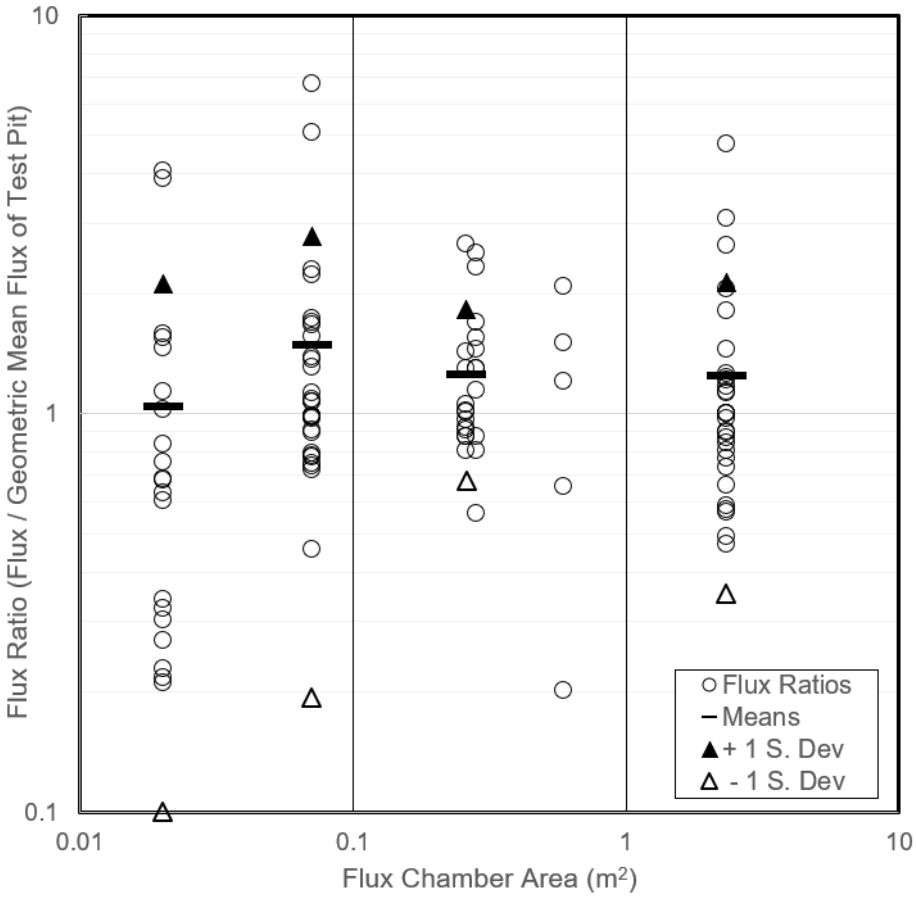

Figure 5.4.2 – Rn fluxes from each chamber, normalized by the geometric mean Rn flux from their respective test pits.

Table 5.4.1 – Summary of flux ratios shown in Figure 5.4.2.

Flux Chamber Designation	Chamber Area (m^2)	Average Flux Ratio	Standard Deviation of Flux Ratio
Extra Small	0.020	1.04	1.07
Small	0.071	1.49	1.29
Medium	0.260	1.25	0.57
Large	2.323	1.24	0.89

While the extra small and small chambers have average flux ratios close to one, there exists significant variability in this observation, as made apparent by the larger standard deviation. The medium chamber area appears to provide flux ratios with the least amount of variability and

a ratio close to one, suggesting that flux chambers with an area of 0.26 m^2 may be large enough to effectively incorporate the scale of the soil structure controlling Rn flux at the four UMTRCA sites visited for this research. The scatter exhibited by the flux ratios produced by the large chambers in this study was not expected and this trend should be investigated further.

It should be noted that flux chambers were placed adjacent to one another in each test pit and were not necessarily taken at the same exact location. Ideally, flux measurements would initially be taken over an area with the smallest chamber size spaced very closely together. This would then be followed by measurements of the same area using the next larger chamber size and so on and so forth. This would provide more confidence that the spatial variation or the soil structure was the main variable in each measurement. For example, the majority of the cracks (or other form of soil structure) in a given test pit may have been completely covered by the large chamber, and the adjacent areas may have been relatively free of structure, or vice versa.

The observations made above may not necessarily be true for all UMTRCA sites or for all conditions. It is possible that sites with very small-scale soil structure, or no soil structure at all may not show any dependence on scale as was observed at these four sites. As-built flux measurements are typically obtained using flux chambers with areas similar to the small chambers used in this study. It is likely that at the time of these measurements, the Rn barrier was relatively free of the macrostructure that is observed after decades of service. Therefore, the use of a small area flux chamber may suffice as the diffusion of Rn through the barrier was likely occurring through the micro-scale pore space of the soil.

6 CONCLUSIONS

Effects of Deep-Rooting Vegetation on Radon Flux

- High Rn fluxes measured from some test pits beneath deep-rooting vegetation relative to control locations that lacked the vegetation suggest the presence of the vegetation is affecting the performance of the Rn barrier at these locations.
    - It is hypothesized that root intrusion, saturation reduction and the associated soil structure formation has caused an increase in Rn flux beneath the vegetation.
- Similar Rn fluxes were measured from some test pits beneath deep-rooting vegetation relative to control test pits that lacked the vegetation.
    - It is hypothesized that soil structure, root intrusion, and changes in saturation at these locations were limited to the near-surface soil and thus did not significantly alter the performance of the Rn barrier.

Effects of Seasonal Ponding on Radon Flux

- Rn fluxes measured from a test pit beneath an ephemeral lake were significantly less than those measured from an adjacent pit without ponding.
    - It is hypothesized that higher saturation levels in the Rn barrier soil beneath the ponding has maintained a lower diffusion coefficient and is the reason for the lower surface flux.

Effects of Animal Burrowing on Radon Flux

- Rn fluxes measured from a test pit beneath an ant mound were significantly greater than those measured from an adjacent control test pit.
    - It is hypothesized that the soil structure created by the ant burrowing has reduced the density and saturation of the Rn barrier soil and is affecting the performance of the barrier at this location.

Effects of Grass Growth in Rip-Rap on Radon Flux

- Similar Rn fluxes were measured from two tests pits excavated beneath bare rip-rap and shallow-rooting grass.
    - It is hypothesized that the root structure did not deeply penetrate the Rn barrier and so any change in soil structure was limited to the near-surface soil.

Radon Fluxes Measured in 2016 / 2017 vs. As-built Radon Fluxes

- Falls City, TX - 2016
    - The geometric mean flux measured in 2016 was approximately four times the magnitude of the as-built geometric mean flux.
- Bluewater, NM - 2016
    - The geometric mean flux measured in 2016 was approximately equal to the magnitude of the as-built geometric mean flux.
- Shirley Basin South, WY - 2017
    - The geometric mean flux measured in 2017 was approximately equal to the magnitude of the as-built geometric mean flux.
- A number of flux measurements from each of the three sites were found to be greater than the largest as-built fluxes from the respective sites. While their exists some bias in the location of our flux measurements, this observation suggests that the Rn attenuating performance of the Rn barrier is changing.

Comparison of Flux Measurement Using Activated Carbon and RAD7

- The two methods are in good agreement for Rn concentration measurement within flux chambers.
- The two methods are not in good agreement when measuring Rn flux.

- The non-linear accumulation of Rn within the flux chambers typically causes the activated carbon method to significantly underestimate Rn flux.
- The multiple, inconsistent factors that contribute to the non-linear buildup of Rn within accumulation chambers suggest that the single point AC method is not a reliable alternative to RAD7 or conventional AC methods.

Effects of Scale on Radon Flux Measurements

- Rn fluxes measured at four sites using four different sizes flux chambers suggest that a chamber with an area of 0.26 m^2 or greater may be most representative of Rn flux in field conditions.
- It is likely that the minimum representative area for Rn flux relies heavily on the scale of the structure controlling Rn flux and thus is likely site/condition dependent.

7 REFERENCES

Albright, W. H., Benson, C. H., Gee, G. W., Abichou, T., Tyler, S. W., & Rock, S. (2006). Field performance of a compacted clay landfill final cover at a humid site. Journal of Geotechnical and Geoenvironmental Engineering, 132 (November), 1393–1403.

ASTM International. (2003). standard test methods for determination of the soil water characteristic curve for desorption using a hanging column, pressure extractor , chilled mirror hygrometer , and / or centrifuge. ASTM D6836-16. West Conshohocken, PA

ASTM International. (2005). Standard Test Methods for Liquid Limit, Plastic Limit, and Plasticity Index of Soils. ASTM D4318, ASTM D 4318-10, & D4318-05. West Conshohocken, PA

ASTM International. (2007). Standard Test Method for Particle-Size Analysis of Soils. ASTM D 422. West Conshohocken, PA

ASTM International. (2008). Standard Practice for Thin-Walled Tube Sampling of Soils for Geotechnical Purposes. ASTM D1587-8. West Conshohocken, PA

ASTM International. (2010). Standard Test Methods for Laboratory Determination of Water (Moisture) Content of Soil and Rock by Mass. ASTM D2216-10. West Conshohocken, PA

ASTM International. (2014). Standard Test Methods for Specific Gravity of Soil Solids by Water Pycnometer. ASTM D854-14. West Conshohocken, PA.

ASTM International. (2015). Standard Practices for Obtaining Undisturbed Block (Cubical and Cylindrical) Samples of Soils. ASTM D7015-13. West Conshohocken, PA

ASTM International. (2017). Standard Test Methods for Measurement of Hydraulic Conductivity of Saturated Porous Materials Using a Flexible Wall Permeameter. ASTM D5084-16a. West Conshohocken, PA.

Benson, C. H., Abichou, T., Olson, M. A., & Bosscher, P. J. (1995). winter effects on hydraulic conductivity of compacted clay. Journal of Geotechnical Engineering, 121(1), 69–79.

Benson, C. H., Albright, W. H., Fratta, D. O., Tinjum, J. M., Kucukkirca, E., Lee, S. H., Scalia, J., Schlicht, P. D., & Wang, X. (2011). Engineered Covers for Waste Containment: Changes in Engineering Properties and Implications for Long-Term Performance Assessment. Office of Nuclear Regulatory Research.

Benson, C. H., Sawangsuriya, A., Trzebiatowski, B., & Albright, W. H. (2007). Postconstruction changes in the hydraulic properties of water balance cover soils. Journal of Geotechnical and Geoenvironmental Engineering, 133(4), 349–359.

Canoba, A. C., López, F. O., & Oliveira, A. A. (1999). Radon determination by activated charcoal adsorption and liquid scintillation measurement. Journal of Radioanalytical and Nuclear Chemistry, 240(1), 237–241.

Chan, D. W. T., & Burnett, J. (1997). Determination of Radon Emanation and Back Diffusion Characteristics of Building Materials in Small Chamber Tests, 32(4), 355–362.

Countess, R, J. (1976). Rn Flux Measurement with a Charcoal Canister. Health Physics. 31, 455.

DOE, United States. (1999). Plant Encroachment on the Burrell , Pennsylvania, Disposal Cell : Evaluation of Long-Term Performance and Risk.

DOE, United States. (2013). Uranium Mill Tailings Radiation Control Act Sites Fact Sheet.

Durridge. (2018). RAD7 Electronic Radon Detector User Manual.

EPA, United States. (1993). Protocols for Radon and Radon Decay Product Measurements in Homes. EPA 402-R-92-003.

Hartley, J. N. & Freeman, H. D. (1985) Radon Flux Measurements on Gardinier and Royster Phosphogypsum Piles Near Tampa and Mulberry, Florida. Prepared for US EPA. DE-ACO6-76RLO 1830.

Hinton, T. G., & Whicker, F. W. (1985). A field experiment on rn flux from reclaimed uranium mill tailings. Health Physics, 48(4), 421–427.

International Atomic Energy Agency. (2004). The long term stabilization of uranium mill tailings.

International Atomic Energy Agency. (2013). Measurement and Calculation of Radon Releases from Uranium Mill Tailings.

Jiránek, M. & Hulka, J. (2000). Radon Diffusion Coefficient in Radon-Proof Membranes - Determination and Applicability for the Design of Radon Barriers. International Journal on Architectural Science. 1(4), 149-155.

Kim, W., & Daniel, D. E. (1992). Effects of Freezing on Hydraulic Conductivity of Compacted Clay. Journal of Geotechnical Engineering, 118(7), 1083–1097.

Paschalides, J. S., Marinakis, G. S., & Petropoulos, N. P. (2010). Passive, integrated measurement of radon using 5A synthetic zeolite and blue silica gel. Applied Radiation and Isotopes, 68(1), 155–163.

Rogers, V. C. & Nielson, K. K. (1991). Multiphase Radon Generation and Transport in Porous Materials. Health Physics, 60(6), 807-815.

Rogers, V. C., Overmyer, R. F., Putzig, K. M., Jensen, C. M., Nielson, K. K., & Sermon, B. W.(1980). Characterization of Uranium Tailings Cover Materials for Radon Flux Reduction. NUREG/CR-1081. FBDU-218-2

Shefsky, S. I., Rose, D., & Parsons, C. G. (1993). A Study of Radon adsorption on Activated Carbon as a Function of Temperature. The 1993 International Radon Conference, 12–18.

Stefani, N. (2016). Field and Laboratory Measurement of Radon Flux and Diffusion for Uranium Mill Tailings Cover Systems. (Master of Science) University of Wisconsin-Madison

Waugh, J., Smith, G., Danforth, B., Gee, G., Kothari, V., & Pauling, T. (2006) Performance Evaluation of the engineered cover at the Lakeview, Oregon, Uranium Mill Tailings Site. WM'07 Conference, February 25 - March 1, 2006, Tucson, AZ.

Waugh, W. J. (). Design, Performance, and Sustainability of Engineered Covers for Uranium Mill Tailings. DOE Office of Legacy Management.

Waugh, W. J., Kastens, M. K., Sheader, L. R. L., Benson, C. H., Albright, W. H., Mushovic, P. S. (2008). Monitoring the performance of an alternative landfill cover at the monticello, utah, uranium mill tailings disposal site. WM 2008 Conference, Phoenix, AZ.

APPENDIX I - Radon Fluxes Measured from a Compacted Clay Barrier at the Falls City, TX Uranium Mill Tailings Disposal Site in 2016

ABSTRACT

Radon (Rn) fluxes were measured from the surface of a uranium mill tailings disposal site after 22 years of service. The tailings were contained by a compacted clay Rn barrier of varying thickness as well as protective layers consisting of a growth medium layer and vegetated topsoil or riprap for erosion control. Flux measurements were made with four different-sized flux chambers: extra small (area = 0.018 m^2, volume = 0.002 m^3), small (0.071 m^2, 0.011 m^3), medium (0.59 m^2, 0.204 m^3), and large (2.32 m^2, 0.352 m^3). Rn concentrations were measured concurrently using activated carbon (AC) canisters and continuously monitoring electronic RAD7 detectors with accumulation chambers. Flux measurements were made at the surface of the Rn barrier and from the surface of the underlying tailings at six locations on the disposal cell. Rn fluxes measured at the surface of the Rn barrier were consistently lower than fluxes measured at the surface of the tailings, indicating that significant Rn attenuation was occurring within the barrier. The geometric mean of all flux values measured from the Rn barrier surface were lower than the regulatory maximum of 0.74 Bq/m^2-s. Comparison of measurements from different-sized flux chambers indicated that no scale-dependent flux measurements were evident. The average of all Rn flux measurements obtained in 2016 was 0.227 Bq/m^2s compared with the 1996 average of 0.660 Bq/m^2s, taken immediately after construction of the barrier. Average in-situ water content measurements of the Rn Barrier material were found to have increased slightly from as-built values and were at high levels of saturation (S_{AVG} > 91%) in 2016. Saturated hydraulic conductivity testing on 350 mm diameter block samples obtained from the Rn barrier has been performed on seven blocks and is currently planned for seven additional blocks.

1 FIELD SITE

The Falls City disposal facility is located approximately 40 miles southeast of San Antonio, in the vicinity of the original Uranium processing mill site. The mill processed uranium ore using sulfuric acid leach methods from 1961 to 1973. Decommissioning of the site initially began in 1978 to 1982 and was resumed and completed from 1992 to 1994. The disposal cell was fully encapsulated by 1994 (U.S. Department of Energy, Legacy Management, 2017).

The disposal facility (**Figures 1 and 2**) consists of a disposal cell with an upper deck with a sloped perimeter. The disposal cell has an area of approximately 5.1×10^5 m^2 and contains approximately 6.44 Tg of dry tailings with an estimated 47.2 TBq of radium-226 activity. Schematic cover profiles for the disposal cell are shown in **Figure 3** (MK-Ferguson Company, 1996). The upper deck of the disposal cell was designed to consist of (bottom to top) a compacted clay Rn barrier (0.91 m), a compacted growth medium layer (0.76 m), followed by a topsoil layer (0.15 m) for erosion control. The 5:1 perimeter slopes were designed to consist of a compacted clay Rn barrier (0.61 m), a compacted bedding layer (0.15 m) and a riprap layer (0.41 m) to allow for drainage and to protect from erosion (MK-Ferguson Company, 1996). The upper deck of the disposal cell was planted with grasses and still contained grass in 2016 (**Figure 4**).

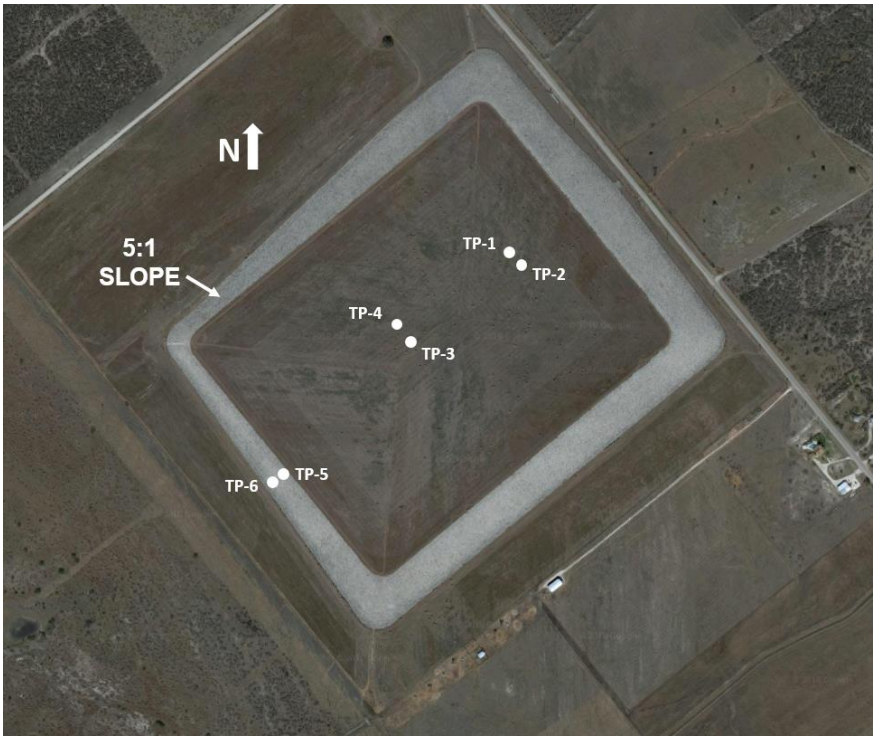

Figure 1 – Satellite image of the Falls City, TX disposal site (Google Earth).

Figure 2 – Granite monument at the Falls City, TX disposal cell.

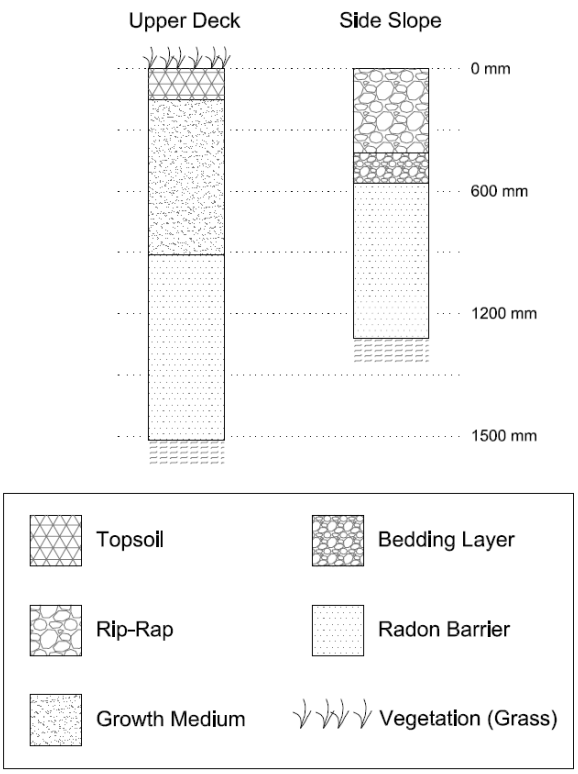

Figure 3 – Falls City, TX “as-designed” cover profiles.

Figure 4 – Grass on the upper deck of the disposal cell.

Figure 5 – Riprap on 5:1 slope.

2 RESULTS

Results from Rn fluxes measured at six test pits are summarized below. Approximate locations of the test pits are shown in **Figure 1**. After Rn flux measurements were made at the top surface of the Rn barrier, an excavation was made through the Rn barrier to expose the underlying uranium mill tailings so that a flux measurement could be taken directly from the tailings.

The locations of the test pits were chosen to be in the vicinity of areas that included surface features that were believed to influence the performance of the Rn barrier. Additionally, “control” test pits that lacked the surface feature were chosen in the vicinity of each test pit.

2.1 Radon Flux Measurements

The methods for the determination of Rn flux from AC and RAD7 were the same methods described in sections 4.1.1 and 4.1.2, respectively. Rn buildup curves from the surface of the Rn barrier and from the surface of the tailings from each test pit are shown in **Appendix I**. It should be noted that the rate of Rn concentration buildup from the flux tests taken directly from the surface of the tailings is much greater than the rate of buildup from the tests taken on the surface of the Rn. This shows that Rn is decaying significantly within the barrier, as it is intended to do.

Fluxes measured from the six test pits using the RAD7 are summarized in **Figure 6** (below) and **Table A2 in Appendix A**. Fluxes measured from test pits using AC canisters are summarized in **Table A3 in Appendix A**. Test pit descriptions are summarized in **Table 1**.

The compiled results of all flux tests do not indicate that there was an impact of measurement scale on flux at this site. **Figure 7** shows each flux value normalized by the geometric mean flux from that respective test pit. If the flux measurements were scale-dependent, it would be expected that the scatter between the flux ratios presented in **Figure 7** would decrease and cluster near a value of one as chamber area increased (and perhaps reach an “optimum” size), however, this trend was not apparent.

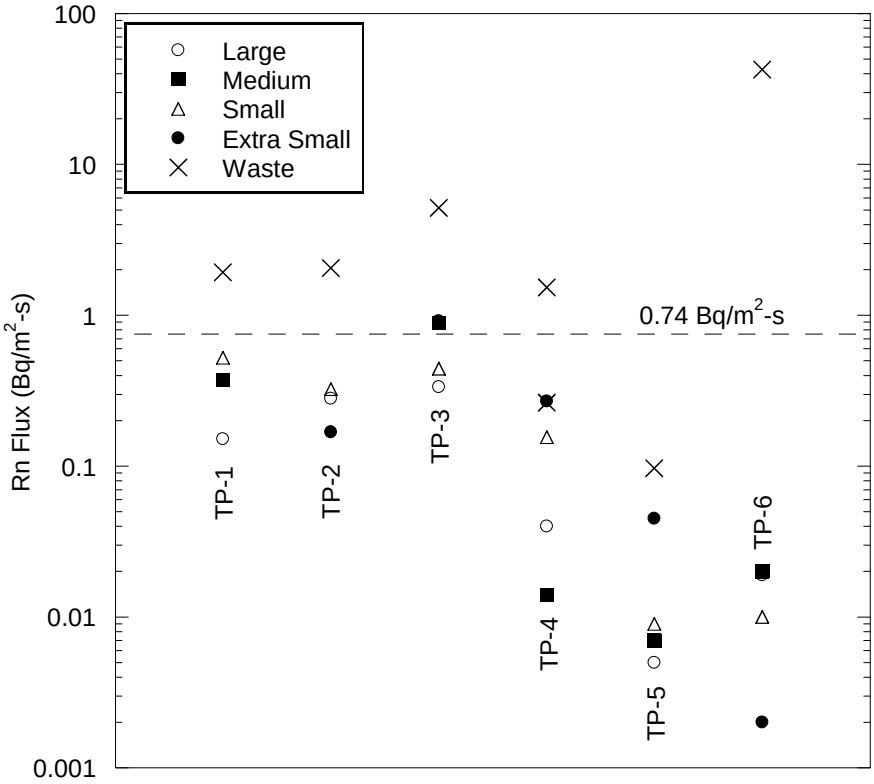

Figure 6 - Summary of fluxes measured with the RAD7 radon detector at the surface of the Rn barrier and the surface of the underlying tailings. DC-X = Disposal Cell X. The dashed horizontal line represents the maximum allowable surface flux specified by UMTRCA (0.74 Bq/m2s).

Table 1 - Test pit descriptions.

Test Pit	Location	Pairing	Surface Feature Description
TP-1	Upper Deck	Pair	Mesquite Tree
TP-2	Upper Deck		Shallow Grass. Control for TP-1
TP-3	Upper Deck	Pair	Mesquite Tree
TP-4	Upper Deck		Shallow Grass. Control for TP-3
TP-5	Side Slope	Pair	Top of 5:1 Rip-Rap Slope
TP-6	Side Slope		Middle of 5:1 Rip-Rap Slope

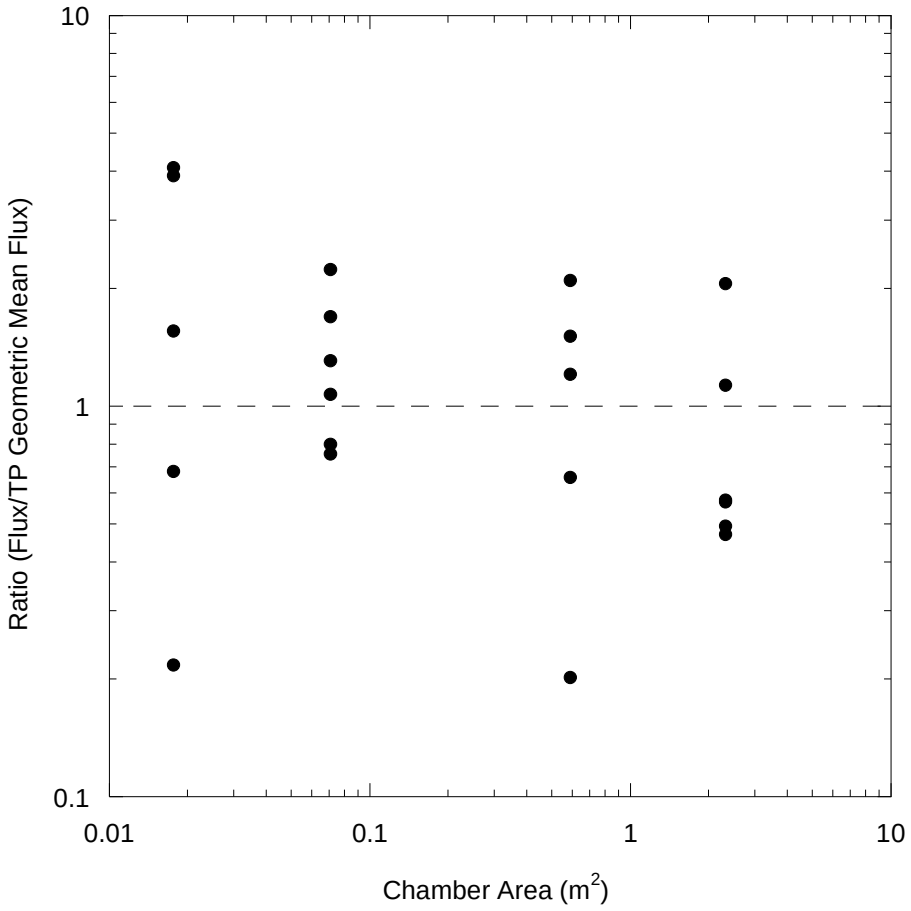

Figure 7 - Fluxes normalized by the geometric mean flux from each test pit.

2.2 Comparison of Fluxes in 2017 to As-Built Fluxes

The Falls City, Texas Final Completion report (MK-Ferguson Company, 1996) reported that upon completion of the Rn Barrier construction at the site, 100 “as-built” surface flux measurements were taken to confirm that the surface flux was below the 0.74 Bq/m^{2}s UMTRCA limit per the guidelines (40 CFR 192.02). These flux measurements were

made using activated charcoal granules placed over a wire mesh within flux chambers that were placed directly on the Rn Barrier and the test durations were approximately 24 hours for each flux test (DOE, 1996). **Table 2** and **Figure 8** below, summarize the flux measurements taken in 1996 and 2016.

Table 2 – Summary of average as-built and 2016 Rn flux measurements from the Falls City, TX disposal site.

	1994 Flux	2016 Flux
Average Flux (Bq/m^2s)	0.018	0.074
Number of Measurements	100	22

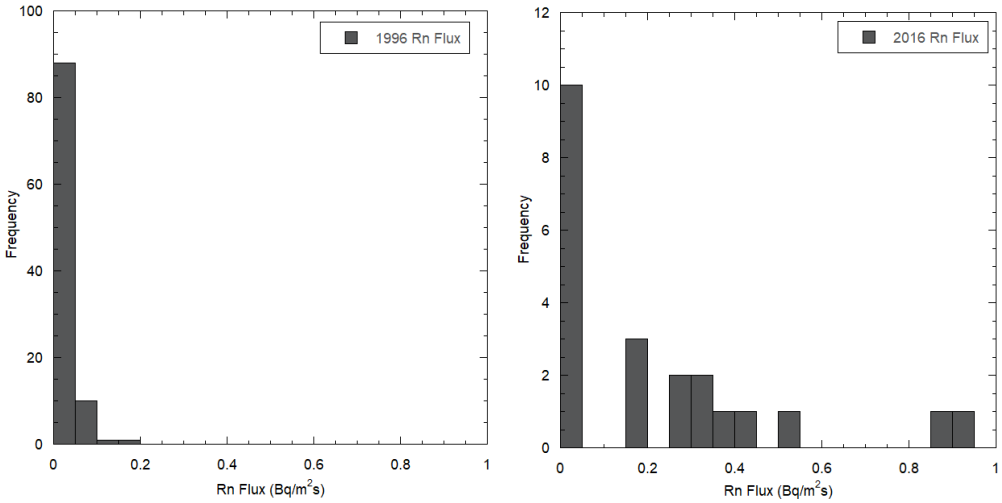

Figure 8 – Histograms showing the frequency of Rn fluxes measured in 1996 (left) and in 2016.

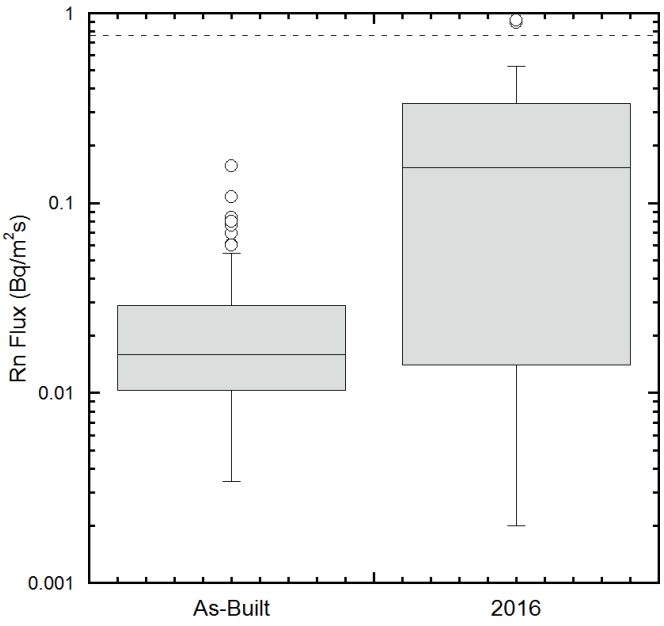

Figure 9 – Box and whisker plot showing the distribution of fluxes measured in 2016 and 1996.

2.3 Water Content Profiles

Thin-walled (Shelby) tube samples (diameter 70 mm) obtained from the Rn Barrier were cut in the lab into sections approximately 40 - 50 mm in length to obtain profiles of water content with depth (see section 4.1.4 laboratory methods). Additionally, the dimensions and masses of each of the sections were measured so that dry unit weight, volumetric water content, and saturation profiles could be created (a compilation of water content, dry density, and saturation profiles can be found in **Appendix F, G, and H**, respectively). The large-scale “block” samples (350 mm diameter) obtained from the site were also used to determine in-situ water content and dry unit weight in the laboratory. The average water content values from both the thin-walled tube samples and large-scale block samples (referred to as “2016 values”) are compared to the in-situ, “as-built” values from the completion report in **Table 3.**

Table 3 – Summary of water content and dry density values for both as-built and 2016 conditions.

	As-Built*		2016	
Parameter	Value	n	Value	n
Gravimetric Water Content	42.2	1377	38.0	82
Dry Density (g/cm^3)	1.18^	-	1.24	34

* Department of Energy, Albuquerque Operation Office, Falls City, Texas Final Completion Report, 1996

* This dry density value was used to calculate the diffusion coefficient and is not an as-built condition.

2.4 Saturated Hydraulic Conductivity

Saturated hydraulic conductivity testing has been performed on seven out of fourteen large-scale undisturbed block samples (350 mm diameter) excavated from the Rn barrier at the Shirley Basin South, WY site (see section 4.1.5 for methods). Testing of the remaining seven blocks is currently ongoing. The results of saturated hydraulic conductivity testing are summarized in **Figure 10** (below) and **Table E3 in Appendix E**.

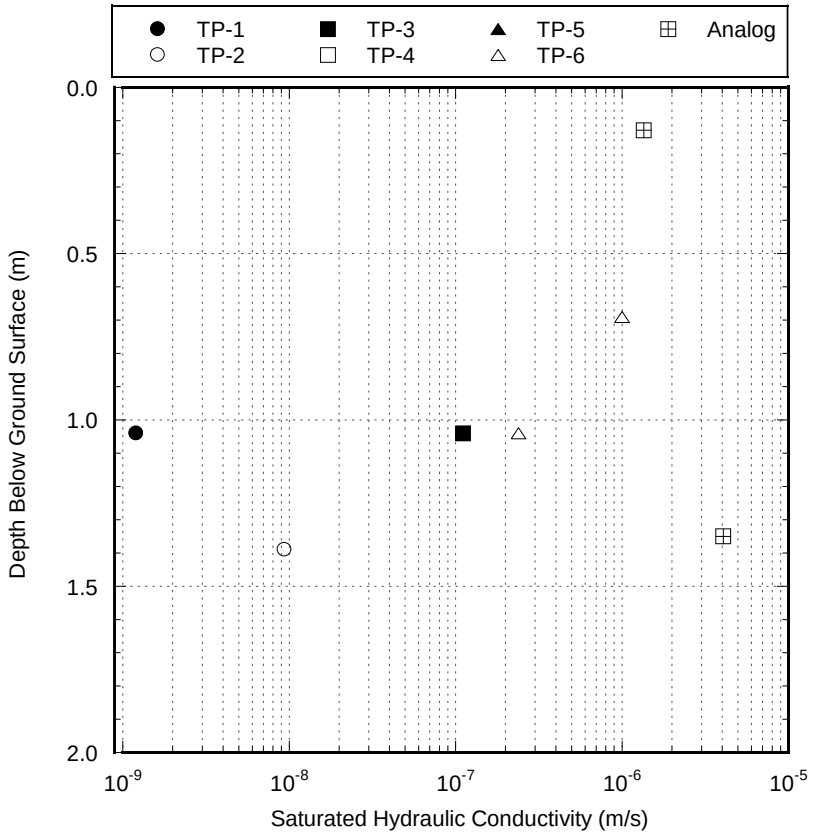

Figure 10 – Summary of saturated hydraulic conductivity measured from 350 mm diameter block samples.

3 SUMMARY

Rn fluxes were measured from six test pits excavated at the uranium mill tailings disposal site in Falls City, TX in 2016. The cover system had been in service for approximately 22 years at the time of the performed field work. Flux measurements were taken from the surface of the Rn barrier to observe if soil structure caused by pedogenesis had caused any changes in Rn flux. Four flux chamber sizes were used to observe if soil structure was causing any scale-dependent Rn flux. Rn concentrations and fluxes were measured with activated carbon (AC) canisters and RAD7 continuous monitors and

accumulation chambers. AC canisters recorded a single concentration point while RAD7 monitors provided continuous concentration measurements.

Rn fluxes measured from the surface of the Rn barrier were significantly lower than the fluxes measured directly from the tailings beneath. This indicates that the Rn barrier is still effective at reducing the Rn flux at the surface, and Rn gas is attenuating significantly within it before reaching the atmosphere. Only one measurement of Rn flux was measured to be above the UMTRCA maximum allowed flux of 0.74 Bq/m^2s. All other flux measurements were below the limit. The overall geometric mean of Rn flux measured from the surface of the Rn barrier was 0.074 Bq/m^2s. This value is significantly greater than the average as-built flux of 0.018 Bq/m^2s measured in 2001. No apparent impacts of measurement scale were observed based on the fluxes measured at this field site.

Water content measurements taken from both thin-walled tube samples and large-scale block samples obtained in the field in 2016 showed that the average water content of the Rn Barrier soil had decreased slightly from as-built measurements.

Testing for the saturated hydraulic conductivity of large-scale block samples obtained in the field is currently ongoing.

REFERENCES

MK-Ferguson Company (1996).Department of Energy Contract No. DE-AC04 83AL18796. Falls City, Texas Final Completion Report. Volumes 1 – 5.

U.S. Department of Energy, Legacy Management (2017). UMTRCA Title II Falls City, Texas, Disposal Site. Fact Sheet.

APPENDIX A – ADDITIONAL TABLES AND FIGURES

Table 4 - Flux chamber areas and volumes.

Chamber Designation	Area [m^2]	Volume [m^3]
Extra Small	0.020	0.002
Small	0.071	0.011
Medium	0.59	0.204
Large	2.323	0.352

Table 5 – Tabulated summary of flux measurements from all test pits using RAD7.

Test Pit	Chamber Size	Flux	Geometric Mean Flux of Test Pit	Tailings Flux (Small Chamber)
		[Bq/m^2s]	[Bq/m^2s]	[Bq/m^2s]
1	Large	0.152	0.309	1.928
	Medium	0.372		
	Small	0.523		
2	Large	0.280	0.248	2.058
	Small	0.323		
	Extra Small	0.169		
3	Large	0.334	0.589	5.151
	Medium	0.888		
	Small	0.443		
	Extra Small	0.915		
4	Large	0.040	0.069	0.264 - 1.536
	Medium	0.014		
	Small	0.155		
	Extra Small	0.270		
5	Large	0.005	0.011	0.097
	Medium	0.007		
	Small	0.009		
	Extra Small	0.045		
6	Large	0.019	0.009	42.479
	Medium	0.020		
	Small	0.010		
	Extra Small	0.002		

Table 6 – Tabulated summary of flux measurements from all test pits using AC.

Test Pit	Chamber Size	Flux	Tailings Flux (Small Chamber)
		[Bq/m^{2}s]	[Bq/m^{2}s]
1	Large	0.036	0.263
	Small	0.004	
2	Large	0.012	0.122
	Small	0.016	
3	Large	0.036	0.282
	Small	0.033	
4	Large	0.013	0.014
	Small	0.023	
5	Large	0.004	0.003
	Small	0.003	
6	Large	0.007	2.216
	Small	0.001	

APPENDIX B – TEST PIT EXCAVATION PHOTOS

Figure 11 – Test pit with rip-rap layer removed to expose Rn barrier.

Figure 12 – Replacement and compaction of Rn barrier material.

APPENDIX C – FLUX MEASUREMENT PHOTOS

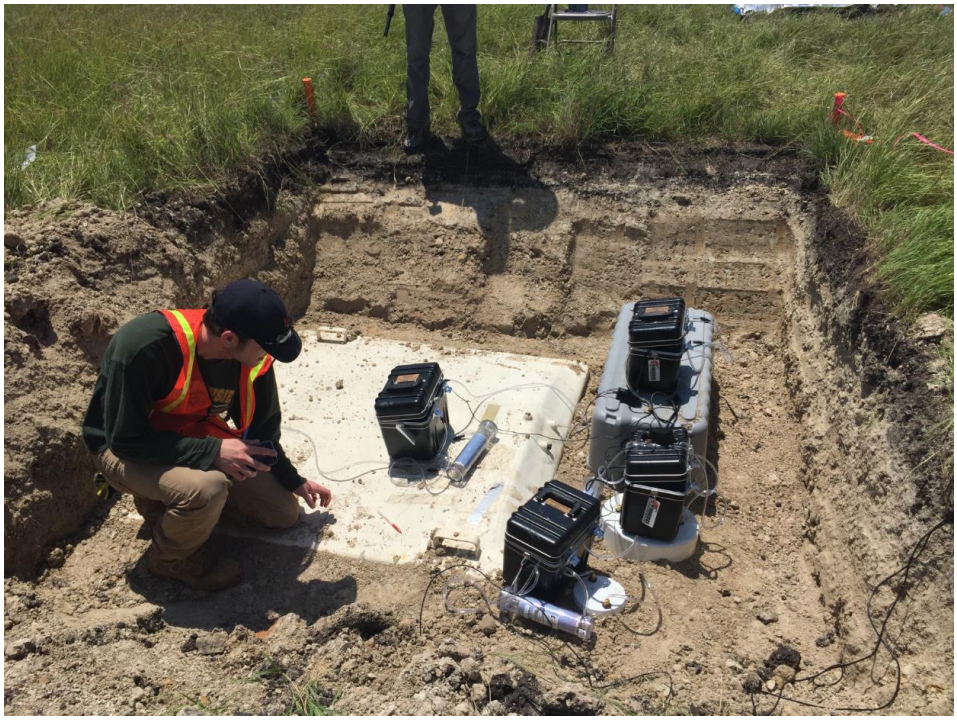

Figure 13 – Installation of flux chambers on the Rn barrier surface.

Figure 14 – Small flux chamber placed directly on tailings.

APPENDIX D – SOIL SAMPLING PHOTOS

Figure 15 – Pushing a thin-walled tube sample through the Rn barrier with an excavator bucket.

Figure 16 – Excavating a 350 mm diameter block sample using a shovel.

Figure 17 – Securing the excavated 350 mm diameter block sample in a protective casing.

APPENDIX E – SUMMARY OF LABORATORY TEST DATA

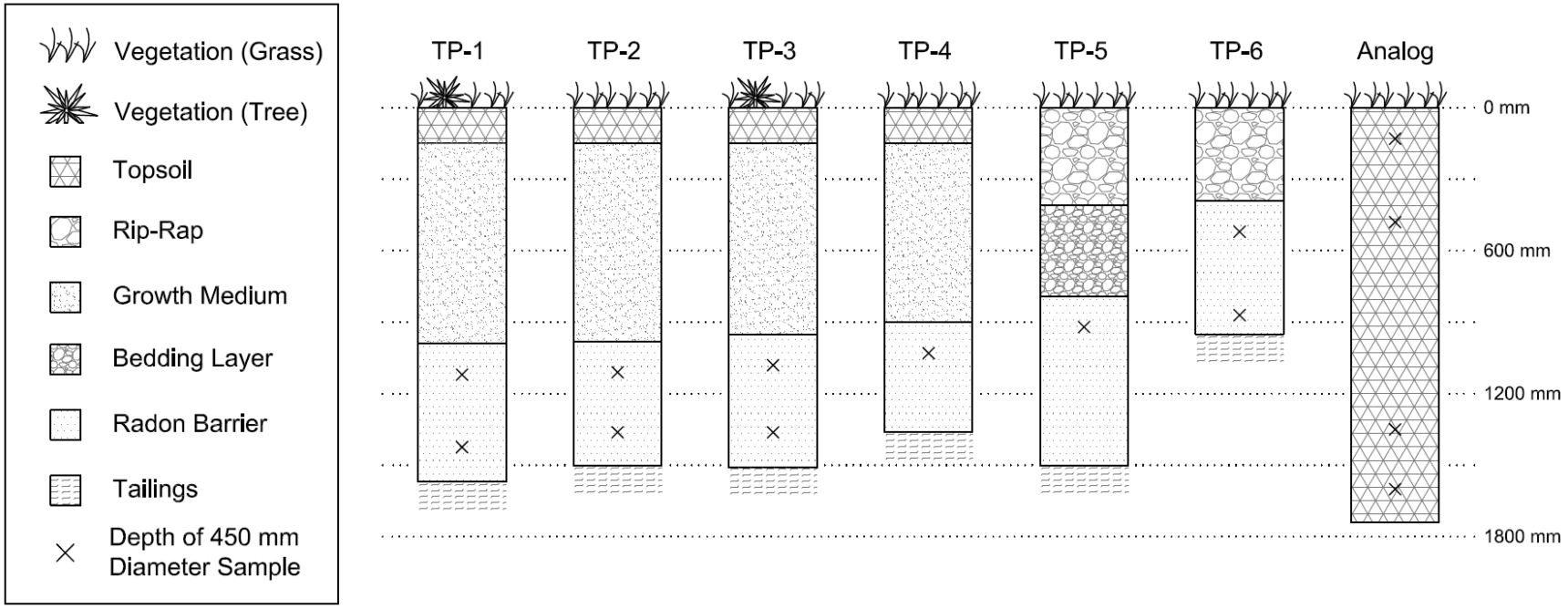

Figure 18 – Cover profiles for test pits excavated at the Falls City, TX site in 2016.

Table 7 – Summary of 350 mm diameter block samples collected at the Falls City, TX site in 2016.

Test Pit	Sample Designation	Depth of Top of Block Sample bgs (m)	Depth of Bottom of Block Sample bgs (m)	AVG Depth	% Gravel	% Sand	% Fines	% Clay	LL	PL	PI	G_s	XRD
1	A	0.99	1.24	1.12	0	9	91	51	-	-	-	-	-
	B	1.35	1.60	1.47									
2	A	0.98	1.23	1.11	0	11	89	48	-	-	-	-	-
	B	1.34	1.59	1.46									
3	A	0.95	1.20	1.08	2	17	81	50	-	-	-	-	-
	B	1.31	1.56	1.43									
4	A	0.90	1.15	1.03	0	20	80	45	-	-	-	-	-
5	A	0.79	1.04	0.92	0	17	82	43	-	-	-	-	-
6	A	0.39	0.64	0.52	0	17	83	42	79	38	41	2.66	-
	B	0.75	1.00	0.87									
Analog	A	0.00	0.25	0.13	0	27	73	51	69	23	46	2.65	-
	B	0.36	0.61	0.48									
	C	1.22	1.47	1.35									
	D	1.47	1.73	1.60									

Table 8 - Summary of 70 mm Diameter (Thin-Wall Tube) Samples Collected at the Falls City, TX site in 2016.

Test Pit	70 mm Diameter (Shelby Tube) Sample ID	Depth of Top of Sample Below Rn Barrier Surface (m)	Depth of Bottom of Sample Below Rn Barrier Surface (m)	Water Content Profile*
1	A	0.00	0.31	x
	B	0.00	0.42	x
2	A	0.00	0.35	x
	B	0.00	0.51	x
3	A	0.00	0.52	x
	B	0.00	0.45	x
4	A	0.00	0.40	x
	B	0.00	-	NM
	C	0.00	0.40	x
5	A	0.00	0.32	x
	B	0.00	0.33	x
	C	0.00	0.33	x
6	A	0.00	0.32	x
	B	0.00	0.33	x
	C	0.00	0.28	x
Analog	No Tubes Collected			

* Water content profiles can be found in Appendix F

NM = Not Measured

Table 9 - Summary of Hydraulic Properties from 350 mm Diameter Block Samples Collected at the Falls City, TX site in 2016.

Test Pit	Sample Designation	Gravimetric Water Content (%) *	γ_d (kN/m^3)	Saturated Hydraulic Conductivity (m/s) †	Soil Water Characteristic Curve §			
					θ_r	θ_s	α	n
1	A	NM	NM	1.21×10^{-9}	-	-	-	-
	B	IP	IP	IP	-	-	-	-
2	A	IP	IP	IP	-	-	-	-
	B	40.5	NM	9.37×10^{-9}	-	-	-	-
3	A	39.4	NM	1.11×10^{-7}	-	-	-	-
	B	NM	NM	IP	-	-	-	-
4	A	IP	IP	IP	-	-	-	-
5	A	NM	NM	IP	-	-	-	-
6	A	44.1	11.82	9.99×10^{-7}	-	-	-	-
	B	39.3	11.40	2.39×10^{-7}	-	-	-	-
Analog	A	IP	IP	IP	-	-	-	-
	B	30.1	14.23	1.35×10^{-6}	-	-	-	-
	C	IP	IP	IP	-	-	-	-
	D	37.9	12.21	4.06×10^{-6}	-	-	-	-

* ASTM D 2216

† ASTM D 5084

§ ASTM D 6836 - 02 (Method A and D)

NM = Not Measured

IP = In Progress

APPENDIX F – GRAVIMETRIC WATER CONTENT PROFILES

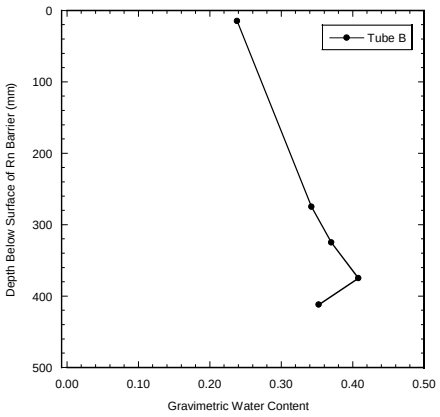

TP-1
Tube B

Depth (mm)	Water Content
15	0.24
275	0.34
325	0.37
375	0.41
412	0.35
Mean	0.34

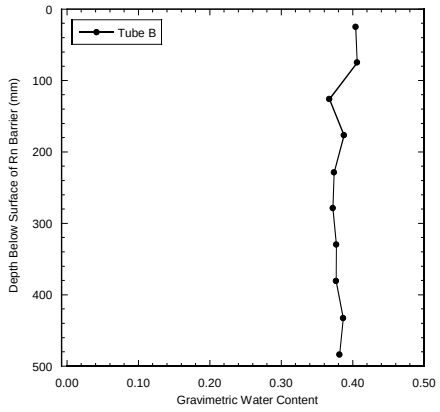

TP-2
Tube B

Depth (mm)	Water Content
25	0.40
75	0.41
126	0.37
177	0.39
229	0.37
279	0.37
330	0.38
381	0.38
433	0.39
484	0.38
Mean	0.38

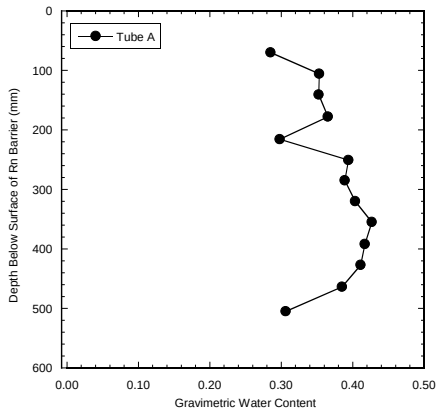

TP-3
Tube A

Depth (mm)	Water Content
70	0.29
106	0.35
141	0.35
178	0.37
216	0.30
251	0.39
285	0.39
320	0.40
355	0.43
392	0.42
427	0.41
464	0.39
505	0.31
Mean	0.37

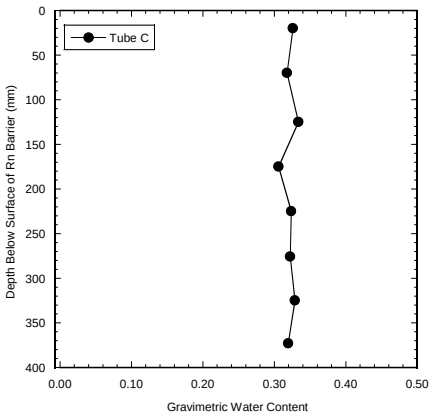

TP-4

Tube C

Depth (mm)	Water Content
20	0.33
70	0.32
125	0.33
175	0.31
225	0.32
276	0.32
325	0.33
373	0.32
Mean	0.32

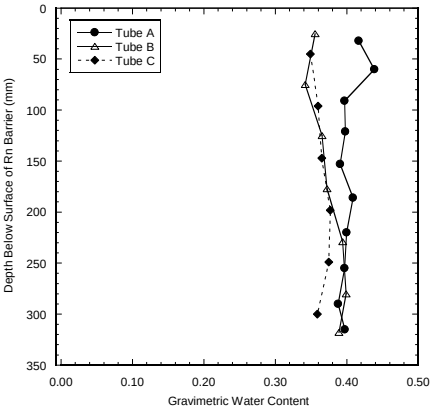

TP-5

Tube A

Depth (mm)	Water Content
32	0.42
60	0.44
91	0.40
121	0.40
153	0.39
186	0.41
220	0.40
255	0.40
290	0.39
315	0.40
Mean	0.4031

Tube B

Depth (mm)	Water Content
25	0.36
75	0.34
125	0.37
177	0.37
229	0.39
280	0.40
318	0.39
Mean	0.37

Tube C

Depth (mm)	Water Content
45	0.35
96	0.36
147	0.36
198	0.38
249	0.37
300	0.36
Mean	0.36

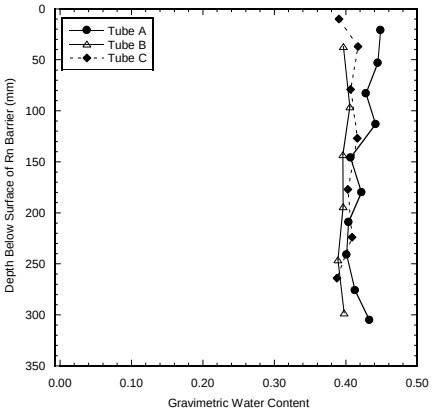

TP-6

Tube A

Depth (mm)	Water Content
21	0.45
53	0.44
83	0.43
113	0.44
146	0.41
180	0.42
209	0.40
241	0.40
276	0.41
305	0.43
Mean	0.42

Tube B

Depth (mm)	Water Content
37	0.40
96	0.41
143	0.40
194	0.40
246	0.39
298	0.40
Mean	0.40

Tube C

Depth (mm)	Water Content
10	0.39
37	0.42
79	0.41
127	0.42
177	0.40
224	0.41
264	0.39
Mean	0.40

APPENDIX G – DRY DENSITY PROFILES

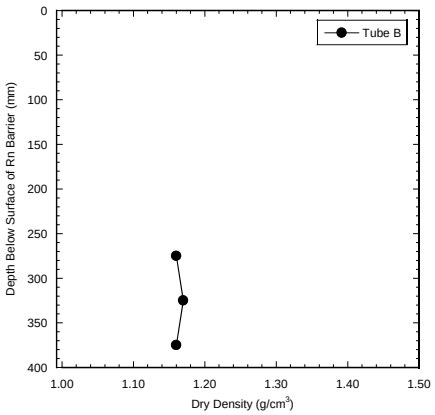

TP-1
Tube B

Depth (mm)	Dry Density (g/cm^3)
275	1.16
325	1.17
375	1.16
Mean	1.16

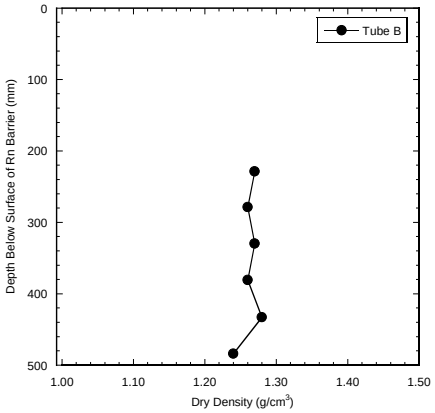

TP-2
Tube B

Depth (mm)	Dry Density (g/cm^3)
229	1.27
279	1.26
330	1.27
381	1.26
433	1.28
484	1.24
Mean	1.26

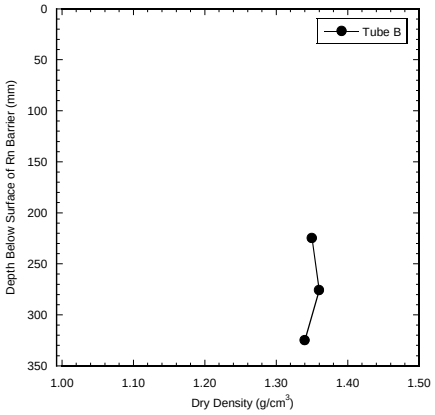

TP-4
Tube B

Depth (mm)	Dry Density (g/cm^3)
225	1.35
276	1.36
325	1.34
Mean	1.35

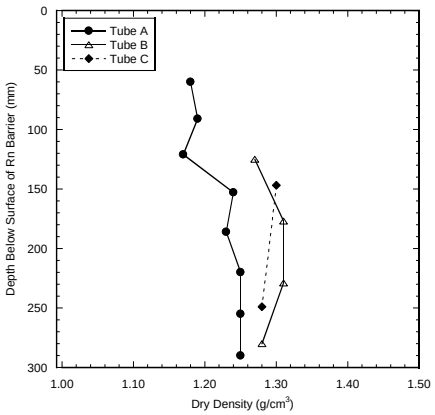

TP-5

Tube A

Depth (mm)	Dry Density (g/cm^3)
60	1.18
91	1.19
121	1.17
153	1.24
186	1.23
220	1.25
255	1.25
290	1.25
Mean	1.22

Tube B

Depth (mm)	Dry Density (g/cm^3)
125	1.27
177	1.31
229	1.31
280	1.28
Mean	1.29

Tube C

Depth (mm)	Dry Density (g/cm^3)
147	1.30
249	1.28
Mean	1.29

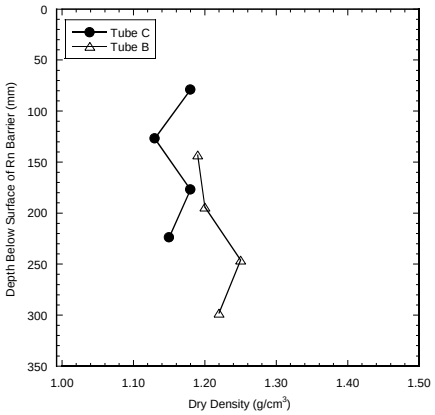

TP-6

Tube B

Depth (mm)	Dry Density (g/cm^3)
143	1.19
194	1.20
246	1.25
298	1.22
Mean	1.21

Tube C

Depth (mm)	Dry Density (g/cm^3)
79	1.18
127	1.13
177	1.18
224	1.15
Mean	1.16

APPENDIX H – SATURATION PROFILES

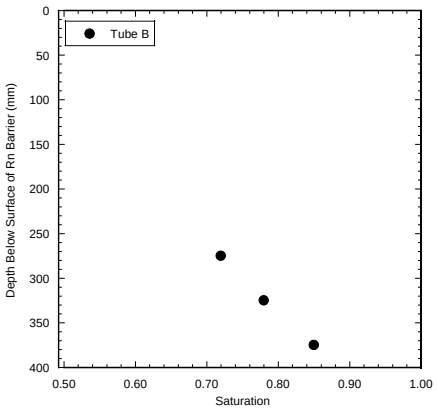

TP-1
Tube B

Depth (mm)	Saturation
275	0.72
325	0.78
375	0.85
Mean	0.79

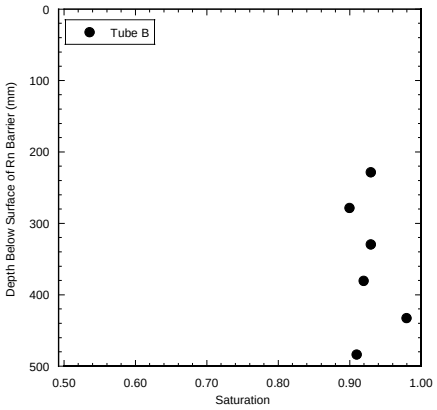

TP-2
Tube B

Depth (mm)	Saturation
229	0.93
279	0.90
330	0.93
381	0.92
433	0.98
484	0.91
Mean	0.93

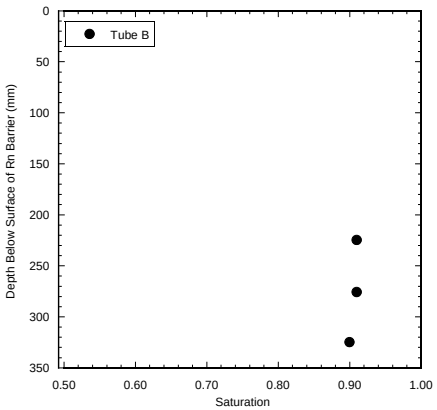

TP-4
Tube B

Depth (mm)	Saturation
225	0.91
276	0.91
325	0.90
Mean	0.91

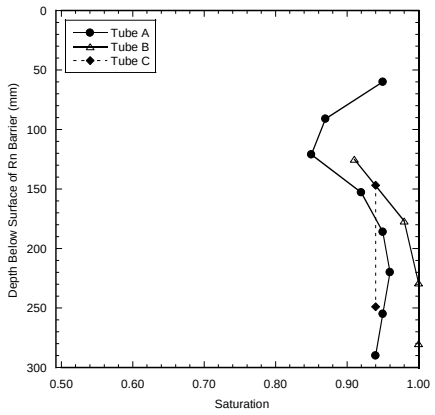

TP-5

Tube A

Depth (mm)	Saturation
60	0.95
91	0.87
121	0.85
153	0.92
186	0.95
220	0.96
255	0.95
290	0.94
Mean	0.92

Tube B

Depth (mm)	Saturation
125	0.91
177	0.98
229	1.03
280	1.00
Mean	0.98

Tube C

Depth (mm)	Saturation
147	0.94
249	0.94
Mean	0.94

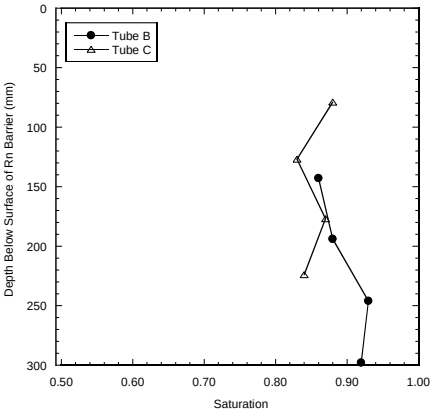

TP-6

Tube B

Depth (mm)	Saturation
143	0.86
194	0.88
246	0.93
298	0.92
Mean	0.90

Tube C

Depth (mm)	Saturation
79	0.88
127	0.83
177	0.87
224	0.84
Mean	0.85

APPENDIX I – RADON CONCENTRATION BUILDUP CURVES

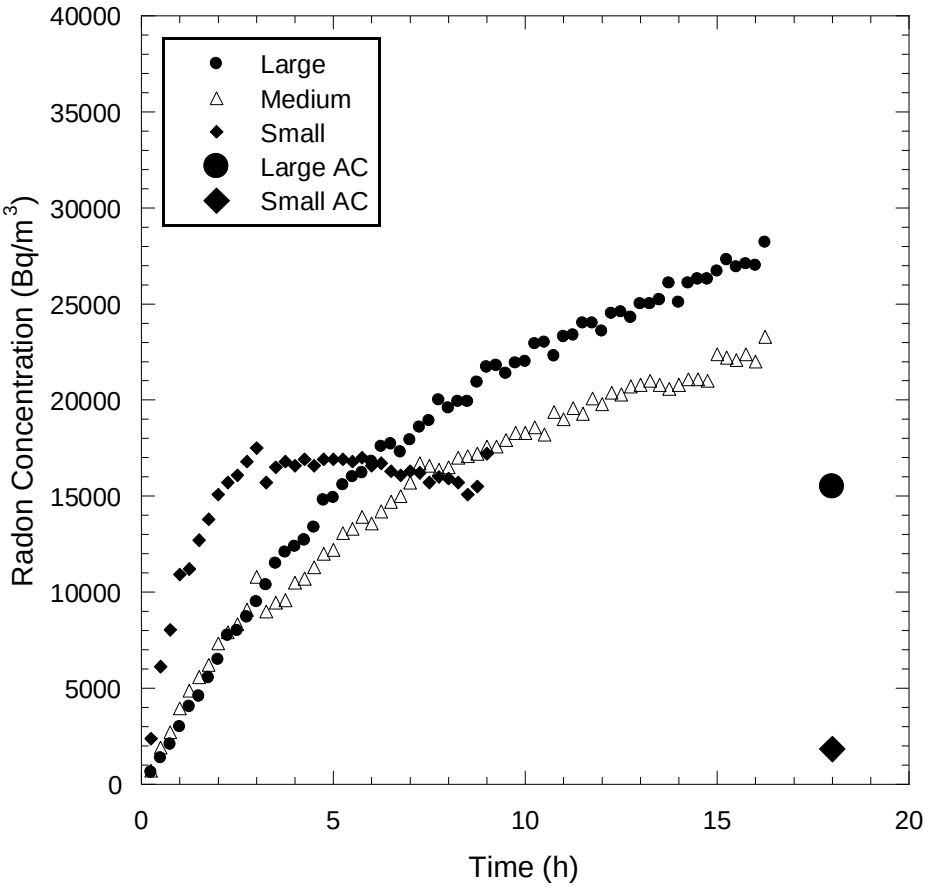

Fig. I19a – Radon concentration buildup curves measured at TP-1 at Falls City, TX.

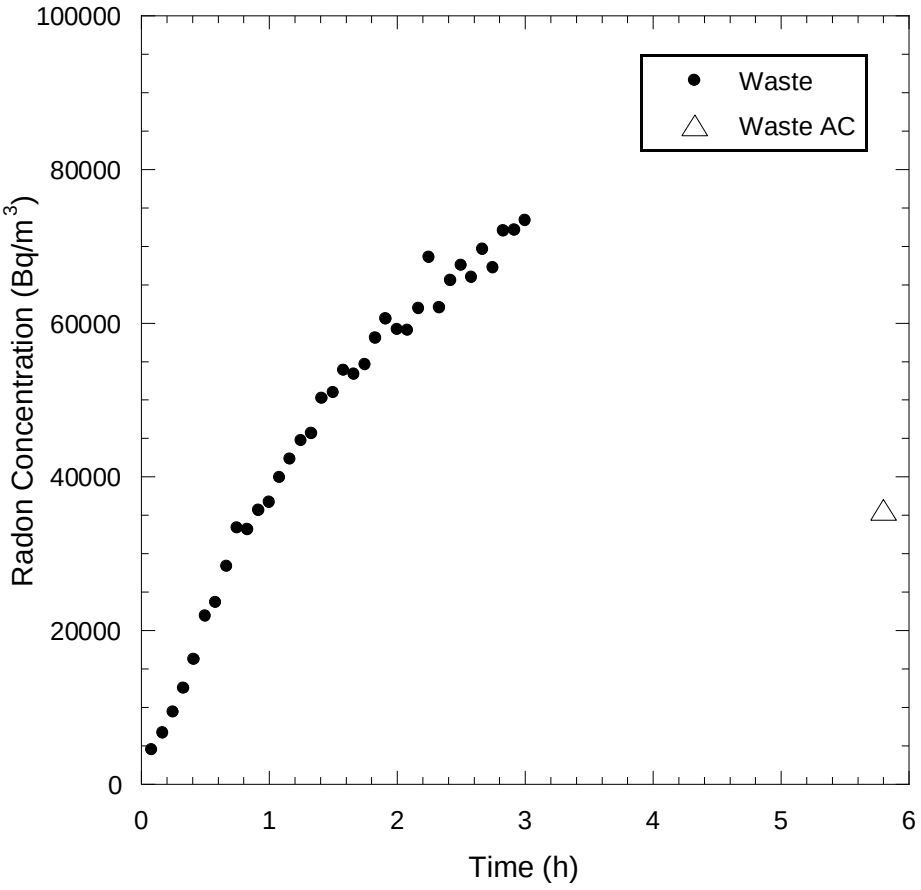

Figure 20 - Radon concentration buildup curves measured from the tailings at TP-1 at Falls City, TX.

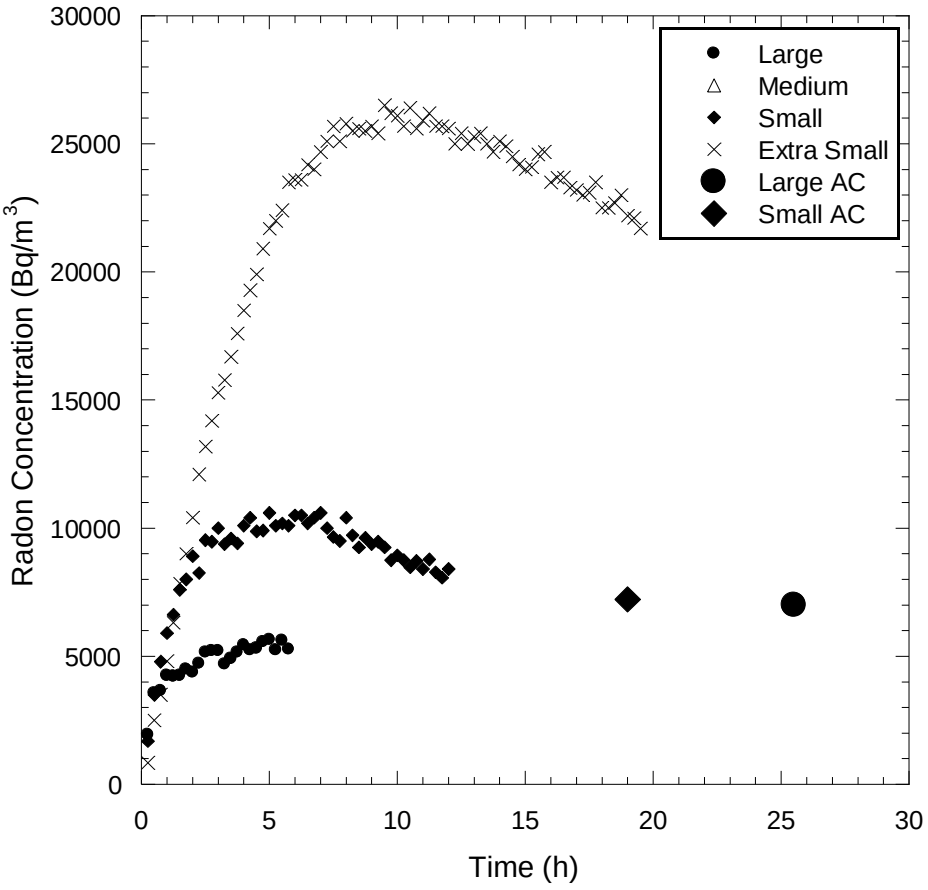

Figure 21 – Radon concentration buildup curves measured at TP-2 at Falls City, TX.

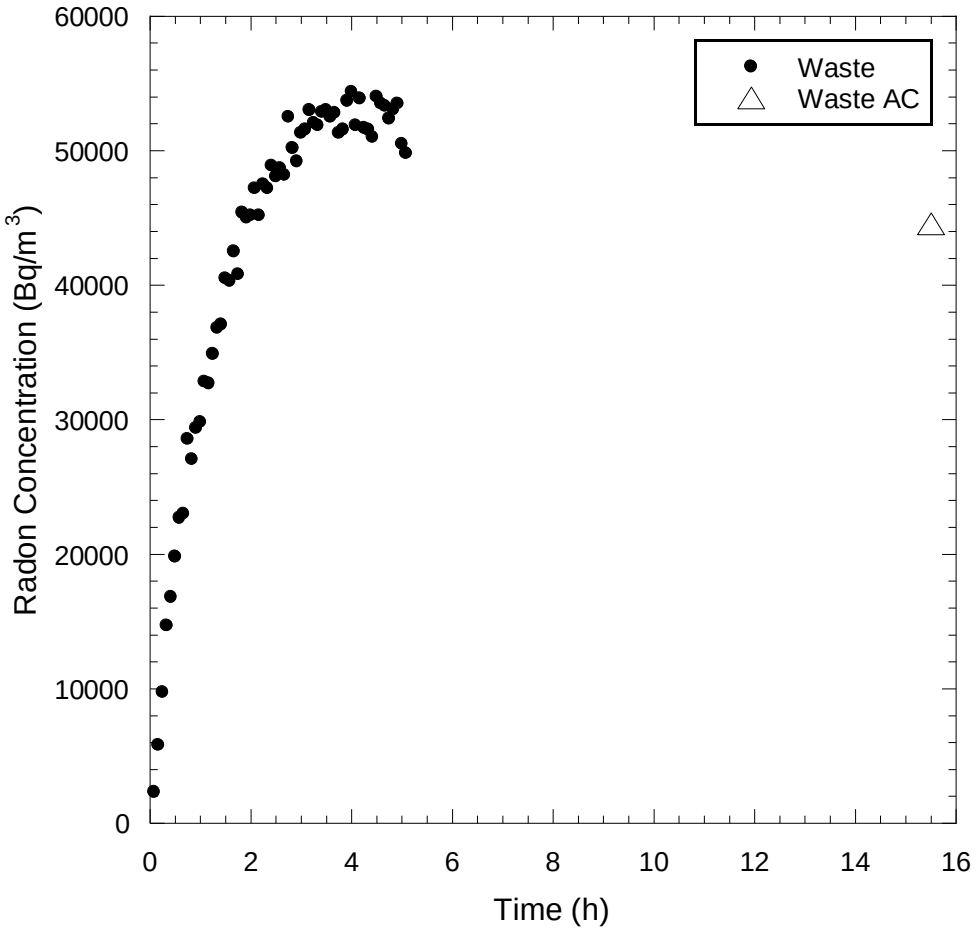

Figure 22 - Radon concentration buildup curves measured from the tailings at TP-2 at Falls City, TX.

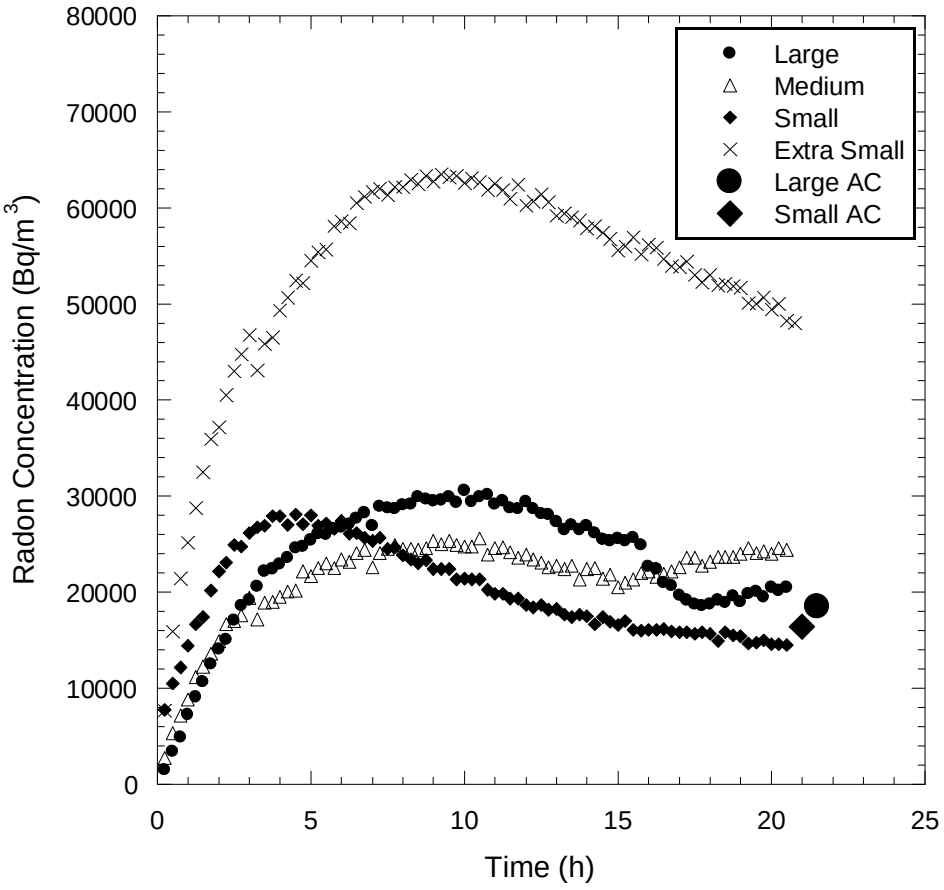

Figure 23 – Radon concentration buildup curves measured at TP-3 at Falls City, TX.

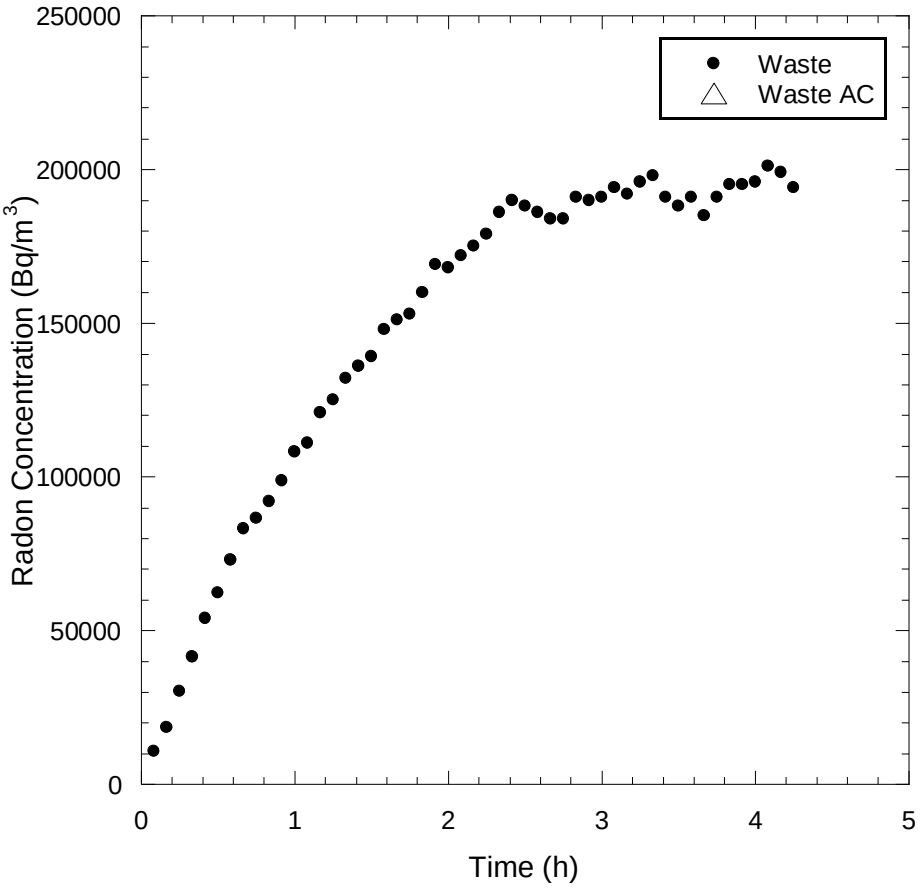

Figure 24 - Radon concentration buildup curves measured from the tailings at TP-3 at Falls City, TX.

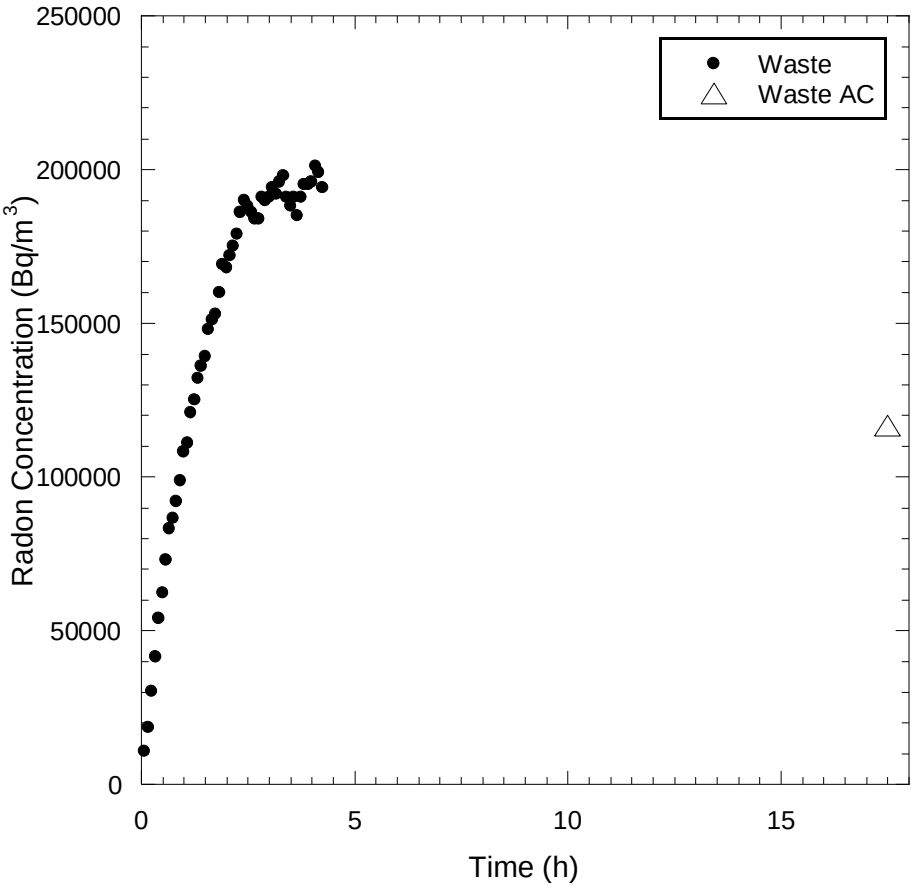

Figure 25 - Radon concentration buildup curves measured from the tailings at TP-3 at Falls City, TX.

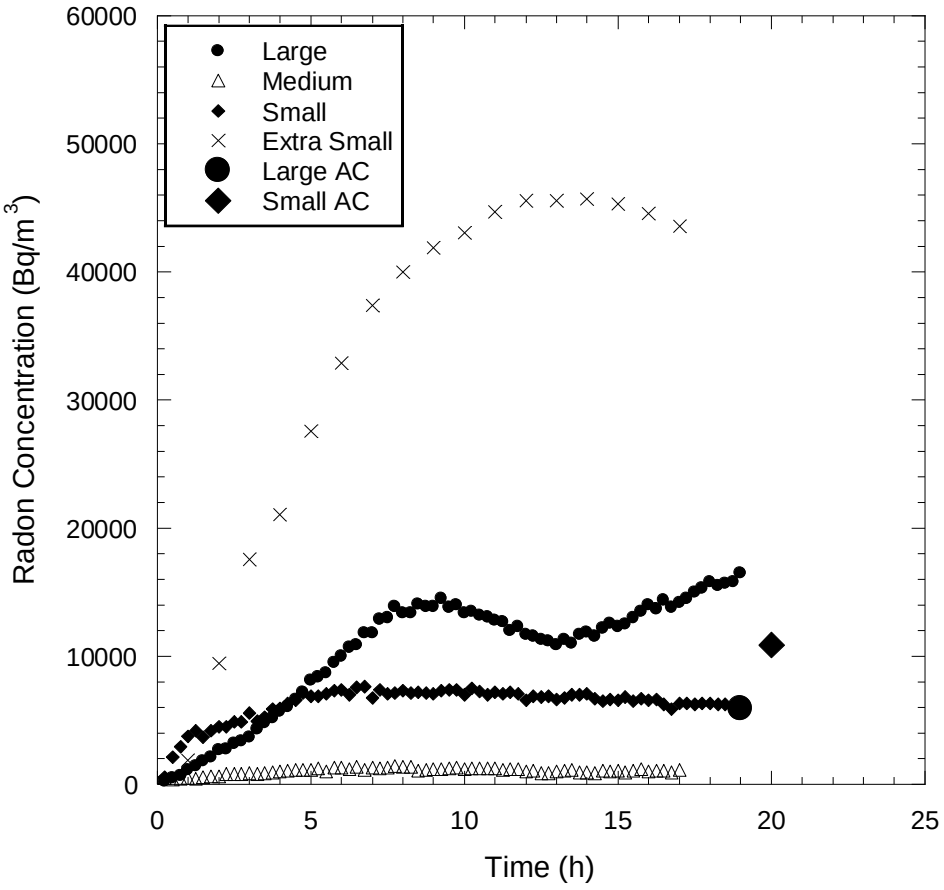

Figure 26 – Radon concentration buildup curves measured at TP-4 at Falls City, TX.

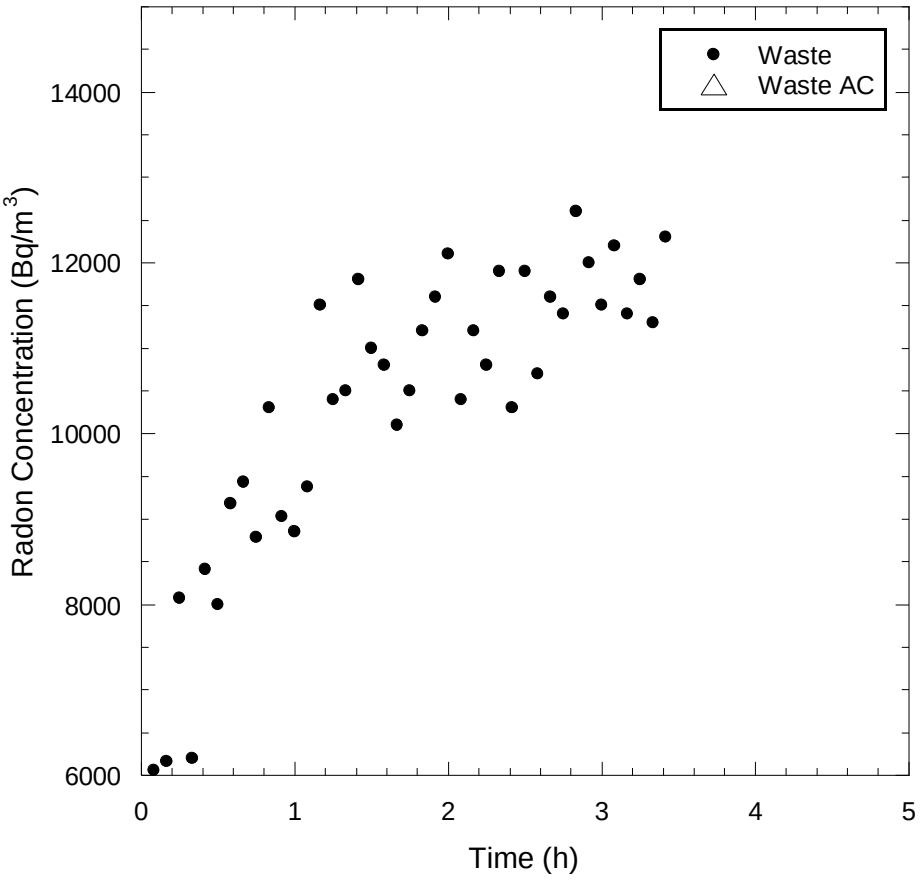

Figure 27 - Radon concentration buildup curves measured from the tailings at TP-4 at Falls City, TX.

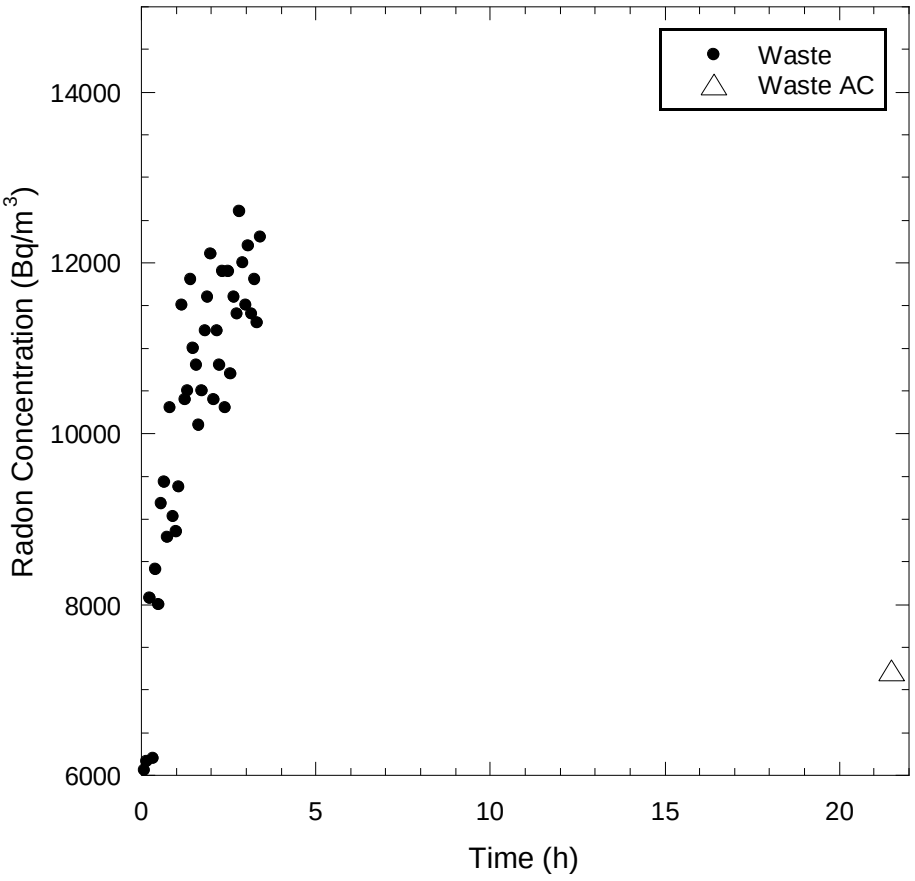

Figure 28 - Radon concentration buildup curves measured from the tailings at TP-4 at Falls City, TX.

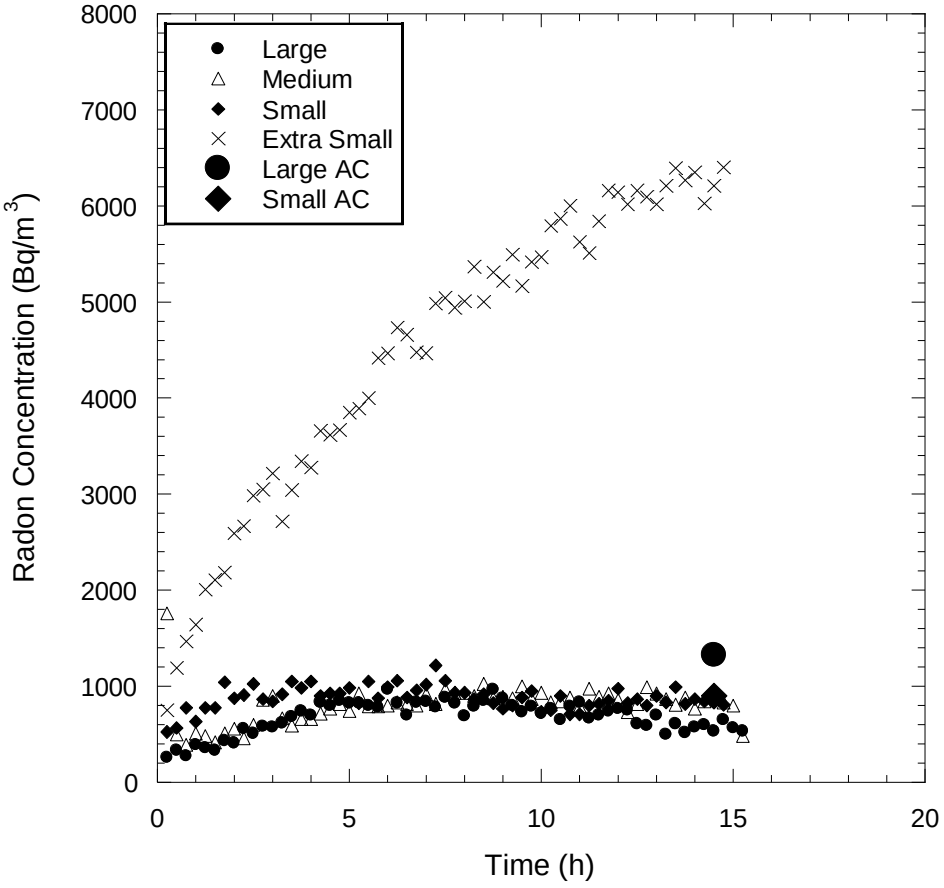

Figure 29 – Radon concentration buildup curves measured at TP-5 at Falls City, TX.

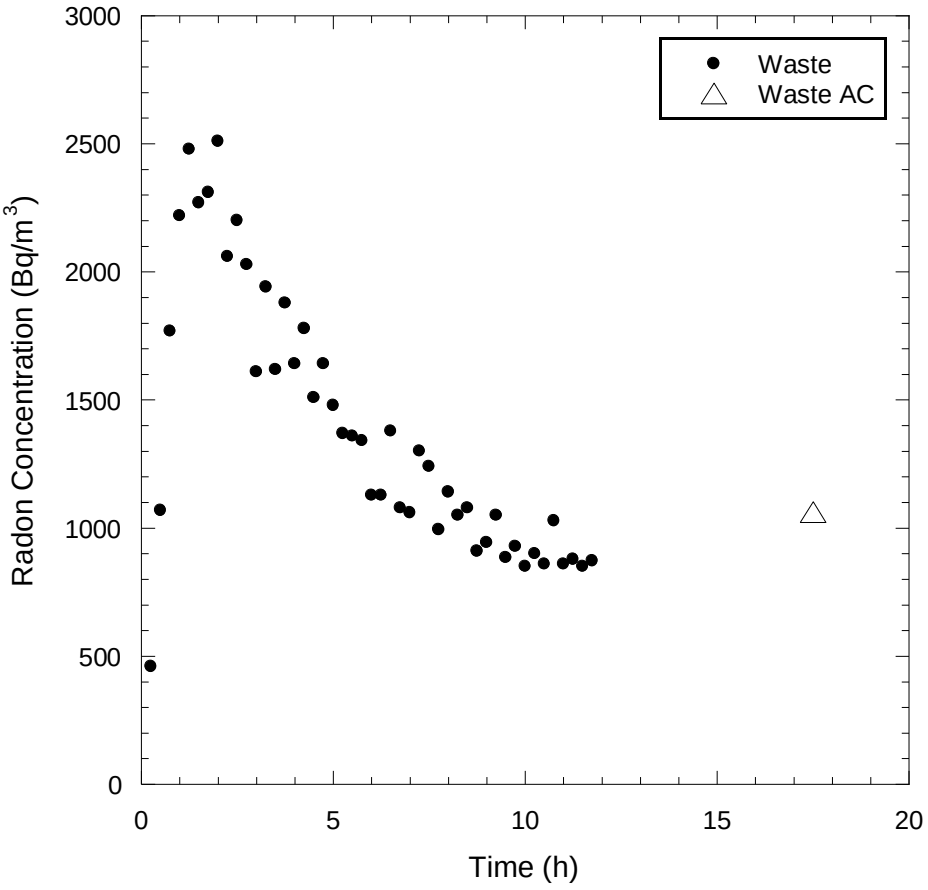

Figure 30 - Radon concentration buildup curves measured from the tailings at TP-5 at Falls City, TX.

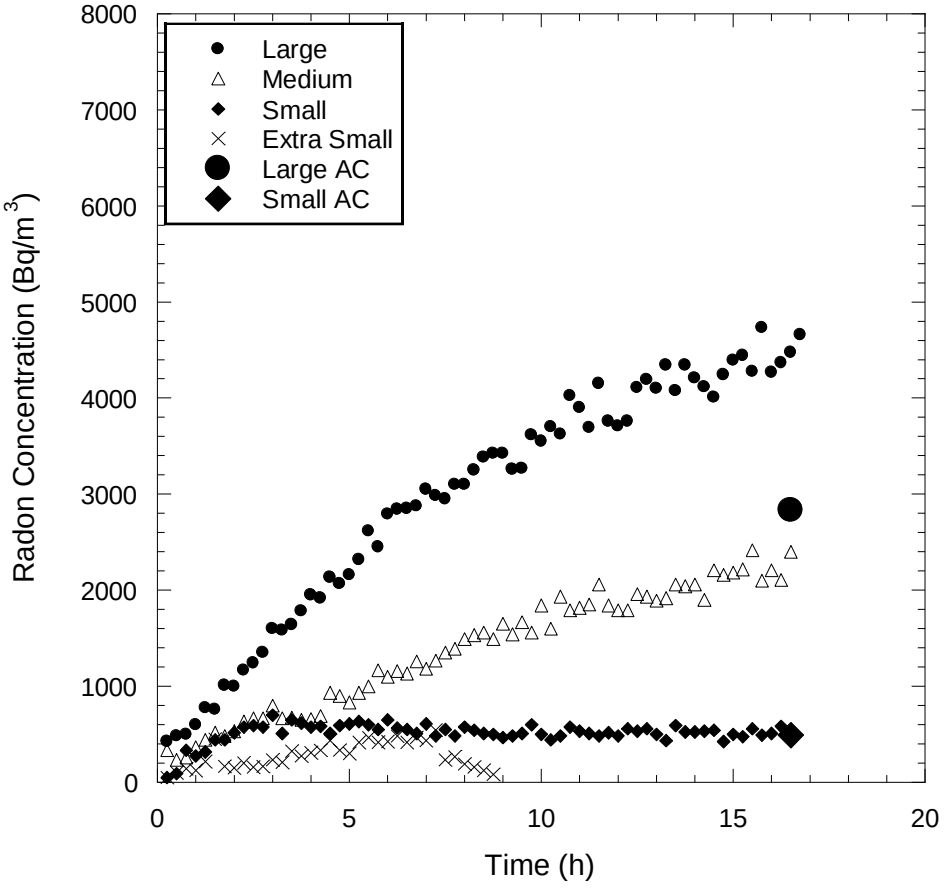

Figure 31 - Radon concentration buildup curves measured at TP-6 at Falls City, TX.

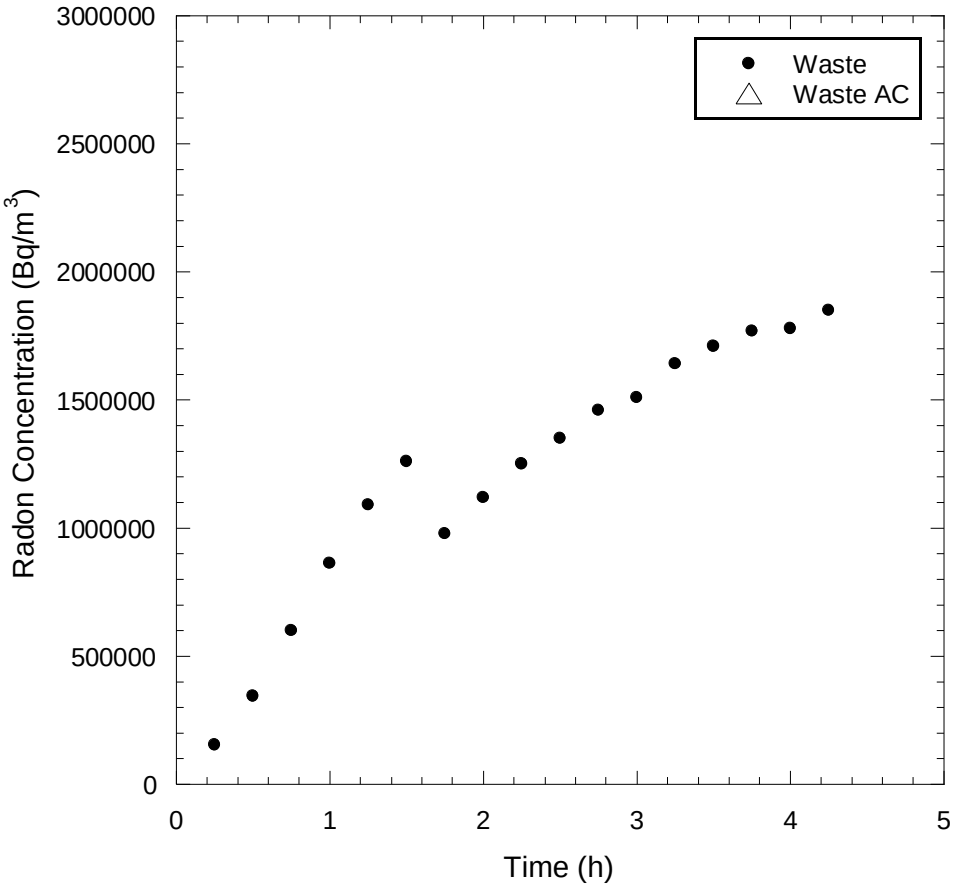

Figure 32 - Radon concentration buildup curves measured from the tailings at TP-6 at Falls City, TX.

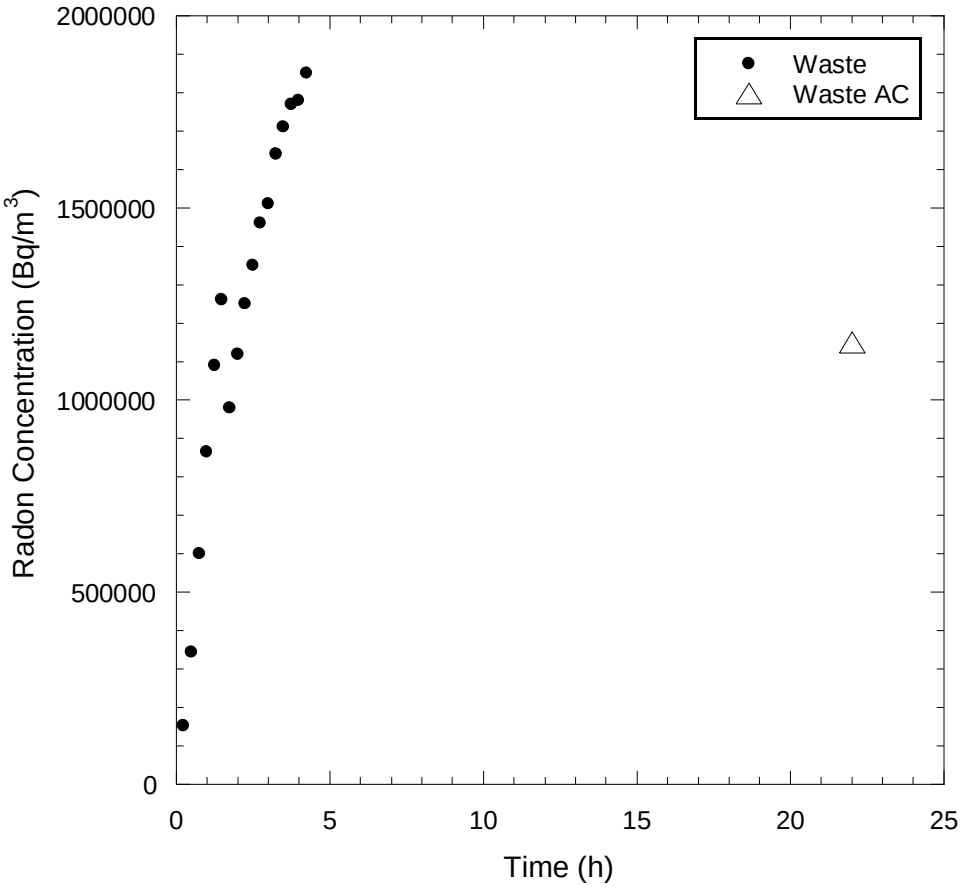

Figure 33 - Radon concentration buildup curves measured from the tailings at TP-6 at Falls City, TX.

APPENDIX II - Radon Fluxes Measured from a Compacted Clay Rn Barrier at the Bluewater, NM Uranium Mill Tailings Disposal Site in 2016

ABSTRACT

Radon (Rn) fluxes were measured from the surface of a uranium mill tailings disposal site after 21 years of service. The tailings were contained by a Rn barrier of varying thickness as well as protective layers consisting of riprap or vegetated topsoil for erosion control. Flux measurements were made with four flux different-sized flux chambers: extra small (area = 0.018 m^2, volume = 0.002 m^3), small (0.071 m^2, 0.011 m^3), medium (0.28 m^2, 0.06 m^3), and large (2.32 m^2, 0.35 m^3). Rn concentrations were measured concurrently using activated carbon (AC) canisters and continuously monitoring electronic RAD7 detectors with accumulation chambers. Flux measurements were made at the surface of the Rn barrier and from the surface of the underlying tailings at nine locations representing features that are believed to cause structure within soil. Rn fluxes measured at the surface of the Rn barrier were consistently lower than fluxes measured at the surface of the tailings, indicating that significant Rn attenuation was occurring within the barrier. The geometric mean of all flux values measured from the Rn barrier surface were lower than the regulatory maximum of 0.74 Bq/m^2-s. Comparison of measurements from different sized flux chambers indicated that no scale-dependent flux measurements were evident. Greater Rn fluxes were observed at three test pit locations adjacent to surface features that were expected to create structure within the soil relative to their paired control test pits. Average in-situ water content measurements of the Rn Barrier material were found to have decreased from as built values, however, were in good agreement with the long-term predicted water content used in the design of the barrier. Saturated hydraulic conductivity was determined from large-scale block samples and was

found to be greatest within the top 25 cm of the Rn Barrier.

1. FIELD SITE

The Bluewater Uranium disposal facility is located approximately 9 miles northwest of Grants, New Mexico in the vicinity of the original Uranium processing mill site. The mill was constructed in 1953 and operations were seized in 1982. Reclamation of the site began in 1991 and concluded in 1995. The disposal facility (**Figure 1**) consists of six disposal areas including the main tailings pile (MTP) disposal cell, the carbonate tailings disposal cell, an asbestos disposal cell, a polychlorinated biphenyl (PCB) disposal cell, and two small landfills. A small section of the MTP is distinguished as the acid tailings disposal cell. The MTP contains approximately 90 percent of the total tailings contained at the site (U.S. Department of Energy, Office of Legacy Management, 2016). The test pits excavated as a part of this study were located within the main tailings, acid tailings and carbonate disposal cells.

The “as-designed” cover profiles for the Bluewater, NM disposal facility are shown in **Figure 2** (Atlantic Richfield Company, 1996). The clay material that was used to construct the Rn Barrier was sourced from a borrow area adjacent to the site. The top deck of the MTP disposal cell consists of (bottom to top) a compacted clay Rn barrier (0.3 m to 0.98 m) and a riprap/erosion control layer (0.11 m). The side slopes of the MTP disposal cell consist of a compacted clay Rn barrier (1.04 m), a filter rock layer (0.15 m), and a riprap/erosion control layer (0.19 m). The MTP covers an area of approximately 1.43 x 10^6 m^2 and contains approximately 20.9 Tg of tailings and other contaminated waste and 414.4 TBq of ^{226}Ra (U.S. Department of Energy, Office of Legacy Management, 2016).

Grasses, brush, shrubs and other types of vegetation were observed growing from the riprap layer of the MTP (**Figure 3**).

The top deck of the acid tailings portion of the MTP disposal cell consists of a compacted clay Rn barrier (0.24 m) and topsoil (0.20 m) seeded with native grasses as erosion control (**Figure 4**). The side slopes of the acid tailings portion consist of a compacted clay Rn barrier (0.24 m), a filter rock layer (0.15 m), and a riprap/erosion control layer (0.19 m).

The top deck of the carbonate tailings disposal cell consists of a compacted clay Rn barrier (3.69 m) and a riprap/erosion control layer (0.11 m). The side slopes of the carbonate tailings disposal cell consist only of a filter rock erosion control layer (0.15 m) since all of the contaminated tailings are contained beneath the top deck of the disposal cell. The carbonate tailings disposal cell covers an area of approximately 21.9 x 10^4 m^2 and contains approximately 1.2 Tg of contaminated materials and 41.8 TBq of ^{226}Ra (U.S. Department of Energy, Office of Legacy Management, 2016).

Table 1 summarizes some of the soil parameters from the borrow soil used to construct the Rn Barrier, the soil parameters used in the design of the Rn Barrier, and the as-built soil parameters obtained after construction of the Rn Barrier.

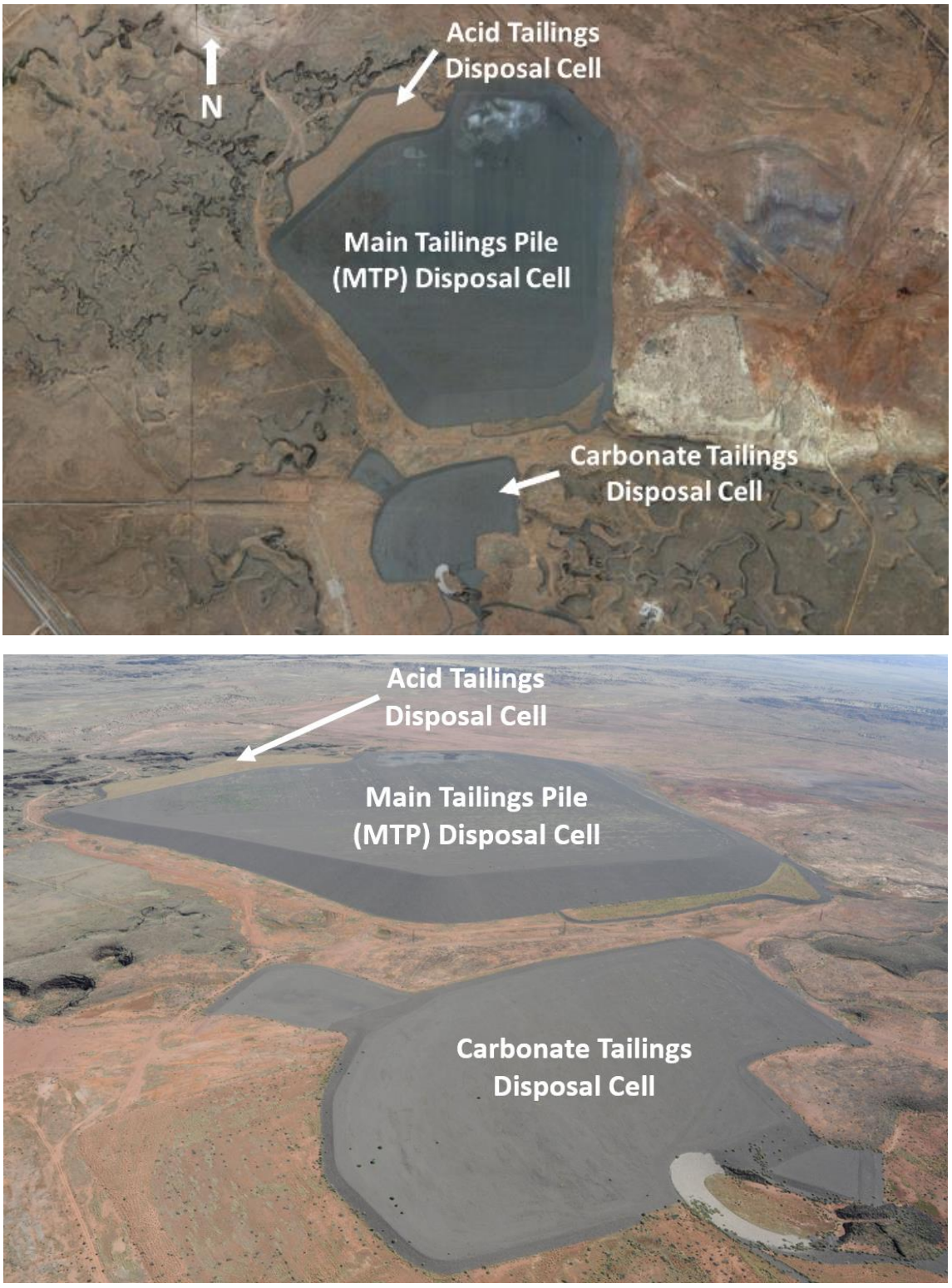

Figure 34 - Aerial views of the Bluewater, NM disposal site (Left, Google Earth & right, The Center for Land Use Interpretation).

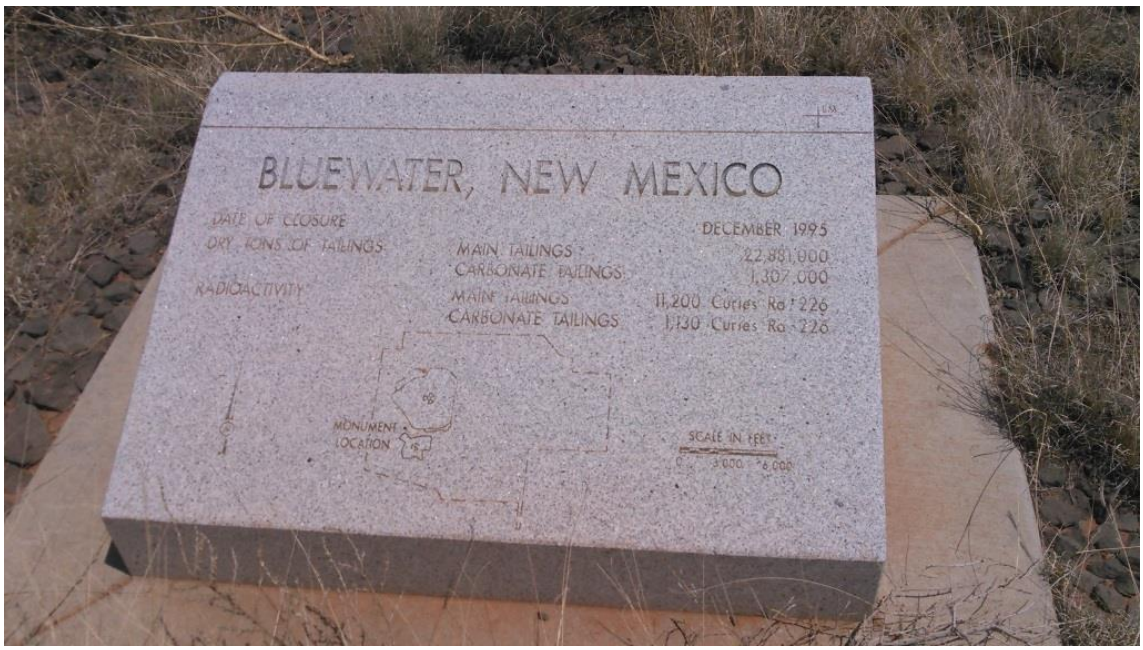

Figure 35 – Granite monument at the Bluewater, NM disposal cell.

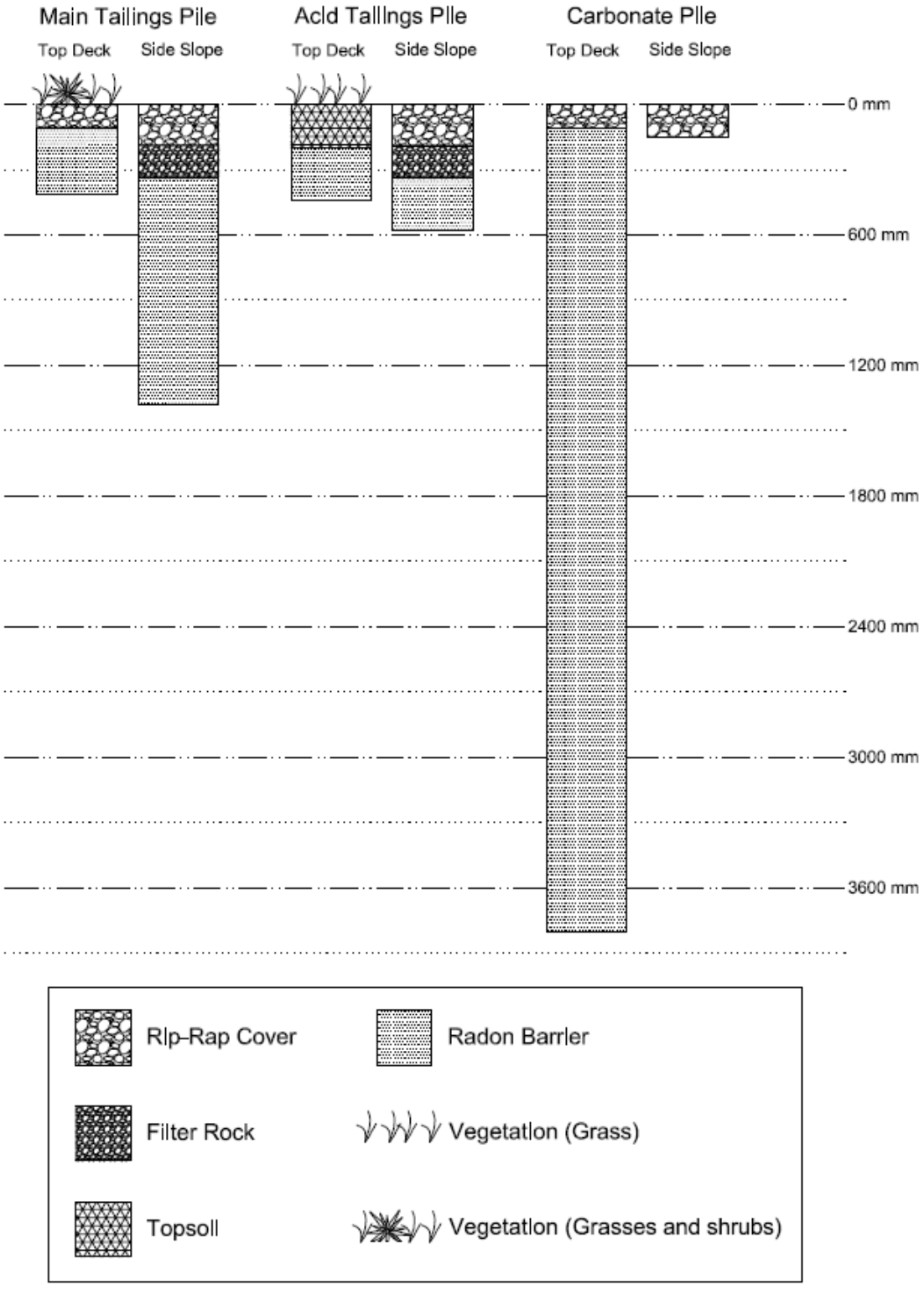

Figure 36 – Bluewater, NM “as-designed” cover profiles.

Table 10 – Summary of soil parameters from borrow soil and as-built soil.

Parameter	Value	Source
- Borrow Soil -	-	-
Average % Fines	33.9 (range 49.2 - 24.6)	4 tests[a]
Borrow Soil % Clay (<2 µm)	23.6	4 tests[a]
Liquid Limit	32 ± 7	10 tests[a]
Plasticity Index	19 ± 6	10 tests[a]
Specific Gravity	2.68 ± 0.02	10 tests[a]
Original Dry Density (Borrow Soil)	1.68	25 tests[b]
Original Gravimetric Water Content (Borrow Soil)	10.4	25 tests[b]
Rn Flux (Bq/m^2-s) (measured background)	0.033 ± 0.022	5 tests[b]
- Soil Parameters Used for Diffusion Coefficient -	-	-
Long Term Gravimetric Water Content	9.5%	[b]
Dry Density (g/cm^3)	1.70	[b]
- As-Built -	-	-
Estimated Diffusion Coefficient (m^2/s)	1.8E-06	[b]
Gravimetric Water Content	-	-
Main Tailings Pile (incl. Acid Tailings Pile)	12.1	2139 tests[c]
Carbonate Pile	12.4	604 tests[c]
Dry Density (g/cm^3)	-	-
Main Tailings Pile (incl. Acid Tailings Pile)	1.851	2139 tests[c]
Carbonate Pile	1.847	604 tests[c]
Surface Rn Flux (Bq/m^2-s)	-	-
Main Tailings Pile (incl. Acid Tailings Pile)	0.079 ± 0.112	125 tests[d]
Carbonate Pile	0.048	100 tests[d]

a - Characterization of Borrow Soil at the Bluewater Uranium Mill Site, Rogers and Associates Engineering Corporation (1987)

b - Arco Coal Co. Bluewater Mill Reclamation Plan: Volumes 1 -3 (1990)

c - Atlantic Richfield Company Bluewater Uranium Mill Completion Report: Volume 3 (1996)

d - Atlantic Richfield Company Bluewater Uranium Mill Completion Report: Volume 4 (1996)

Figure 37 – Clockwise from top left: 1. Unvegetated riprap erosion cover. 2. Grasses growing in the riprap cover layer. 3. Ant mound protruding from the riprap cover (Test Pit 6). 4. Salt bush growing from the riprap layer (ATV for scale).

Figure 38 - Vegetated topsoil cover at the acid tailings pile disposal cell.

2. RESULTS

Results from Rn fluxes measured at nine test pits are summarized below. Approximate locations of the test pits are shown in **Figure 9** (Appendix A). Test pits were chosen to be adjacent to surface features that were believed to influence the performance of the Rn barrier. Additionally, “control” test pits that lacked the surface feature were chosen in the vicinity of each test pit. Six out of the nine test pits were divided into halves and the flux measurements from each half were designated as “Test Pit #A” and “Test Pit #B”. After Rn flux measurements were made at the top surface of the Rn barrier, an excavation was made through the Rn barrier to expose the underlying uranium mill tailings so that a flux measurement could be taken directly from the tailings.

2.1 Radon Flux Measurements

The methods for the determination of Rn flux from AC and RAD7 were the same methods described in sections 4.1.1 and 4.1.2, respectively. Rn buildup curves from the surface of the Rn barrier and from the surface of the tailings from each test pit are shown in **Appendix I**. It should be noted that the rate of Rn concentration buildup from the flux tests taken directly from the surface of the tailings is much greater than the rate of buildup from the tests taken on the surface of the Rn. This shows that Rn is decaying significantly within the barrier, as it is intended to do.

Fluxes measured from the nine test pits using the RAD7 are summarized in **Figure 6** (below) and **Table 7** in **Appendix A**. Test pit descriptions are summarized in **Table 2**, below.

The compiled results of all flux tests do not indicate that there was an impact of measurement scale on flux at this site. **Figure 7** shows each flux value normalized by the geometric mean flux from that respective test pit. If the flux measurements were scale-dependent, it would be expected that the scatter between the flux ratios presented in **Figure 7** would decrease and cluster near a value of one as chamber area increased (and perhaps reach an "optimum" size), however, this trend was not apparent.

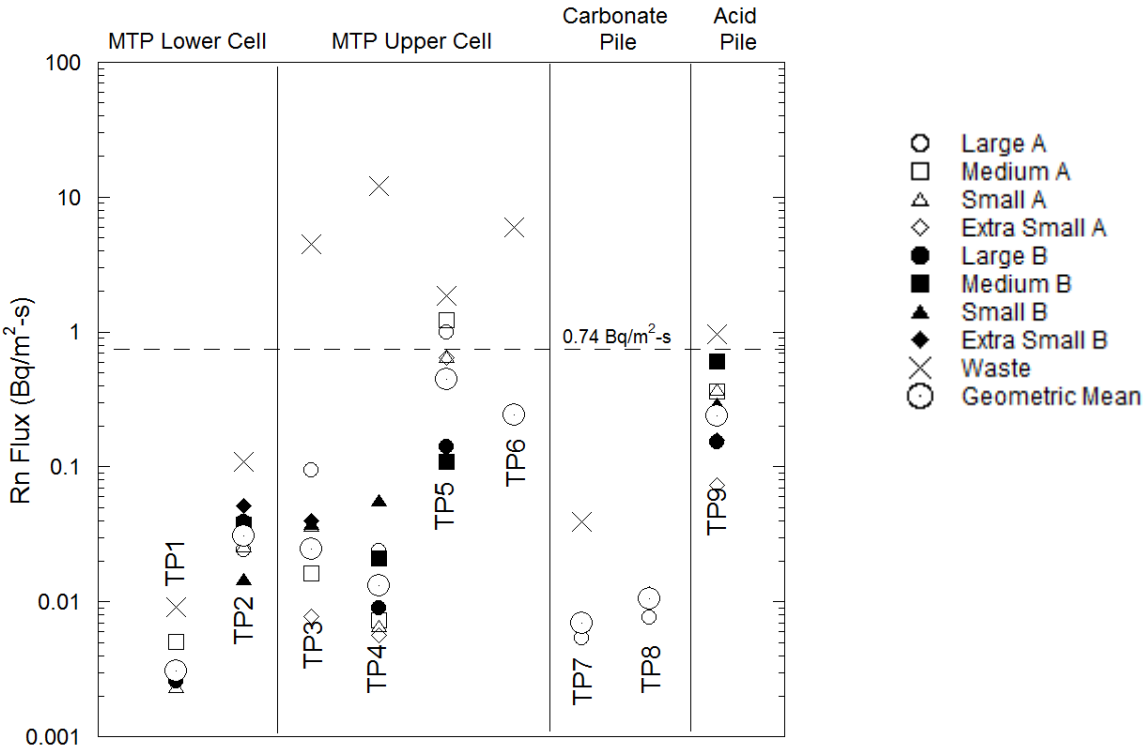

Figure 39 - Summary of fluxes measured with the RAD7 radon detector at the surface of the Rn barrier and the surface of the underlying tailings. TPX = Test Pit X. The dashed horizontal line represents the maximum allowable surface flux specified by UMTRCA (0.74 Bq/m^{2}s).

Table 11 - Test pit descriptions.

Test Pit	Location	Surface Feature Description
1	MTP	Seasonal ponding
2		Paired Pit w/TP-1 w/o ponding
3		Sparse vegetation
4		Unvegetated control for TP 5 & 6
5		Mature Salt Bush colony
6		Ant mound
7	Carbonate Pile	Small Salt Bush
8		Paired Pit w/TP-7 w/o Salt Bush
9	Acid Pile	Vegetated Topsoil

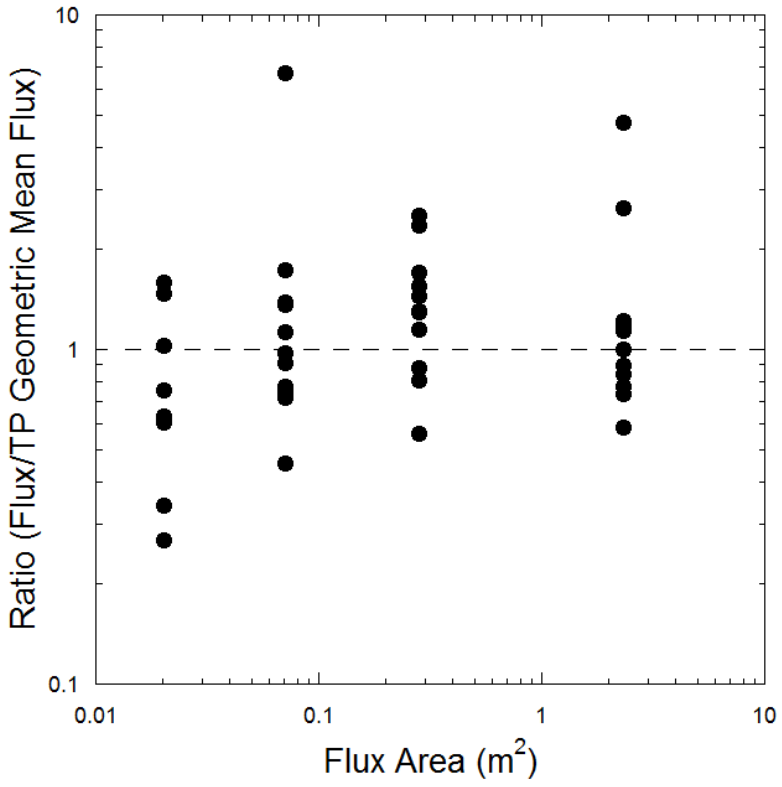

Figure 40 - Fluxes normalized by the geometric mean flux from each test pit.

2.2 Comparison of Fluxes in 2017 to As-Built Fluxes

The Bluewater Completion Report (1996) reported that upon completion of the Rn Barrier construction at the site, a number of "as-built" surface flux measurements were taken from each region to confirm that the surface flux was below the 0.74 Bq/m^2s UMTRCA limit per the guidelines (40 CFR 192.02). These flux measurements were made using adsorptive methods and activated charcoal granules placed over a wire mesh within flux chambers that were placed directly on the Rn Barrier and the test durations were approximately 24 hours for each flux test (Petrotomics Company, 2001). **Table 3** and **Figure 8** below, summarize the flux measurements taken in 2000 and 2017.

It must be noted that when the as-built flux measurements were taken, compaction had recently been completed, thus the moisture content was close to an optimum moisture content for compaction purposes. For example, the average as-built moisture content on the main tailings pile was reported to be 12.1% (versus the average 9.6% in 2016 – additional discussion on water content to follow). Thus, the diffusion coefficient at the time of as-built flux measurements was likely lower than what should be considered representative of the steady-state Rn Barrier conditions resulting in a lower surface Rn flux. In either case, it appears as if the average flux from both the Main Tailings Pile and the Carbonate Tailings Pile in 2016 was very similar to as-built values.

Table 12 – Summary of average as-built and 2016 flux measurements from the Bluewater, NM disposal site.

		As-Built (AC) (Bq/m^2s)	2016 RAD7 (Bq/m^2s)
MTP	**AVG Flux**	0.076	0.147
	SD	0.120	0.296
Carbonate Pile	**AVG Flux**	0.047	0.009
	SD	0.068	0.003
Acid Pile	**AVG Flux**	0.435	0.296
	SD	0.724	0.181

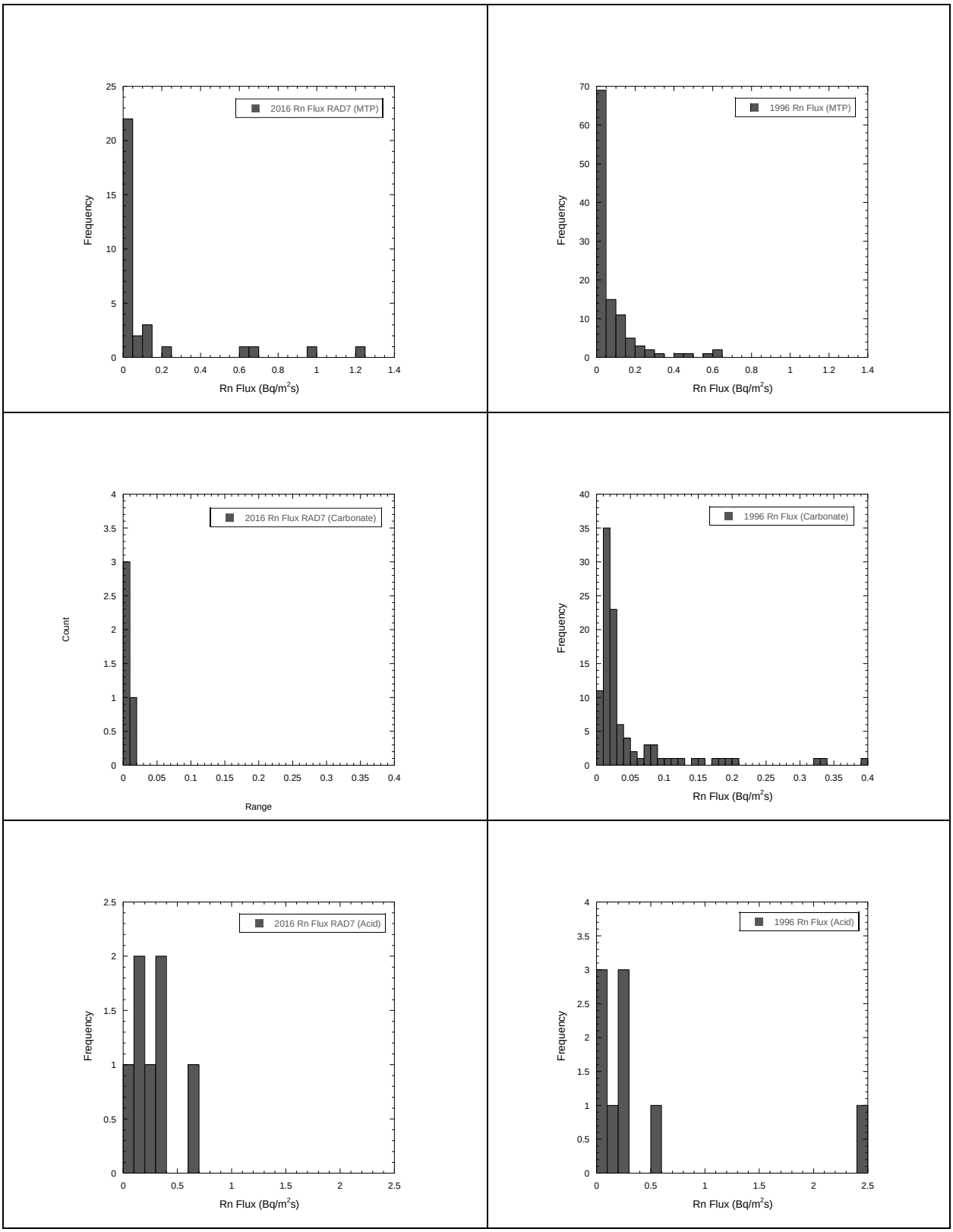

Figure 41 – Histograms showing the frequency of Rn fluxes measured in 2016 (left) and 1996 (right) at three distinct regions of the site.

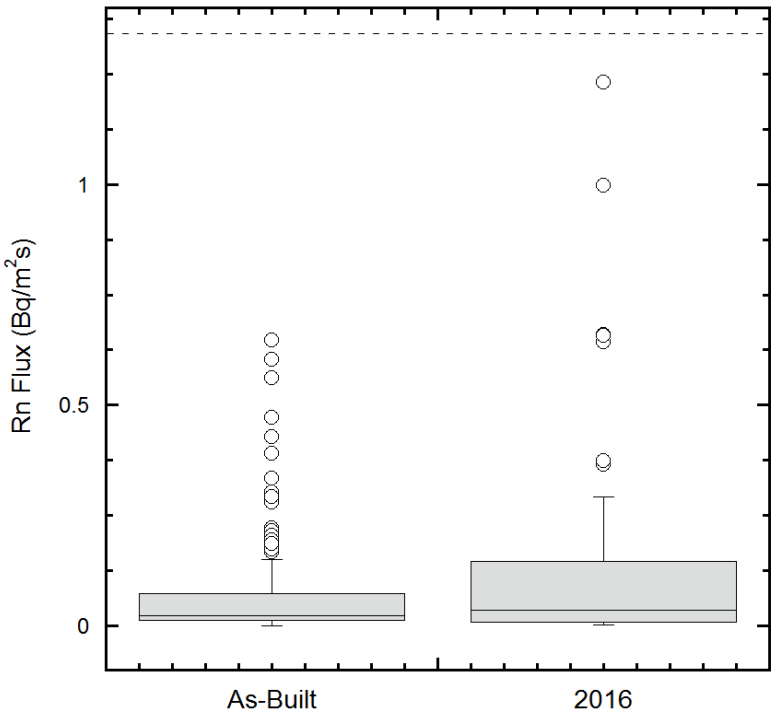

Figure 42 - Box plot showing as-built and 2016 measurements of Rn flux.

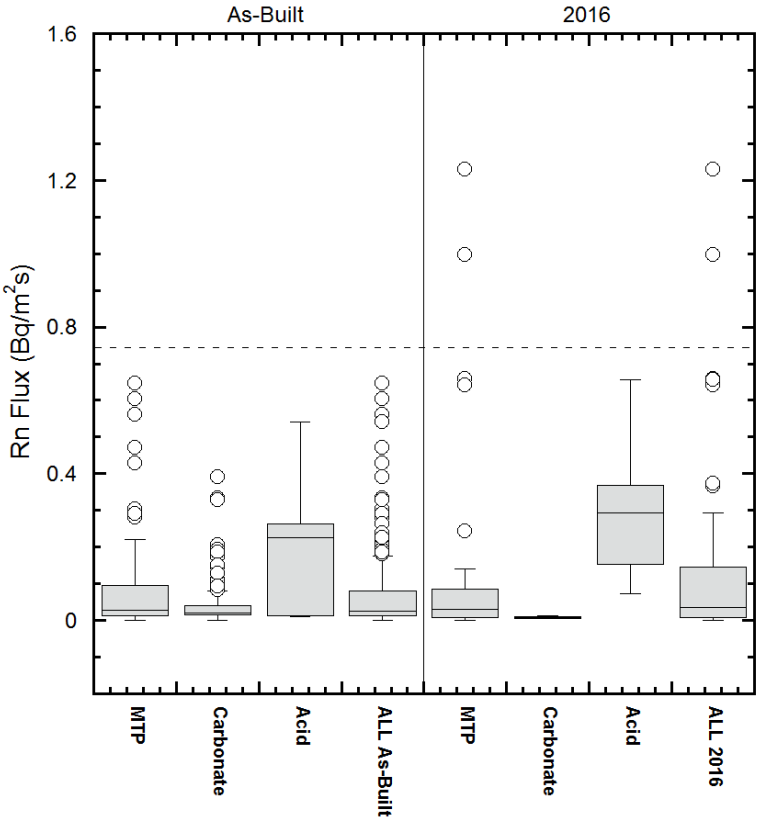

Figure 43 - Box plot showing as-built and 2016 measurements of Rn flux separated by location.

2.3 Water Content Profiles

Thin-walled (Shelby) tube samples (diameter 70 mm) obtained from the Rn Barrier were cut in the lab into sections approximately 40 - 50 mm in length to obtain profiles of water content with depth (see section 4.1.4 laboratory methods). When possible, the dimensions and masses of each of the sections were measured so that dry unit weight, volumetric water content, and saturation profiles could be created (a compilation of water content, dry density, and saturation profiles can be found in **Appendix F, G, and H**, respectively). The large-scale "block" samples (350 mm diameter) obtained from the site were also used to determine in-situ water content and dry unit weight in the laboratory. The average water content values from both the thin-walled tube samples and large-scale block samples (referred to as "2016 values") are compared to the in-situ, "as-built" values from the completion report in **Table 4.**

Table 13 – Summary of as-built and 2016 measurements of water content and dry unit weight.

		As-Built Value		***2016 Value***	
Parameter	***Location***	***Value***	***# of Samples***	***Value***	***# of Samples***
Average Moisture Content (%)	Main Tailings Pile (incl. Acid Tailings)	12.1	2282	9.6	19
	Carbonate Pile	12.4	604	10.7	14
Dry Density (g/cm^3)	Main Tailings Pile (incl. Acid Tailings)	1.851	2282	1.848	19
	Carbonate Pile	1.847	604	1.743	14

It should be noted that the average water content in 2016 was measured to be lower than as-built values for both the Main Tailings Pile and the Carbonate Tailings locations. More specifically, the water contents in 2016 at the Main Tailings Pile and the Carbonate Tailings locations were found to have decreased by approximately 21% and 14%, respectively, when compared to as-built averages for both locations. While this does

insist that the Rn Barrier has dried significantly, it should also be noted that the predicted, long-term moisture content that was used to determine the design diffusion coefficient and thus the thickness of the Rn Barrier at the Bluewater site was 9.5 % (see **Table 1**). The higher as-built water contents were more than likely due to the required optimum water content for compaction purposes. The long-term moisture content value was determined based on average rainfall in the area as well as a number of soil borings taken from the clay borrow area adjacent to the site.

2.4 Saturated Hydraulic Conductivity

Saturated hydraulic conductivity testing was completed on 18 large-scale, undisturbed block samples (350 mm diameter) taken from the Bluewater, NM site. Fifteen blocks were exhumed from the Rn Barrier and three from an Analog location adjacent to the location of the source of borrow material for construction of the Rn Barrier. The blocks were trimmed to a testing diameter of approximately 305 mm and height of 152 mm using the procedures previously described section 4.1.5. The results of the saturated hydraulic conductivity testing are summarized in **Figure 11 and Table 5**, below.

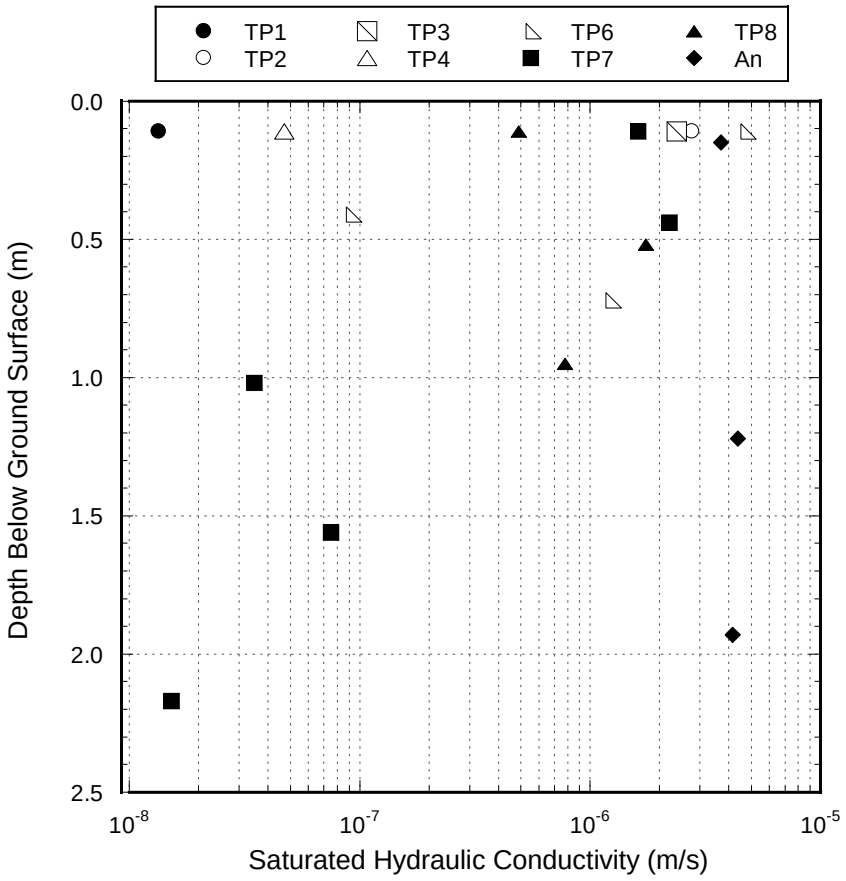

Figure 44 - Summary of saturated hydraulic conductivity of eighteen large-scale block samples taken from the Bluewater, NM disposal site.

Table 14 - Summary of saturated hydraulic conductivity of eighteen large-scale block samples taken from the Bluewater, NM disposal site.

TP	Depth BGS to Middle of Sample (m)	Hydraulic Conductivity (m/s)
1	0.24	1.34E-08
2	0.22	2.77E-06
3	0.21	2.38E-06
4	0.19	4.71E-08
6A	0.25	9.21E-08
6-TOP	0.55	4.72E-06
6-BOT	0.86	1.23E-06
7	0.27	1.62E-06
7	0.60	2.21E-06
7	1.18	3.50E-08
7	1.72	7.49E-08
7	2.33	1.53E-08
8	0.17	4.90E-07
8	0.58	1.75E-06
8	1.01	7.77E-07
Analog 3	0.28	3.69E-06
Analog 3	1.35	4.38E-06
Analog 3	2.06	4.16E-06

The saturated hydraulic conductivity varied across all samples approximately two orders of magnitude. The block from TP-1, taken near the surface of the Rn Barrier was found to have the lowest k_{sat} (1.34×10^{-8} m/s) while the block taken from near the surface at TP-6 was found to have the greatest k_{sat} (4.72×10^{-6} m/s). Of the fifteen blocks tested from Rn Barrier soil, the geometric mean k_{sat} was 3.6×10^{-5} cm/s. The geometric mean k_{sat} of the three blocks exhumed from the analog location was 4.1×10^{-4} cm/s and did not change significantly with depth. The hydraulic conductivity of the analog samples may be an indication of what the long term hydraulic conductivity of the Rn barrier will be.

3 SUMMARY

Rn fluxes were measured from nine test pits excavated at the uranium mill tailings disposal site in Bluewater, NM in 2016. The cover system had been in service for approximately 21 years at the time of the performed field work. Flux measurements were taken from the surface of the Rn barrier to observe if soil structure caused by pedogenesis had caused any changes in Rn flux. Four flux chamber sizes were used to observe if soil structure was causing any scale-dependent Rn flux. Rn concentrations and fluxes were measured with activated carbon (AC) canisters and RAD7 continuous monitors. AC canisters recorded a single concentration point while RAD7 monitors provided continuous concentration measurements.

Rn fluxes measured from the surface of the Rn barrier were significantly lower than the fluxes measured directly from the tailings beneath. This indicates that the Rn barrier is still effective at reducing the Rn flux at the surface, and Rn gas is attenuating significantly within it before reaching the atmosphere. Two measurements of Rn flux were measured to be above the UMTRCA maximum allowed flux of 0.74 Bq/m^2s, while all others (41 tests) were below the limit. The overall geometric mean of Rn flux measured from the surface of the Rn barrier was 0.040 Bq/m^2s. No apparent impacts of measurement scale were observed based on the fluxes measured at this field site.

Higher fluxes were measured at test pit 2 (no seasonal ponding) relative to test pit 1 (seasonal ponding), however the flux from the tailings below test pit 2 was greater than that of test pit 1, which may account for the difference in surface flux. Higher fluxes were measured at test pits 5 (salt bush) and 6 (ant mound) relative to the adjacent test pit 4, which was an unvegetated control. It is believed that the elevated fluxes at these two test

pits were caused by the soil structure created by the biotic processes. Similar Rn fluxes were recorded from test pits 7 and 8, despite the expectation that the salt bush adjacent to test pit 7 would cause an increase in the Rn flux.

Water content measurements taken from both thin-walled tube samples and large-scale block samples obtained in the field in 2016 showed that the average water content of the Rn Barrier soil had decreased from as-built values by 21% and 14% at the Main Tailings Pile and Carbonate Tailings Pile, respectively. However, the predicted long-term water content used in the design of the Rn Barrier was very close to the 2016 in-situ measurements.

The saturated hydraulic conductivity of large-scale block samples obtained at the field site were measured in the laboratory. In general, blocks from close to the surface were found to have greater saturated hydraulic conductivity relative to deeper samples which may indicate that pedogenisis near the surface is affecting hydraulic conductivity. Three blocks from various depths taken from an analog location showed little variation of saturated hydraulic conductivity with depth (Geom. Mean ksat = 4.1×10^{-6} m/s) and may represent the long-term hydraulic conductivity of the Rn Barrier.

REFERENCES

Company, A. R. (1996). Completion Report for Reclamation of the Bluewater Mill Site. Grants, NM.

DOE-LM, U. (1978). Fact Sheet UMTRCA Title II Bluewater , New Mexico , Disposal Site, 1978, 1–3.

APPENDIX A – ADDITIONAL TABLES AND FIGURES

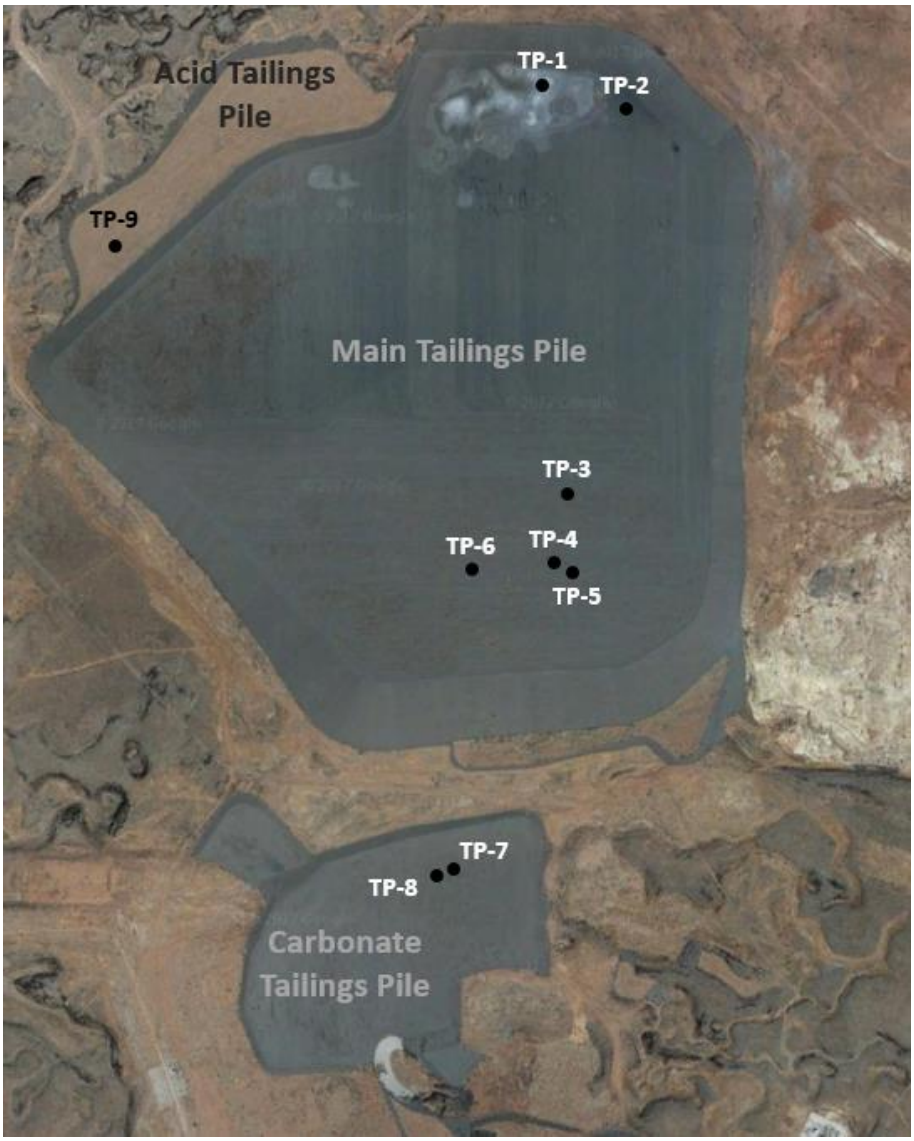

Figure 45 – Approximate locations of test pits excavated at the Bluewater, NM site.

Table 15 - Flux chamber areas and volumes.

Chamber Designation	Area [m^2]	Volume [m^3]
Extra Small	0.020	0.002
Small	0.071	0.011
Medium	0.282	0.056
Large	2.323	0.352

Table 16 – Tabulated summary of flux measurements from all test pits using RAD7.

Test Pit	*Test (A/B)*	*Chamber Size*	*Flux*	*Geometric Mean of Test Pit*	*Tailings Flux (Small Chamber)*
			[Bq/m^2-s]	*[Bq/m^2-s]*	*[Bq/m^2-s]*
1	A	Large	0.003	0.003	0.009
		Medium	0.005		
		Small	0.002		
	B	Large	0.003		
2	A	Large	0.024	0.031	0.109
		Medium	0.037		
		Small	0.026		
	B	Large	0.040		
		Medium	0.037		
		Small	0.015		
		Extra Small	0.051		
3	A	Large	0.138	0.032	4.508
		Medium	0.016		
		Small	0.040		
		Extra Small	0.008		
	B	Small	0.038		
		Extra Small	0.040		
4	A	Large	0.024	0.013	11.985
		Medium	0.007		
		Small	0.007		
		Extra Small	0.006		
	B	Large	0.009		
		Medium	0.021		
		Small	0.061		
		Extra Small	0.013		
5A	A	Large	0.997	0.849	1.854
		Medium	1.230		
		Small	0.660		
		Extra Small	0.642		
5B	B	Large	0.141	0.124	
		Medium	0.109		
6	A	Large	0.244	0.244	5.954
7	A	Large	0.005	0.007	N/A
		Medium	0.009		
8	A	Large	0.008	0.010	N/A
		Small	0.014		
9	A	Medium	0.366	0.240	1.025
		Small	0.373		
		Extra Small	0.074		
	B	Large	0.152		
		Medium	0.657		
		Small	0.293		
		Extra Small	0.157		

Table 17 - Tabulated summary of flux measurements from all test pits using AC.

Test Pit	Test (A/B)	Chamber Size	Flux	Geometric Mean of Test Pit	Tailings Flux (Small
			[Bq/m^2-s]	[Bq/m^2-s]	[Bq/m^2-s]
1	A	Large	0.002	0.001	0.005
	A	Small	0.001	-	
2	A	Large	0.013	0.009	0.021
	A	Small	0.006	-	
3	B	Large	0.018	0.016	6.933
	B	Medium	0.015	-	
	B	Small	0.014	-	
4	B	Large	0.008	0.015	1.616
	B	Medium	0.017	-	
	B	Small	0.024	-	
5B	B	Large	0.127	0.073	9.459
	B	Medium	0.076	-	
	B	Small	0.087	-	
	B	Extra Small	0.033	-	
6	Bottom	Small	0.805	0.805	0.805
7	A	Large	0.006	0.001	0.039
	A	Medium	0.003	-	
	A	Small	0.000	-	
	A	Extra Small	0.001	-	
9	A	Small	0.133	0.130	N/A
	A	Large	0.135	-	
	A	Medium	0.283	-	
	A	Small	0.138	-	
	A	Extra Small	0.053	-	
	B	Large	0.274	0.165	
	B	Medium	0.282	-	
	B	Small	0.161	-	
	B	Small	0.163	-	
	B	Extra Small	0.061	-	

APPENDIX B – TEST PIT EXCAVATION PHOTOS

Figure 46 – Removal of the rip-rap layer to expose the top of the Rn barrier.

Figure 47 – Repair and compaction of the Rn barrier soil.

APPENDIX C – FLUX MEASUREMENT PHOTOS

Figure 48 – Installation of flux chambers on the surface of the Rn barrier.

Figure 49 – Installation of a small flux chamber on the exposed tailings.

APPENDIX D – SOIL SAMPLING PHOTOS

Figure 50 – Obtaining a thin-walled tube sample of Rn barrier soil.

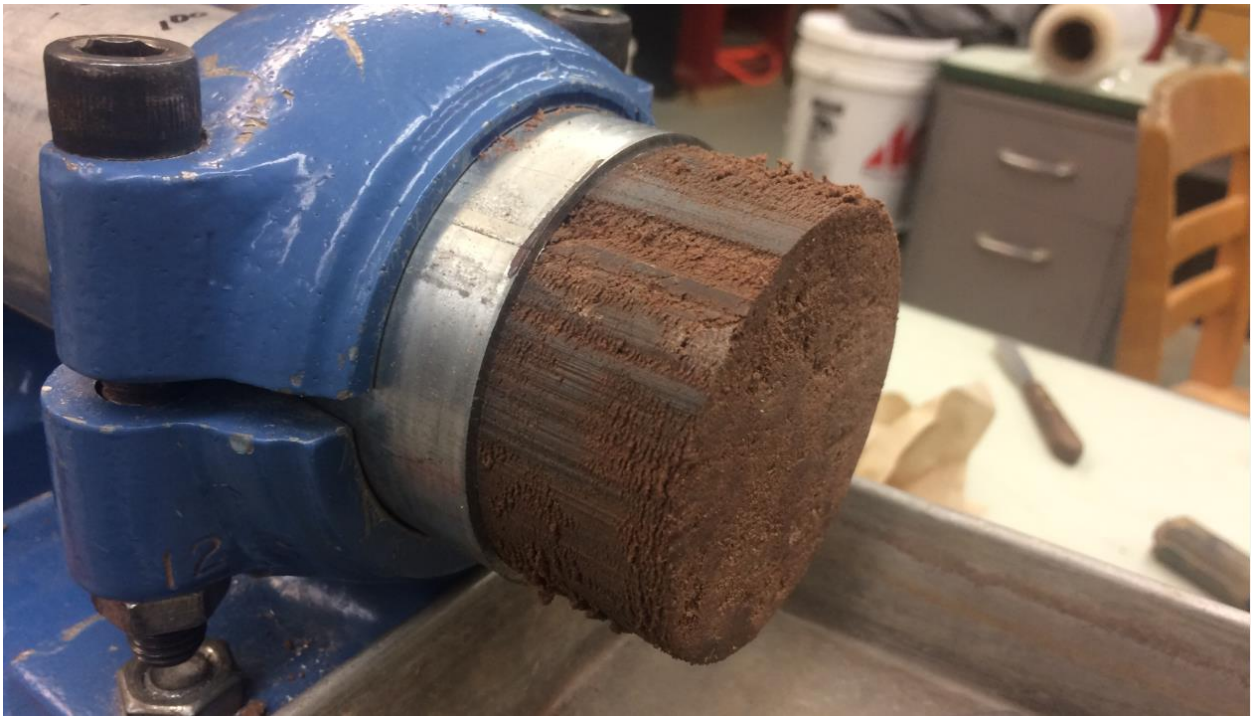

Figure 51 – Extraction of a 70 mm diameter (Shelby) tube sample in the lab.

a.

b.

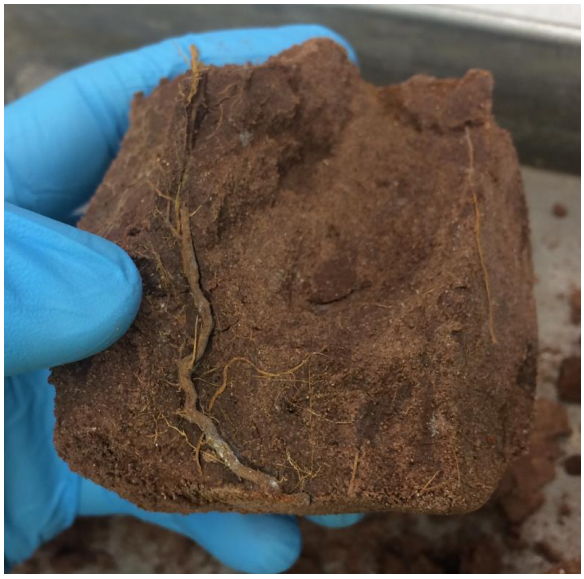

c.

d.

Figure 52 – Various roots encountered during 70 mm diameter sample extraction.

Figure 53 – Excavating a 350 mm diameter block sample from the Rn barrier with a shovel.

Figure 54 – Removal of a 350 mm diameter block sample from the Rn barrier.

Figure 55 – Trimming 350 mm diameter block sample for saturated hydraulic conductivity test.

Figure 56 – 350 mm diameter block sample with flexible membrane installed for saturated hydraulic conductivity testing.

APPENDIX E – SUMMARY OF LABORATORY TEST DATA

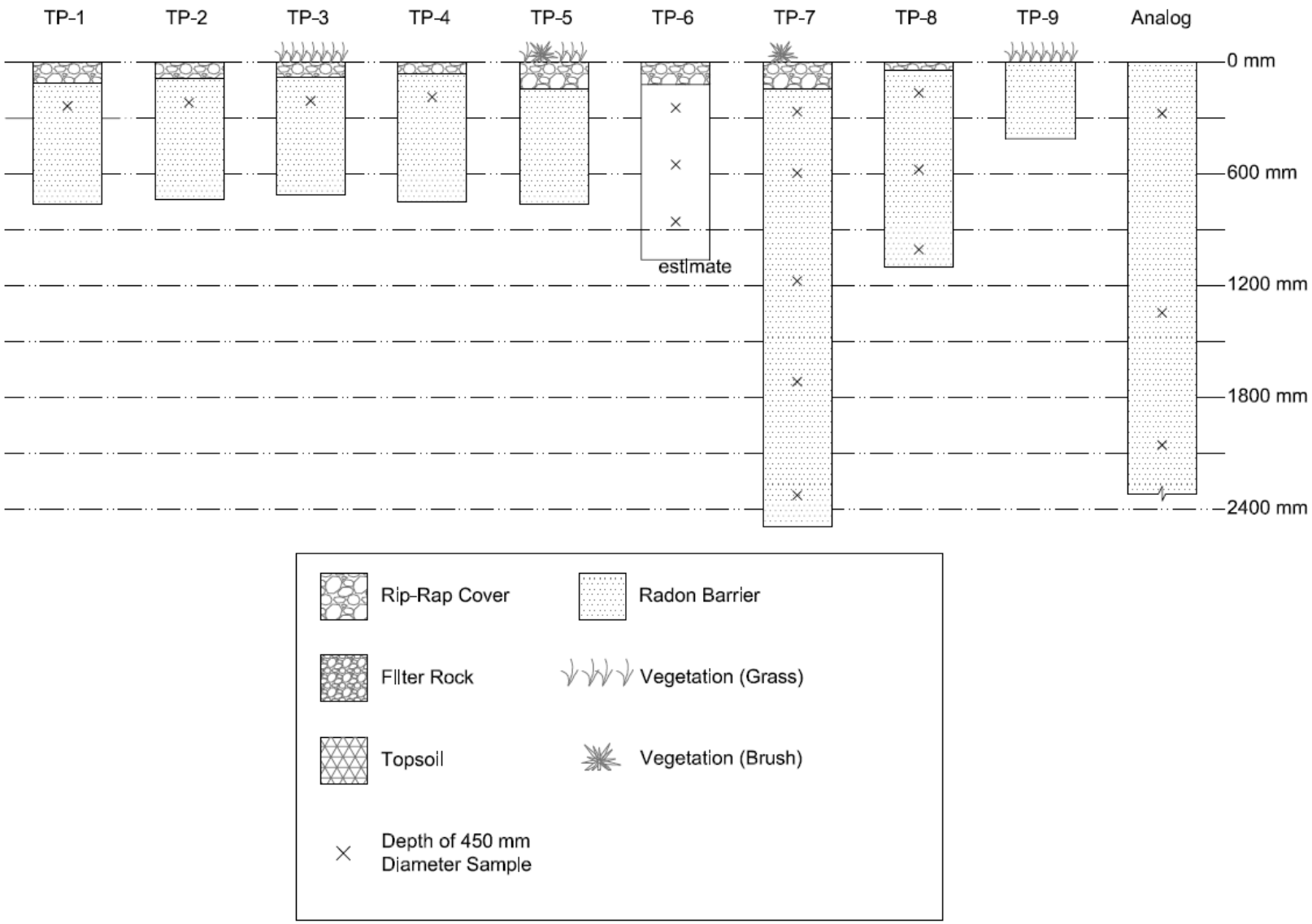

Figure 57 – Cover profiles at each test pit excavated at the Bluewater, NM site in 2016.

Table 18 – Summary of 350 mm Diameter Block Samples Collected at the Bluewater, NM Site in 2016.

Test Pit	Sample Designation	Depth of Top of Block Sample bgs (m)	Depth of Bottom of Block Sample bgs (m)	% Gravel	% Sand	% Fines	% Clay	LL	PL	PI	G_s	XRD
1	A	0.11	0.36	0	65	35	18	-	-	-	-	-
2	A	0.11	0.36	0	32	68	NM	-	-	-	-	-
3	A	0.11	0.36	0	66	34	12	-	-	-	-	-
4	A	0.11	0.36	0	65	34	11	28	15	13	-	-
5	No Block Samples Obtained							-	-	-	-	x
6	B (TOP)	0.11	0.36	0	52	48	NM	-	-	-	-	-
	A*	0.41	0.67	1	64	35	17	28	18	10	2.60	-
	C (BOT)	0.72	0.97	0	53	47	26	33	16	17	-	-
7	A	0.11	0.36	0	72	28	NM	-	-	-	-	-
	B	0.44	0.69	0	57	43	NM	-	-	-	-	-
	C	1.02	1.27	0	60	40	14	32	15	17	-	-
	D	1.56	1.81	0	60	40	NM	-	-	-	-	-
	E	2.17	2.42	0	58	42	NM	-	-	-	-	-
8	A	0.11	0.36	0	70	30	12	-	-	-	-	-
	B	0.52	0.77	1	57	42	NM	-	-	-	-	x
	C	0.95	1.20	0	64	36	NM	-	-	-	2.58	-
9	No Block Samples Obtained							-	-	-	-	-
Analog 3 (Clay Borrow Area)	A	0.15	0.40	0	60	40	NM	35	18	17	-	-
	B	1.22	1.47	0	68	32	NM	22	NP	-	-	-
	C	1.93	2.18	0	51	49	25	33	16	17	-	-

NM = Not Measured

Table 19 – Summary of 70 mm Diameter (Thin-Wall Tube) Samples Collected at the Bluewater, NM Site in 2016.

Test Pit	70 mm Diameter (Shelby Tube) Sample ID	Depth of Top of Sample Below Rn Barrier Surface (m)	Depth of Bottom of Sample Below Rn Barrier Surface (m)	Water Content Profile*
1	A	0.00	0.45	x
	B	0.00	0.44	x
2	A	0.00	0.25	x
	B	0.00	0.50	x
3	A	0.00	0.45	x
	B	0.00	0.50	x
4	A	0.00	0.48	x
	B	0.00	0.47	x
5	A	0.00	0.42	x
	B	0.00	0.40	x
	C	0.00	0.40	x
	D	0.00	0.47	x
6	A	0.00	0.46	x
	B	0.00	NM	
7	A	0.00	0.51	x
	B	0.00	NM	
	C	0.36	0.71	x
	D	1.45	1.87	x
	E	1.83	2.15	x
8	A	0.00	0.51	x
	B	0.00	0.47	x
	C	0.40	0.99	x
	D	0.81	NM	
	E	0.84	1.21	x
	F	1.07	NM	
9	No Thin-Wall Tube Samples Collected			
Analog 3	No Thin-Wall Tube Samples Collected			

* Water content profiles can be found in Appendix C

NM = Not Measured

Table 20 – Summary of Hydraulic Properties from 350 mm Diameter Block Samples Collected at the Bluewater, NM Site in 2016.

Test Pit	Sample Designation	Gravimetric Water Content (%) *	γ_d (kN/m^3)	Saturated Hydraulic Conductivity (m/s) †	Soil Water Characteristic Curve §			
					θ_r	θ_s	α	n
1	A	12.9	18.96	1.34×10^{-8}	-	-	-	-
2	A	10.6	17.63	2.77×10^{-6}	-	-	-	-
3	A	8.1	17.62	2.38×10^{-6}	0.0	28.7	0.1	1.3
4	A	12.7	19.08	4.71×10^{-8}	-	-	-	-
5	No Block Samples Obtained							
6	B (TOP)	10.2	16.97	4.72×10^{-6}	-	-	-	-
	A	7.3	18.08	9.21×10^{-8}				
	C (BOT)	12.7	17.08	1.23×10^{-6}	-	-	-	-
7	A	7.2	16.67	1.62×10^{-6}	-	-	-	-
	B	12.6	17.62	2.21×10^{-6}	0.0	28.0	0.2	1.1
	C	11.3	16.24	3.50×10^{-8}	-	-	-	-
	D	12.8	16.89	7.49×10^{-8}	-	-	-	-
	E	11.5	16.21	1.53×10^{-8}	-	-	-	-
8	A	16.8	15.28	4.90×10^{-7}	-	-	-	-
	B	10.7	16.87	1.75×10^{-6}	-	-	-	-
	C	11.9	17.35	7.77×10^{-7}	-	-	-	-
9	No Block Samples Obtained							
Analog 3 (Clay Borrow Area)	A	8.6	14.38	3.69×10^{-6}	-	-	-	-
	B	3.3	15.44	4.38×10^{-6}	-	-	-	-
	C	8.8	16.04	4.16×10^{-6}	-	-	-	-

* ASTM D 2216

† ASTM D 5084

§ ASTM D 6836 - 02 (Method A and D)

APPENDIX F – GRAVIMETRIC WATER CONTENT PROFILES

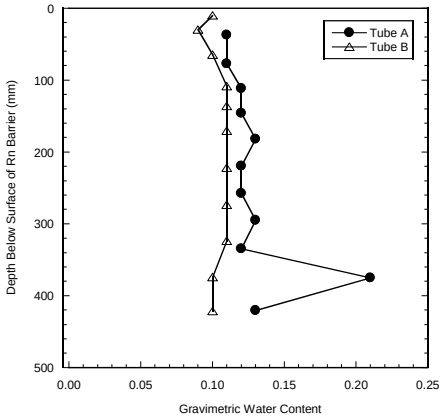

TP-1

Tube A		Tube B	
Depth (mm)	Water Content	Depth (mm)	Water Content
37	0.11	10	0.10
77	0.11	30	0.09
112	0.12	65	0.10
146	0.12	109	0.11
182	0.13	136	0.11
220	0.12	170	0.11
258	0.12	222	0.11
295	0.13	274	0.11
335	0.12	323	0.11
375	0.21	374	0.10
421	0.13	421	0.10
Mean	0.13	Mean	0.10

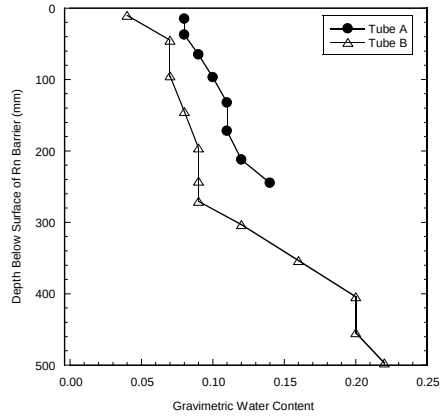

TP-2

Tube A		Tube B	
Depth (mm)	Water Content	Depth (mm)	Water Content
15	0.08	10	0.04
37	0.08	45	0.07
65	0.09	95	0.07
97	0.10	145	0.08
133	0.11	196	0.09
172	0.11	242	0.09
212	0.12	271	0.09
245	0.14	303	0.12
Mean	0.10	354	0.16
		404	0.20
		455	0.20
		497	0.22
		Mean	0.12

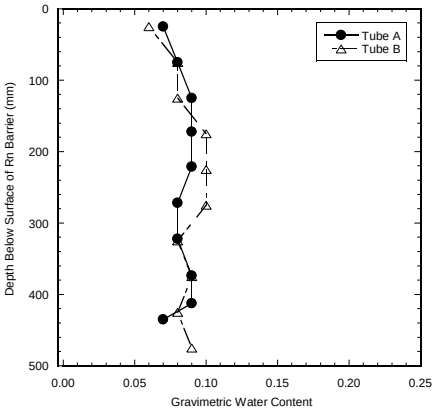

TP-3

Tube A		Tube B	
Depth (mm)	Water Content	Depth (mm)	Water Content
25	0.07	25	0.06
75	0.08	75	0.08
125	0.09	125	0.08
172	0.09	175	0.10
221	0.09	225	0.10
272	0.08	275	0.10
322	0.08	325	0.08
374	0.09	375	0.09
412	0.09	425	0.08
435	0.07	475	0.09
Mean	0.08	Mean	0.08

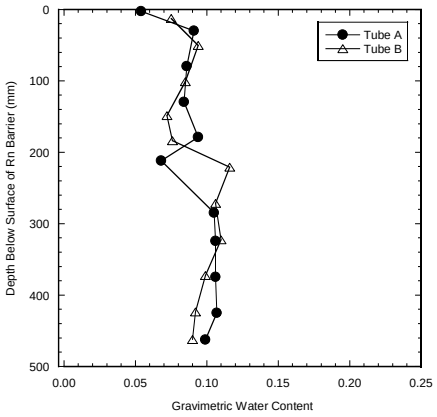

TP-4

Tube A		Tube B	
Depth (mm)	Water Content	Depth (mm)	Water Content
3	0.05	13	0.08
30	0.09	50	0.09
80	0.09	101	0.09
129	0.08	149	0.07
179	0.09	184	0.08
212	0.07	221	0.12
285	0.10	272	0.11
324	0.11	323	0.11
375	0.11	373	0.10
425	0.11	424	0.09
463	0.10	462	0.09
Mean	0.09	Mean	0.09

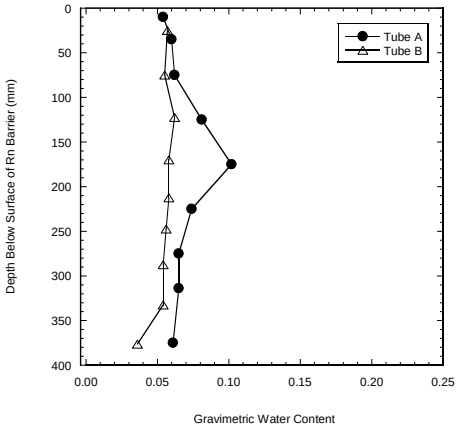

TP-5

Tube A		Tube B	
Depth (mm)	Water Content	Depth (mm)	Water Content
10	0.05	25	0.06
35	0.06	75	0.06
75	0.06	123	0.06
125	0.08	170	0.06
175	0.10	213	0.06
225	0.07	248	0.06
275	0.07	288	0.05
314	0.06	333	0.05
375	0.06	377	0.04
Mean	0.07	Mean	0.05

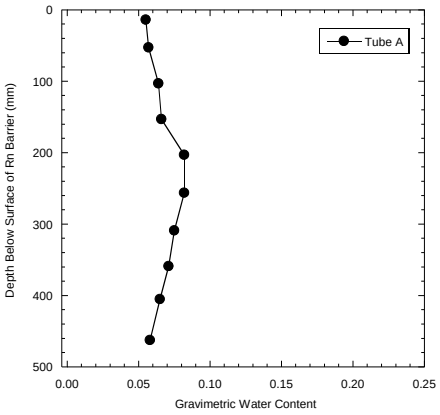

TP-6

Tube A	
Depth (mm)	Water Content
14	0.05
53	0.06
103	0.06
153	0.07
203	0.08
256	0.08
309	0.08
359	0.07
405	0.07
463	0.06
Mean	0.07

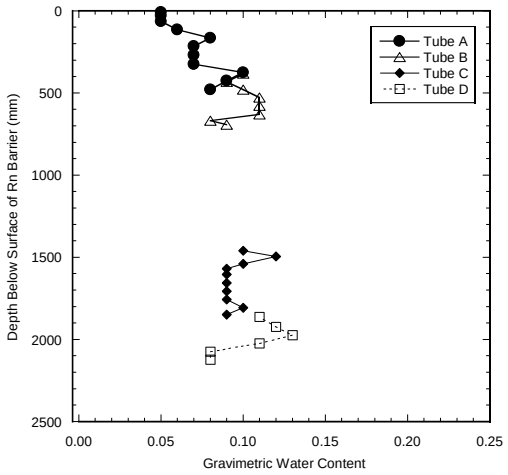

TP-7

Tube A

Depth (mm)	Water Content
10	0.05
30	0.05
65	0.05
115	0.06
165	0.08
215	0.07
269	0.07
324	0.07
375	0.10
425	0.09
480	0.08
Mean	0.07

Tube B

Depth (mm)	Water Content
383	0.10
432	0.09
479	0.10
529	0.11
579	0.11
630	0.11
668	0.08
693	0.09
Mean	0.10

Tube C

Depth (mm)	Water Content
1460	0.10
1495	0.12
1541	0.10
1569	0.09
1604	0.09
1656	0.09
1707	0.09
1758	0.09
1808	0.10
1850	0.09
Mean	0.10

Tube D

Depth (mm)	Water Content
1864	0.11
1924	0.12
1974	0.13
2024	0.11
2074	0.08
2124	0.08
Mean	0.10

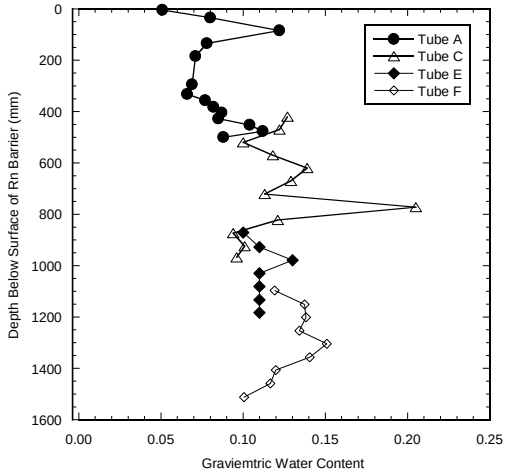

TP-8

Tube A

Depth (mm)	Water Content
5	0.05
35	0.08
85	0.12
135	0.08
185	0.07
295	0.07
333	0.07
358	0.08
383	0.08
405	0.09
428	0.08
453	0.10
478	0.11
500	0.09
Mean	0.08

Tube C

Depth (mm)	Water Content
420	0.13
470	0.12
520	0.10
570	0.12
620	0.14
670	0.13
721	0.11
772	0.20
822	0.12
873	0.09
925	0.10
968	0.10
Mean	0.12

Tube E

Depth (mm)	Water Content
871	0.10
928	0.11
979	0.13
1030	0.11
1081	0.11
1133	0.11
1184	0.11
Mean	0.11

Tube F

Depth (mm)	Water Content
1097	0.1191
1151	0.1373
1202	0.1383
1254	0.1343
1305	0.1509
1357	0.1405
1407	0.1198
1459	0.1165
1512	0.1005
Mean	0.13

APPENDIX G – DRY DENSITY PROFILES

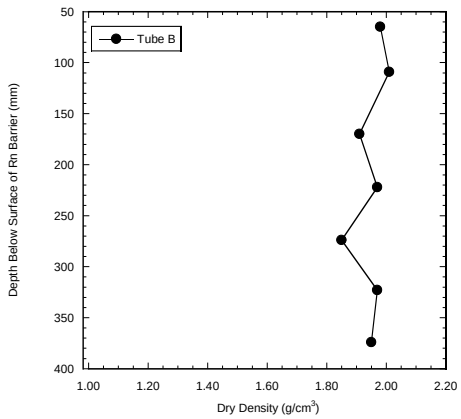

TP-1
Tube B

Depth (mm)	Dry Density (g/cm^3)
65	1.98
109	2.01
170	1.91
222	1.97
274	1.85
323	1.97
374	1.95
Mean	1.95

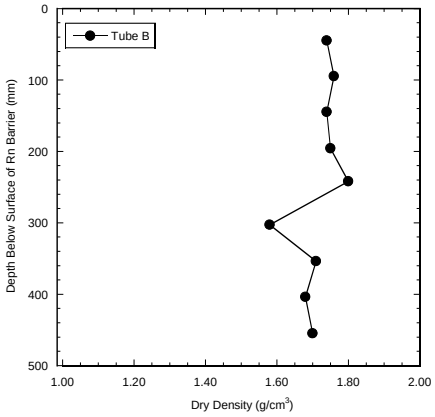

TP-2
Tube B

Depth (mm)	Dry Density (g/cm^3)
45	1.74
95	1.76
145	1.74
196	1.75
242	1.80
303	1.58
354	1.71
404	1.68
455	1.70
Mean	1.72

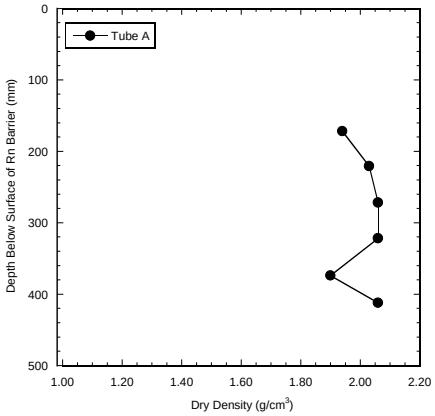

TP-3
Tube A

Depth (mm)	Dry Density (g/cm^3)
172	1.94
221	2.03
272	2.06
322	2.06
374	1.90
412	2.06
Mean	2.01

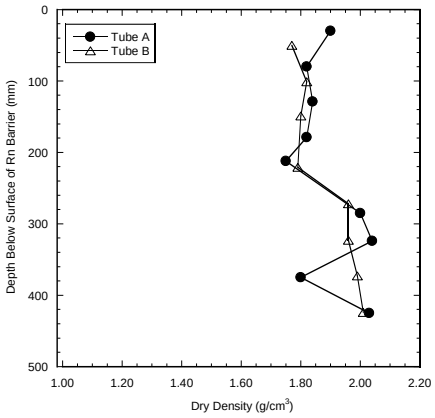

TP-4

Tube A		Tube B	
Depth (mm)	Dry Density (g/cm^3)	Depth (mm)	Dry Density (g/cm^3)
30	1.90	50	1.77
80	1.82	101	1.82
129	1.84	149	1.80
179	1.82	221	1.79
212	1.75	272	1.96
285	2.00	323	1.96
324	2.04	373	1.99
375	1.80	424	2.01
425	2.03	Mean	1.89
Mean	1.89		

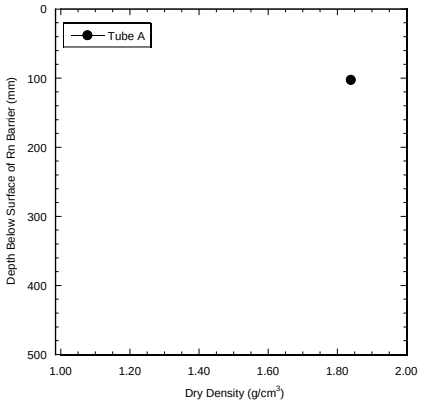

TP-6

Tube A

Depth (mm)	Dry Density (g/cm^3)
103	1.84

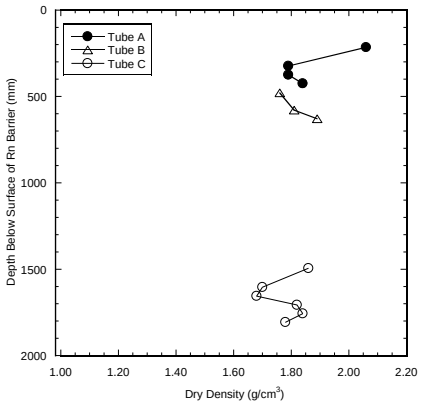

TP-7

Tube A		Tube B		Tube C	
Depth (mm)	Dry Density (g/cm^3)	Depth (mm)	Dry Density (g/cm^3)	Depth (mm)	Dry Density (g/cm^3)
215	2.06	479	1.76	1495	1.86
324	1.79	579	1.81	1604	1.70
375	1.79	630	1.89	1656	1.68
425	1.84	Mean	1.82	1707	1.82
Mean	1.87			1758	1.84
				1808	1.78
				Mean	1.78

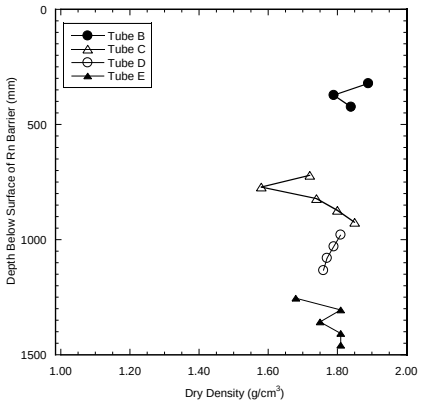

TP-8

Tube B

Depth (mm)	Dry Density (g/cm^3)
322	1.89
373	1.79
424	1.84
Mean	1.84

Tube C

Depth (mm)	Dry Density (g/cm^3)
721	1.72
772	1.58
822	1.74
873	1.80
925	1.85
Mean	1.74

Tube D

Depth (mm)	Dry Density (g/cm^3)
979	1.81
1030	1.79
1081	1.77
1133	1.76
Mean	1.78

Tube E

Depth (mm)	Dry Density (g/cm^3)
1254	1.68
1305	1.81
1357	1.75
1407	1.81
1459	1.81
Mean	1.77

APPENDIX H – SATURATION PROFILES

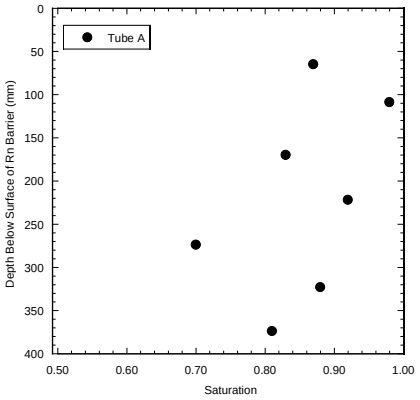

TP-1
Tube B

Depth (mm)	Saturation
65	0.87
109	0.98
170	0.83
222	0.92
274	0.70
323	0.88
374	0.81
Mean	0.86

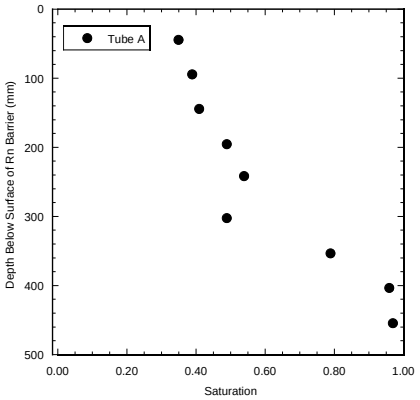

TP-2
Tube B

Depth (mm)	Saturation
45	0.35
95	0.39
145	0.41
196	0.49
242	0.54
303	0.49
354	0.79
404	0.96
455	0.97
Mean	0.60

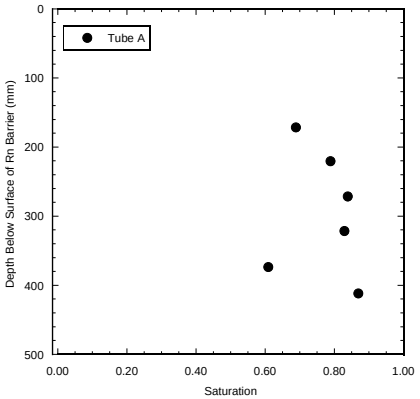

TP-3
Tube A

Depth (mm)	Saturation
172	0.69
221	0.79
272	0.84
322	0.83
374	0.61
412	0.87
Mean	0.77

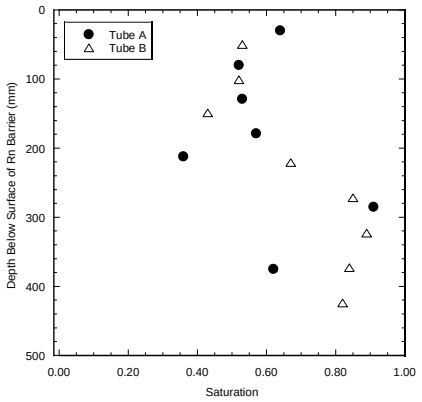

TP-4

Tube A

Depth (mm)	Saturation
30	0.64
80	0.52
129	0.53
179	0.57
212	0.36
285	0.91
324	1.02
375	0.62
425	1.01
Mean	0.69

Tube B

Depth (mm)	Saturation
50	0.53
101	0.52
149	0.43
221	0.67
272	0.85
323	0.89
373	0.84
424	0.82
Mean	0.69

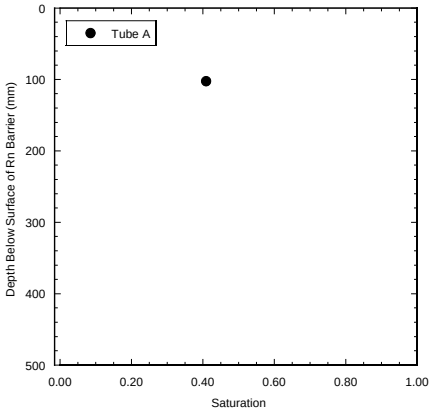

TP-6

Tube A

Depth (mm)	Saturation
103	0.41

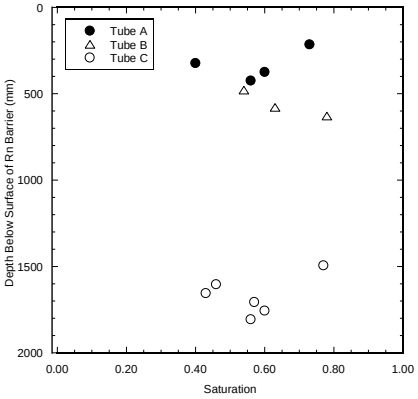

TP-7

Tube A

Depth (mm)	Saturation
215	0.73
324	0.40
375	0.60
425	0.56
Mean	0.57

Tube B

Depth (mm)	Saturation
479	0.54
579	0.63
630	0.78
Mean	0.65

Tube C

Depth (mm)	Saturation
1495	0.77
1604	0.46
1656	0.43
1707	0.57
1758	0.60
1808	0.56
Mean	0.57

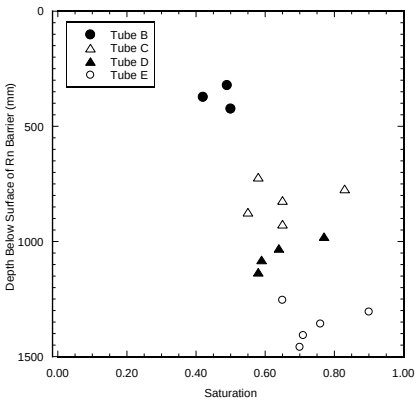

TP-8

Tube B

Depth (mm)	Saturation
322	0.49
373	0.42
424	0.50
Mean	0.47

Tube C

Depth (mm)	Saturation
721	0.58
772	0.83
822	0.65
873	0.55
925	0.65
Mean	0.65

Tube D

Depth (mm)	Saturation
979	0.77
1030	0.64
1081	0.59
1133	0.58
Mean	0.65

Tube E

Depth (mm)	Saturation
1254	0.65
1305	0.90
1357	0.76
1407	0.71
1459	0.70
Mean	0.74

APPENDIX I – RADON CONCENTRATION BUILDUP CURVES

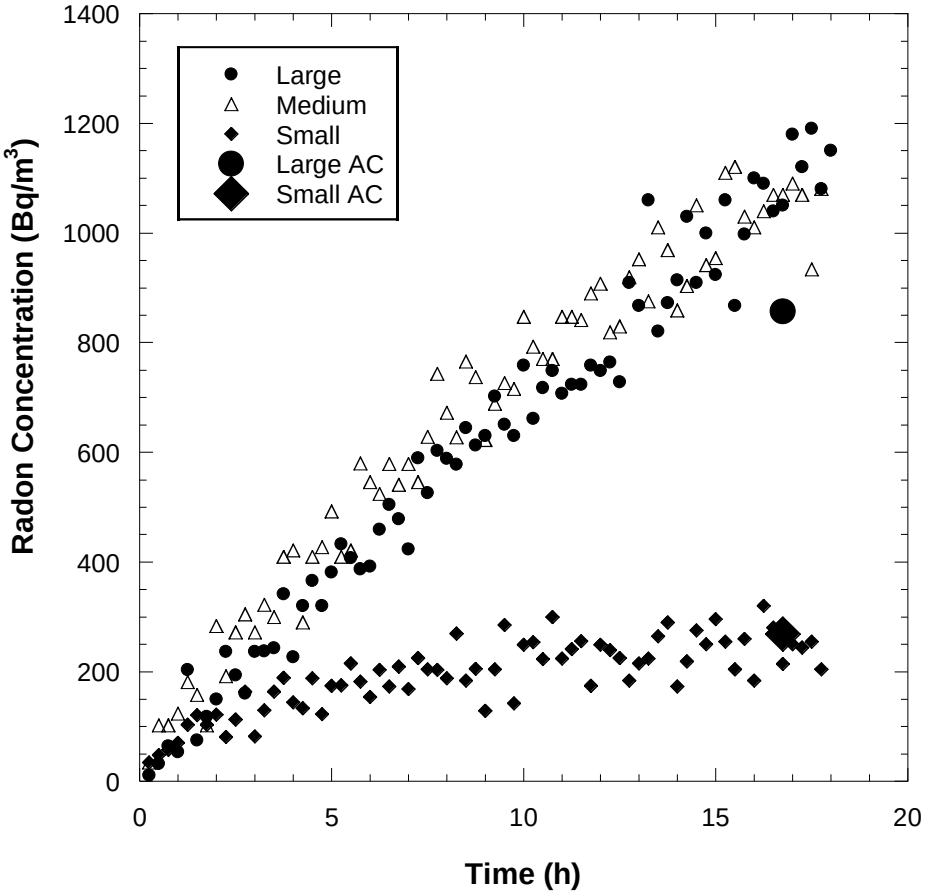

Fig. P58 – Radon concentration buildup curves measured at TP-1A at Bluewater, NM.

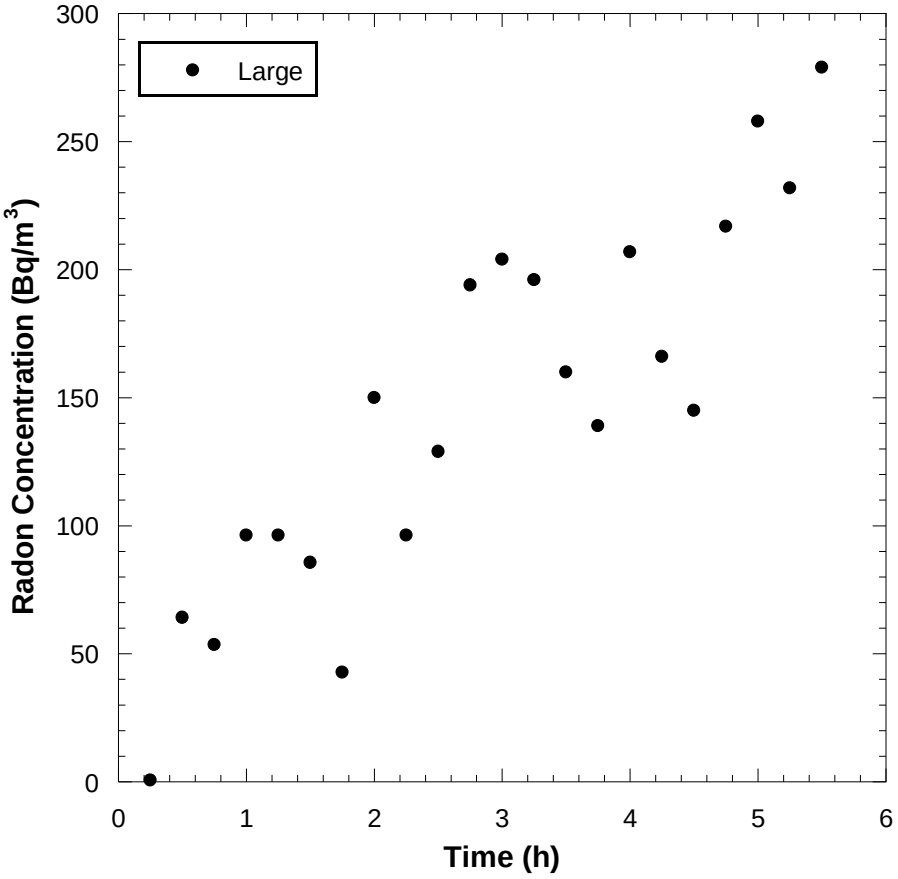

Fig. P59 - Radon concentration buildup curve measured at TP-1B at Bluewater, NM.

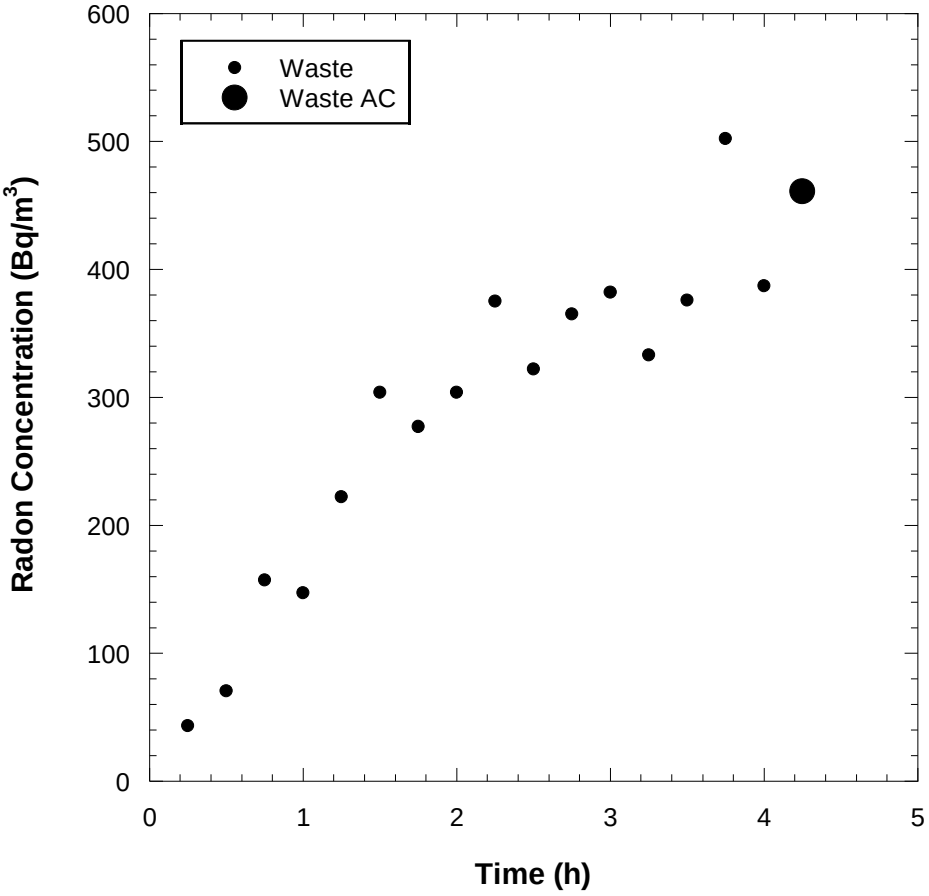

Fig. P60 – Radon concentration buildup curve measured from tailings at TP-1 at Bluewater, NM.

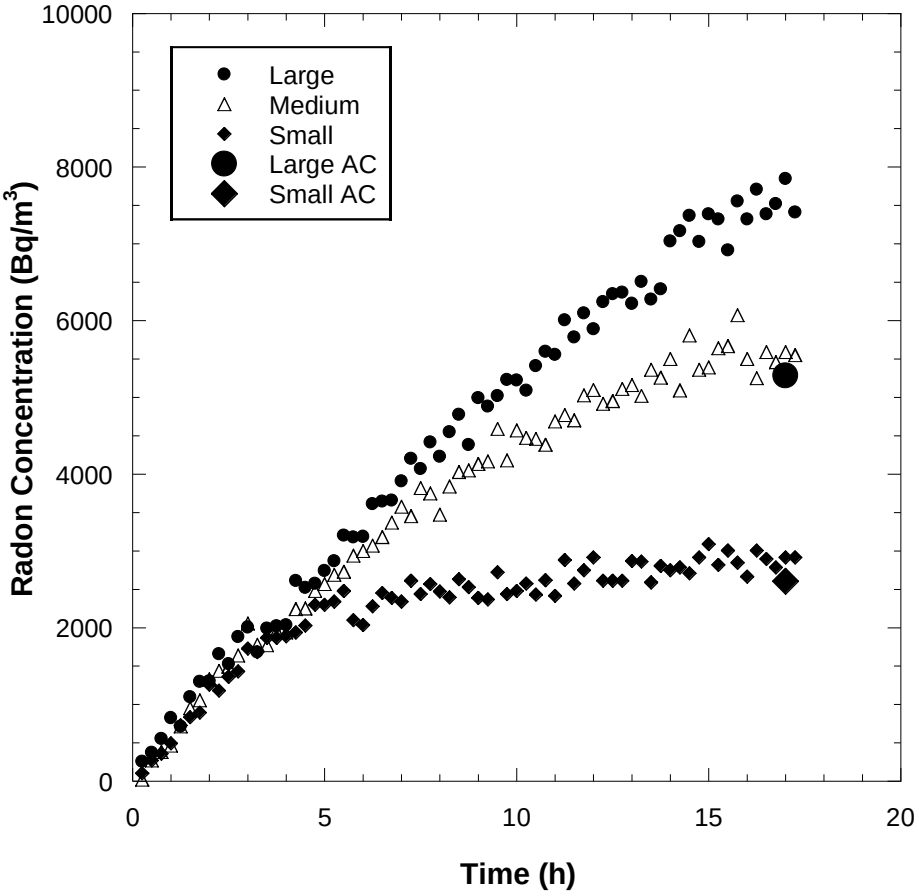

Fig. P61 -– Radon concentration buildup curve measured TP-2A at Bluewater, NM.

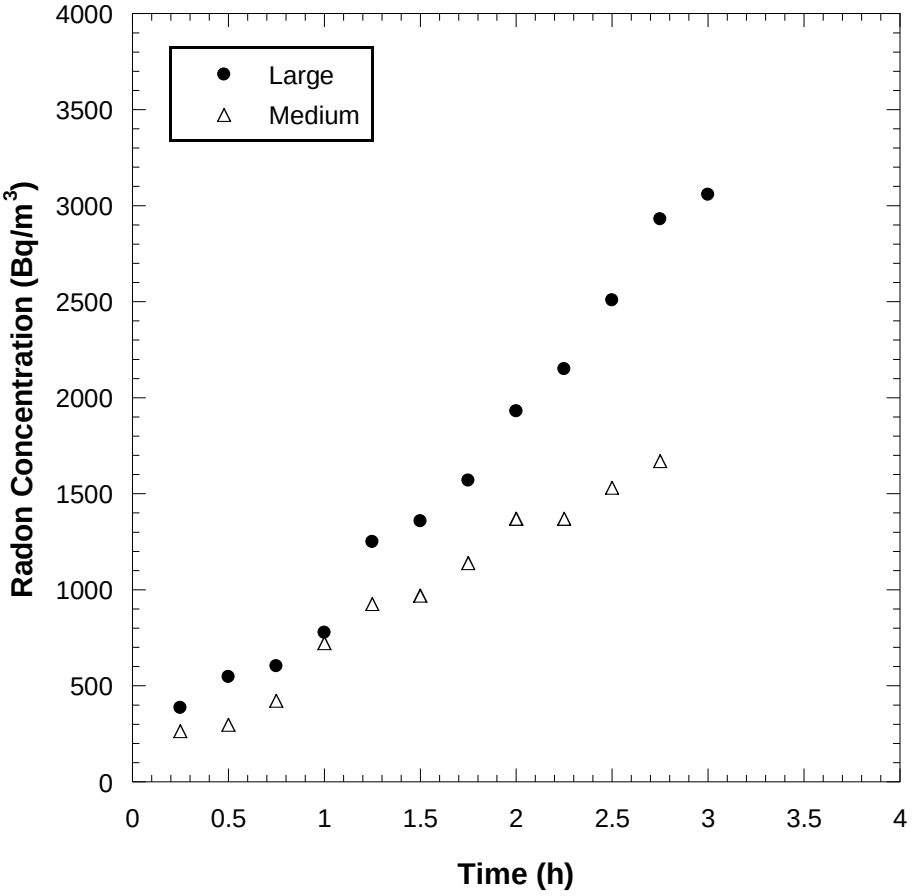

Fig. P62 - Radon concentration buildup curve measured at TP-2B at Bluewater, NM.

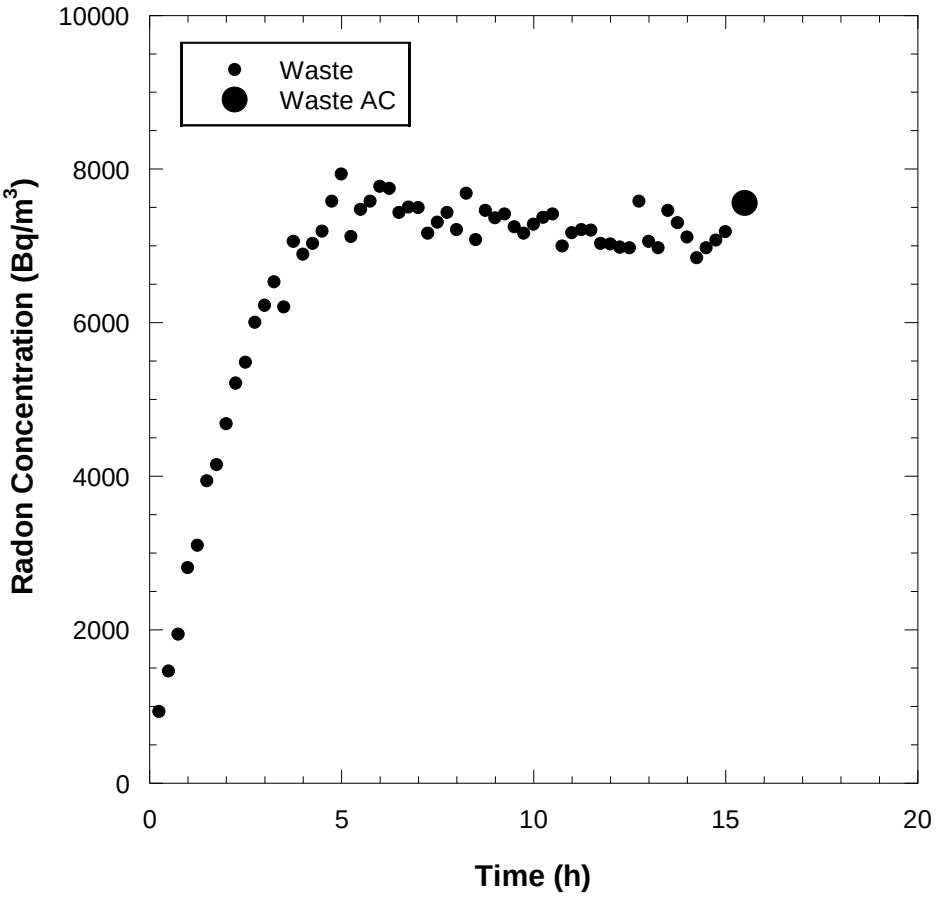

Fig. P63 – Radon concentration buildup curve measured from tailings at TP-2 at Bluewater, NM.

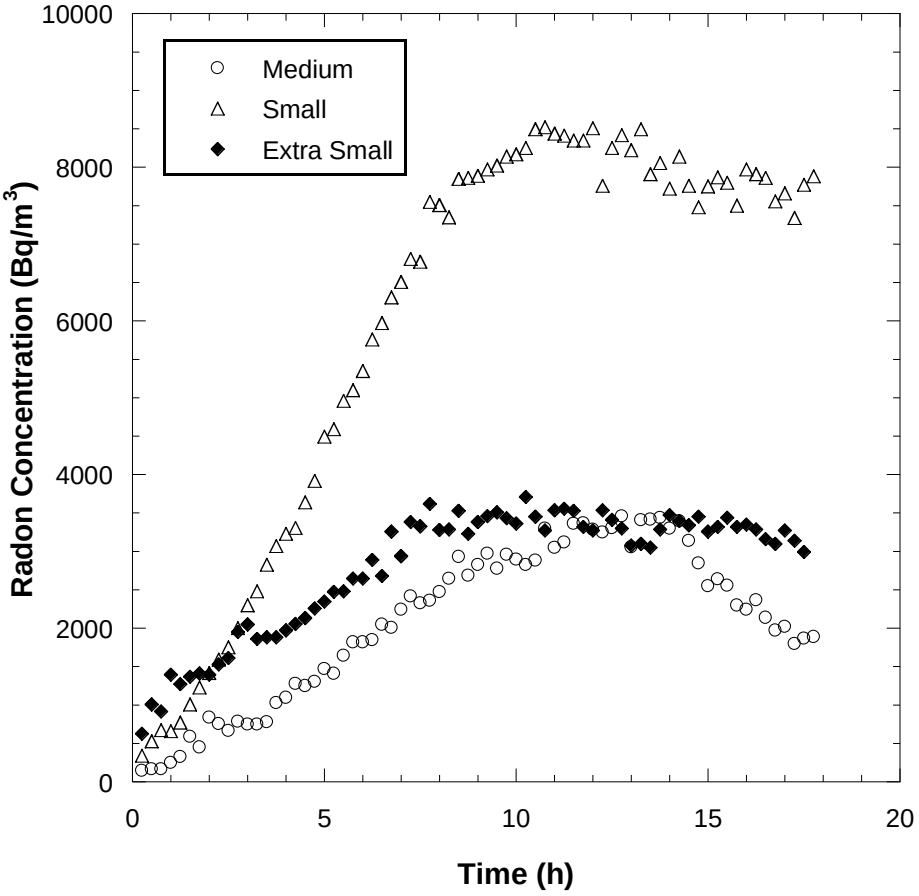

Fig. P64 – Radon concentration buildup curves measured at TP-3A at Bluewater, NM.

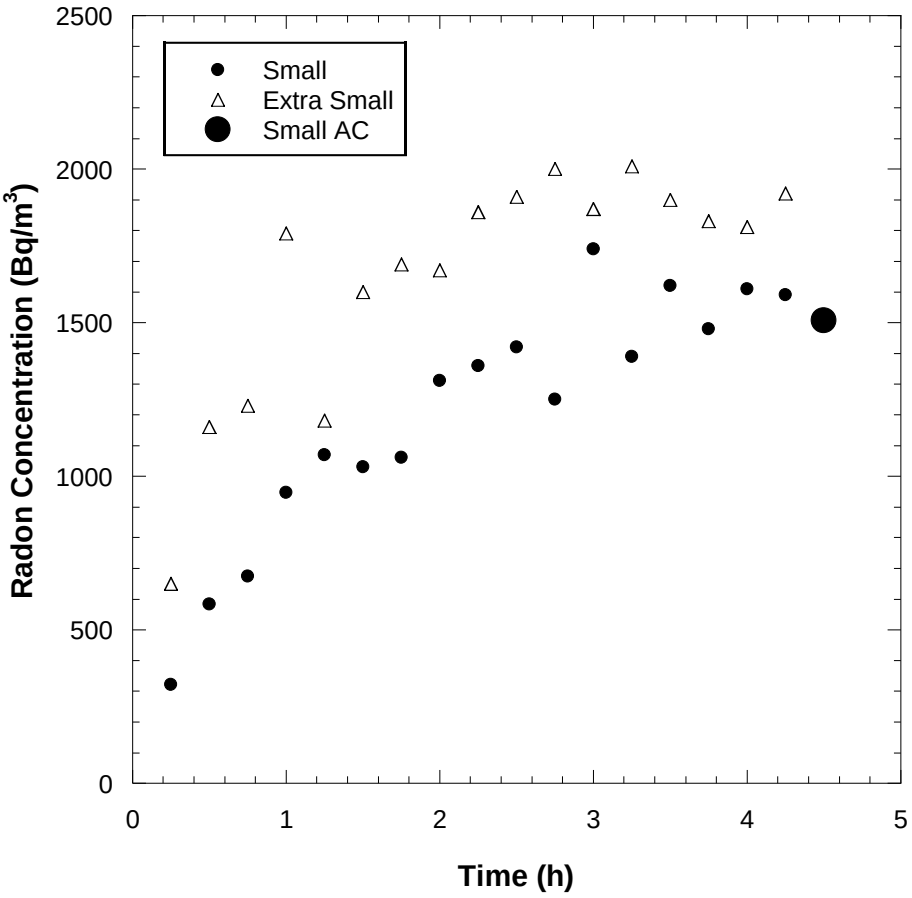

Fig. P65 – Radon concentration buildup curves measured at TP-3B at Bluewater, NM.

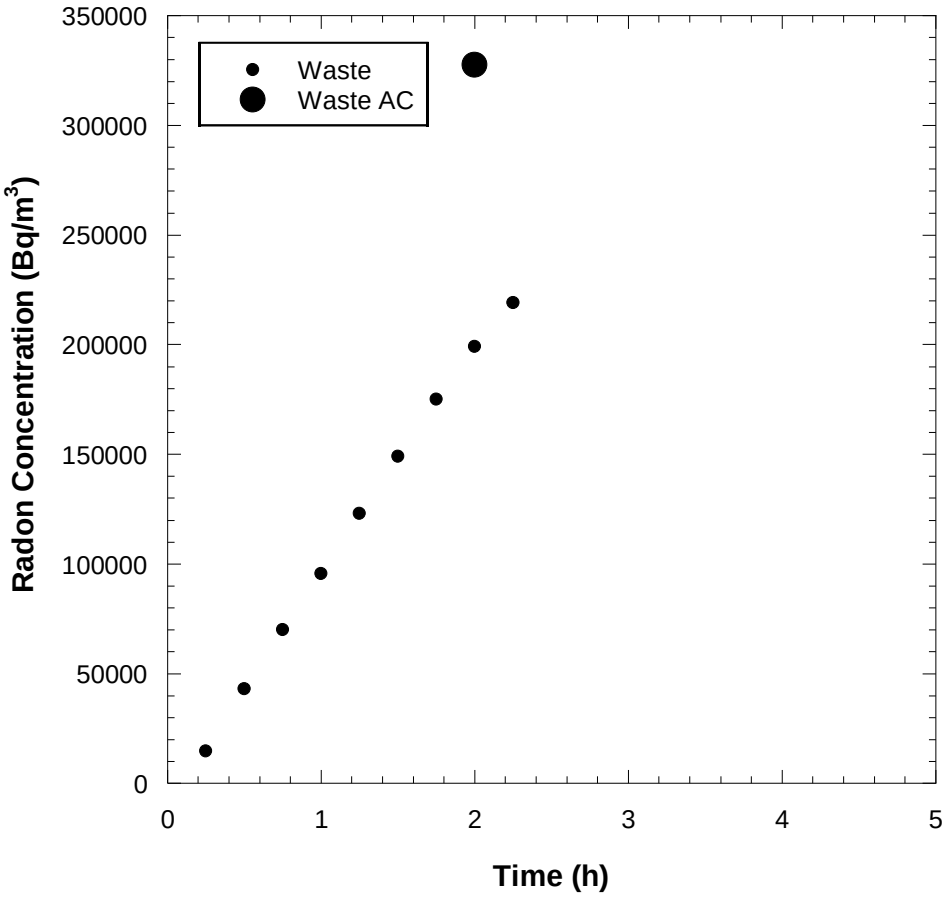

Fig. P66 – Radon concentration buildup curve measured from tailings at TP-3 at Bluewater, NM.

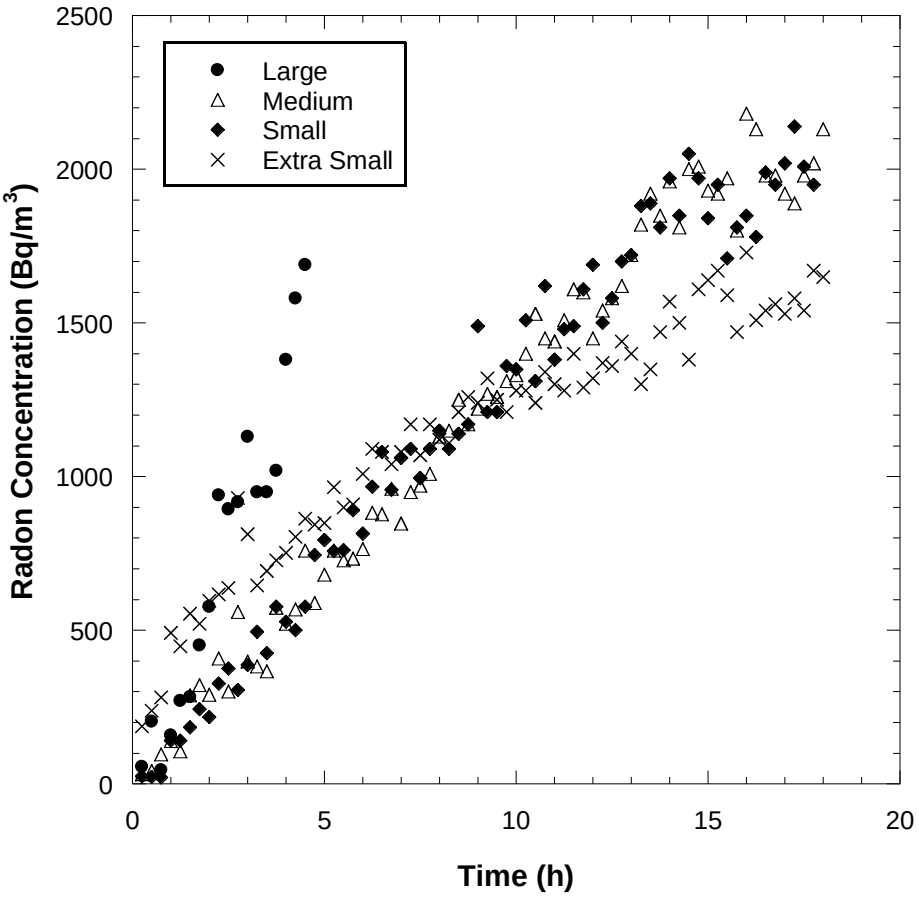

Fig. P67 – Radon concentration buildup curves measured at TP-4A at Bluewater, NM.

.

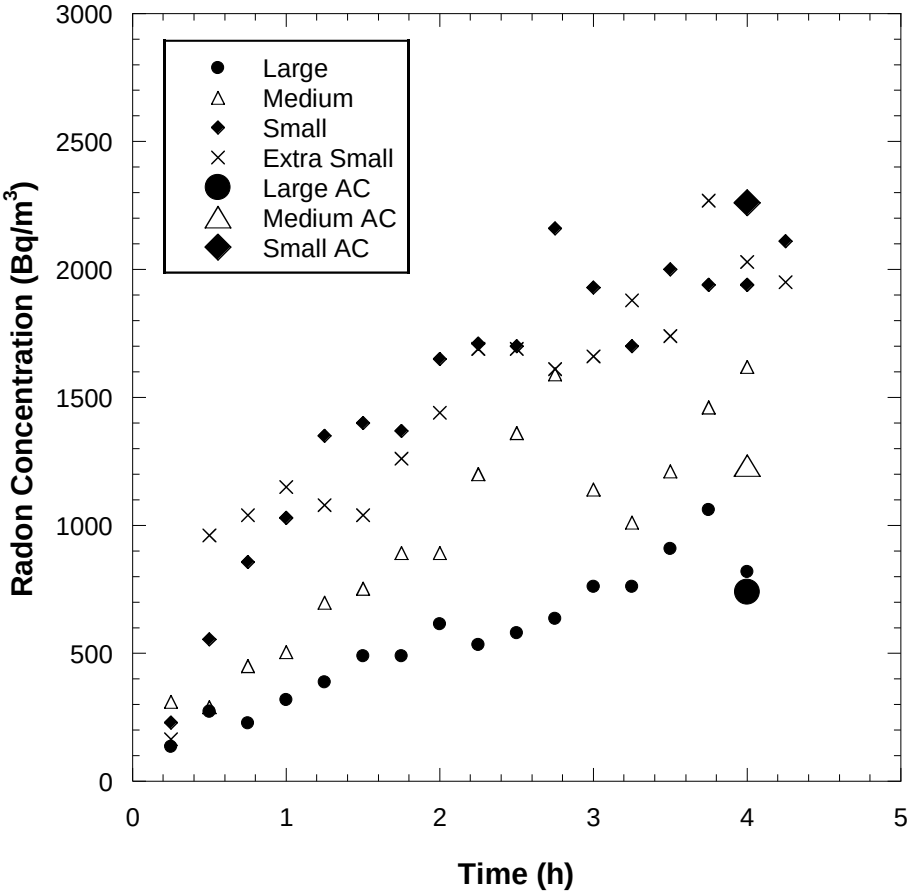

Fig. P68 – Radon concentration buildup curves measured at TP-4B at Bluewater, NM.

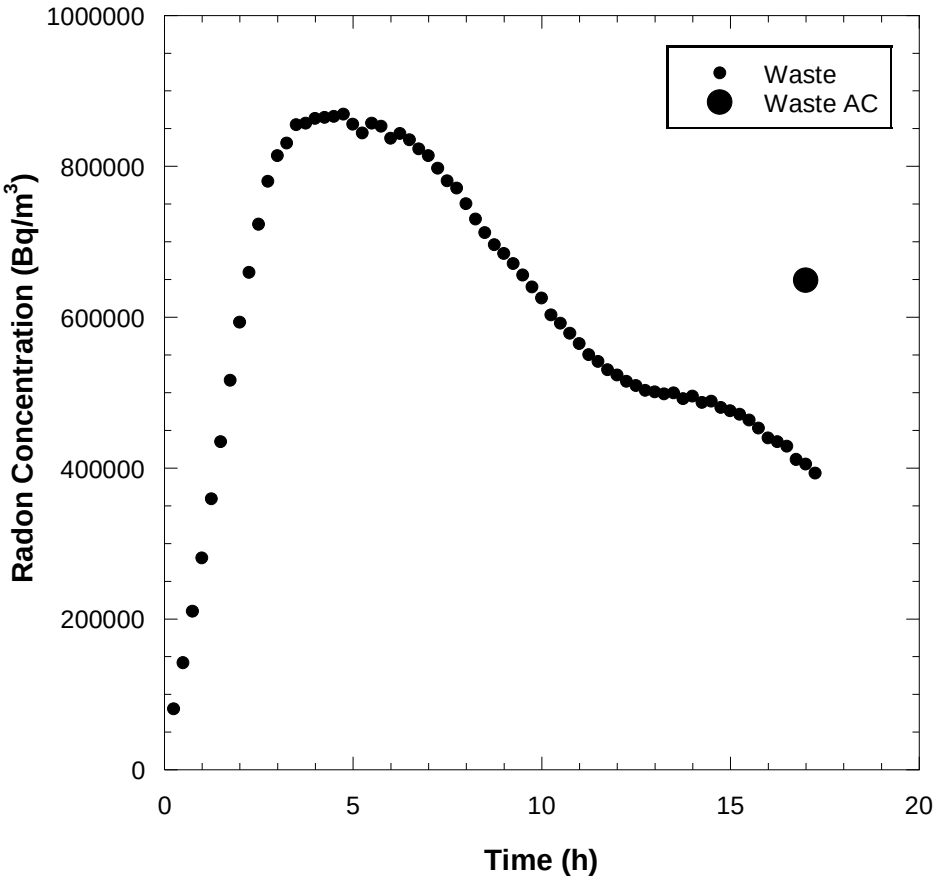

Fig. P69 – Radon concentration buildup curve measured from tailings at TP-4 at Bluewater, NM.

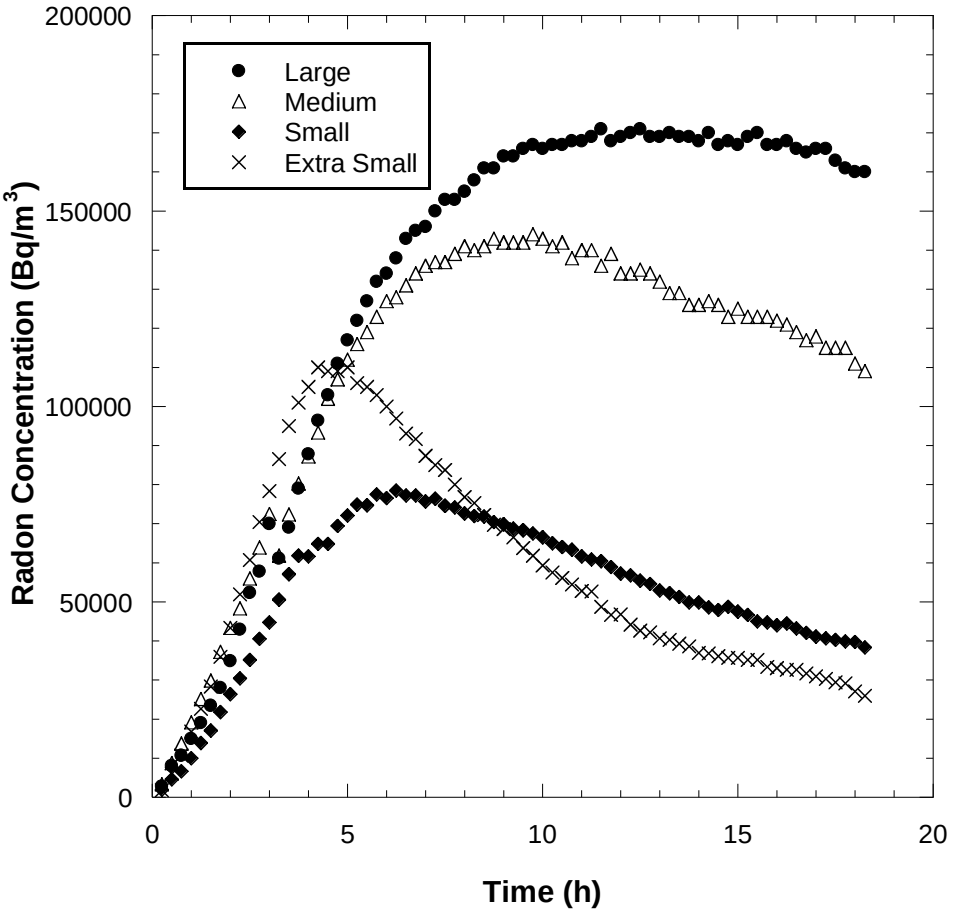

Fig. P70 – Radon concentration buildup curves measured at TP-5A at Bluewater, NM.

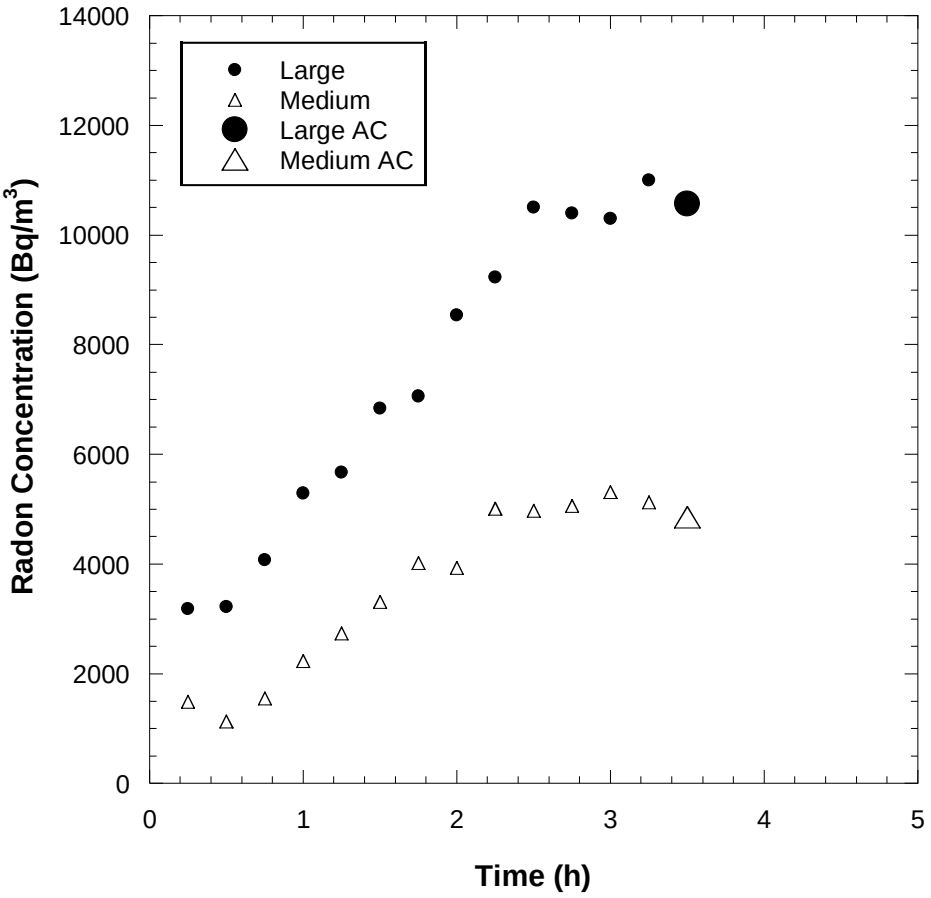

Fig. P71 – Radon concentration buildup curves measured at TP-5B at Bluewater, NM.

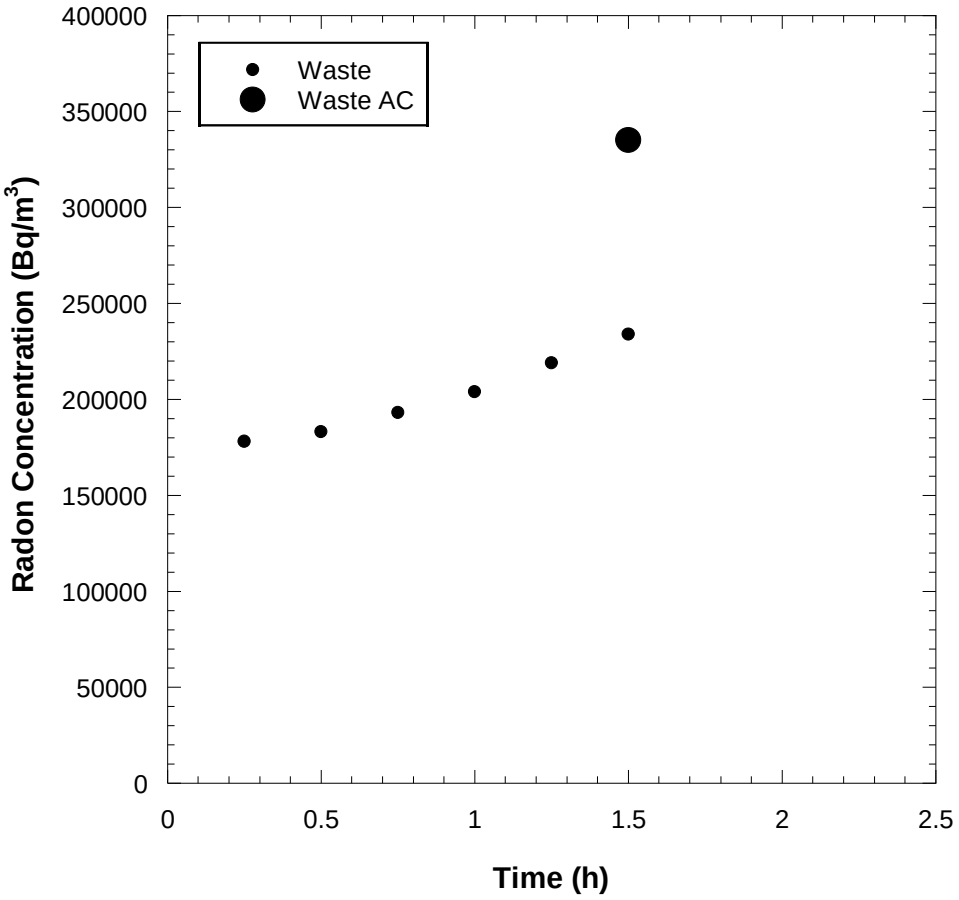

Fig. P72 – Radon concentration buildup curve measured from tailings at TP-5 at Bluewater, NM.

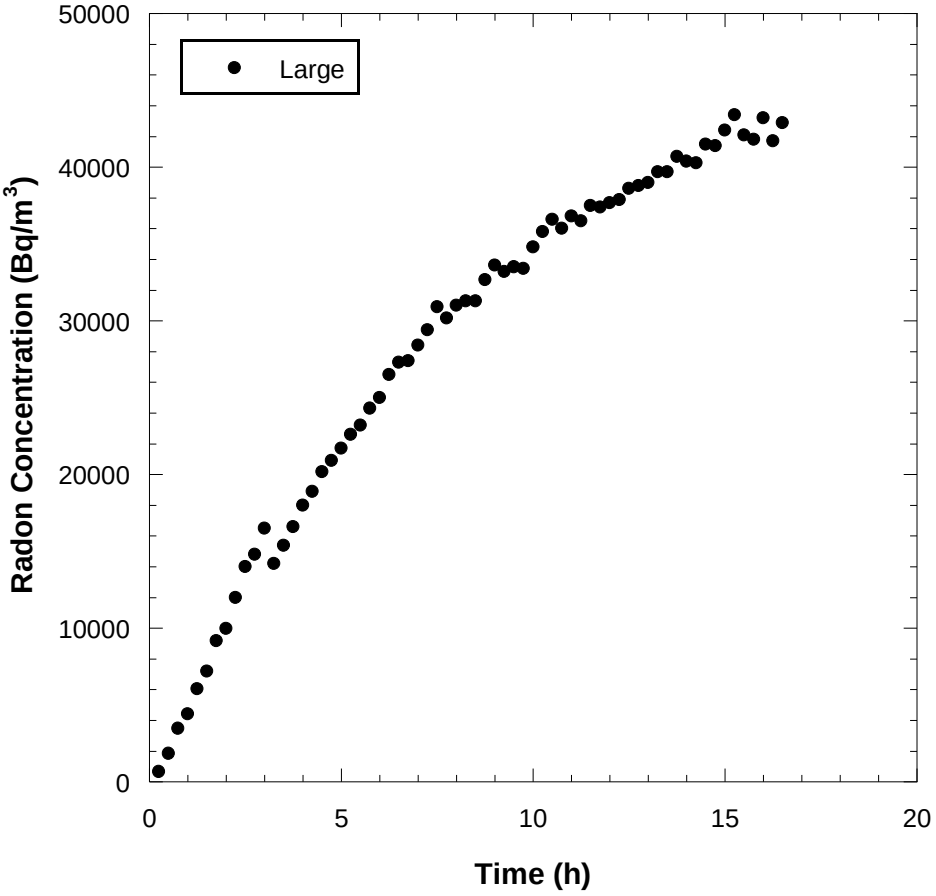

Fig. P73 – Radon concentration buildup curve measured at TP-6 at Bluewater, NM.

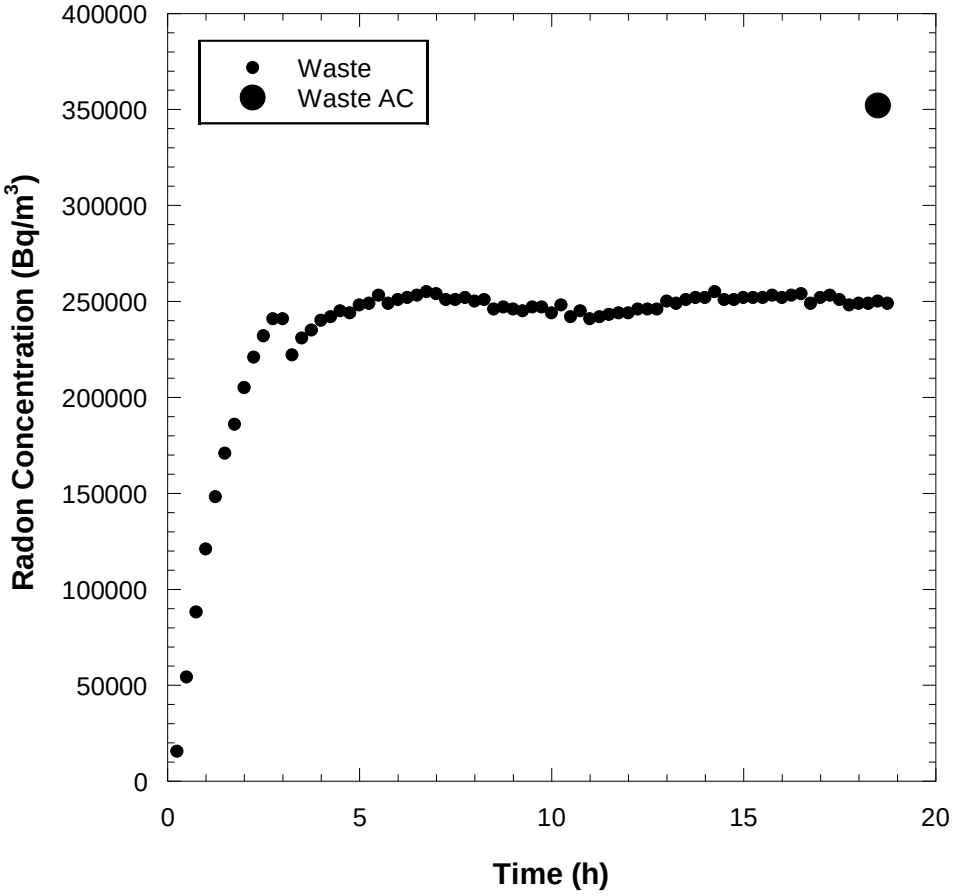

Fig. P74 – Radon concentration buildup curve measured from tailings at TP-6 at Bluewater, NM.

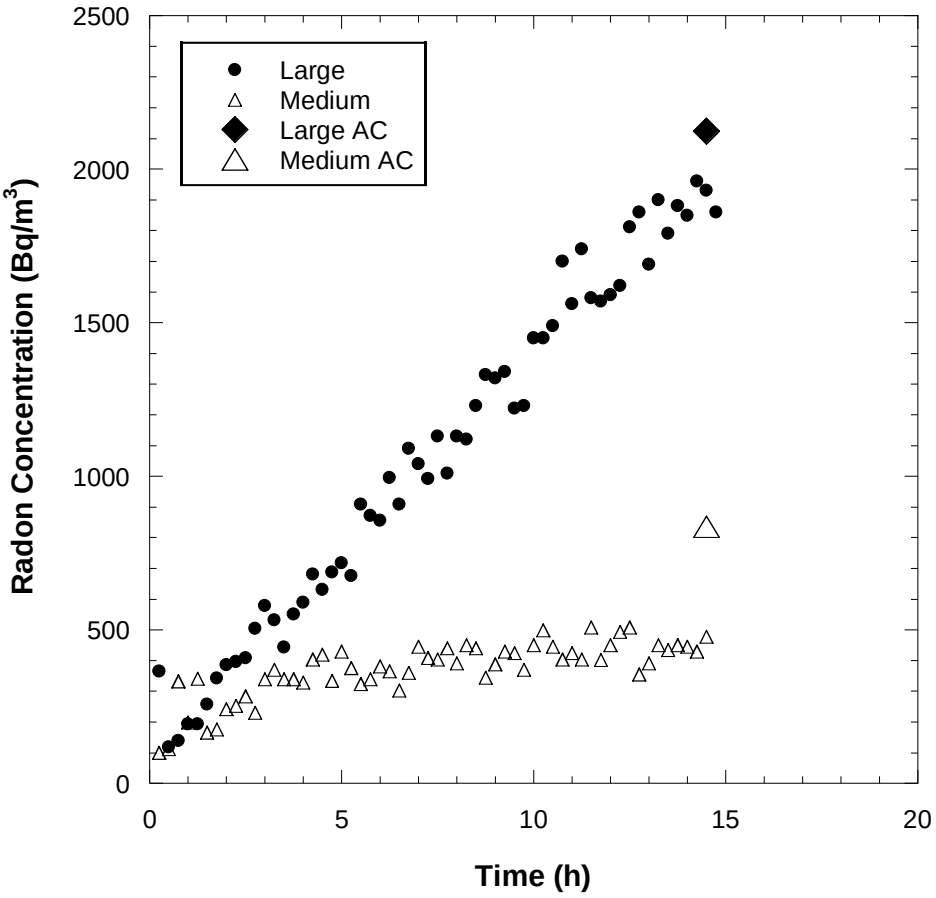

Fig. P75 – Radon concentration buildup curves measured at TP-7 at Bluewater, NM.

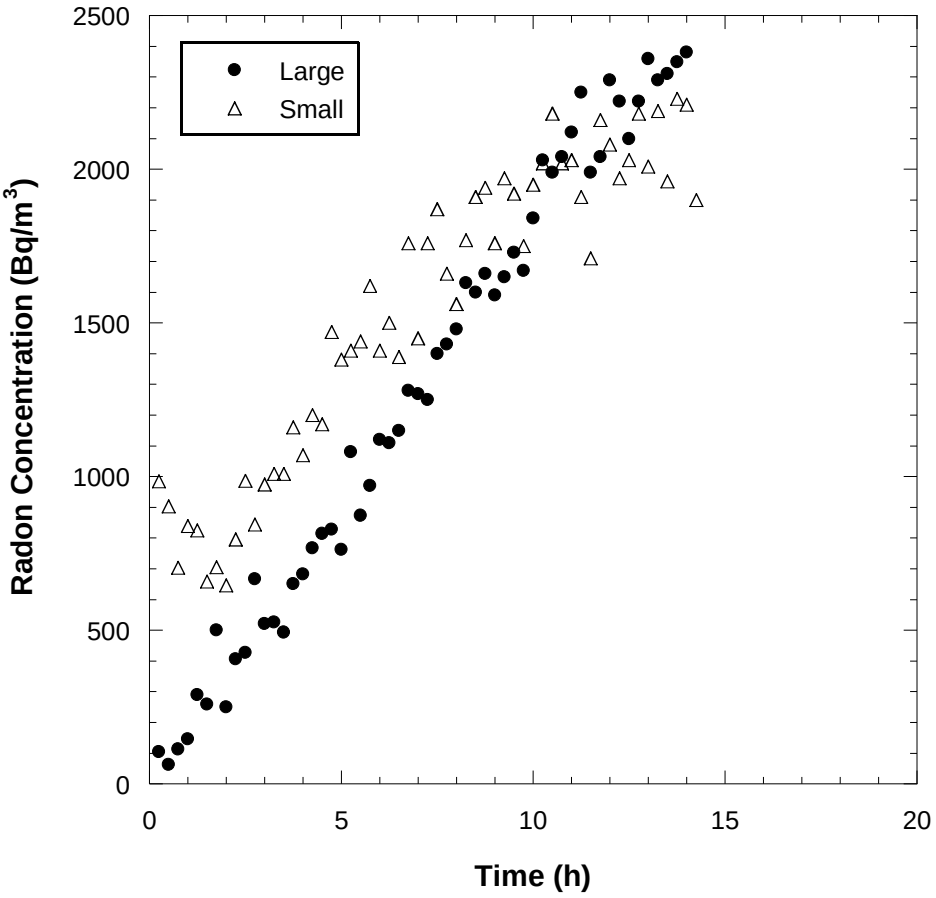

Fig. P76 – Radon concentration buildup curves measured at TP-8 at Bluewater, NM.

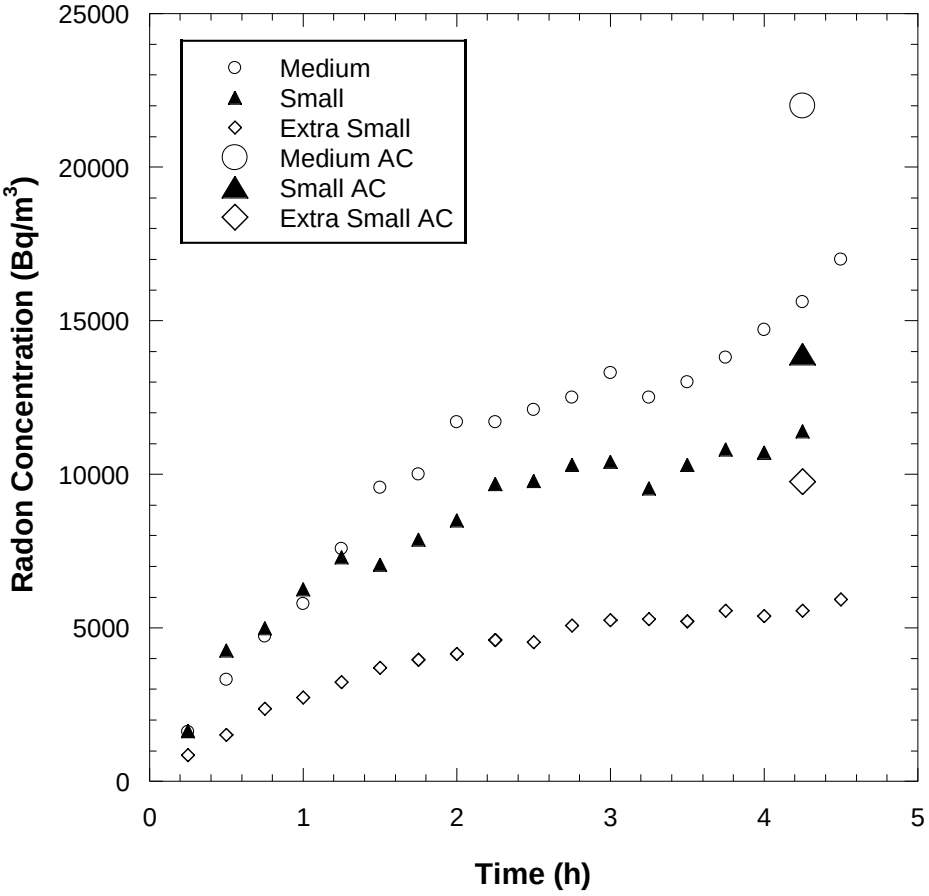

Fig. P77 – Radon concentration buildup curves measured at TP-9A at Bluewater, NM.

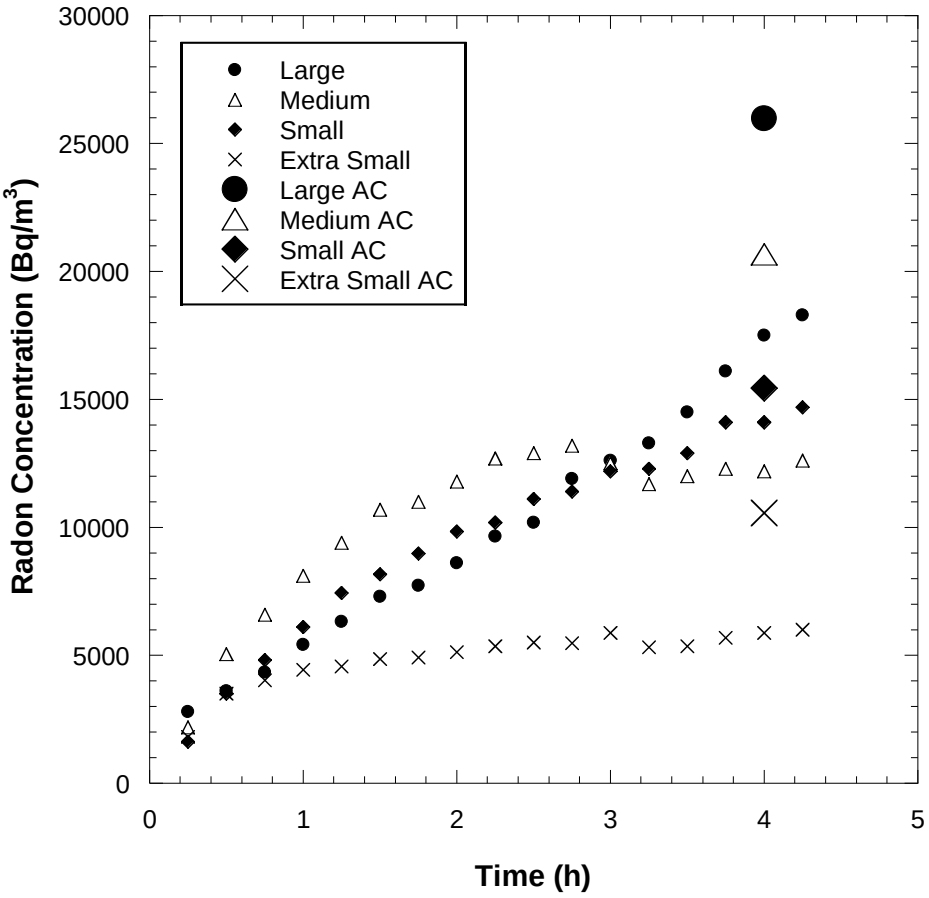

Fig. P78 – Radon concentration buildup curves measured at TP-9B at Bluewater, NM.

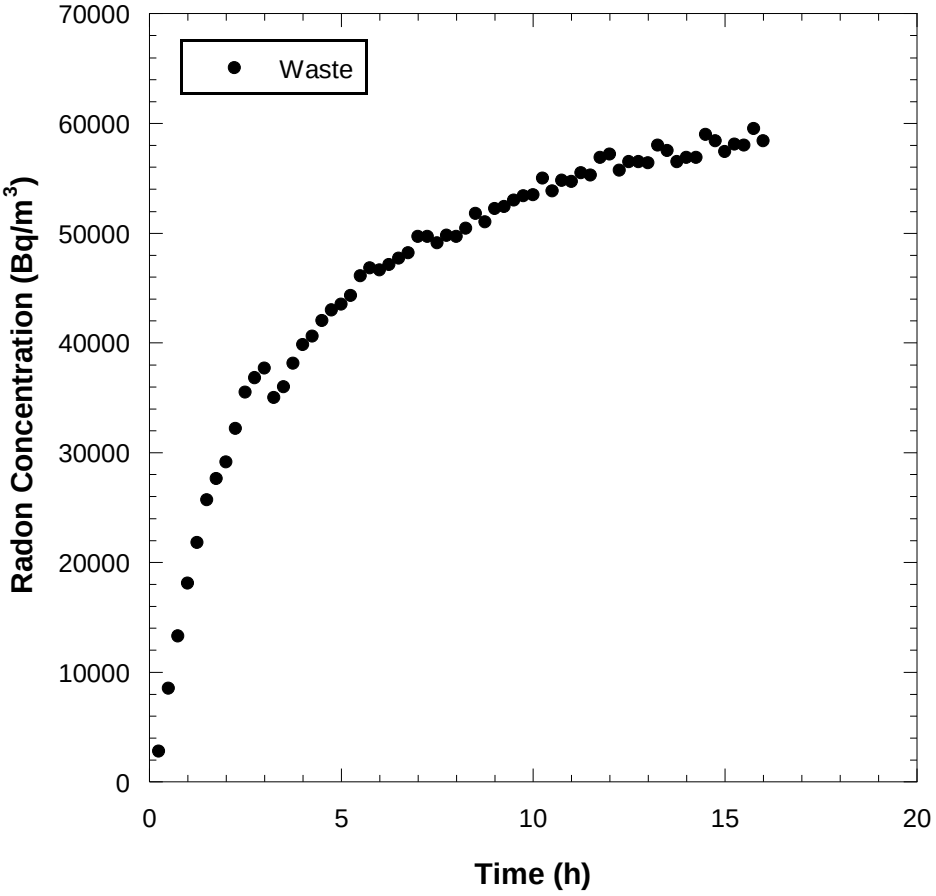

Fig. P79 – Radon concentration buildup curve measured from tailings at TP-9 at Bluewater, NM.

APPENDIX III - Radon Fluxes Measured from a Compacted Clay Barrier at the Shirley Basin South, WY Uranium Mill Tailings Disposal Site in 2017

ABSTRACT

Radon (Rn) fluxes were measured from the surface of a uranium mill tailings disposal site after 17 years of service. The tailings were contained by a compacted clay Rn barrier of varying thickness as well as protective layers consisting of compacted sand, vegetated topsoil or riprap for erosion control. Flux measurements were made with four different-sized flux chambers: extra small (area = 0.018 m^2, volume = 0.002 m^3), small (0.071 m^2, 0.011 m^3), medium (0.26 m^2, 0.035 m^3), and large (2.32 m^2, 0.352 m^3). Rn concentrations were measured concurrently using activated carbon (AC) canisters and continuously monitoring electronic RAD7 detectors with accumulation chambers. Flux measurements were made at the surface of the Rn barrier and from the surface of the underlying tailings at five locations on the disposal cell. Rn fluxes measured at the surface of the Rn barrier were consistently lower than fluxes measured at the surface of the tailings, indicating that significant Rn attenuation was occurring within the barrier. The geometric mean of all flux values measured from the Rn barrier surface were lower than the regulatory maximum of 0.74 Bq/m^2-s. Comparison of measurements from different-sized flux chambers indicated that no scale-dependent flux measurements were evident. The average of all Rn flux measurements obtained in 2017 was 0.051 Bq/m^2s compared with the 2001 average of 0.049 Bq/m^2s, taken immediately after construction of the barrier. This may indicate that physical changes within the barrier soil have not significantly affected the performance of the Rn barrier at this site. Average in-situ water content measurements of the Rn Barrier material were found to have increased slightly

from as-built values and were at high levels of saturation (S_{AVG} > 89%) in 2017. Saturated hydraulic conductivity testing on 350 mm diameter block samples obtained from the Rn barrier is currently in progress.

1 FIELD SITE

The Shirley Basin South Uranium disposal facility is located approximately 60 miles south of Casper, Wyoming in the vicinity of the original Uranium processing mill site. The mill processed uranium ore using acid leach processes from 1962 to 1974 and from 1978 to 1985. Decommissioning of the site began in 1985 and the disposal cell was fully encapsulated by 2000 (Petrotomics Company, 2001).

The disposal facility (**Figures 1 and 2**) consists of a two-tiered disposal cell with an upper and lower deck, separated by a riprap covered slope. The disposal cell has an area of approximately 5.8 x 10^5 m^2 and contains approximately 5.72 Tg of tailings with an estimated 36.0 TBq of radium-226. Schematic cover profiles for the disposal cell are shown in **Figure 3** (Petrotomics Company, 2001). The upper and lower decks of the disposal cell were designed to consist of (bottom to top) a compacted clay Rn barrier (0.62 m), a compacted sandy overburden layer (0.61 m), followed by a topsoil layer (0.24 m) for erosion control. The 5:1 slope between the upper and lower decks was designed to consist of a compacted clay Rn barrier (0.62 m), a compacted sandy overburden layer (0.63 m), a filter blanket layer (0.10 m), and a riprap layer (0.13 m) to allow for drainage and to protect from erosion (Petrotomics Company, 2001). The upper and lower decks of the disposal cell were planted with grasses and still contained grass in 2017 (**Figure 4**). The entire cell is actively grazed by cattle. The majority of the 5:1 riprap slope consisted

of bare riprap; however, a portion of the slope was filled in with windblown fines where vegetation was present (**Figure 5**).

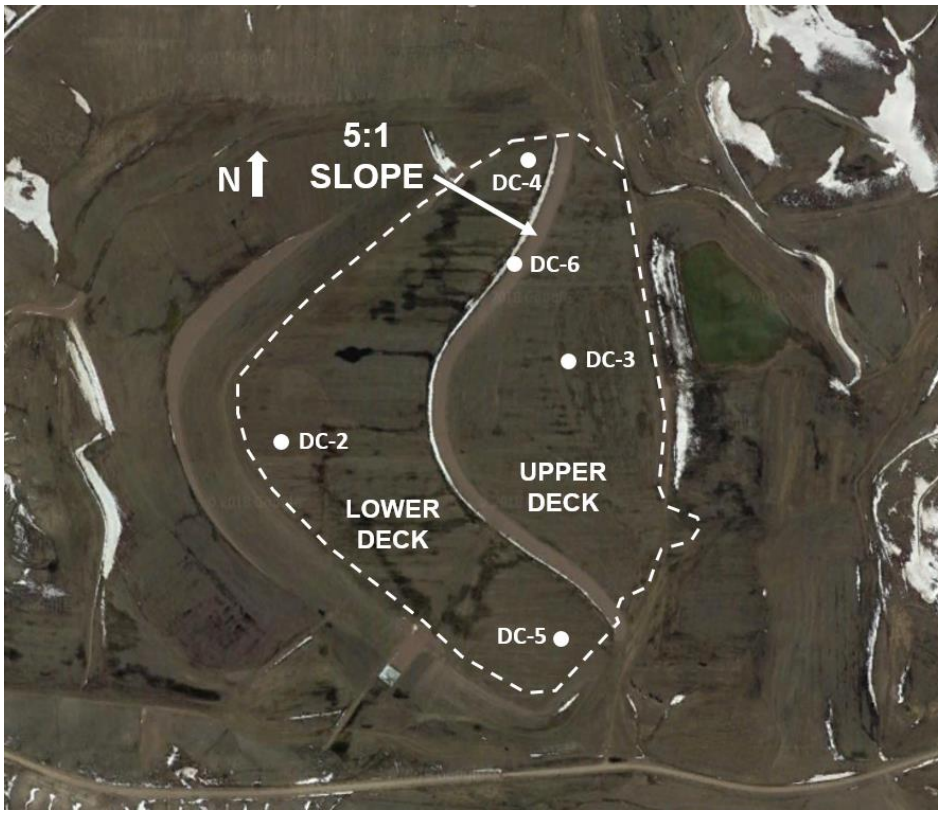

Figure 80 – Satellite image of the Shirley Basin South, WY disposal site (Google Earth). The extents of the disposal cell are shown by the dotted line. The white areas of the image are snow.

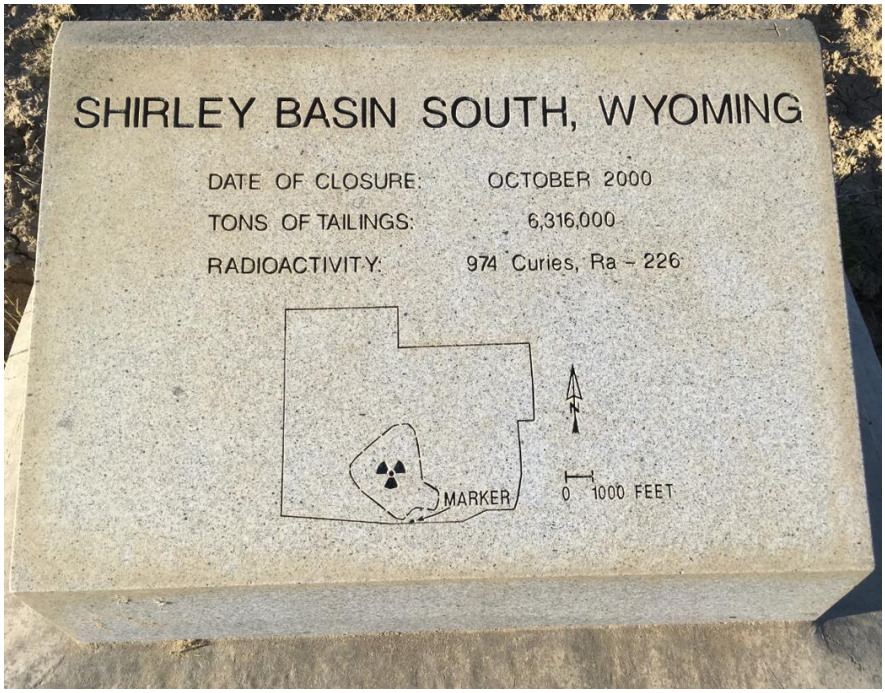

Figure 81 – Granite monument at the Shirley Basin South, WY disposal cell.

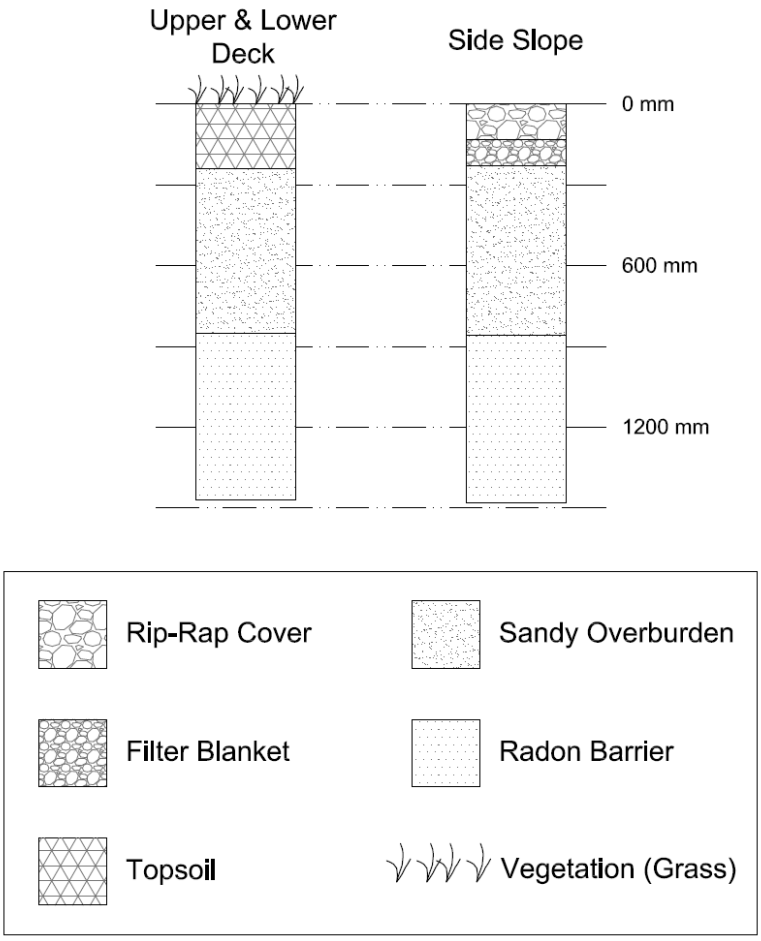

Figure 82 – Shirley Basin South, WY “as-designed” cover profiles.

Figure 83 – Grass on the lower deck of the disposal cell.

Figure 84 – Riprap on 5:1 slope looking North from lower deck.

2 RESULTS

Results from Rn fluxes measured at five test pits are summarized below. Approximate locations of the test pits are shown in **Figure 1**. Three of the five test pits were divided into halves and the flux measurements from each half were designated as “Test Pit #A” and “Test Pit #B”. After Rn flux measurements were made at the top surface of the Rn barrier, an excavation was made through the Rn barrier to expose the underlying uranium mill tailings so that a flux measurement could be taken directly from the tailings.

The locations of the test pits were chosen to be in the vicinity of areas where high as-built Rn fluxes were measured in 2000, with the exception of test pit 6. Test pit 6 was chosen at a location on the 5:1 riprap slope that had accumulations of wind-blown soil. The soil had filled in much of the voids and vegetation was found growing from the surface. This location was chosen because it represented a surface condition that had undergone significant change since its construction.

2.1 Radon Flux Measurements

The methods for the determination of Rn flux from AC and RAD7 were the same methods described in sections 4.1.1 and 4.1.2, respectively. Rn buildup curves from the surface of the Rn barrier and from the surface of the tailings from each test pit are shown in **Appendix I**. It should be noted that the rate of Rn concentration buildup from the flux test taken directly from the surface of the tailings is much greater than the rate of buildup from the test taken on the surface of the Rn. This shows that Rn is decaying significantly within the barrier, as it is intended to do.

Fluxes measured from the five test pits using the RAD7 are summarized in **Figure 6 and 7** (below) and **Table A2 in Appendix A**. Fluxes measured from test pits using AC canisters are summarized in **Table A3 in Appendix A**. Test pit descriptions are summarized in **Table 1**. Tailings were not encountered in test pit 4, as it was later discovered that the test pit was excavated over an area where no tailings existed.

The compiled results of all flux tests do not indicate that there was an impact of measurement scale on flux at this site. **Figure 8** shows each flux value normalized by the geometric mean flux from that respective test pit. If the flux measurements were scale-dependent, it would be expected that the scatter between the flux ratios presented in **Figure 8** would decrease and cluster near a value of one as chamber area increased (and perhaps reach an “optimum” size), however, this trend was not apparent.

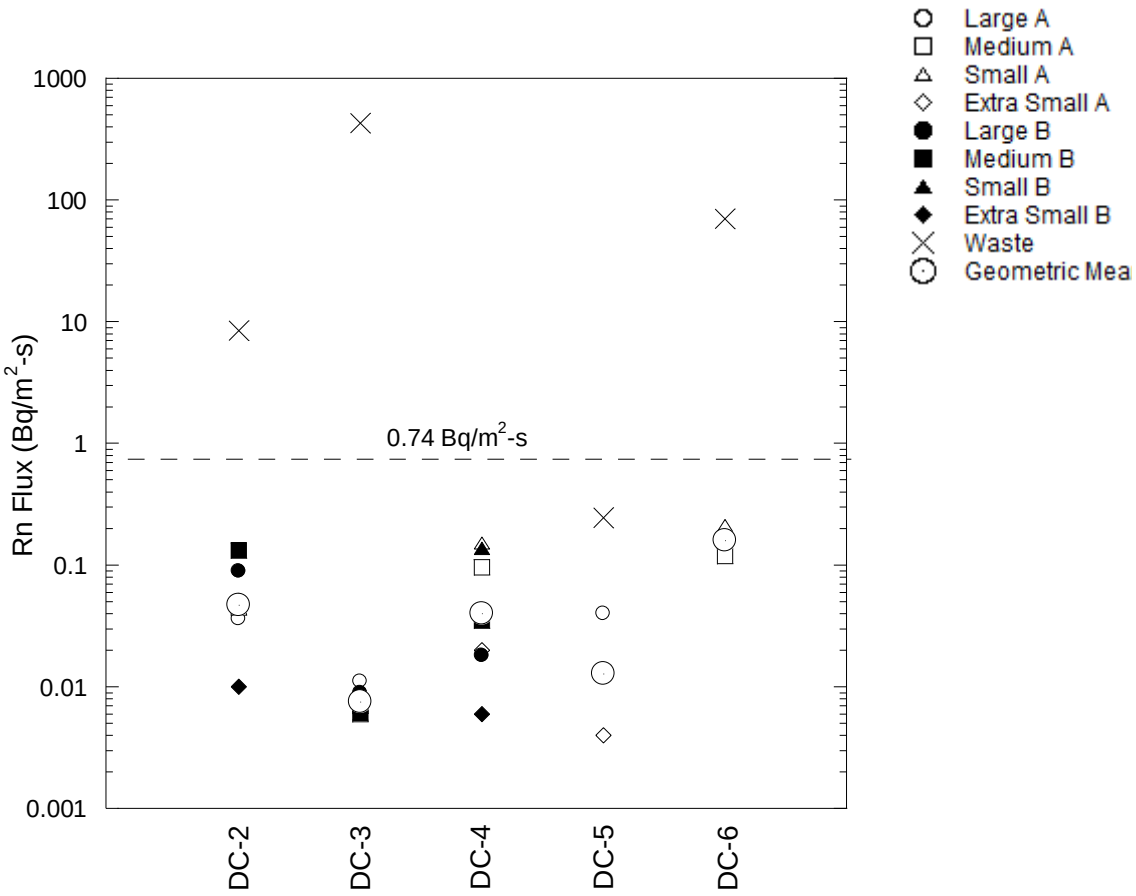

Figure 85 - Summary of fluxes measured with the RAD7 radon detector at the surface of the Rn barrier and the surface of the underlying tailings. DC-X = Disposal Cell X. The dashed horizontal line represents the maximum allowable surface flux specified by UMTRCA (0.74 Bq/m2s).

Table 21 - Test pit descriptions.

Test Pit	Location	Surface Feature Description
DC-2	Lower Deck	High As-Built Rn Flux
DC-3	Upper Deck	High As-Built Rn Flux
DC-4	Lower Deck	High As-Built Rn Flux
DC-5	Lower Deck	High As-Built Rn Flux
DC-6	Side Slope	Vegetated Riprap Cover

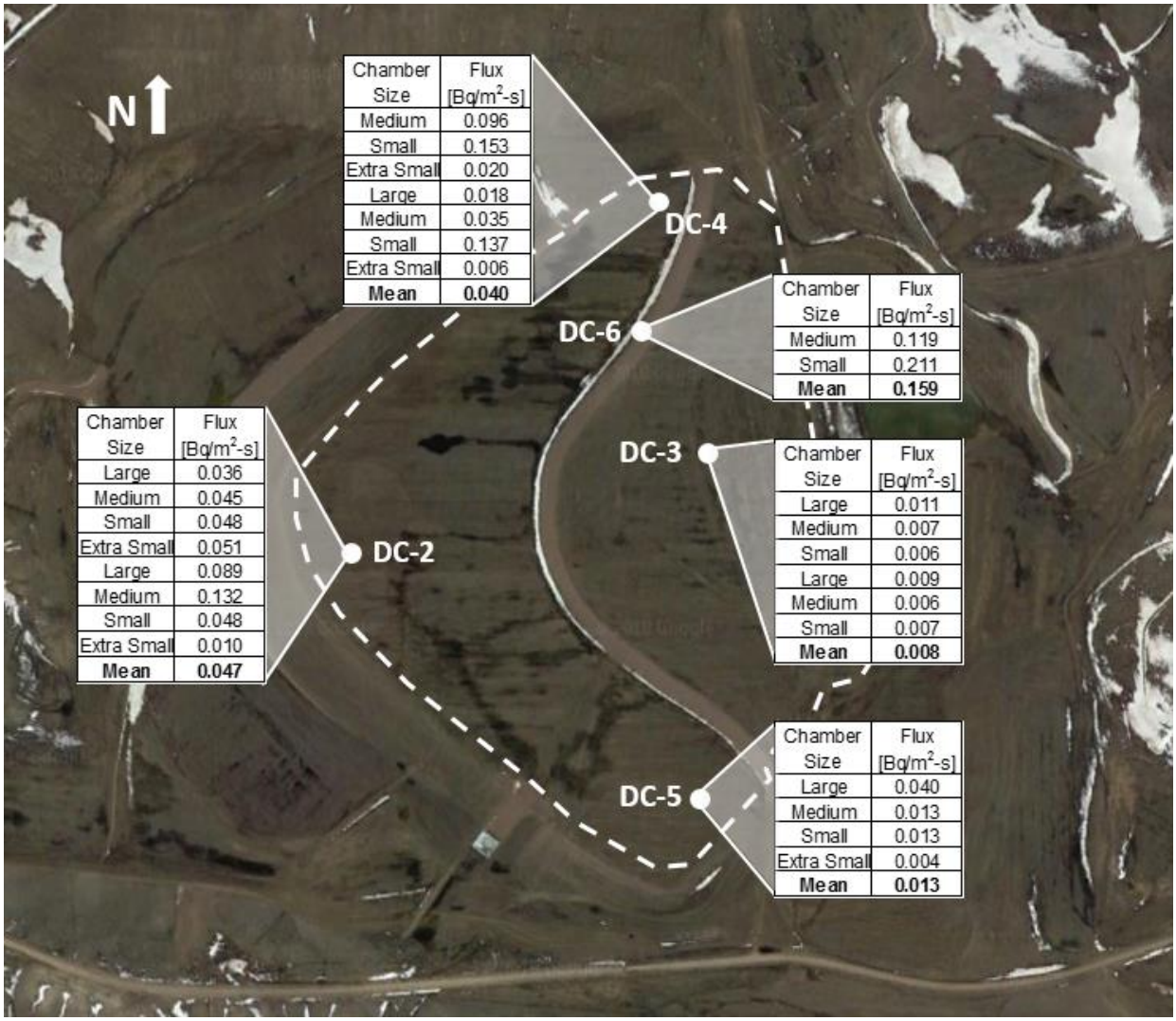

Figure 86 - Summary of fluxes measured with the RAD7 radon detector at the surface of the Rn barrier.

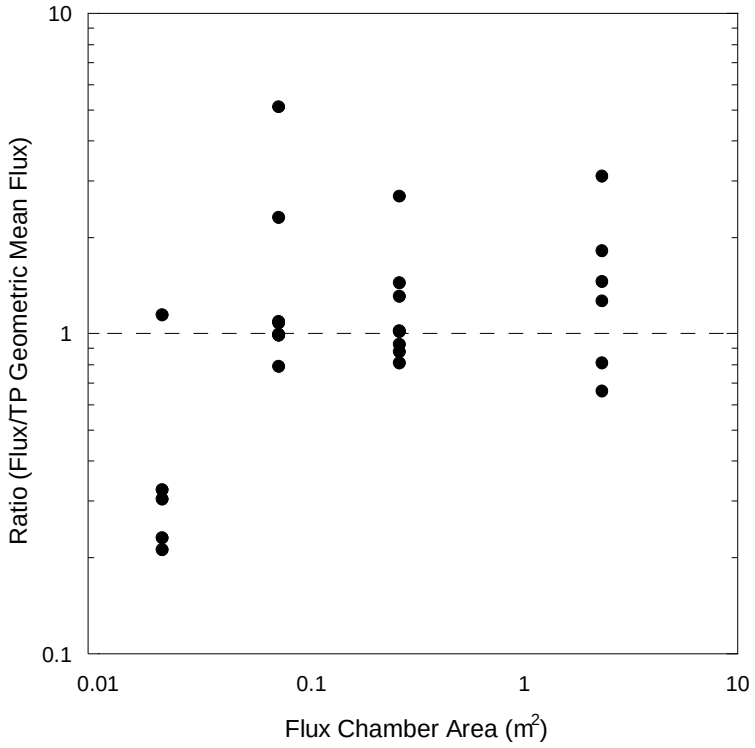

Figure 87 - Fluxes normalized by the geometric mean flux from each test pit.

2.2 Comparison of Fluxes in 2017 to As-Built Fluxes

The Shirley Basin South Completion report (Petrotomics Company, 2001) reported that upon completion of the Rn Barrier construction at the site, 103 “as-built” surface flux measurements were taken to confirm that the surface flux was below the 0.74 Bq/m^2s UMTRCA limit per the guidelines (40 CFR 192.02). These flux measurements were made using activated charcoal granules placed over a wire mesh within flux chambers that were placed directly on the Rn Barrier and the test durations were approximately 24 hours for each flux test (Petrotomics Company, 2001). **Table 2** and **Figure 9** below, summarize the flux measurements taken in 2000 and 2017.

Table 22 – Summary of geometric mean as-built and 2017 Rn flux measurements from the Shirley Basin South, WY disposal site.

	2001 As-Built	2017 RAD7
Geometric Mean Flux (Bq/m^2s)	0.049	0.051
Number of Measurements	103	27

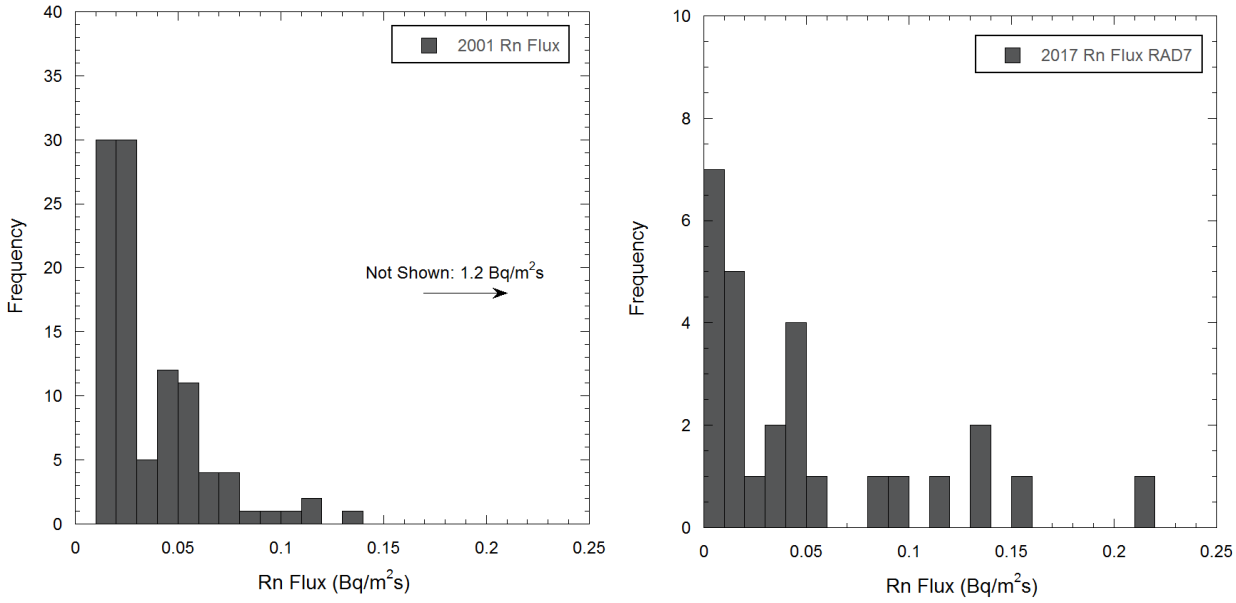

Figure 88 – Histograms showing the frequency of Rn fluxes measured in 2001 (left) and in 2017.

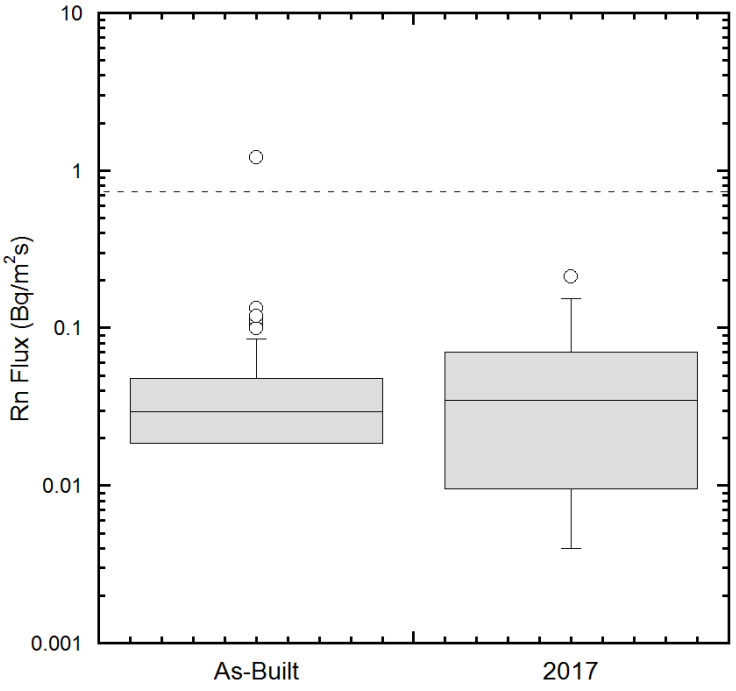

Figure 89 – Box and whisker plot showing as-built and 2016 flux measurements.

2.3 Water Content Profiles

Thin-walled (Shelby) tube samples (diameter 70 mm) obtained from the Rn Barrier were cut in the lab into sections approximately 40 - 50 mm in length to obtain profiles of water content with depth (see section 4.1.4 laboratory methods). Additionally, the dimensions and masses of each of the sections were measured so that dry unit weight, volumetric water content, and saturation profiles could be created (a compilation of water content, dry density, and saturation profiles can be found in **Appendix F, G, and H**, respectively). The large-scale "block" samples (350 mm diameter) obtained from the site were also used to determine in-situ water content and dry unit weight in the laboratory. The average water content values from both the thin-walled tube samples and large-scale block samples (referred to as "2017 values") are compared to the in-situ, "as-built" values from the completion report in **Table 3.**

Table 23 – Summary of soil parameters as-built soil.

			2017					
	As-Built Value		70 mm Diameter Tube		Nuclear Density Gage		Sand Cone	
Parameter	Value	n	Value	n	Value	n	Value	n
Gravimetric Water Content	23.3	518[a]	26.3	8	27.6	5	25.1	2
Dry Density (g/cm^3)	1.54	1078[a]	1.50	8	1.48	4	1.53	2

a - Tailings Reclamation Construction Completion Report. Petrotomics Company, Shirley Basin, WY, November 2001

2.4 Saturated Hydraulic Conductivity

Saturated hydraulic conductivity testing is currently ongoing on 9 large-scale, undisturbed block samples (350 mm diameter) excavated from the Rn barrier at the Shirley Basin South, WY site (see section 4.1.5 for methods). The results of saturated hydraulic conductivity testing are summarized in **Figure 11** (below) and **Table E3 in Appendix E**.

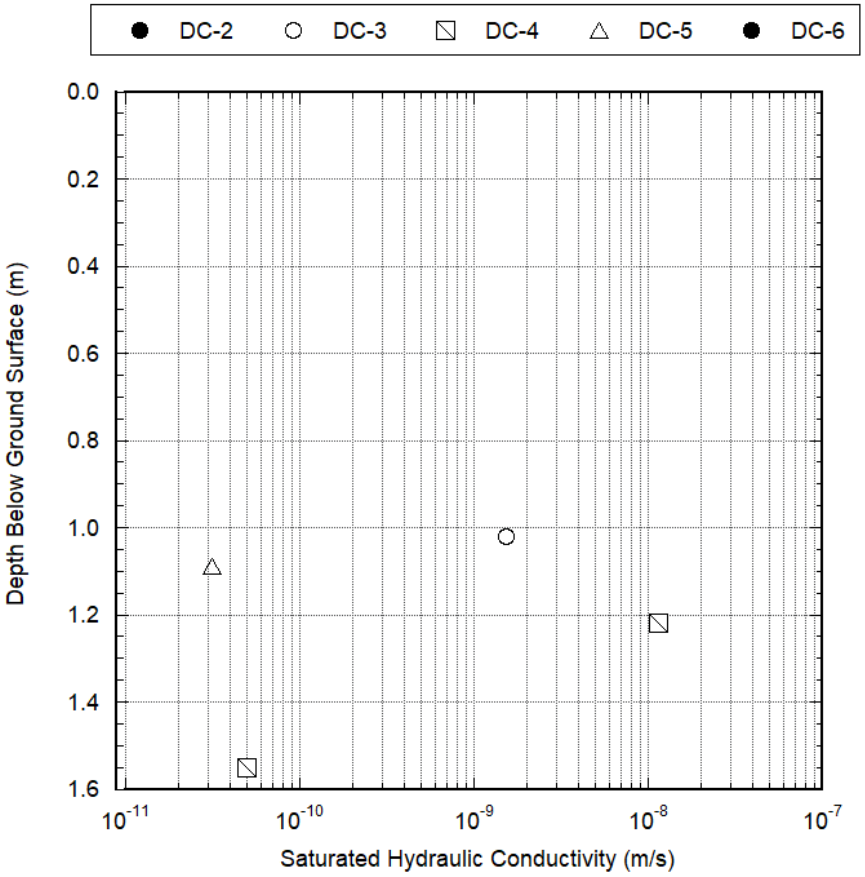

Figure 90 – Summary of saturated hydraulic conductivity measured from 350 mm diameter block samples.

2.5 Diffusion Coefficients Measured in the Laboratory

Rn Diffusion coefficient tests were performed in the laboratory on samples extracted from 70 mm diameter thin wall tube samples obtained from the field following the methods described in section 4.1.3. **Table 4**, below, summarizes the diffusion coefficients measured in the lab as well as the diffusion coefficients calculated using the empirical formula shown in **Equation 5** in **section 4.1.3**. This empirical formula considers the porosity and saturation of the soil that were determined from field measurements.

Table 24 – Summary of Diffusion Coefficients Measured in the Laboratory

Test Pit	Sample ID	Depth of Sample Below Surface of Rn Barrier (mm)	Rn Diffusion Coefficient, Lab (m^2/s)	Rn Diffusion Coefficient, Eqn. 5 (Section 4.1.3) (m^2/s)	Porosity, n (%)	Saturation, S (%)
DC-2	A	447	$8.7x10^{-8}$	$3.2x10^{-8}$	45	91
	B	457	$6.0x10^{-8}$	$1.1x10^{-8}$	44	92
	C	532	$6.8x10^{-8}$	$3.9x10^{-8}$	41	86
DC-5	A	140	$5.4x10^{-8}$	$1.2.x10^{-8}$	49	92
	B					
DC-6	A	35	$8.3x10^{-8}$	$1.3x10^{-7}$	46	80
	B	75	$9.8x10^{-8}$	$1.5x10^{-7}$	46	79

3 SUMMARY

Rn fluxes were measured from five test pits excavated at the uranium mill tailings disposal site in Shirley Basin South, WY in 2017. The cover system had been in service for approximately 17 years at the time of the performed field work. Flux measurements were taken from the surface of the Rn barrier to observe if soil structure caused by pedogenesis had caused any changes in Rn flux. Four flux chamber sizes were used to observe if soil structure was causing any scale-dependent Rn flux. Rn concentrations and fluxes were measured with activated carbon (AC) canisters and RAD7 continuous monitors. AC canisters recorded a single concentration point while RAD7 monitors provided continuous concentration measurements.

Rn fluxes measured from the surface of the Rn barrier were significantly lower than the fluxes measured directly from the tailings beneath. This indicates that the Rn barrier is still effective at reducing the Rn flux at the surface, and Rn gas is attenuating significantly within it before reaching the atmosphere. No measurements of Rn flux were measured to be above the UMTRCA maximum allowed flux of 0.74 Bq/m^2s. The overall

geometric mean of Rn flux measured from the surface of the Rn barrier was 0.051 Bq/m^2s. This value is very close to the average as-built flux of 0.049 Bq/m^2s measured in 2001. No apparent impacts of measurement scale were observed based on the fluxes measured at this field site.

Water content measurements taken from both thin-walled tube samples and large-scale block samples obtained in the field in 2017 indicated that the average water content of the Rn Barrier soil had increased slightly from as-built measurements. The Rn barrier was very wet and saturation levels were greater than 89%, on average.

Rn diffusion testing was performed on 70 mm diameter samples extracted from thin walled tube samples obtained at the site. The mean diffusion coefficient was found to be 1.9 x 10^{-8} m^2/s and values compared well with those determined via a common empirical equation.

The saturated hydraulic conductivity of large-scale block samples obtained in the field is currently ongoing. The saturated hydraulic conductivity of four samples tested to date has been very low with a geometric mean of 4.1 x 10^{-10} m/s.

REFERENCES

Petrotomics Company (2001). Tailings Reclamation Construction Comlpetion Report, Shirley Basin Wyoming, NRC Source Material License SUA-551. Vol. 1 – 2.

U.S. Department of Energy, Legacy Management (2017). UMTRCA Title II Shirley Basin South, Wyoming, Disposal Site. Fact Sheet.

APPENDIX A – ADDITIONAL TABLES AND FIGURES

Table A25 - Flux chamber areas and volumes.

Chamber Designation	Area [m^2]	Volume [m^3]
Extra Small	0.020	0.002
Small	0.071	0.011
Medium	0.260	0.032
Large	2.323	0.352

Table A26 – Tabulated summary of flux measurements from all test pits using RAD7.

Test Pit	Test (A/B)	Chamber Size	Flux	Geometric Mean of Test Pit	Tailings Flux (Small Chamber)
			[Bq/m^2-s]	[Bq/m^2-s]	[Bq/m^2-s]
DC-2	A	Large	0.036	0.047	8.38
		Medium	0.045		
		Small	0.048		
		Extra Small	0.051		
	B	Large	0.089		
		Medium	0.132		
		Small	0.048		
		Extra Small	0.010		
DC-3	A	Large	0.011	0.0075	370.26
		Medium	0.007		
		Small	0.006		
	B	Large	0.009		
		Medium	0.006		
		Small	0.007		
DC-4	A	Medium	0.096	0.0397	NM
		Small	0.153		
		Extra Small	0.020		
	B	Large	0.018		
		Medium	0.035		
		Small	0.137		
		Extra Small	0.006		
DC-5	A	Large	0.040	0.0128	0.24
		Medium	0.013		
		Small	0.013		
		Extra Small	0.004		
DC-6	A	Medium	0.119	0.1586	69.93
		Small	0.211		

Table A27 - Tabulated summary of flux measurements from all test pits using AC.

Test Pit	Test (A/B)	Chamber Size	Flux	Geometric Mean of Test Pit	Tailings Flux (Small Chamber)
			[Bq/m^2-s]	[Bq/m^2-s]	[Bq/m^2-s]
DC-2	A	Large	0.027	0.021	0.09
		Medium	0.024		
		Small	0.027		
		Extra Small	0.012		
	B	Large	0.148		
		Medium	0.034		
		Small	0.010		
		Extra Small	0.004		
DC-3	A	Large	0.008	0.002	N/A
		Medium	0.003		
		Small	0.002		
		Extra Small	0.000		
	B	Large	0.006		
		Medium	0.002		
		Small	0.001		
DC-4	A	Large	0.008	0.006	0.01
		Medium	0.036		
		Small	0.023		
		Extra Small	0.001		
	B	Large	0.005		
		Medium	0.002		
		Small	0.004		
DC-5	A	Large	0.017	0.005	0.09
		Medium	0.002		
		Small	0.004		
DC-6	A	Medium	0.015	0.007	30.62
		Medium	0.002		
		Small	0.010		

APPENDIX B – TEST PIT EXCAVATION PHOTOS

Figure B91 – Removal and stockpiling of the topsoil layer to expose the sandy overburden layer.

Figure B92 – Removal of the sandy overburden layer to expose the top surface of the Rn Barrier.

Figure B93 – Reconstruction of the Rn barrier and protective layers using a remote controlled sheep's foot compactor.

APPENDIX C – FLUX MEASUREMENT PHOTOS

Figure C94 – Installation of flux chambers on the Rn Barrier surface.

Figure C95 – Installation of a small flux chamber directly on the uranium mill tailings.

APPENDIX D – SOIL SAMPLING PHOTOS

Figure D96 – Obtaining a thin-walled tube sample of Rn barrier soil.

Figure D97 – Sampling soil from a thin-walled tube in the laboratory.

Figure D98 – Trimming a 350 mm diameter sample using a shovel.

Figure D99 – Trimming a 350 mm diameter sample using hand tools to fit protective PVC pipe around sample.

Figure D100 – 350 mm diameter sample with protective PVC pipe in place.

Figure D101 – 350 mm diameter sample after removal.

Figure D102 – Trimming a 350 mm diameter block sample prior to saturated hydraluic conductivity
testing in the laboratory.

Figure D103 - A 350 mm diameter block sample with flexible membrane in place prior to saturated hydraluic conductivity testing in the laboratory.

APPENDIX E – SUMMARY OF LABORATORY TEST DATA

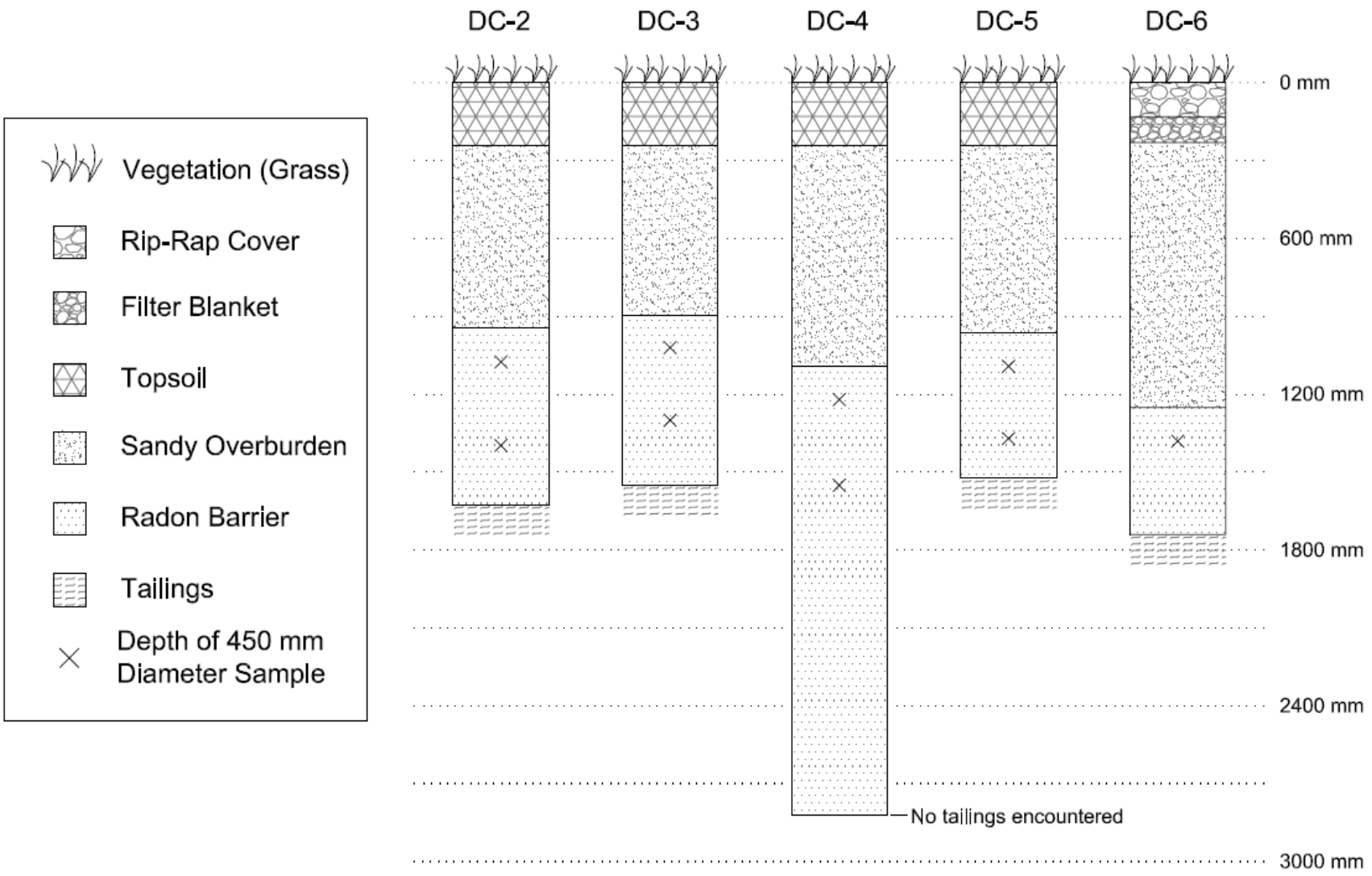

Figure E104 – Cover profiles for test pits excavated at the Shirley Basin South, WY site in 2017.

Table E28 – Summary of 350 mm Diameter Block Samples Collected at the Shirley Basin South, WY Site in 2017.

Test Pit	Sample Designation	Depth of Top of Block Sample BGS (m)	Depth of Bottom of Block Sample BGS (m)	% Gravel	% Sand	% Fines	% Clay	LL	PL	PI	G_s	XRD
DC-2	A	0.95	1.20	3	20	77	59	-	-	-	-	x
	B	1.26	1.52					-	-	-	-	-
DC-3	A	0.90	1.15	5	30	65	34	67	29	38	-	x
	B	1.18	1.43					-	-	-	-	-
DC-4	A	1.09	1.35	1	33	67	49	-	-	-	-	-
	B	1.42	1.68					-	-	-	-	-
DC-5	A	0.97	1.22	0	6	93	66	-	-	-	2.70	-
	B	1.25	1.50					-	-	-	-	-
DC-6	A	1.25	1.51	IP	IP	74	IP	67	28	39	2.69	-

NM = Not Measured

IP = In Progress

Table E29 – Summary of 70 mm Diameter (Thin-Wall Tube) Samples Collected at the Shirley Basin South, WY Site in 2017.

Test Pit	70 mm Diameter Sample ID	Depth of Top of Sample Below Rn Barrier Surface (m)	Depth of Bottom of Sample Below Rn Barrier Surface (m)	Water Content Profile*
DC-2	A	0.00	0.44	x
	B	0.24	0.59	x
	C	0.24	0.67	x
DC-3	A	0.00	0.36	x
	B	0.32	0.64	x
DC-4	A	0.00	0.44	x
	B	0.51	-	NM
DC-5	A	0.00	-	NM
	B	0.00	-	NM
	C	0.00	0.30	x
	D	0.15	0.42	x
DC-6	A	0.00	0.36	x
	B	0.00	-	NM

* Water content profiles can be found in Appendix F

NM = Not Measured

IP = In Progress

Table E30 – Summary of Hydraulic Properties from 350 mm Diameter Block Samples Collected at the Shirley Basin South, WY in 2017

Test Pit	Sample Designation	Gravimetric Water Content (%) *	γ_d (kN/m^3)	Saturated Hydraulic Conductivity (m/s) †	Soil Water Characteristic Curve §			
					θ_r	θ_s	α	n
DC-2	A	-	-	-	-	-	-	-
	B	-	-	-	-	-	-	-
DC-3	A	27.6	14.3	1.53×10^{-9}	-	-	-	-
	B	-	-	-	-	-	-	-
DC-4	A	25.0	15.6	1.14×10^{-8}	-	-	-	-
	B	20.6	15.8	5.01×10^{-11}	IP	IP	IP	IP
DC-5	A	32.0	14.8	3.15×10^{-11}	IP	IP	IP	IP
	B	-	-	-	-	-	-	-
DC-6	A	26.5	14.9	IP	-	-	-	-

* ASTM D 2216

† ASTM D 5084

§ ASTM D 6836 - 02 (Method A and D)

Table E31 - Summary of Diffusion Coefficients Determined from 70 mm Diameter Samples Collected at the Shirley Basin South, WY in 2017

Test Pit	Sample ID	Depth of Sample Below Surface of Rn Barrier (mm)	Rn Diffusion Coefficient, Lab (m^2/s)	Rn Diffusion Coefficient, Eqn. 5 (Section 4.1.3) (m^2/s)
DC-2	A	45	2.4×10^{-8}	8.9×10^{-9}
	B	46	1.6×10^{-8}	1.1×10^{-8}
	C	55	1.8×10^{-8}	4.3×10^{-8}
DC-5	A	14	1.5×10^{-8}	$1.2. \times 10^{-8}$
	B			
DC-6	A	35	2.2×10^{-8}	$1.3. \times 10^{-7}$
	B	IP	IP	IP

APPENDIX F – GRAVIMETRIC WATER CONTENT PROFILES

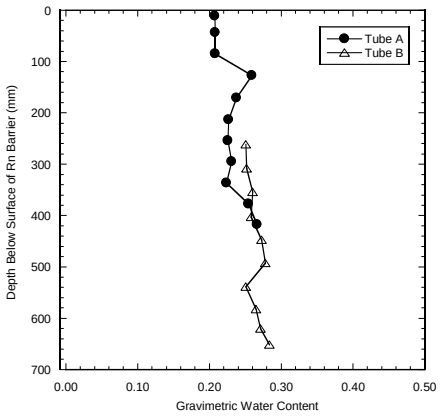

DC-2

Tube A		Tube B	
Depth (mm)	Water Content	Depth (mm)	Water Content
11	0.21	261	0.25
43	0.21	308	0.25
85	0.21	354	0.26
127	0.26	403	0.26
171	0.24	447	0.27
213	0.23	492	0.28
254	0.23	538	0.25
295	0.23	582	0.26
336	0.22	620	0.27
377	0.25	651	0.28
417	0.27	Mean	0.26
Mean	0.23		

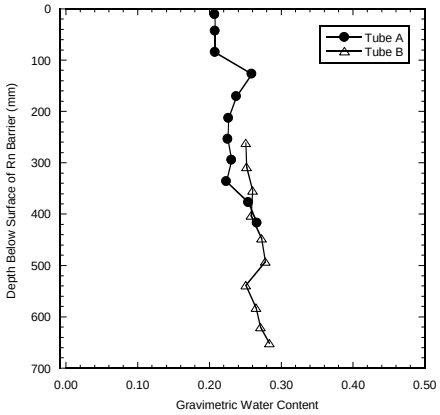

DC-3

Tube A		Tube B	
Depth (mm)	Water Content	Depth (mm)	Water Content
5	0.25	341	0.27
30	0.28	386	0.24
69	0.28	433	0.17
110	0.26	473	0.23
151	0.17	513	0.24
193	0.19	592	0.24
234	0.27	625	0.20
275	0.31	Mean	0.23
311	0.32		
341	0.21		
Mean	0.25		

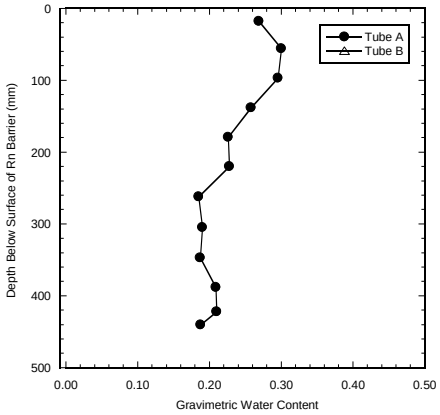

DC-4

Tube A		Tube B	
Depth (mm)	Water Content	Depth (mm)	Water Content
18	0.27		
56	0.30		
97	0.30		
138	0.26		
179	0.23		
220	0.23		
262	0.18		
305	0.19	Mean	
347	0.19		
388	0.21		
422	0.21		
440	0.19		
Mean	0.23		

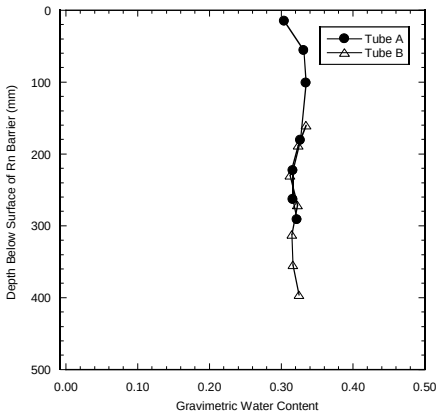

DC-5

Tube A		Tube B	
Depth (mm)	Water Content	Depth (mm)	Water Content
15	0.3041	160	0.3343
56	0.3315	188	0.3237
101	0.3343	230	0.3118
181	0.3265	271	0.3224
223	0.3161	312	0.3146
263	0.3164	354	0.3160
291	0.3220	396	0.3246
Mean	0.32	Mean	0.32

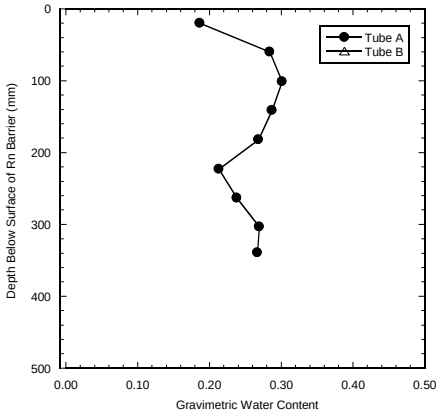

DC-6

Tube A		Tube B	
Depth (mm)	Water Content	Depth (mm)	Water Content
20	0.1864		
60	0.2841		
101	0.3012		
141	0.2871		
182	0.2683		
223	0.2130		
263	0.2382		
303	0.2695	Mean	
339	0.2665		
Mean	0.26		

APPENDIX G – DRY DENSITY PROFILES

DC-2

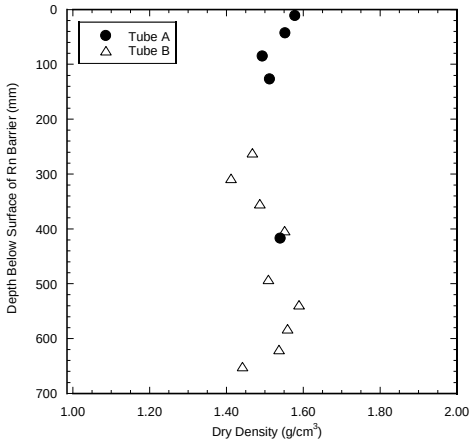

Tube A

Depth (mm)	Dry Density (g/cm^3)
43	1.55
85	1.49
127	1.51
417	1.54
Mean	1.52

Tube B

Depth (mm)	Dry Density (g/cm^3)
261	1.47
308	1.41
354	1.49
403	1.55
492	1.51
538	1.59
582	1.56
620	1.54
651	1.44
Mean	1.51

DC-3

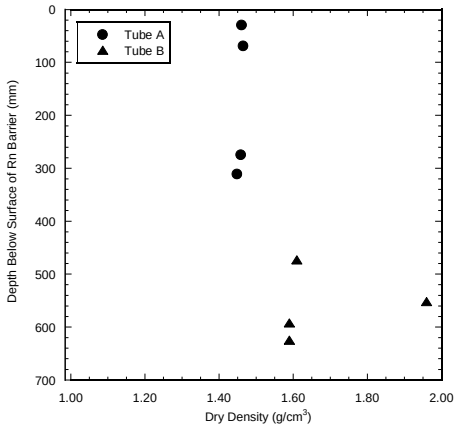

Tube A

Depth (mm)	Dry Density (g/cm^3)
30	1.46
69	1.47
275	1.46
311	1.45
Mean	1.46

Tube B

Depth (mm)	Dry Density (g/cm^3)
473	1.61
552	1.96
592	1.59
625	1.59
Mean	1.69

DC-4

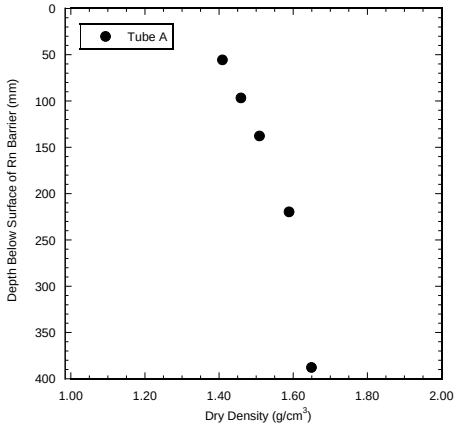

Tube A

Depth (mm)	Dry Density (g/cm^3)
56	1.41
97	1.46
138	1.51
220	1.59
388	1.65
Mean	1.53

Tube B

Depth (mm)	Dry Density (g/cm^3)
Mean	

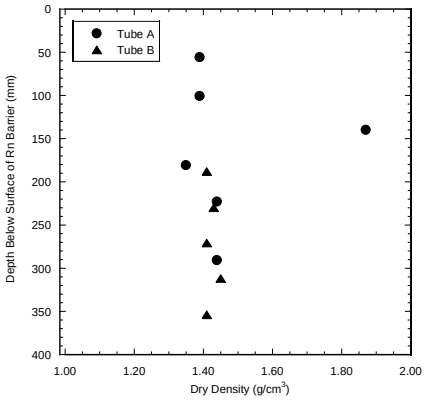

DC-5

Tube A

Depth (mm)	Dry Density (g/cm^3)
56	1.39
101	1.39
140	1.87
181	1.35
223	1.44
291	1.44
Mean	1.48

Tube B

Depth (mm)	Dry Density (g/cm^3)
188	1.41
230	1.43
271	1.41
312	1.45
354	1.41
Mean	1.42

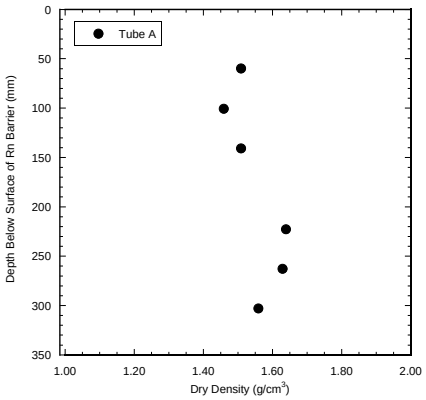

DC-6

Tube A

Depth (mm)	Dry Density (g/cm^3)
60	1.51
101	1.46
141	1.51
223	1.64
263	1.63
303	1.56
Mean	1.55

Tube B

Depth (mm)	Dry Density (g/cm^3)
Mean	

APPENDIX H – SATURATION PROFILES

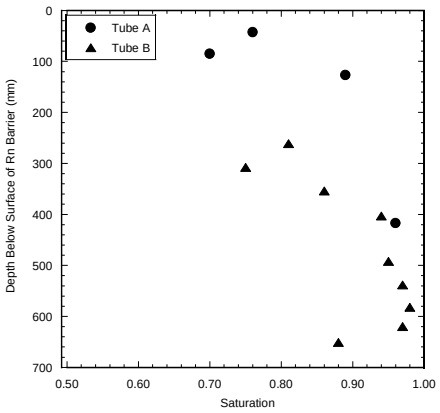

DC-2

Tube A

Depth (mm)	Saturation
43	0.76
85	0.70
127	0.89
417	0.96
Mean	0.83

Tube B

Depth (mm)	Saturation
261	0.81
308	0.75
354	0.86
403	0.94
492	0.95
538	0.97
582	0.98
620	0.97
651	0.88
Mean	0.90

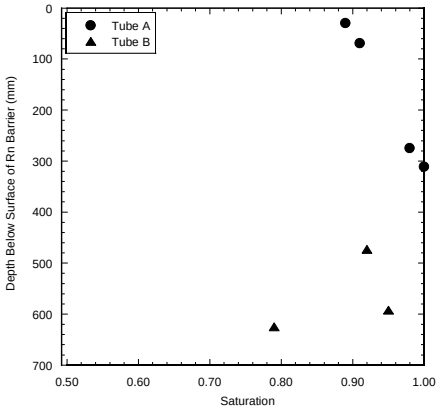

DC-3

Tube A

Depth (mm)	Saturation
30	0.89
69	0.91
275	0.98
311	1.00
Mean	0.94

Tube B

Depth (mm)	Saturation
473	0.92
592	0.95
625	0.79
Mean	0.89

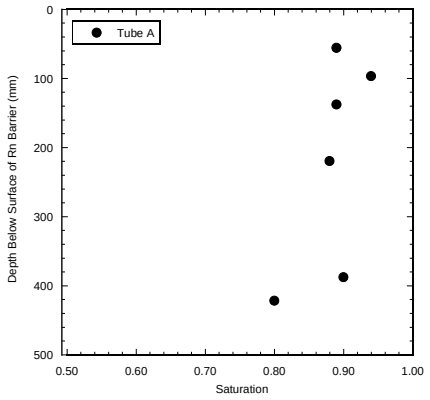

DC-4

Tube A

Depth (mm)	Saturation
56	0.89
97	0.94
138	0.89
220	0.88
388	0.90
Mean	0.90

Tube B

Depth (mm)	Saturation
Mean	

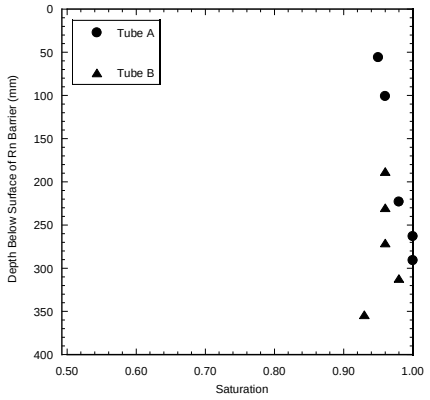

DC-5

Tube A

Depth (mm)	Saturation
56	0.95
101	0.96
223	0.98
263	1.00
291	1.00
Mean	0.98

Tube B

Depth (mm)	Saturation
188	0.96
230	0.96
271	0.96
312	0.98
354	0.93
Mean	0.96

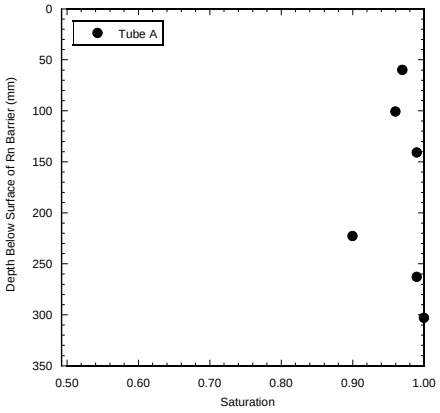

DC-6

Tube A

Depth (mm)	Saturation
60	0.97
101	0.96
141	0.99
223	0.90
263	0.99
303	1.00
Mean	0.97

Tube B

Depth (mm)	Saturation
Mean	

APPENDIX I – RADON CONCENTRATION BUILDUP CURVES

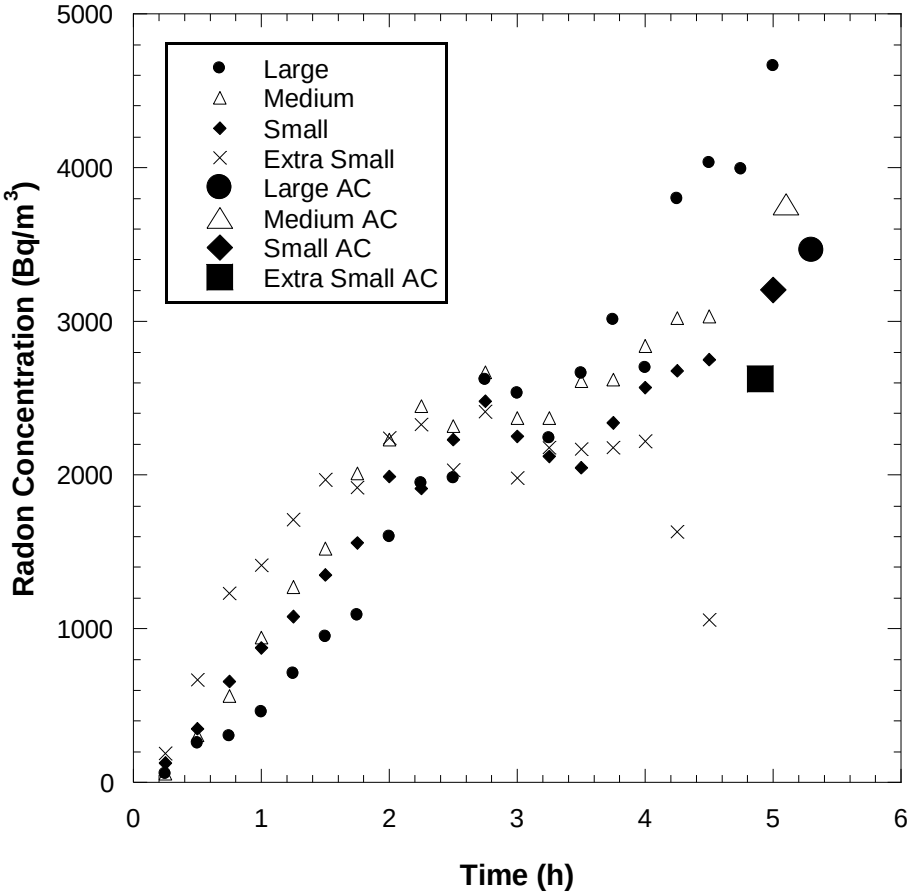

Fig. I105a – Radon concentration buildup curves measured at DC-2A at Shirley Basin South, WY.

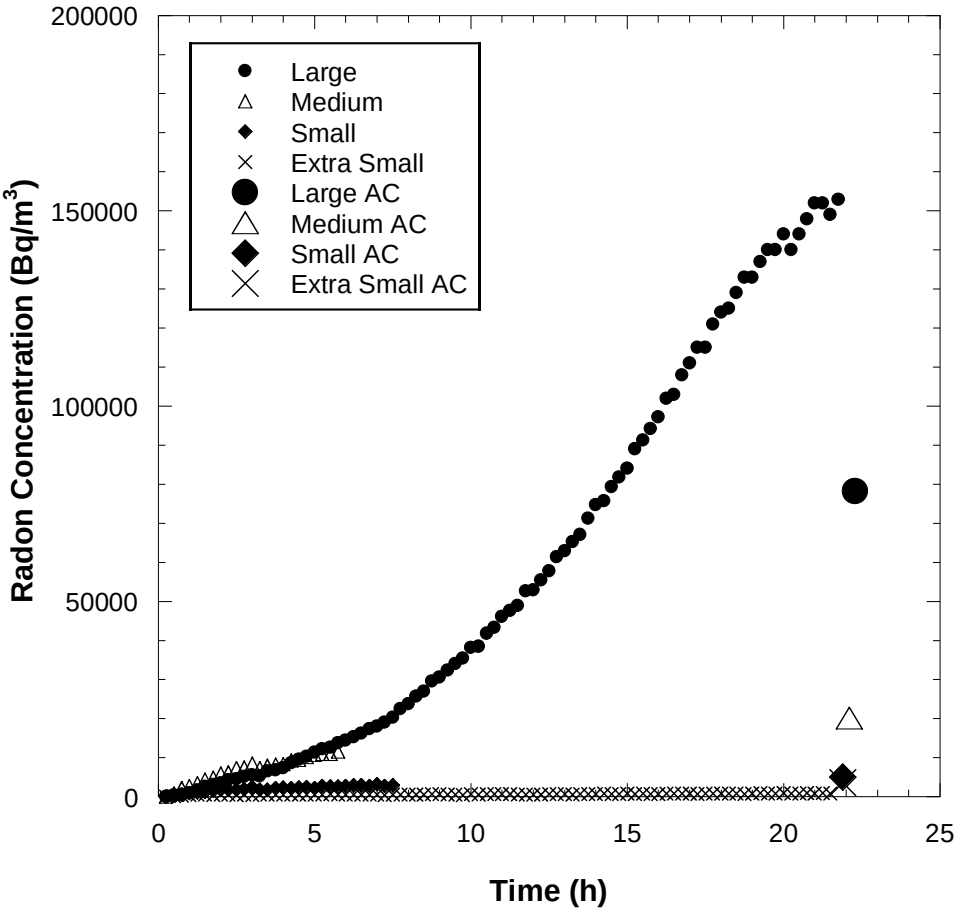

Fig. IP106 - Radon concentration buildup curves measured at DC-2B at Shirley Basin South, WY.

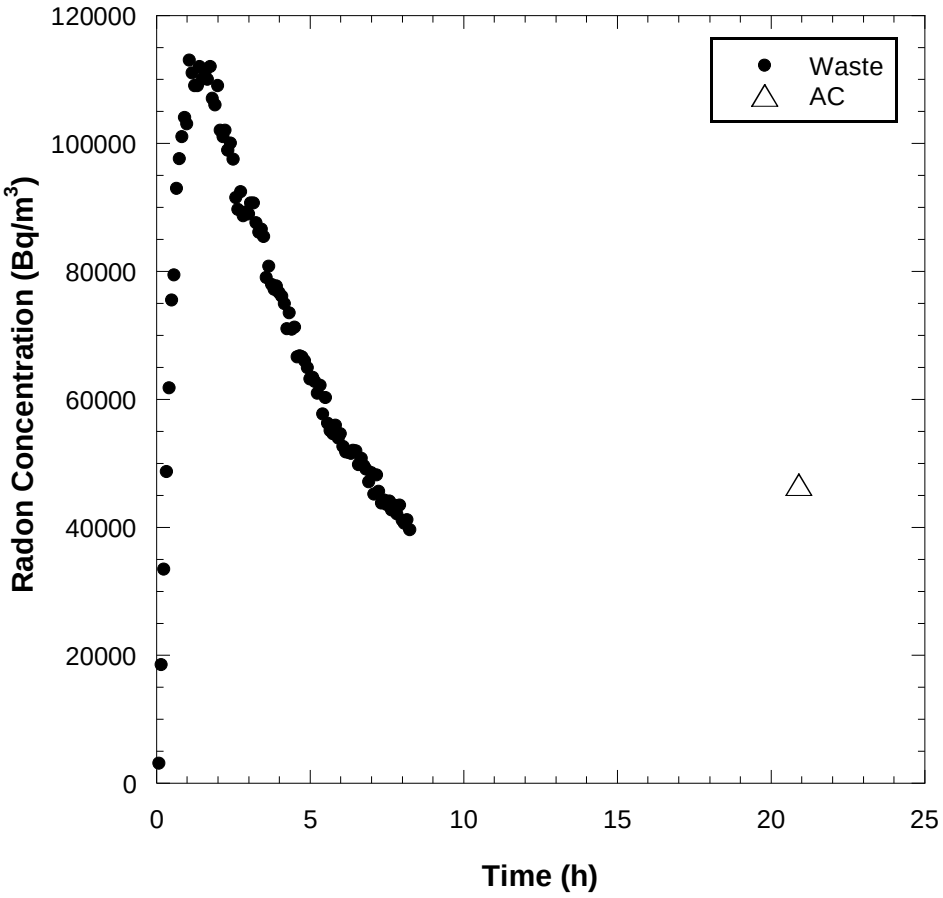

Fig. I107 – Radon concentration buildup curve measured from tailings at DC-2 at Shirley Basin South, WY.

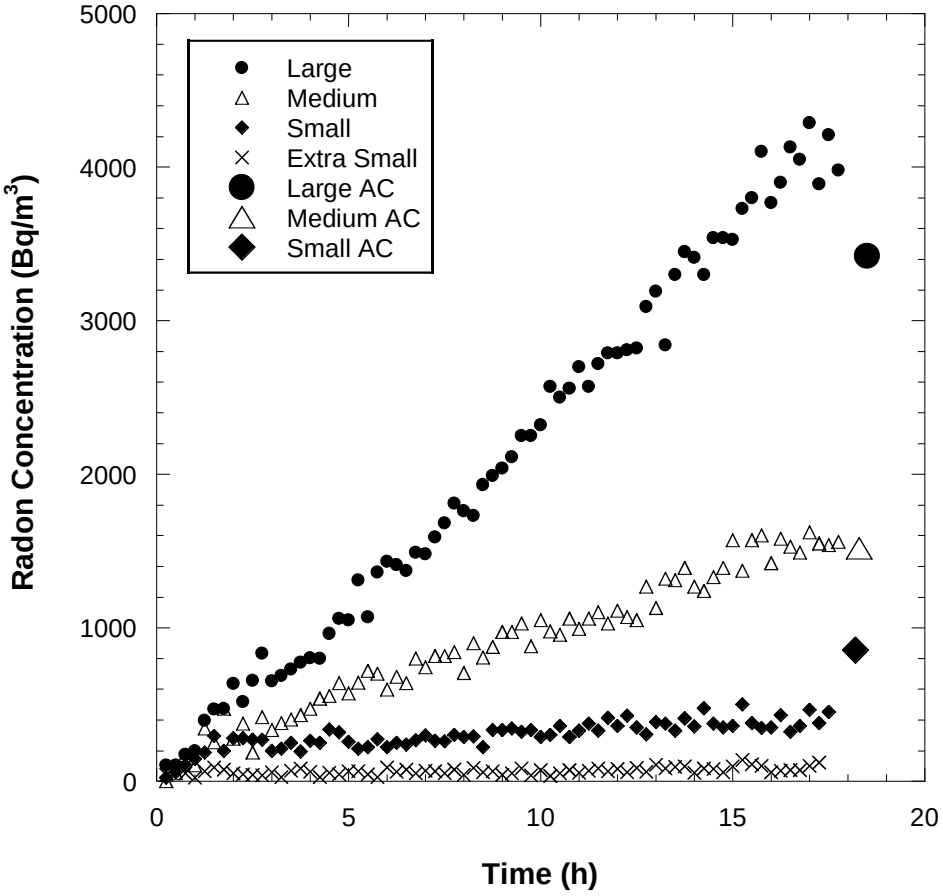

Fig. I108 – Radon concentration buildup curves measured at DC-3A at Shirley Basin South, WY.

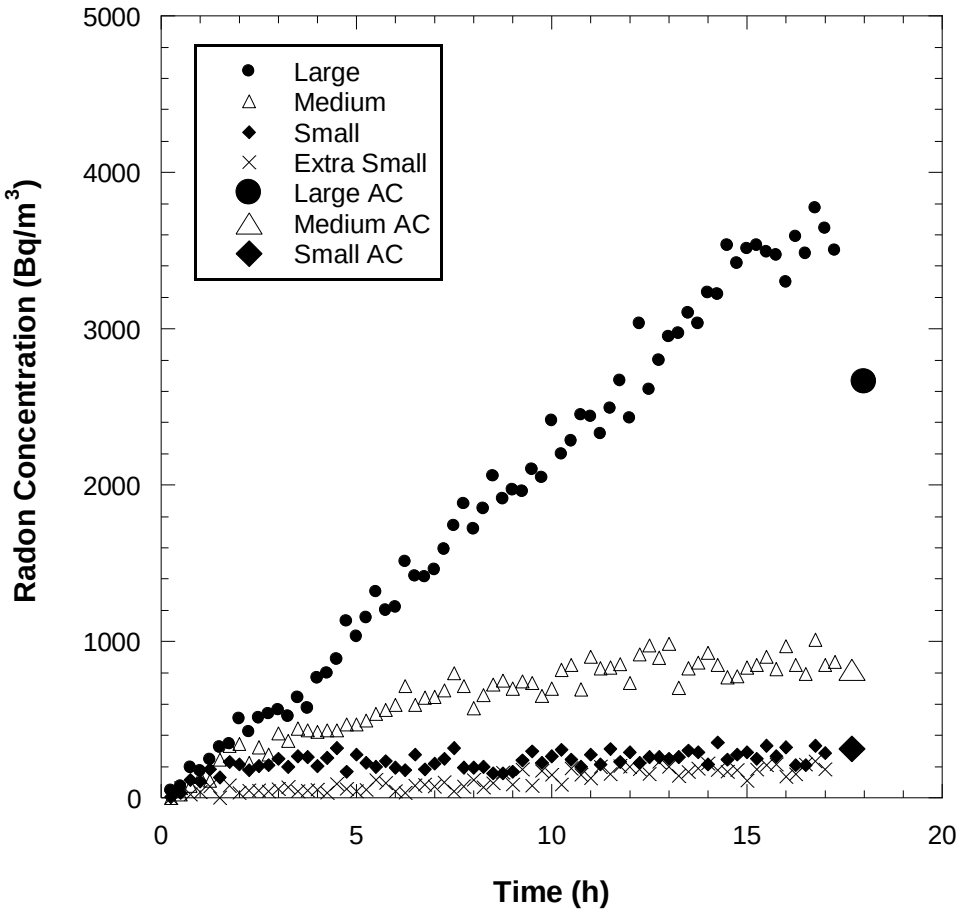

Fig. I109 – Radon concentration buildup curves measured at DC-3B at Shirley Basin South, WY.

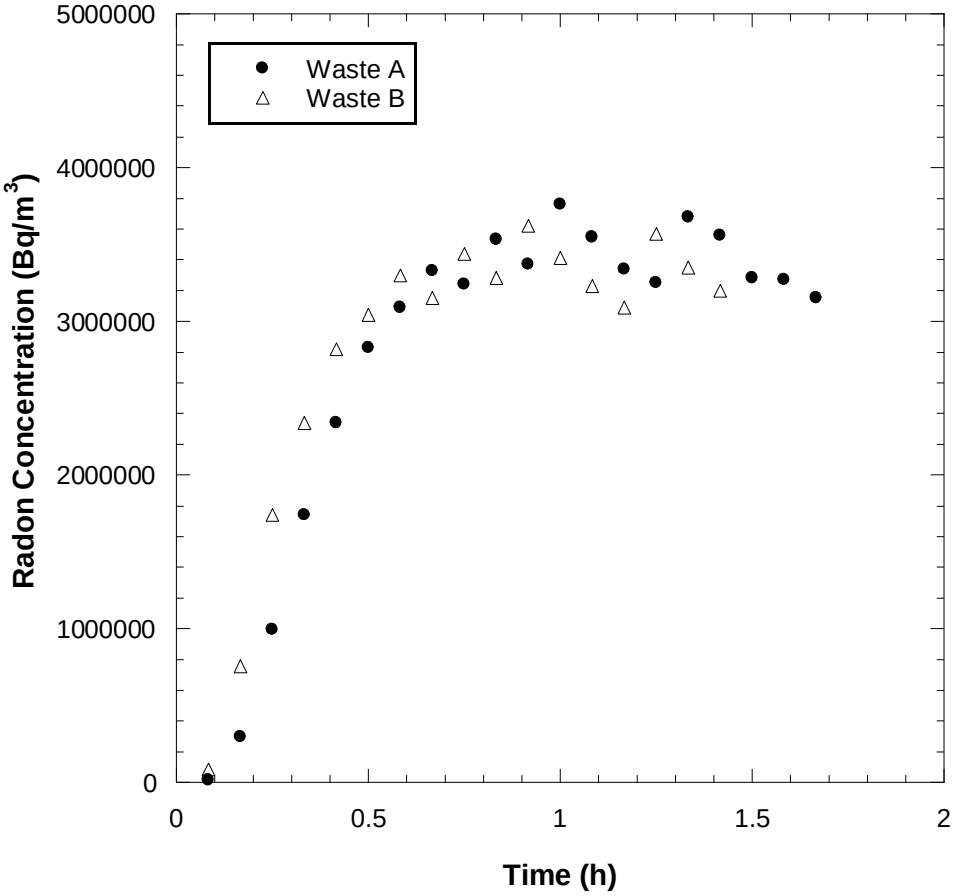

Fig. I110 - Radon concentration buildup curves measured from tailings at DC-3 at Shirley Basin South, WY.

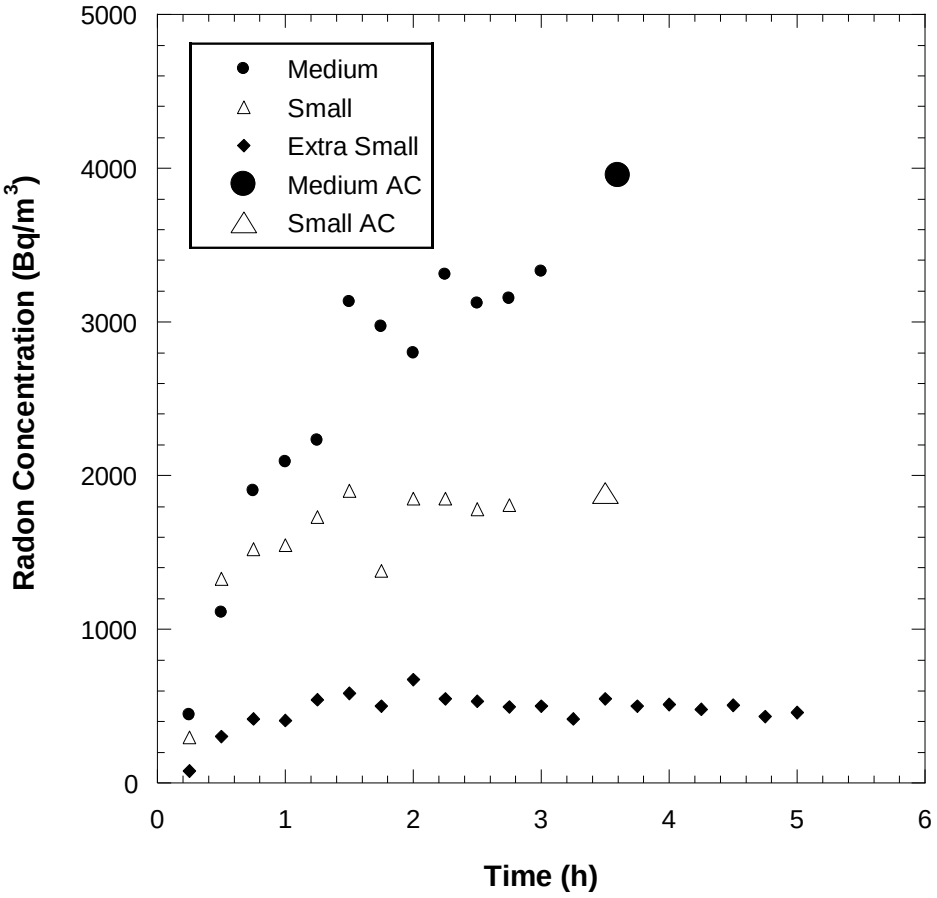

Fig. I111 - Radon concentration buildup curves measured at DC-4A at Shirley Basin South, WY.

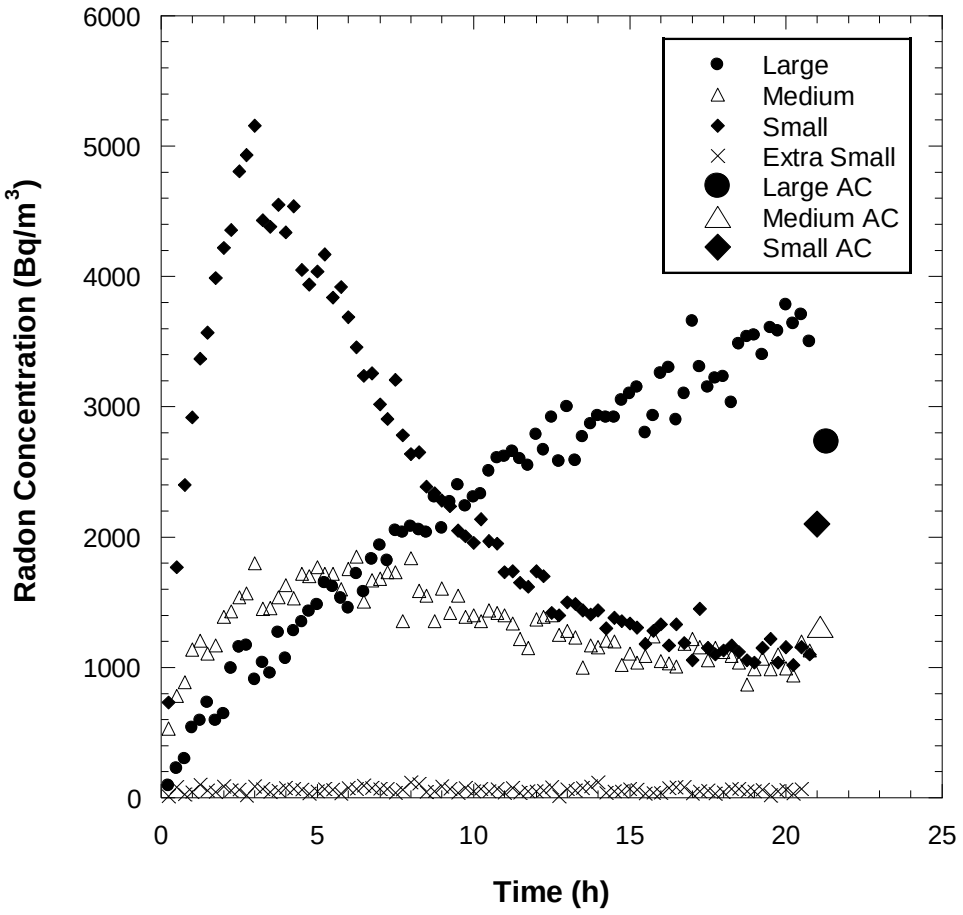

Fig. I112 - Radon concentration buildup curves measured at DC-4B at Shirley Basin South, WY.

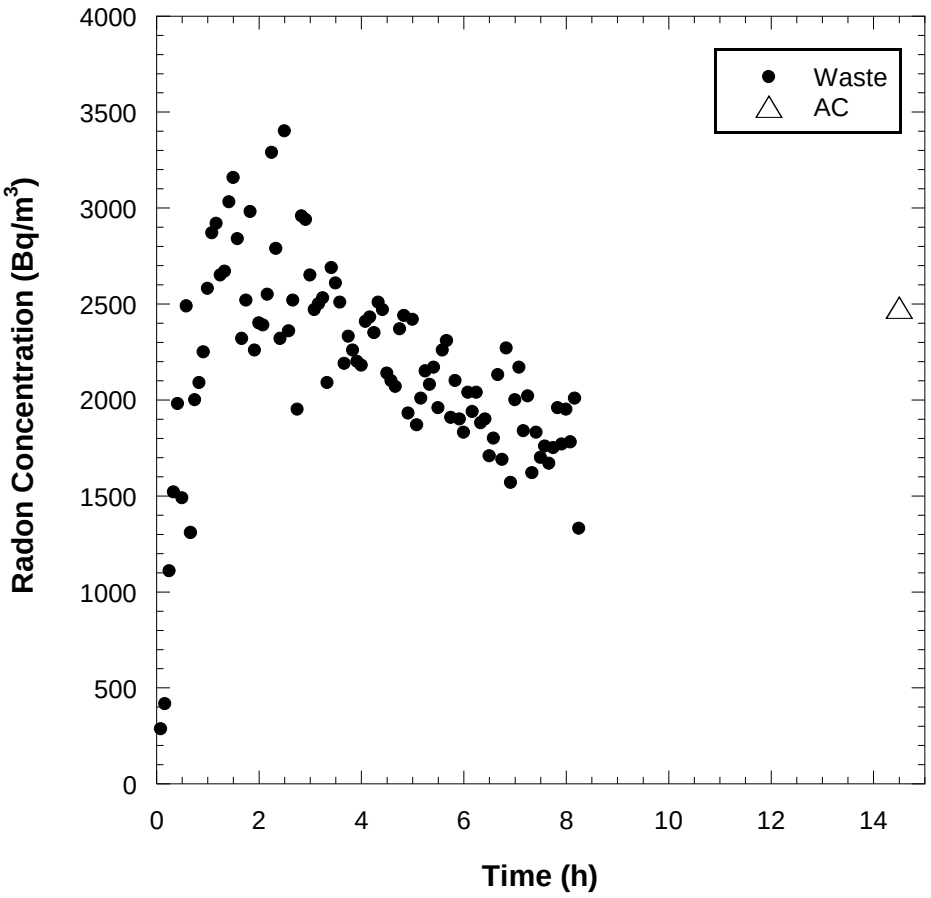

Fig. I113 - Radon concentration buildup curve measured from tailings at DC-4 at Shirley Basin South, WY.

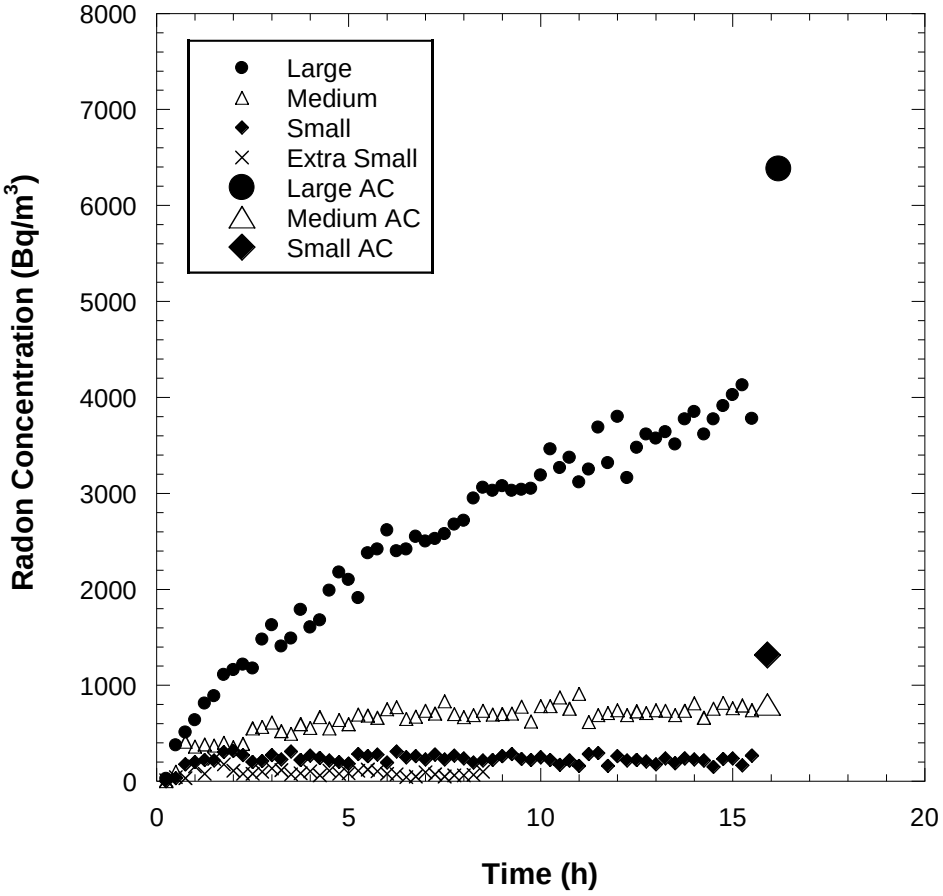

Fig. I114 – Radon concentration buildup curves measured at DC-5 at Shirley Basin South, WY.

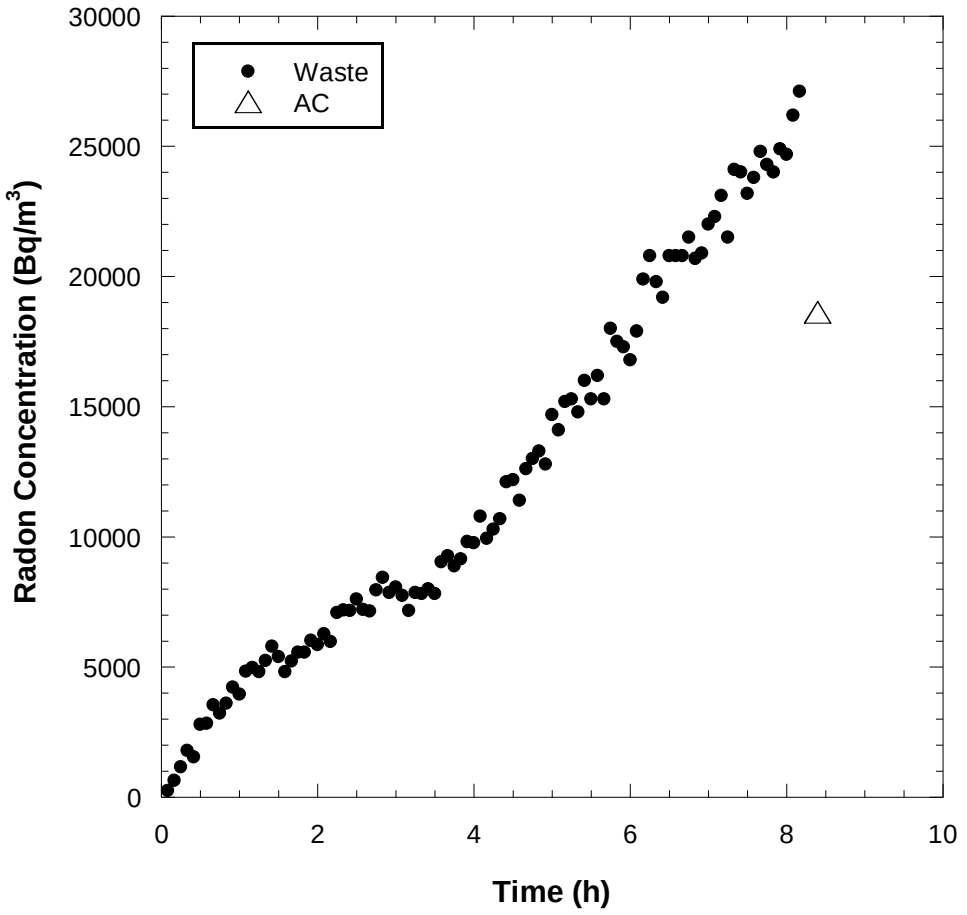

Fig. I115 - Radon concentration buildup curve measured from tailings at DC-5 at Shirley Basin South, WY.

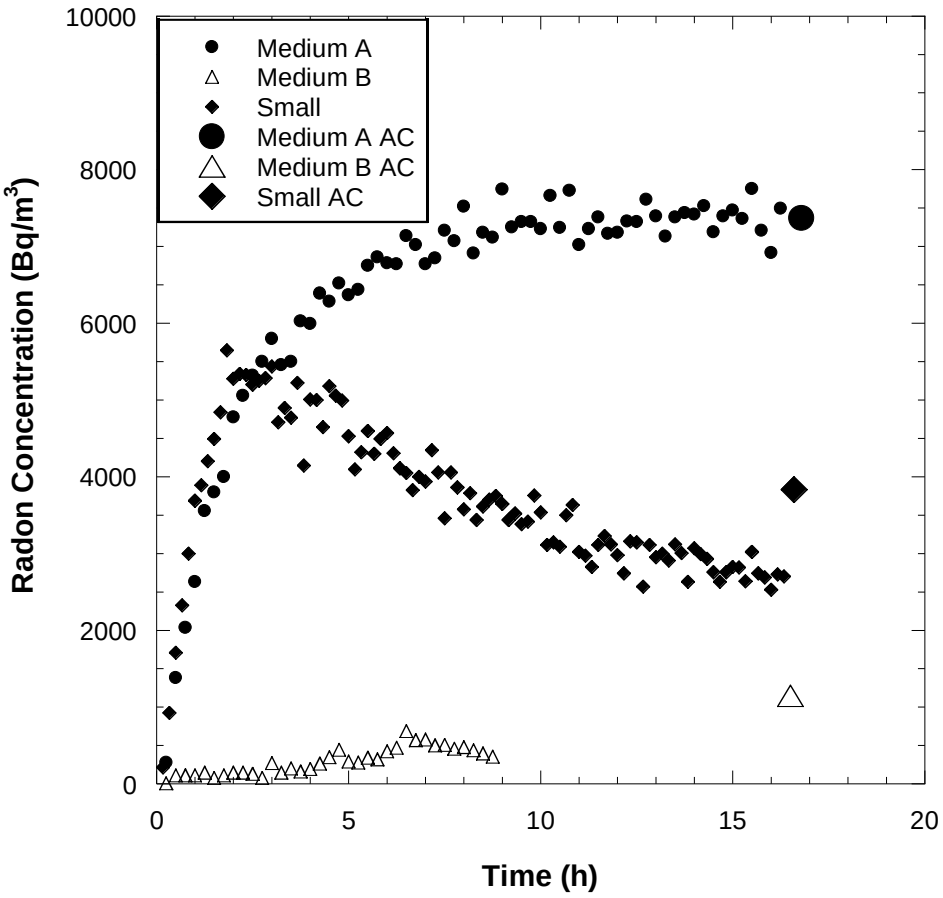

Fig. I116 – Radon concentration buildup curves measured at DC-6 at Shirley Basin South, WY.

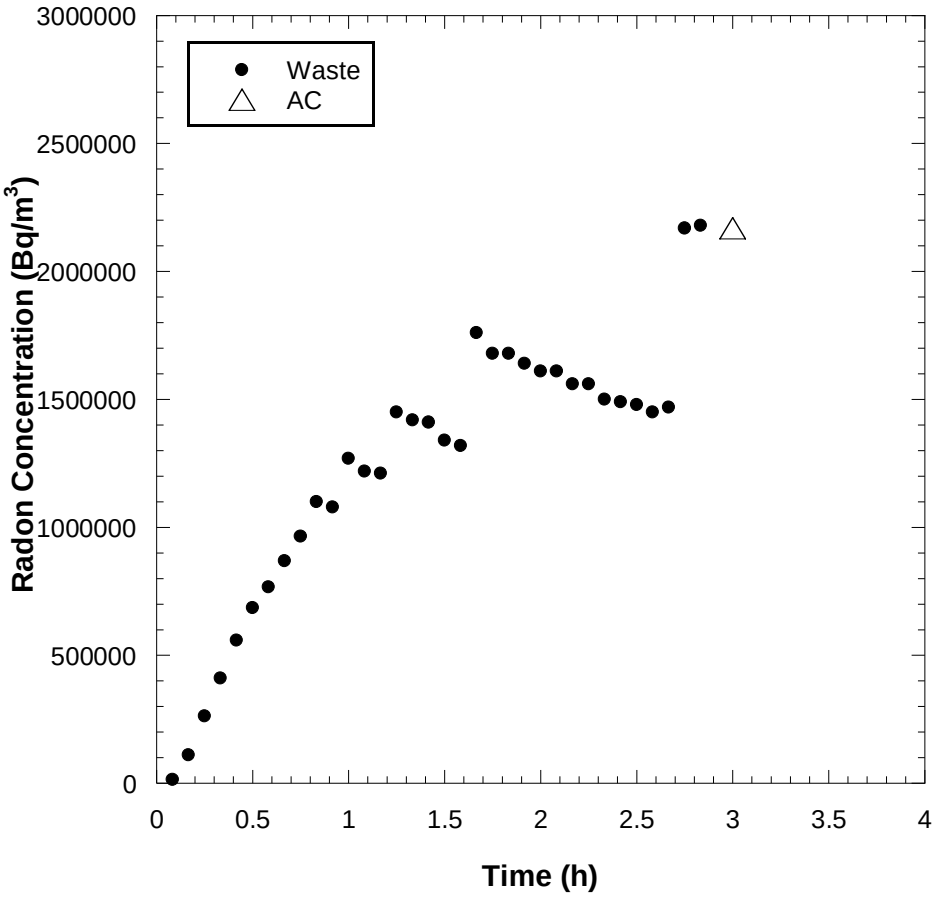

Fig. I117 - Radon concentration buildup curve measured from tailings at DC-6 at Shirley Basin South, WY.

APPENDIX IV - Radon Fluxes Measured from a Compacted Clay Rn Barrier at the Lakeview, OR Uranium Mill Tailings Disposal Site in 2017

ABSTRACT

Radon (Rn) fluxes were measured from the surface of a uranium mill tailings disposal site after 29 years of service. The tailings were contained by a compacted clay Rn barrier of varying thickness as well as protective layers consisting of a rock/soil matrix, a sandy drainage layer, and/or riprap for erosion control. Flux measurements were made with four different-sized flux chambers: extra small (area = 0.018 m^2, volume = 0.002 m^3), small (0.071 m^2, 0.011 m^3), medium (0.26 m^2, 0.035 m^3), and large (2.32 m^2, 0.352 m^3). Rn concentrations were measured concurrently using activated carbon (AC) canisters and continuously monitoring electronic RAD7 detectors with accumulation chambers. Flux measurements were made at the surface of the Rn barrier and from the surface of the underlying tailings at seven locations on the disposal cell. Rn fluxes measured at the surface of the Rn barrier were consistently lower than fluxes measured at the surface of the tailings, indicating that significant Rn attenuation was occurring within the barrier. The geometric mean of all flux values measured from the Rn barrier surface were lower than the regulatory maximum of 0.74 Bq/m^2-s. The majority of the surface flux measurements were low enough to be considered background. This means that the fluxes that were measured were likely from the cover soil alone, and the tailings were not contributing. Comparison of measurements from different sized flux chambers indicated that no scale-dependent flux measurements were observed. The geometric mean of all Rn flux measurements obtained in 2017 was 0.008 Bq/m^2s. Average in-situ water content measurements of the Rn Barrier material were found to have decreased slightly from as

built values. Saturated hydraulic conductivity testing on 350 mm diameter samples obtained from the Rn barrier is currently in progress.

1 FIELD SITE

The Lakeview Uranium disposal site is located approximately 7 miles Northwest of Lakeview, Oregon. The original processing facility was located approximately 1.5 miles northwest of Lakeview, and the contaminated tailings were transported to the final disposal area. The mill processed uranium ore for only three years, from 1958 to 1961. Removal and relocation of the contaminated tailings began in 1986 and the material was fully encapsulated by June of 1988 (U.S. Department of Energy, Legacy Management, 2017).

The disposal facility (**Figures 1, 2 and 3**) consists of an engineered landfill excavated into a hillside. The disposal cell has an area of approximately 6.5 x 10^4 m^2 and contains approximately 0.67 Tg of dry tailings with an estimated 1.6 TBq of radium-226. The cover profiles for the disposal cell are shown in **Figure 4**. The upper deck of the disposal cell was designed to consist of (bottom to top) a compacted clay Rn barrier (0.46 m), a sandy filter layer (0.15 m), followed by a rock/soil matrix layer (0.46 m). The 5:1 slope on the west and north perimeters of the cell was designed to consist of a compacted silt Rn barrier (0.46 m), a sandy filter layer (0.15 m), followed by a riprap layer (0.30 m) to allow for drainage and to protect from erosion (U.S. Department of Energy, Legacy Management, 2017). Native grasses and brush were found growing on the upper deck (**Figures 2, 5 and 6**), while the riprap slope was relatively free of windblown soil and vegetation (**Figures 6, 7 and 8**).

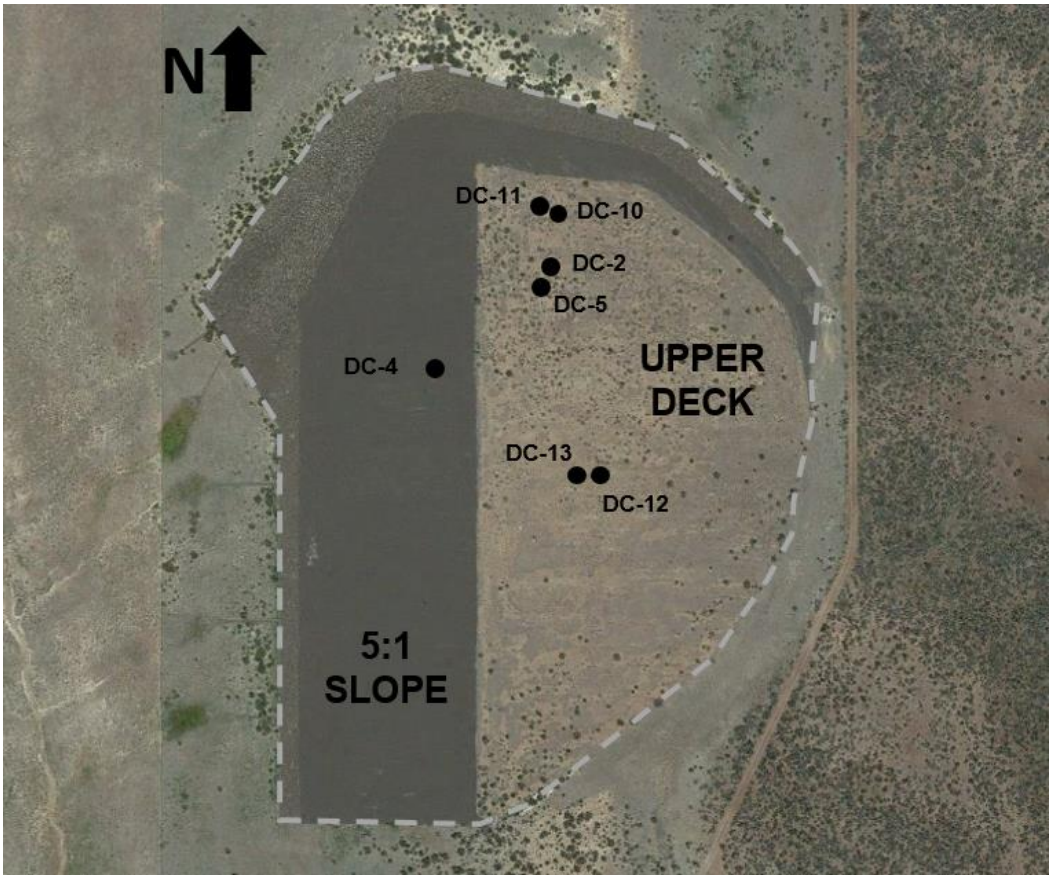

Figure 118 – Satellite image of the Lakeview, OR disposal site (Google Earth). The extents of the disposal cell are shown by the dotted line.

Figure 119 – View of the Lakeview, OR disposal cell looking south.

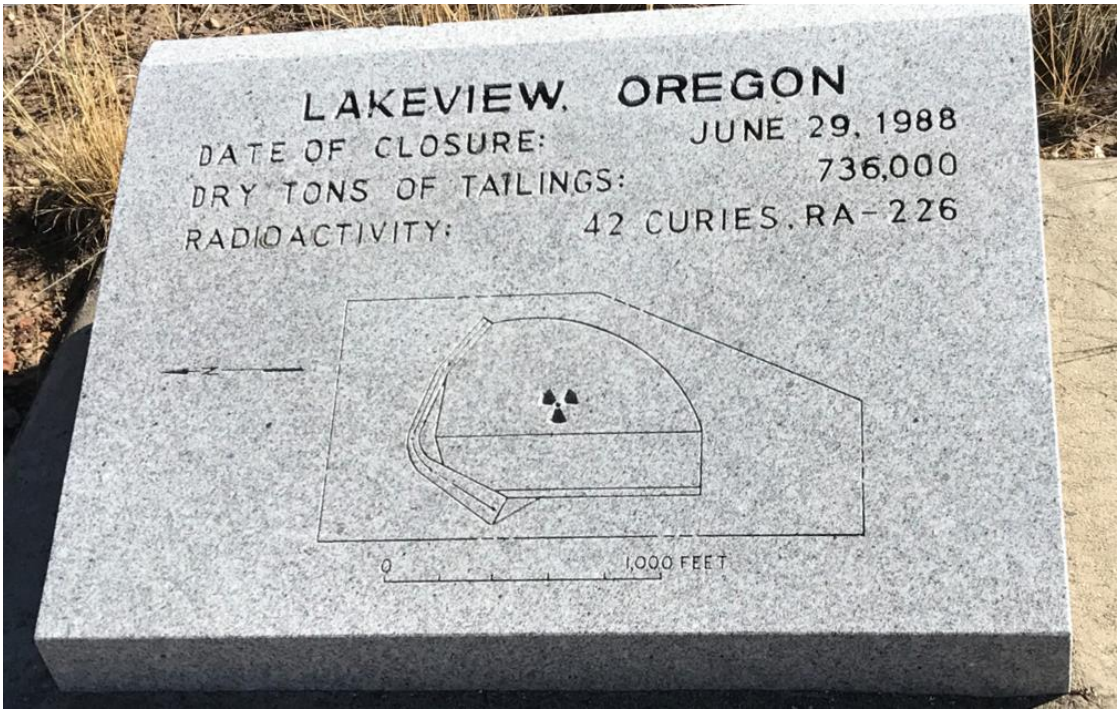

Figure 120 – Granite monument at the Lakeview, OR disposal cell.

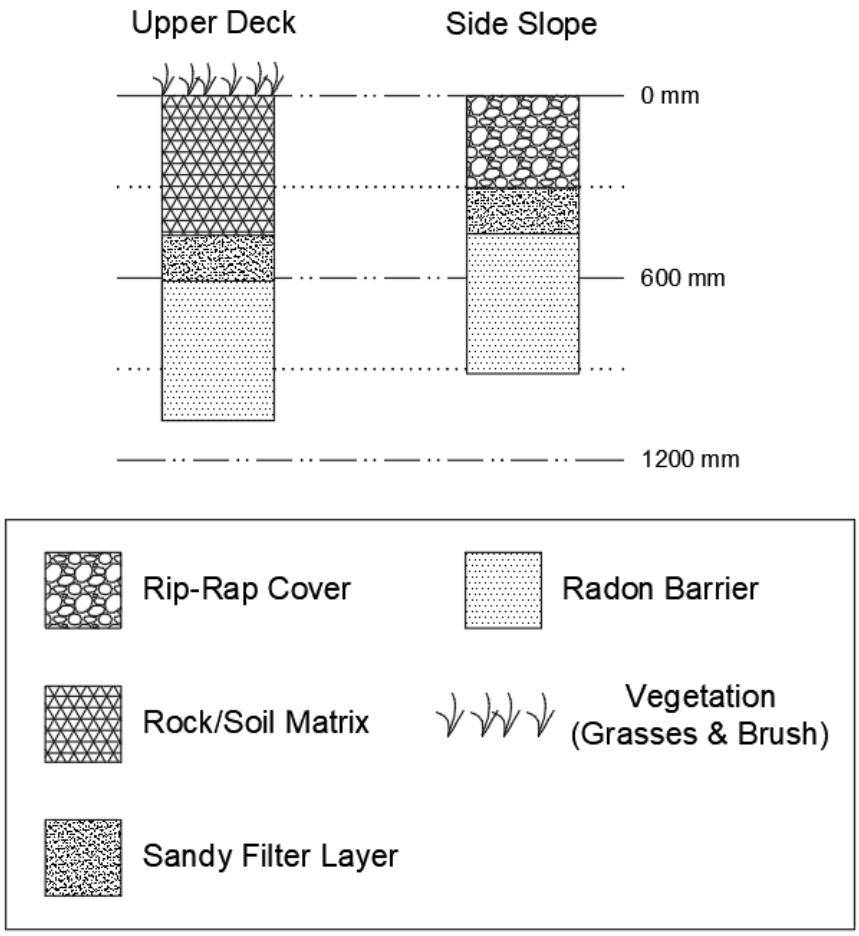

Figure 121 – Lakeview, OR as-built cover profiles.

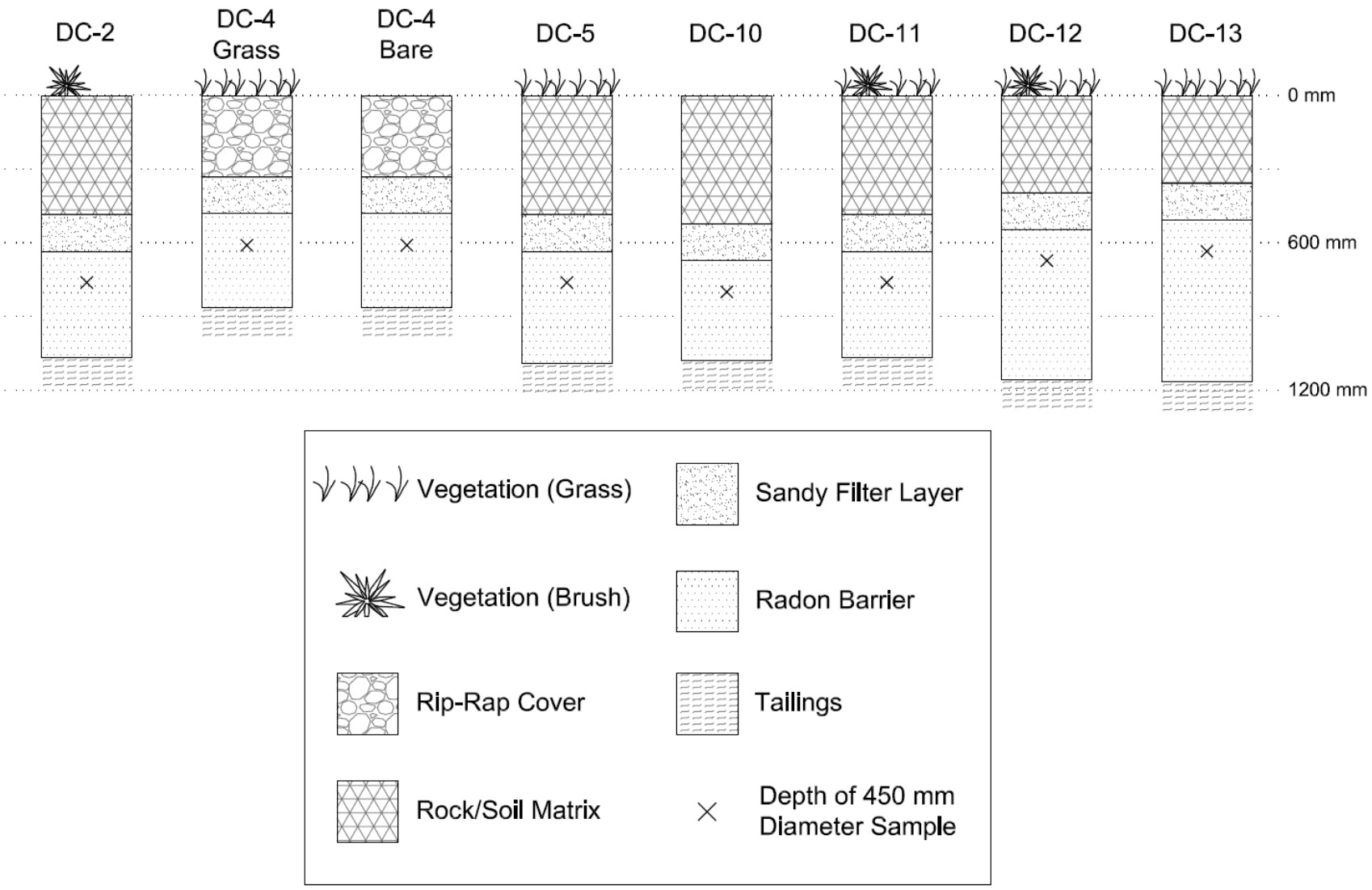

Figure 122 - Cover profiles at test pits excavated at the Lakeview, OR site in 2017.

Figure 123 – Various vegetation growth on the upper deck of the disposal cell.

Figure 124 – View from the edge of the 5:1 slope looking North.

Figure 125 - Riprap covered slope of the disposal cell looking East.

Figure 126 - Riprap covered slope of the disposal cell looking North.

2 RESULTS

Results from Rn fluxes measured at seven test pits are summarized below. Approximate locations of the test pits are shown in **Figure 1**. After Rn flux measurements were made at the top surface of the Rn barrier, an excavation was made through the Rn barrier to expose the underlying uranium mill tailings so that a flux measurement could be taken directly from the tailings.

The locations of the test pits were chosen to be in the vicinity of areas with distinct surface features, such as vegetation (brush and grasses), animal burrows, or lack thereof, that were expected to cause physical change within the cover. When possible, test pits were paired with an adjacent test pit that lacked the surface feature and served as a control test pit.

2.1 Radon Flux Measurements

The methods for the determination of Rn flux from AC and RAD7 were the same methods described in sections 4.1.1 and 4.1.2, respectively. Rn buildup curves from the surface of the Rn barrier and from the surface of the tailings from each test pit are shown in **Appendix I**. It should be noted that the rate of Rn concentration buildup from the flux test taken directly from the surface of the tailings is much greater than the rate of buildup from the test taken on the surface of the Rn. This shows that Rn is decaying significantly within the barrier, as it is intended to do.

Fluxes measured from the seven test pits using the RAD7 are summarized in **Figure 10 and 11** (below) and **Table A2 in Appendix A**. Fluxes measured from test pits

using AC canisters are summarized in **Table A3 in Appendix A**. Test pit descriptions are summarized in **Table 1**.

The compiled results of all flux tests do not indicate that there was an impact of measurement scale on flux at this site. **Figure 12** shows each flux value normalized by the geometric mean flux from that respective test pit. If the flux measurements were scale-dependent, it would be expected that the scatter between the flux ratios presented in **Figure 12** would decrease and cluster near a value of one as chamber area increased (and perhaps reach an “optimum” size), however, this trend was not apparent.

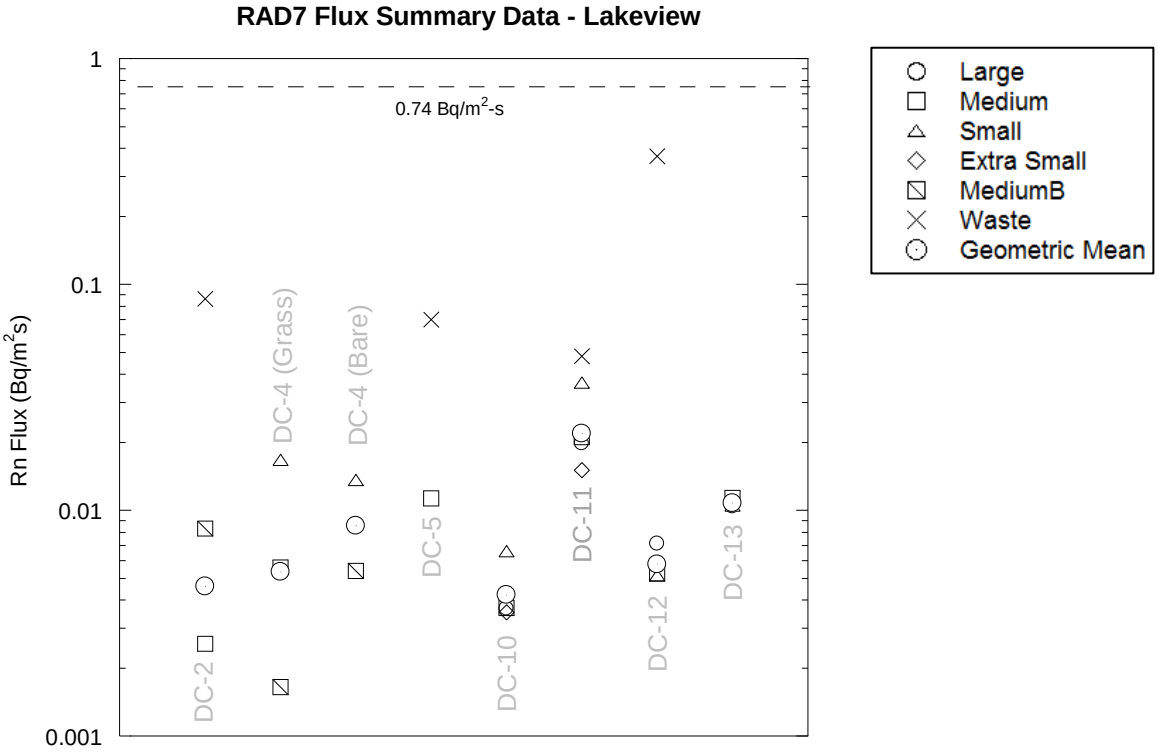

Figure 127 - Summary of fluxes measured with the RAD7 radon detector at the surface of the Rn barrier and the surface of the underlying tailings. DC-X = Disposal Cell X. The dashed horizontal line represents the maximum allowable surface flux specified by UMTRCA (0.74 Bq/m^{2}s).

Table 32 - Test pit descriptions.

	Test Pit	Location	Surface Feature Description
Micro Pit	DC-2	Upper Deck	Bitterbrush to Bare Ground Gradient
Pair	DC-4	Slope	Grass
			Bare
Micro Pit	DC-5	Upper Deck	Animal Burrow
Pair	DC-10	Upper Deck	Bare
	DC-11	Upper Deck	Bitterbrush
Pair	DC-12	Upper Deck	Bitterbrush
	DC-13	Upper Deck	Grass

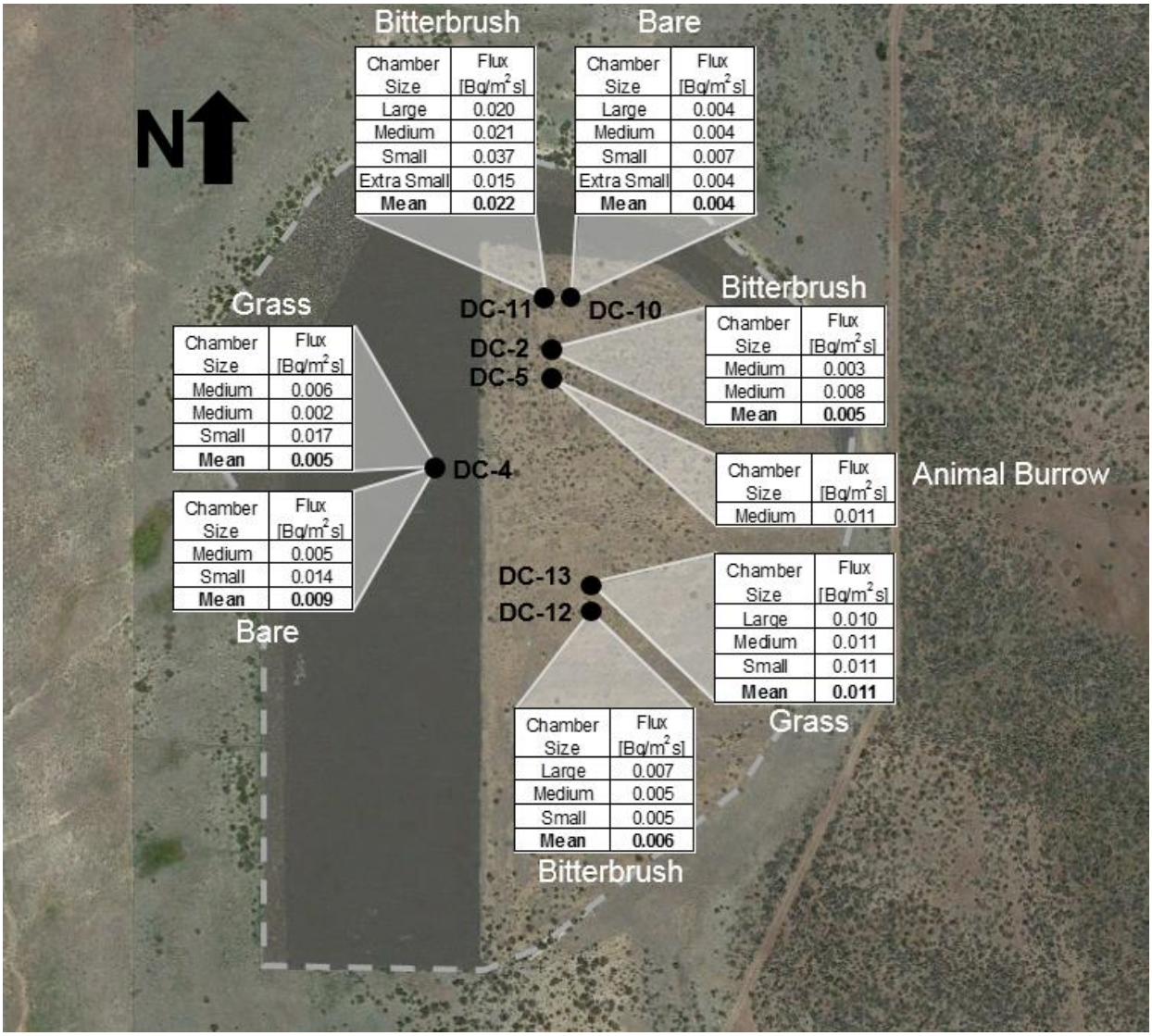

Figure 128 – Summary of Rn fluxes measured with the RAD7 radon detector at the surface of the Rn barrier.

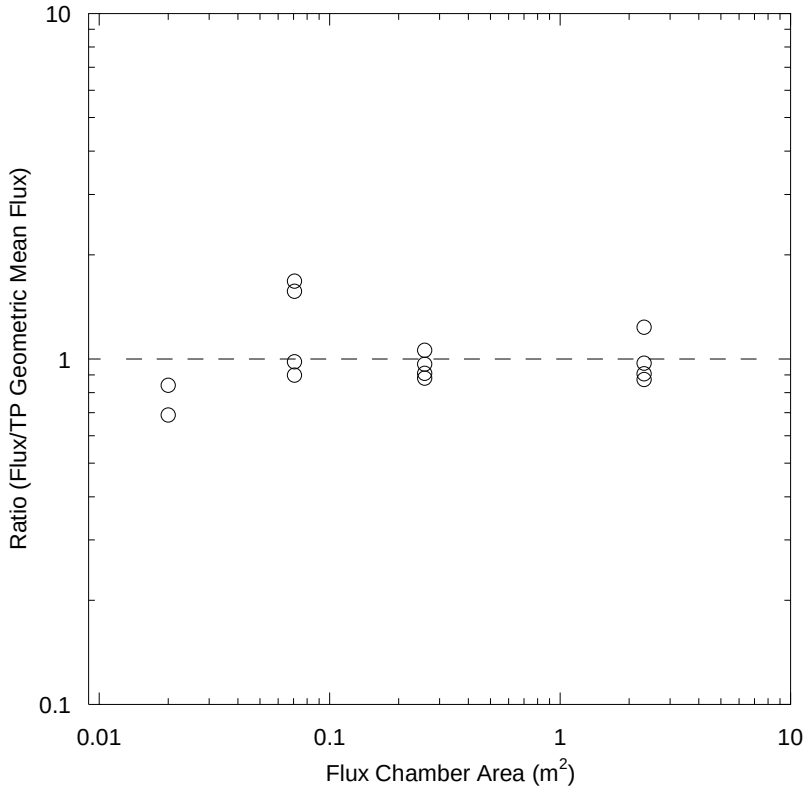

Figure 129 - Fluxes normalized by the geometric mean flux from each test pit.

2.3 Water Content Findings

Thin walled tube samples (diameter 70 mm) obtained from the Rn Barrier were cut in the lab into sections approximately 40 - 50 mm in length to obtain continuous profiles of water content versus depth (see section 4.1.4 laboratory methods). Additionally, the dimensions and masses of each of the sections were measured so that dry unit weight and saturation profiles could be created (a compilation of water content, dry density, and saturation profiles can be found in **Appendix F, G, and H**). The large-scale "block" samples (350 mm diameter) obtained from the site were also used to determine in-situ

water content and dry unit weight in the laboratory. The average water content values from the thin walled tube samples (referred to as “2017 values”) are compared to the in-situ, “as-built” values from the completion report in **Table 2.**

Table 33 – Summary of soil parameters as-built soil.

	As-Built*		2017	
Parameter	Value	n	Value	n
Gravimetric Water Content	40.5	75	35.6	12

* Department of Energy, Albuquerque Operation Office, Lakeview, Oregon Final Completion Report, Volume 3, 1991.

2.4 Saturated Hydraulic Conductivity

Saturated hydraulic conductivity testing is currently ongoing on 12 large-scale, undisturbed block samples (350 mm diameter) excavated from the Rn barrier at the Lakeview, OR site (see section 4.1.5 for methods).

3 SUMMARY

Rn fluxes were measured from seven test pits excavated at the uranium mill tailings disposal site in Lakeview, OR in 2017. The cover system had been in service for approximately 29 years at the time of the performed field work. Flux measurements were taken from the surface of the Rn barrier to observe if soil structure caused by pedogenesis had caused any changes in Rn flux. Four flux chamber sizes were used to observe if soil structure was causing any scale-dependent Rn flux. Rn concentrations and fluxes were measured with activated carbon (AC) canisters and RAD7 continuous monitors using accumulation chambers. AC canisters recorded a single concentration point while RAD7 monitors provided continuous concentration measurements.

Rn fluxes measured from the surface of the Rn barrier were significantly lower than the fluxes measured directly from the tailings beneath. This indicates that the Rn barrier is still effective at reducing the Rn flux at the surface, and Rn gas is attenuating significantly within it before reaching the atmosphere. No measurements of Rn flux were measured to be above the UMTRCA maximum allowed flux of 0.74 Bq/m^2s. The overall geometric mean of Rn flux measured from the surface of the Rn barrier was 0.008 Bq/m^2s. No apparent impacts of measurement scale were observed based on the fluxes measured at this field site.

Water content measurements taken from thin-walled tube samples obtained in the field in 2017 showed that the average water content of the Rn Barrier soil had decreased slightly from as-built measurements. Saturation levels were approximately 88%, on average.

Testing of the saturated hydraulic conductivity of large-scale block samples obtained in the field is currently ongoing.

REFERENCES

MK-Ferguson Company (1991).Department of Energy Contract No. DE-AC04 83AL18796. Lakeview, Oregon Final Completion Report. Volumes 1 – 6.

U.S. Department of Energy, Legacy Management (2017). UMTRCA Title II Lakeview, Oregon, Disposal Site. Fact Sheet.

APPENDIX A – ADDITIONAL TABLES AND FIGURES

Table A34 - Flux chamber areas and volumes.

Chamber Designation	Area [m^2]	Volume [m^3]
Extra Small	0.020	0.002
Small	0.071	0.011
Medium	0.260	0.032
Large	2.323	0.352

Table A35 – Tabulated summary of flux measurements from all test pits using RAD7.

Test Pit	Chamber Size	Flux	Geometric Mean Flux of Test Pit	Tailings Flux (Small Chamber)
		[Bq/m^2-s]	[Bq/m^2-s]	[Bq/m^2-s]
DC-2	Medium	0.003	0.005	0.086
	Medium	0.008		
DC-4 Grass	Medium	0.006	0.005	N/A
	Medium	0.002		
	Small	0.017		
DC-4 No Veg	Medium	0.005	0.009	N/A
	Small	0.014		
DC-5	Medium	0.011	0.011	0.070
DC-10	Large	0.004	0.004	N/A
	Medium	0.004		
	Small	0.007		
	Extra Small	0.004		
DC-11	Large	0.020	0.022	0.048
	Medium	0.021		
	Small	0.037		
	Extra Small	0.015		
DC-12	Large	0.007	0.006	0.368
	Medium	0.005		
	Small	0.005		
DC-13	Large	0.010	0.011	N/A
	Medium	0.011		
	Small	0.011		

Table A36 - Tabulated summary of flux measurements from all test pits using AC.

Test Pit	Chamber Size	Flux	Geometric Mean Flux of Test Pit	Tailings Flux (Small Chamber)
		[Bq/m^2-s]	[Bq/m^2-s]	[Bq/m^2-s]
DC-2	Medium	0.0013	0.0026	0.0022
	Medium	0.0049		
DC-4 (Grass)	Medium	0.0003	0.0003	0.0007
	Medium	0.0006		
	Small	0.0002		
DC-4 (Bare)	Medium	0.0010	0.0007	0.0007
	Small	0.0005		
DC-5	Medium	0.0062	0.0062	0.0055
DC-10	Large	0.0021	0.0015	0.0032
	Medium	0.0016		
	Small	0.0011		
	Extra Small	0.0002		
DC-11	Large	0.0097	0.0030	0.0176
	Medium	0.0041		
	Small	0.0026		
	Extra Small	0.0008		
DC-12	Medium	0.0031	0.0031	0.0198
	Small	0.0032		
DC-13	Large	0.0055	0.0045	0.0005
	Medium	0.0040		
	Small	0.0040		

APPENDIX B – TEST PIT EXCAVATION PHOTOS

Figure 130 – Removal and stockpiling of the topsoil layer.

Figure 131 – Removal of the rip-rap layer.

Figure 132 - Removal of the drainage layer to expose the top surface of the Rn Barrier.

Figure 133 – Replacement and compaction of the Rn barrier soil using a hand operated compactor.

Figure 134 – Replacement of the protective layers using an excavator.

APPENDIX C – FLUX MEASUREMENT PHOTOS

Figure 135 – Installation of flux chambers on the surface of the Rn barrier.

Figure 136 – Flux chambers installed on the Rn Barrier surface.

Figure 137 – Flux chambers installed on exposed tailings.

APPENDIX D – SOIL SAMPLING PHOTOS

Figure 138 – Obtaining a thin-walled tube sample of Rn barrier soil.

Figure 139 - Obtaining a thin-walled tube sample of Rn barrier soil.

Figure 140 – Trimming a 350 mm diameter block sample using a shovel.

Figure 141 – Installing a protective PVC sleeve around a 350 mm diameter sample.

APPENDIX E – SUMMARY OF LABORATORY TEST DATA

Table 37 – Summary of 350 mm Diameter Block Samples Collected at the Lakeview, OR Site in 2017.

Test Pit	Sample Designation	Depth of Top of Block Sample bgs (m)	Depth of Bottom of Block Sample BGS (m)	% Gravel	% Sand	% Fines	% Clay	LL	PL	PI	G_s	XRD
DC-2	A	0.64	0.89	1	32	67	11	-	-	-	-	-
DC-4 (Bare)	A	0.48	0.74	2	24	74	12	47	32	15	-	-
DC-4 (Grass)	A	0.48	0.74	IP	IP	74	IP	-	-	-	-	-
DC-5	A	0.64	0.89	2	31	67	13	-	-	-	-	-
DC-10	A	0.67	0.93	2	35	64	9	-	-	-	-	-
DC-11	A	0.64	0.89	2	37	61	10	45	31	14	2.60	-
	B	0.64	0.89									-
DC-12	A	0.55	0.80	2	35	63	6	-	-	-	2.61	-
DC-13	A	0.51	0.76	4	34	62	6	-	-	-	-	-

NM = Not Measured

IP = In Progress

Table 38 – Summary of 70 mm Diameter (Thin-Wall Tube) Samples Collected at the Lakeview, OR Site in 2017.

Test Pit	70 mm Diameter (Shelby Tube) Sample ID	Depth of Top of Sample Below Rn Barrier Surface (m)	Depth of Bottom of Sample Below Rn Barrier Surface (m)	Water Content Profile*
DC-2	A	0.00	0.34	x
	B	0.00	0.31	x
DC-4 (Bare)	A	0.00	0.36	x
	B	0.00	0.33	x
DC-4 (Grass)	A	0.00	0.33	x
	B	0.00	0.33	x
DC-5	A	0.00	-	NM
	B	0.00	0.35	x
DC-10	A	0.00	0.32	x
	B	0.00	0.35	x
DC-11	A	0.00	0.37	x
	B	0.00	0.38	x
DC-12	A	0.00	0.33	x
	B	0.25	0.50	x
DC-13	A	0.00	0.34	x
	B	0.20	0.56	x

* Water content profiles can be found in Appendix F

NM = Not Measured

Table 39 – Summary of Hydraulic Properties from 350 mm Diameter Block Samples Collected at the Lakeview, OR site in 2017.

Test Pit	Sample Designation	Gravimetric Water Content (%) *	γ_d (kN/m^3)	Saturated Hydraulic Conductivity (m/s) †	Soil Water Characteristic Curve §			
					θ_r	θ_s	α	n
DC-2	A	No Testing Performed to Date						
DC-4 (Bare)	A							
DC-4 (Grass)	A							
DC-5	A							
DC-10	A							
DC-11	A							
	B							
DC-12	A							
DC-13	A							

* ASTM D 2216

† ASTM D 5084

§ ASTM D 6836 - 02 (Method A and D)

APPENDIX F – GRAVIMETRIC WATER CONTENT PROFILES

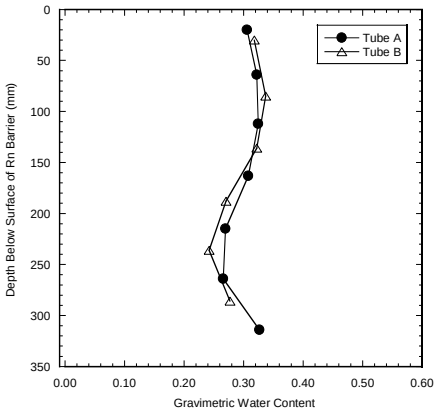

DC-2

Tube A	
Depth (mm)	Water Content
20	0.31
64	0.32
112	0.32
163	0.31
215	0.27
264	0.27
314	0.33
Mean	0.30

Tube B	
Depth (mm)	Water Content
30	0.32
85	0.34
136	0.32
188	0.27
236	0.24
286	0.28
Mean	0.29

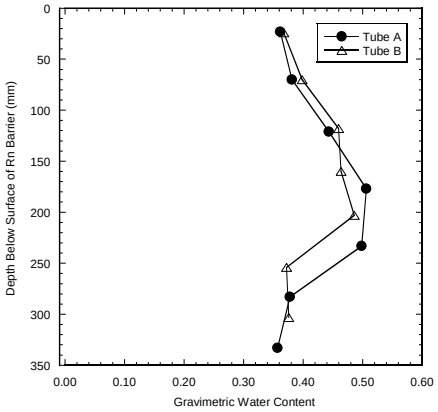

DC-4 (No Grass)

Tube A	
Depth (mm)	Water Content
23	0.36
70	0.38
121	0.44
177	0.51
233	0.50
283	0.38
333	0.36
Mean	0.42

Tube B	
Depth (mm)	Water Content
24	0.37
70	0.40
118	0.46
160	0.46
203	0.49
254	0.37
303	0.38
Mean	0.42

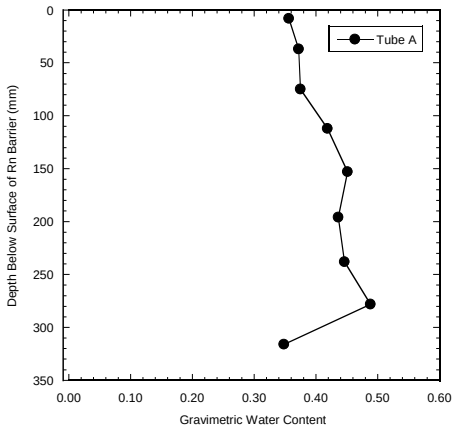

DC-4 (Grass)

Tube A	
Depth (mm)	Water Content
8	0.36
37	0.37
75	0.38
112	0.42
153	0.45
196	0.44
238	0.45
278	0.49
316	0.35
Mean	0.41

Tube B	
Depth (mm)	Water Content
Mean	

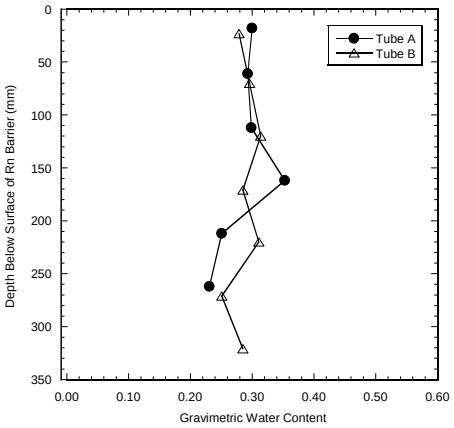

DC-5

Tube A	
Depth (mm)	Water Content
18	0.30
61	0.29
112	0.30
162	0.35
212	0.25
262	0.23
Mean	0.29

Tube B	
Depth (mm)	Water Content
23	0.28
70	0.30
120	0.31
171	0.28
220	0.31
271	0.25
321	0.28
Mean	0.29

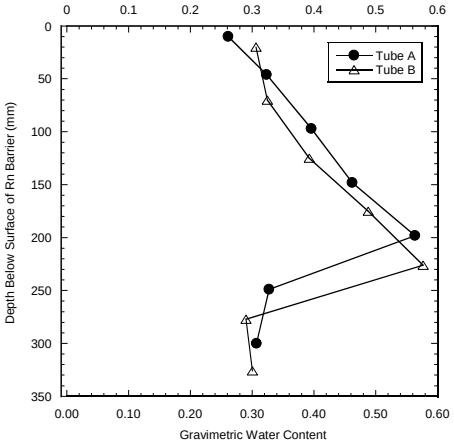

DC-10

Tube A	
Depth (mm)	Water Content
10	0.26
46	0.32
97	0.40
148	0.46
198	0.56
249	0.33
300	0.31
Mean	0.38

Tube B	
Depth (mm)	Water Content
20	0.31
70	0.32
125	0.39
175	0.49
226	0.58
277	0.29
326	0.30
Mean	0.38

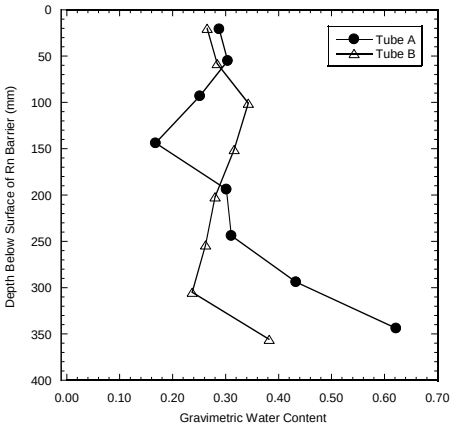

DC-11

Tube A	
Depth (mm)	Water Content
21	0.29
55	0.30
93	0.25
144	0.17
194	0.30
244	0.31
294	0.43
344	0.62
Mean	0.33

Tube B	
Depth (mm)	Water Content
20	0.27
58	0.28
101	0.34
151	0.32
202	0.28
254	0.26
305	0.24
356	0.38
Mean	0.30

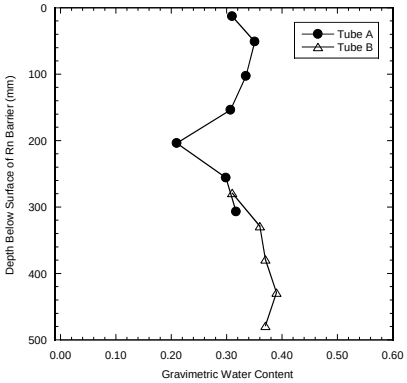

DC-12

Tube A

Depth (mm)	Water Content
13	0.31
51	0.35
103	0.34
154	0.31
204	0.21
256	0.30
307	0.32
Mean	0.30

Tube B

Depth (mm)	Water Content
279	0.31
329	0.36
379	0.37
429	0.39
479	0.37
Mean	0.36

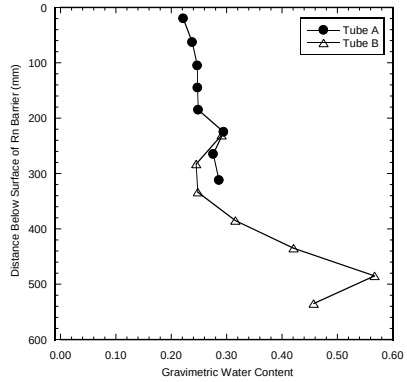

DC-13

Tube A

Depth (mm)	Water Content
20	0.22
63	0.24
105	0.25
145	0.25
185	0.25
225	0.29
265	0.28
312	0.29
Mean	0.26

Tube B

Depth (mm)	Water Content
231	0.29
283	0.25
334	0.25
385	0.32
435	0.42
485	0.57
535	0.46
Mean	0.36

APPENDIX G – DRY DENSITY PROFILES

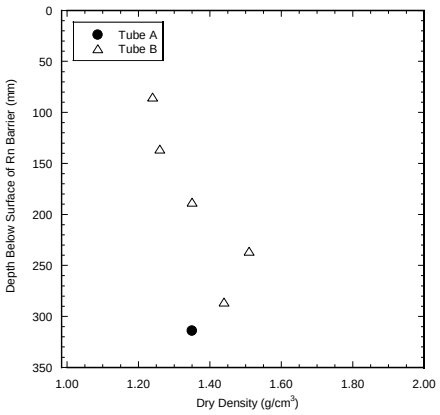

DC-2

Tube A

Depth (mm)	Dry Density (g/cm^3)
314	1.35

Tube B

Depth (mm)	Dry Density (g/cm^3)
85	1.24
136	1.26
188	1.35
236	1.51
286	1.44
Mean	1.36

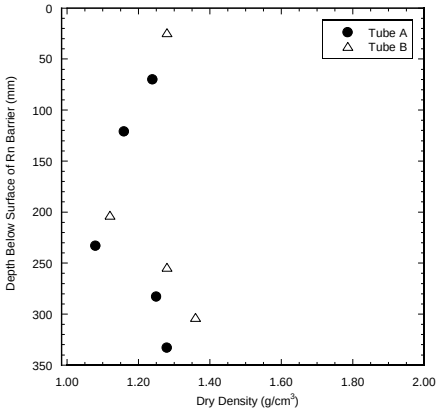

DC-4 (Bare Rip-Rap)

Tube A

Depth (mm)	Dry Density (g/cm^3)
70	1.24
121	1.16
177	0.98
233	1.08
283	1.25
333	1.28
Mean	1.16

Tube B

Depth (mm)	Dry Density (g/cm^3)
24	1.28
203	1.12
254	1.28
303	1.36
Mean	1.26

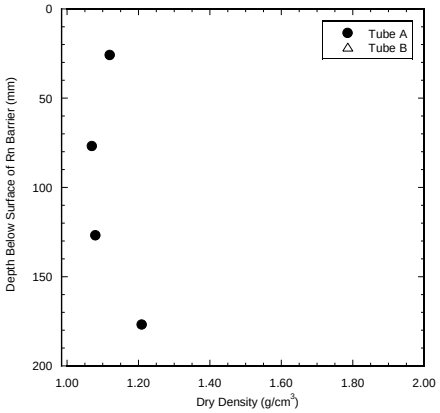

DC-4 (Grass)

Tube B

Depth (mm)	Dry Density (g/cm^3)
26	1.12
77	1.07
127	1.08
177	1.21
Mean	1.12

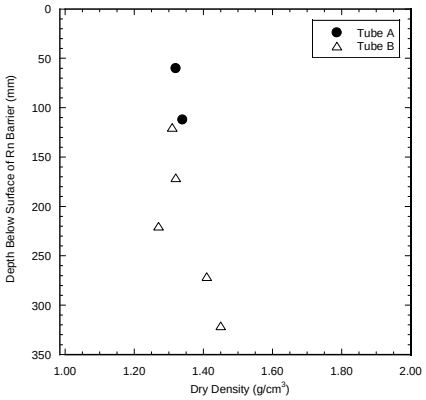

DC-5

Tube A

Depth (mm)	Dry Density (g/cm^3)
60	1.32
112	1.34
Mean	1.33

Tube B

Depth (mm)	Dry Density (g/cm^3)
120	1.31
171	1.32
220	1.27
271	1.41
321	1.45
Mean	1.35

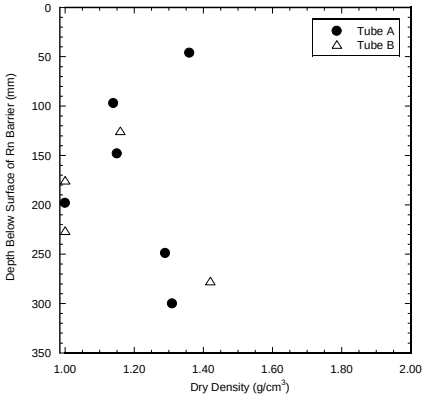

DC-10

Tube A

Depth (mm)	Dry Density (g/cm^3)
46	1.36
97	1.14
148	1.15
198	1.00
249	1.29
300	1.31
Mean	1.21

Tube B

Depth (mm)	Dry Density (g/cm^3)
125	1.16
175	1.00
226	1.00
277	1.42
Mean	1.14

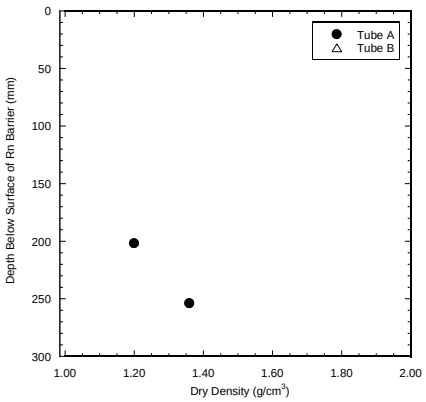

DC-11

Tube B

Depth (mm)	Dry Density (g/cm^3)
202	1.20
254	1.36
Mean	1.28

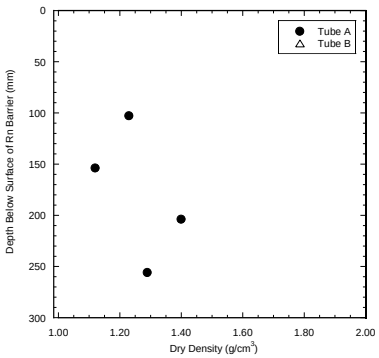

DC-12
Tube A

Depth (mm)	Dry Density (g/cm^3)
103	1.23
154	1.12
204	1.40
256	1.29
Mean	1.26

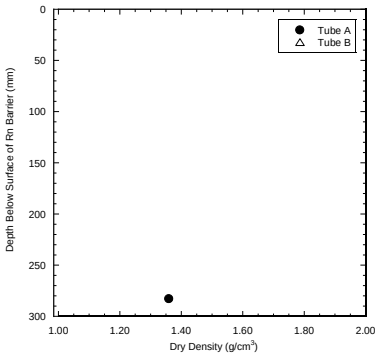

DC-13
Tube A

Depth (mm)	Dry Density (g/cm^3)
283	1.36

APPENDIX H – SATURATION PROFILES

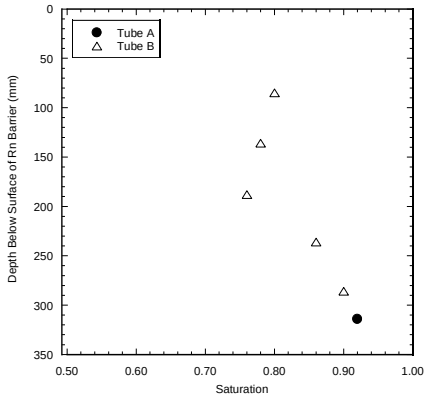

DC-2

Tube A	
Depth (mm)	Saturation
314	0.92

Tube B	
Depth (mm)	Saturation
85	0.80
136	0.78
188	0.76
236	0.86
286	0.90
Mean	0.82

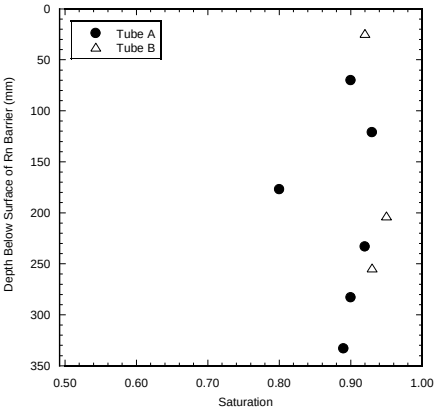

DC-4 (Bare Rip-Rap)

Tube A	
Depth (mm)	Saturation
70	0.90
121	0.93
177	0.80
233	0.92
283	0.90
333	0.89
Mean	0.89

Tube B	
Depth (mm)	Saturation
24	0.92
203	0.95
254	0.93
303	1.06
Mean	0.97

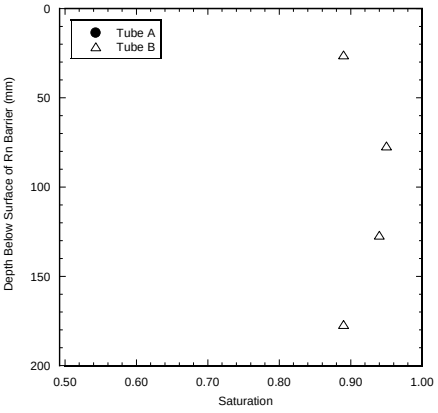

DC-4 (Grass)

Tube B	
Depth (mm)	Saturation
26	0.89
77	0.95
127	0.94
177	0.89
Mean	0.92

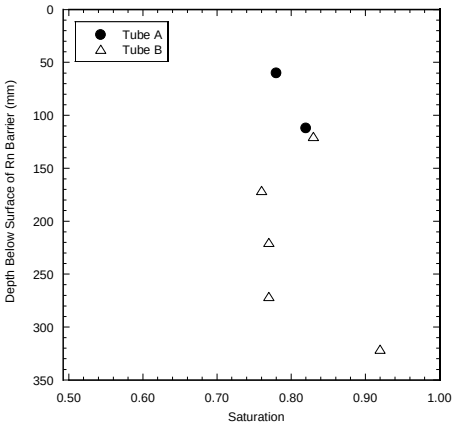

DC-5

Tube A

Depth (mm)	Saturation
60	0.78
112	0.82
Mean	0.80

Tube B

Depth (mm)	Saturation
120	0.83
171	0.76
220	0.77
271	0.77
321	0.92
Mean	0.81

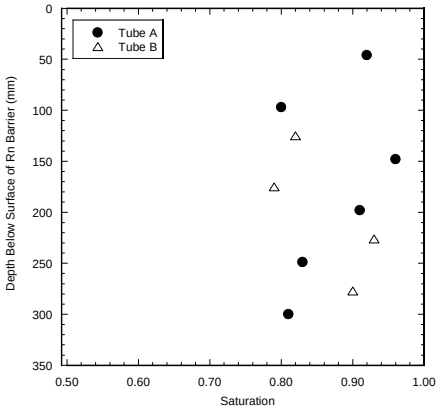

DC-10

Tube A

Depth (mm)	Saturation
46	0.92
97	0.80
148	0.96
198	0.91
249	0.83
300	0.81
Mean	0.87

Tube B

Depth (mm)	Saturation
125	0.82
175	0.79
226	0.93
277	0.90
Mean	0.86

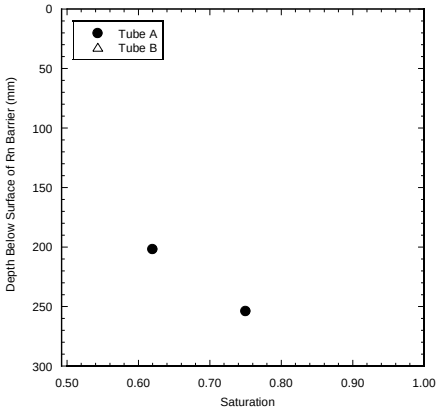

DC-11

Tube B

Depth (mm)	Saturation
202	0.62
254	0.75
Mean	0.68

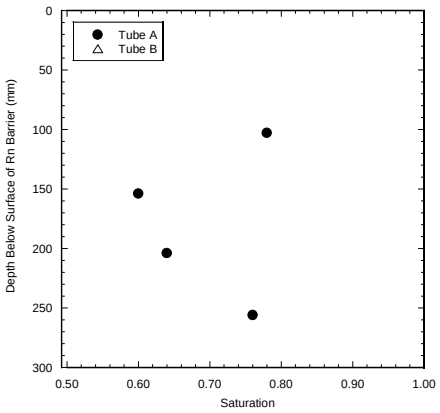

DC-12
Tube A

Depth (mm)	Saturation
103	0.78
154	0.60
204	0.64
256	0.76
Mean	0.69

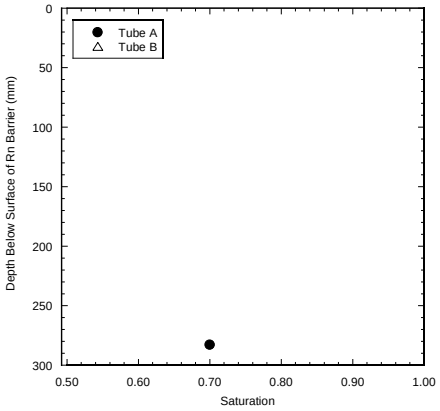

DC-13
Tube A

Depth (mm)	Saturation
283	0.70

APPENDIX I – RADON CONCENTRATION BUILDUP CURVES

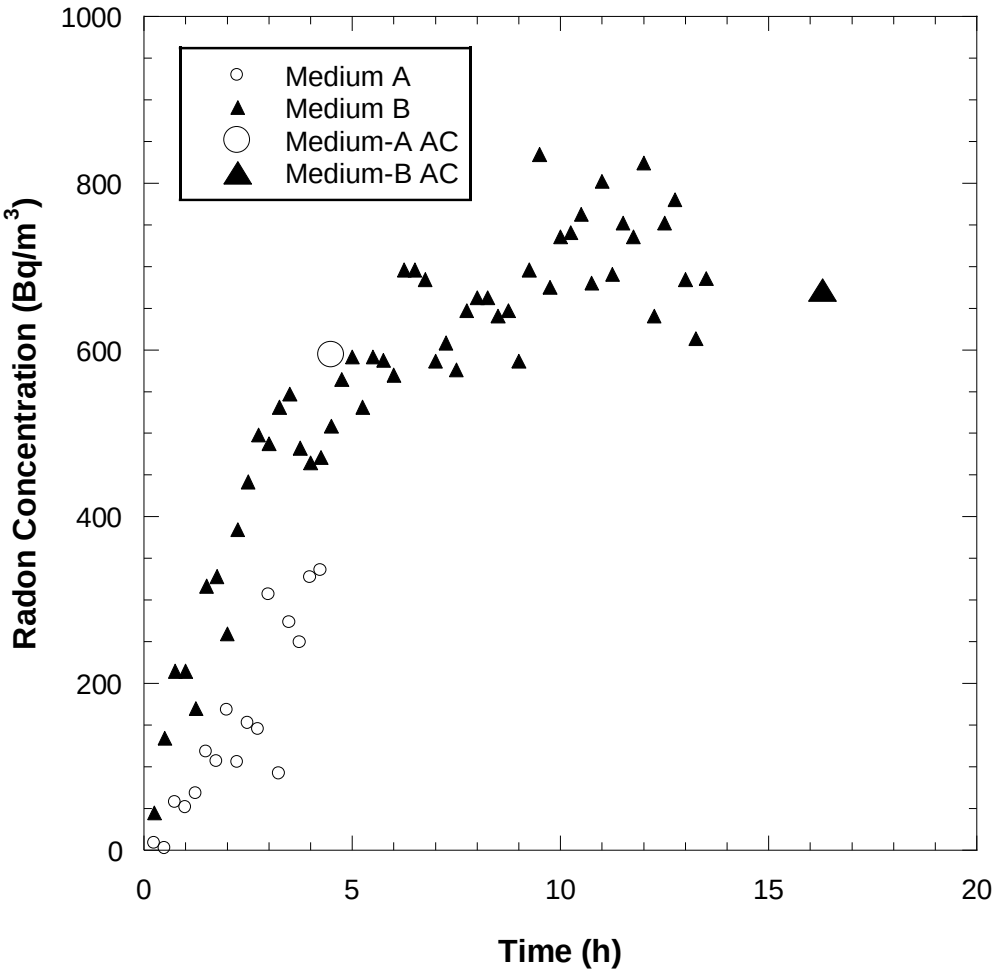

Fig. P142 – Radon concentration buildup curves measured at DC-2 at Lakeview, OR.

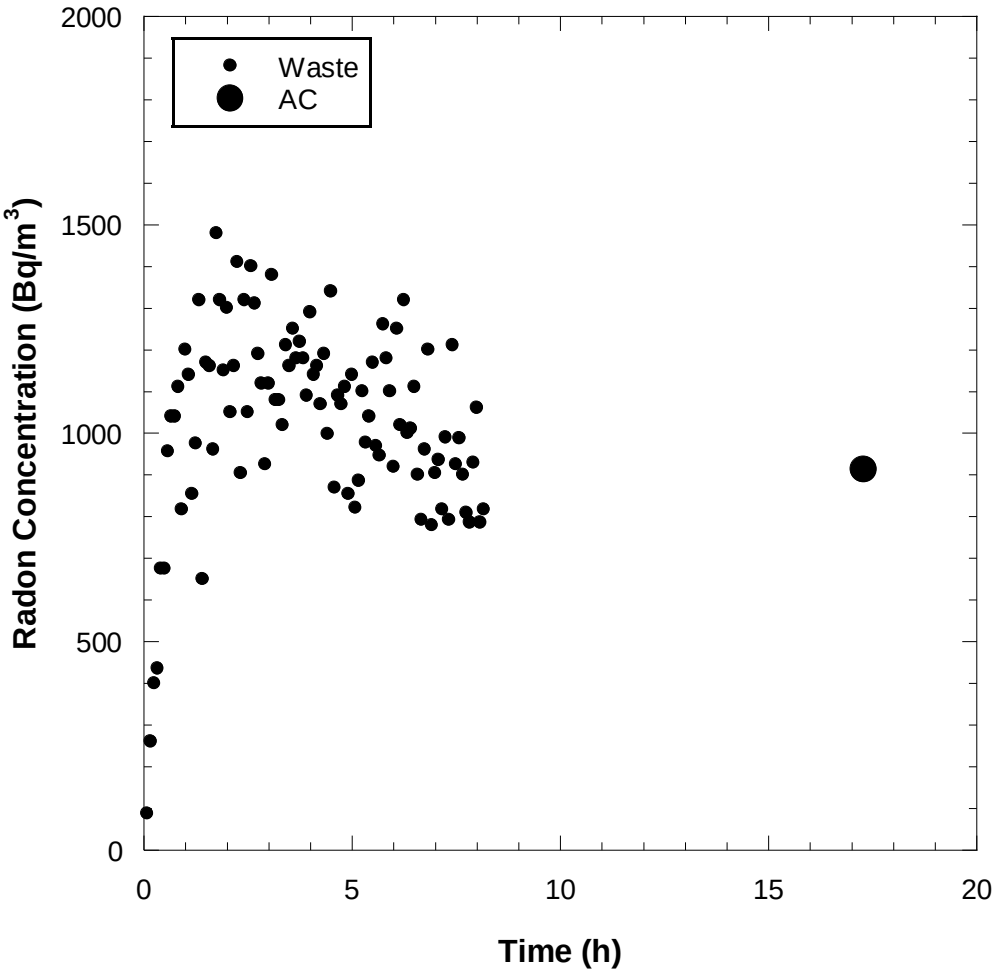

Fig. P143 - Radon concentration buildup curves measured from tailings at DC-2 at Lakeview, OR.

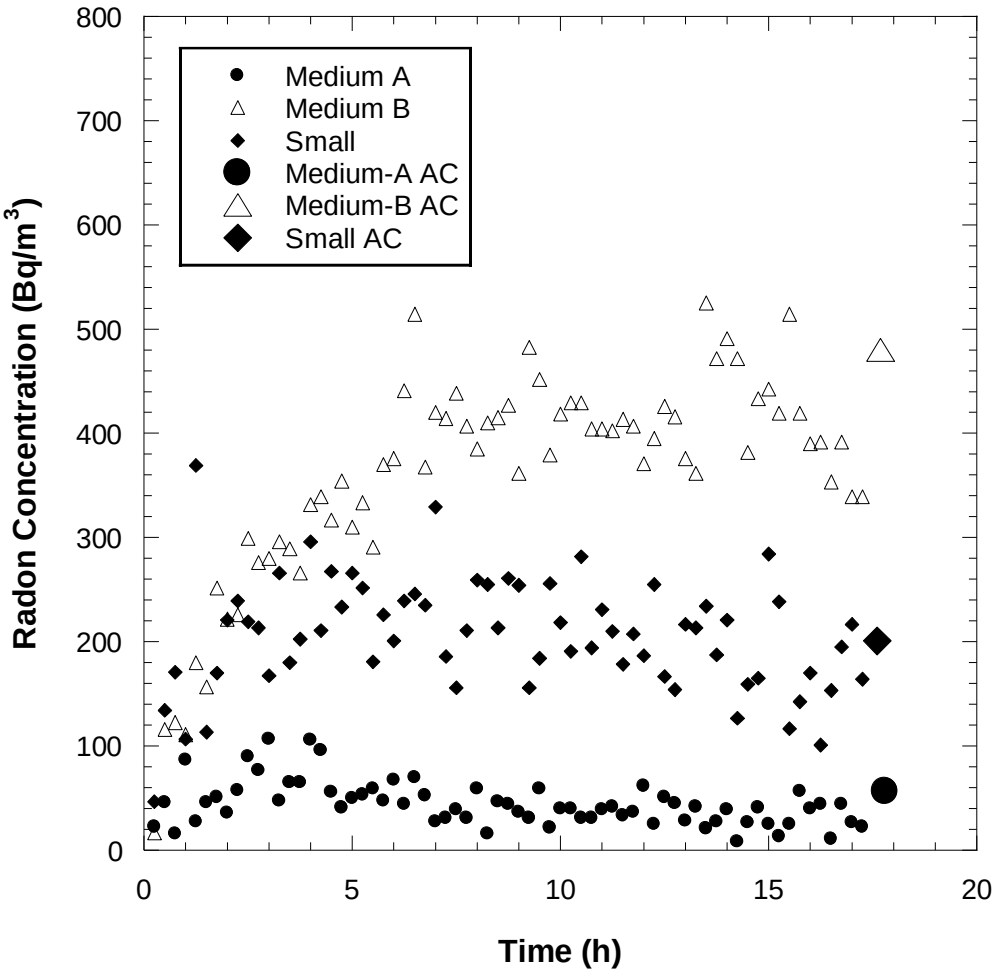

Figure 144 – Radon concentration buildup curves measured at DC-4 (no grass) at Lakeview, OR.

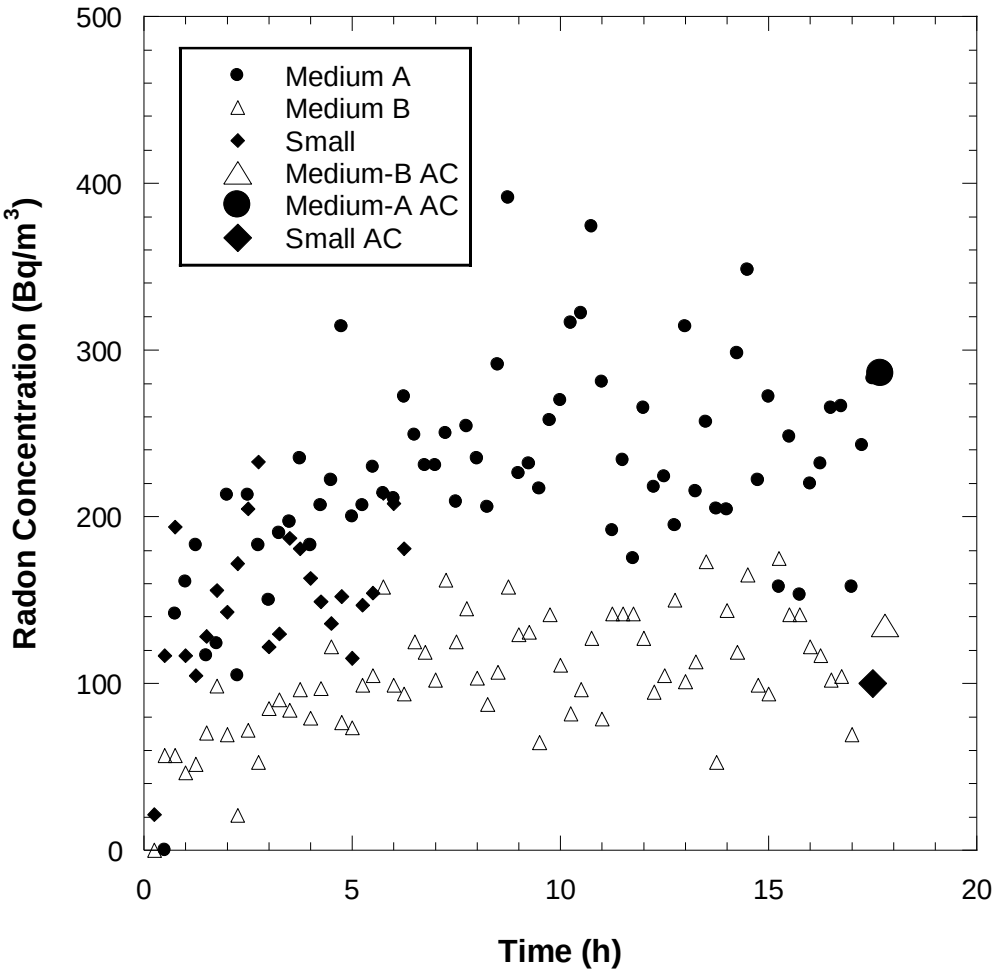

Figure 145 – Radon concentration buildup curves measured at DC-4 (grass) at Lakeview, OR.

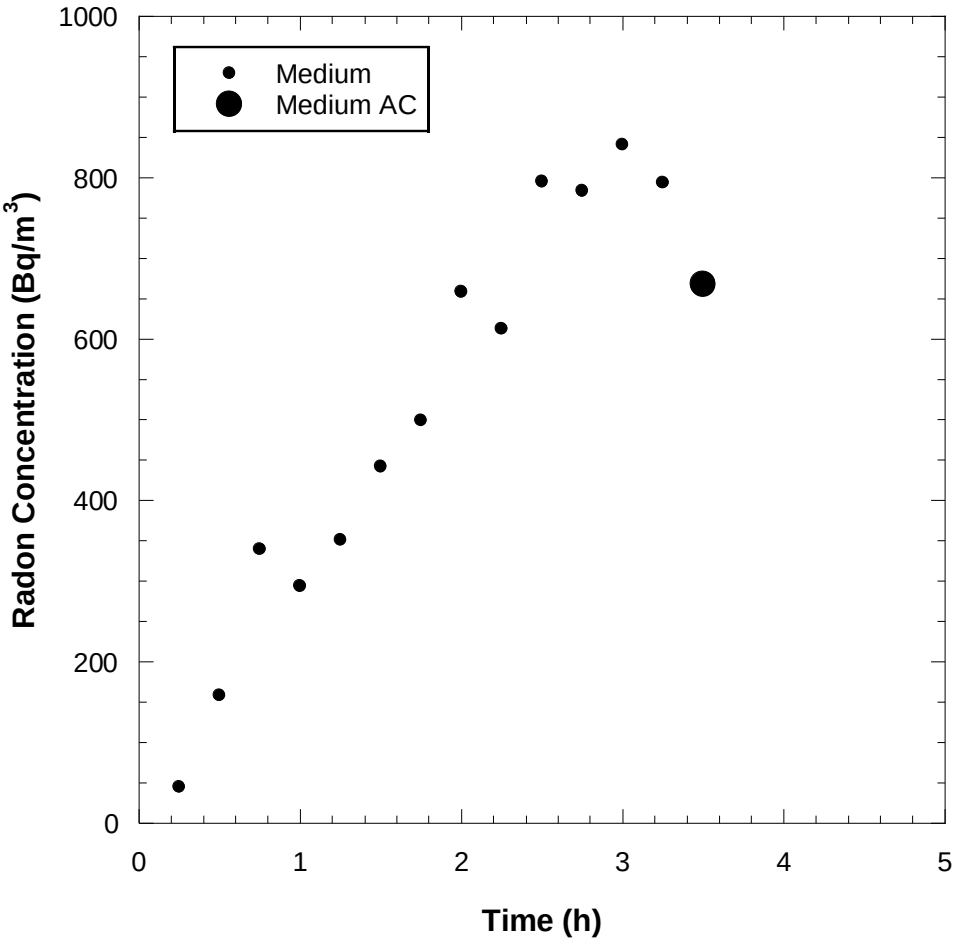

Figure 146 – Radon concentration buildup curves measured at DC-5 at Lakeview, OR.

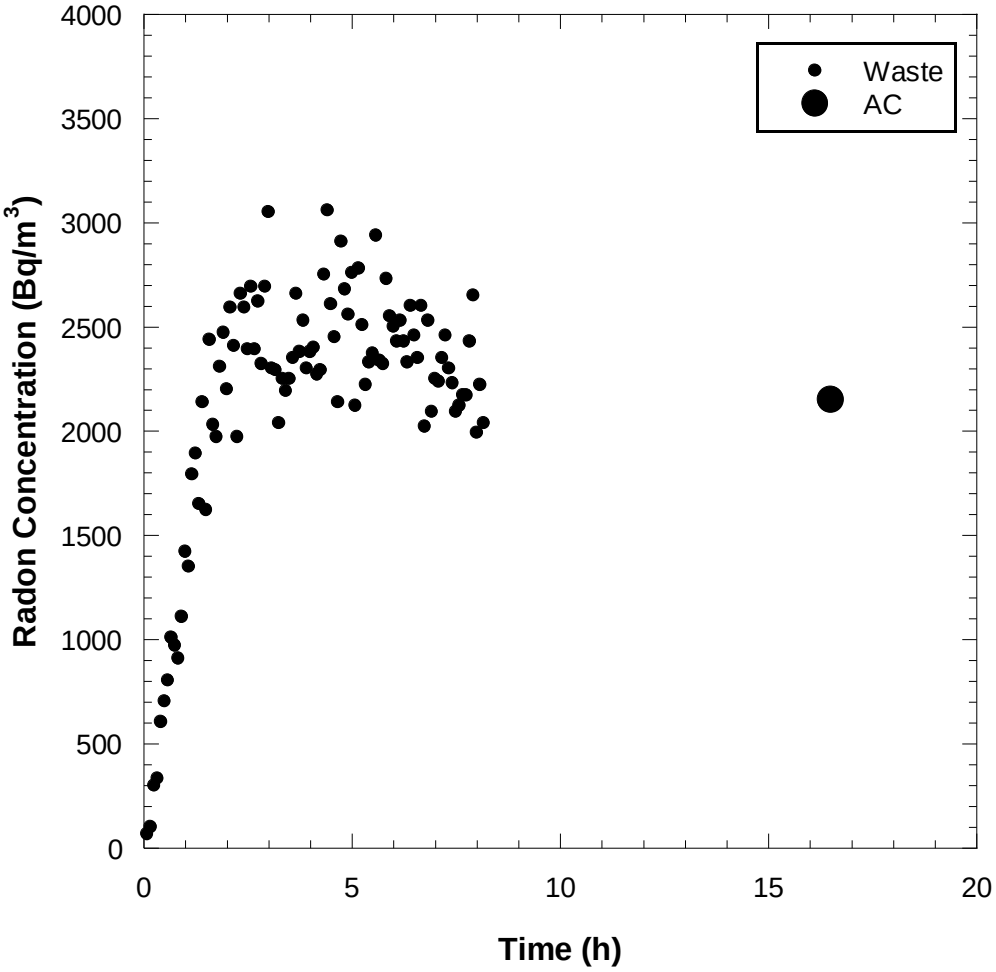

Figure 147 – Radon concentration buildup curves measured from tailings at DC-5 at Lakeview, OR.

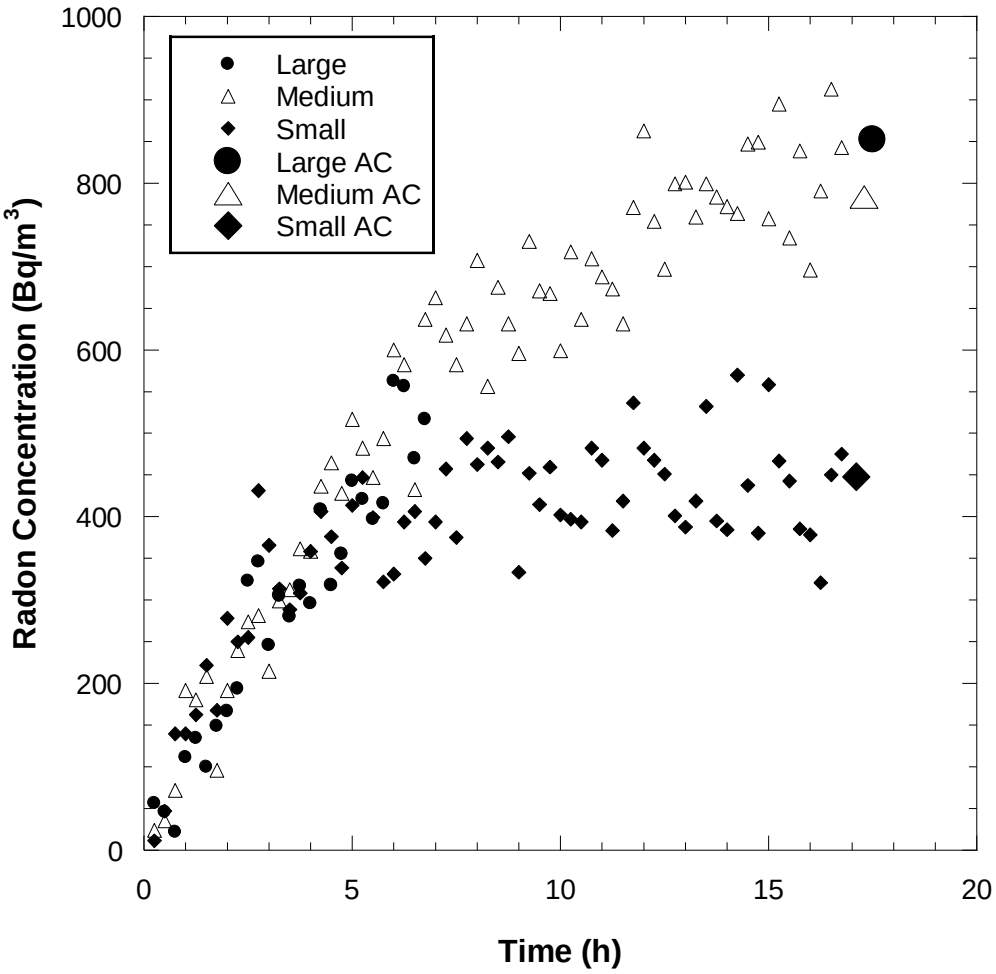

Figure 148 – Radon concentration buildup curves measured at DC-10 at Lakeview, OR.

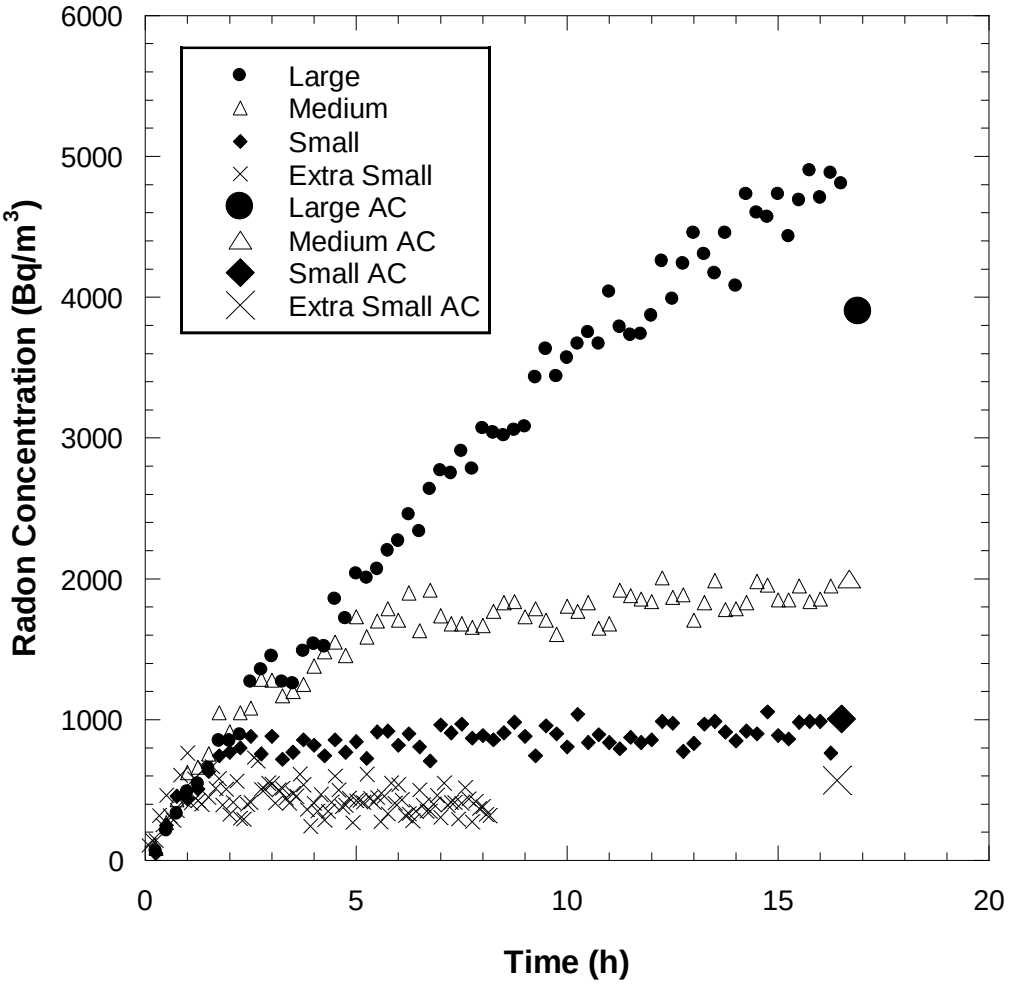

Figure 149 – Radon concentration buildup curves measured at DC-11 at Lakeview, OR.

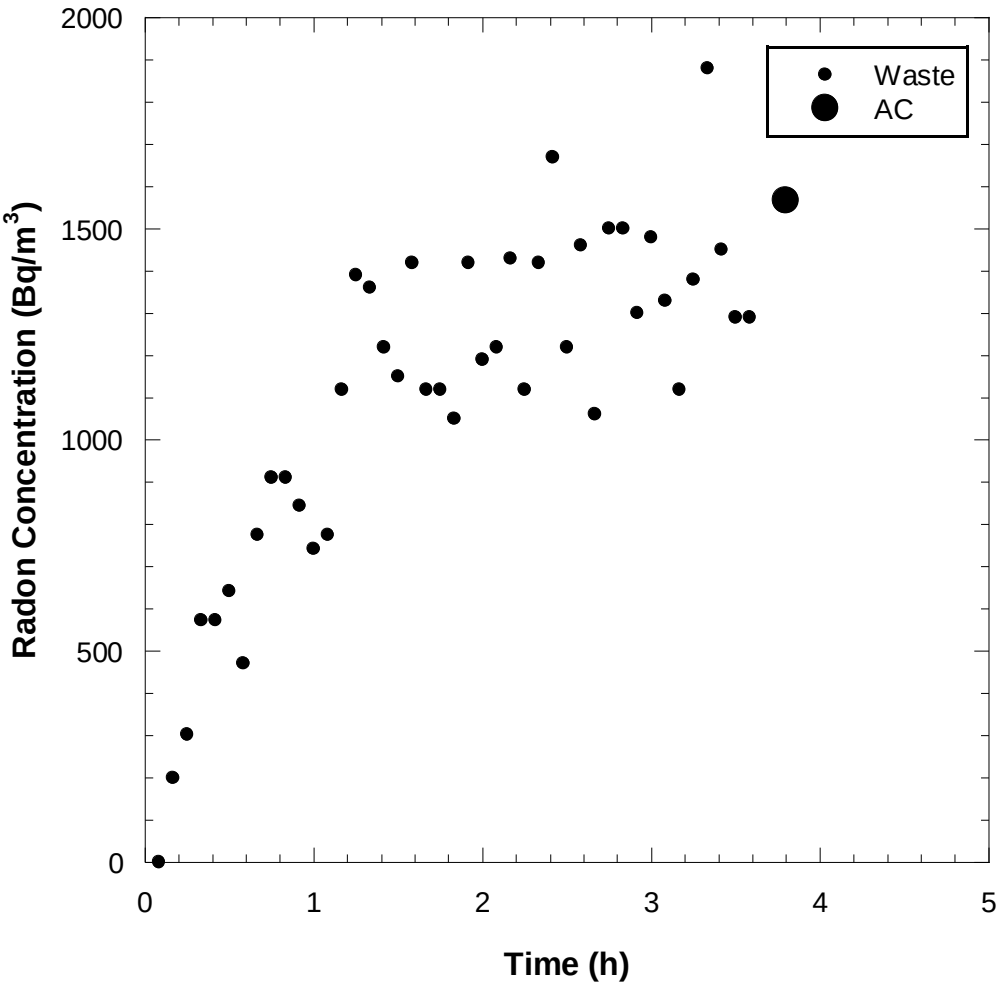

Figure 150 – Radon concentration buildup curves measured from tailings at DC-11 at Lakeview, OR.

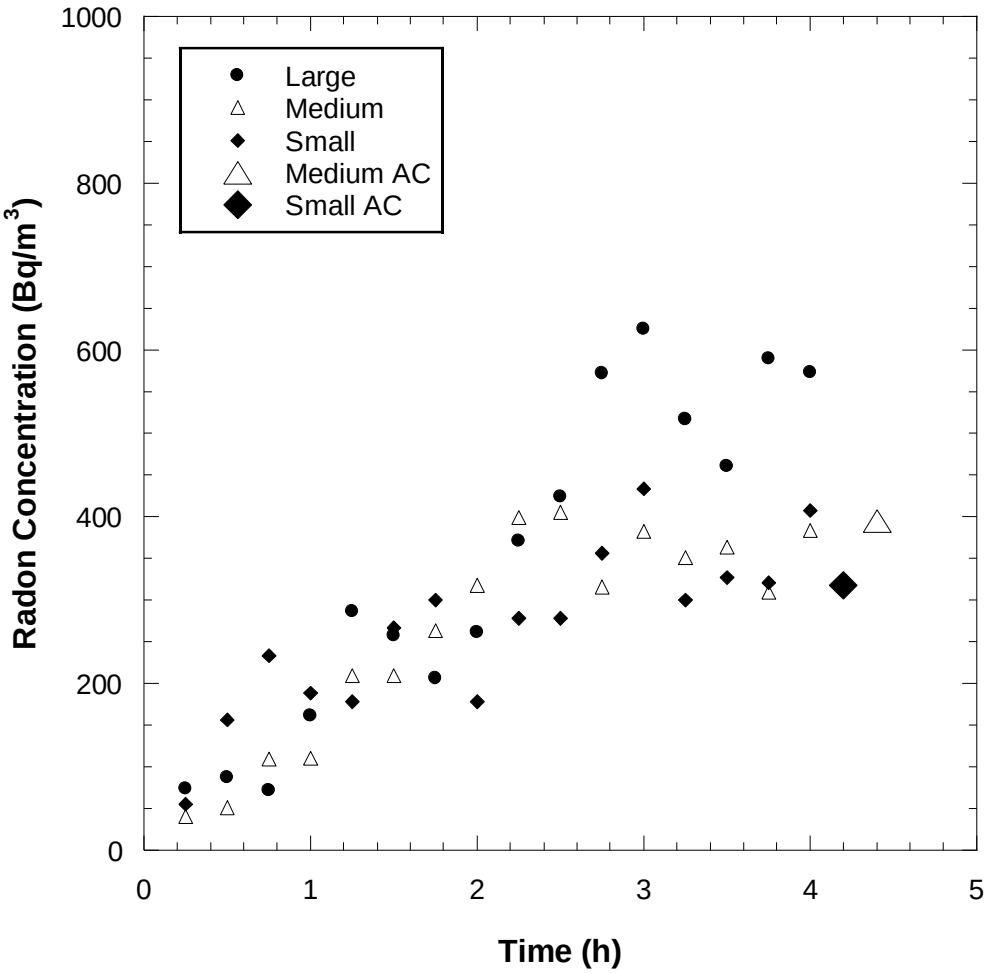

Figure 151 – Radon concentration buildup curves measured at DC-12 at Lakeview, OR.

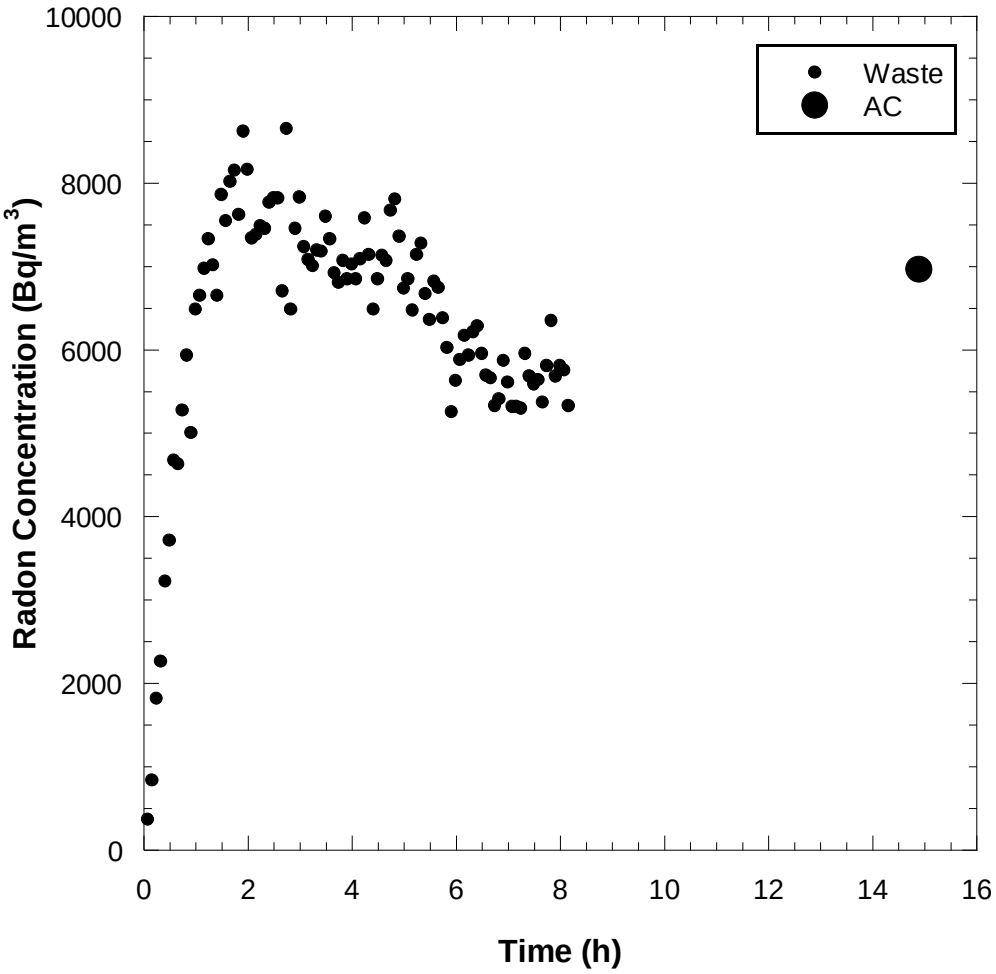

Figure 152 Radon concentration buildup curves measured from tailings at DC-12 at Lakeview, OR.

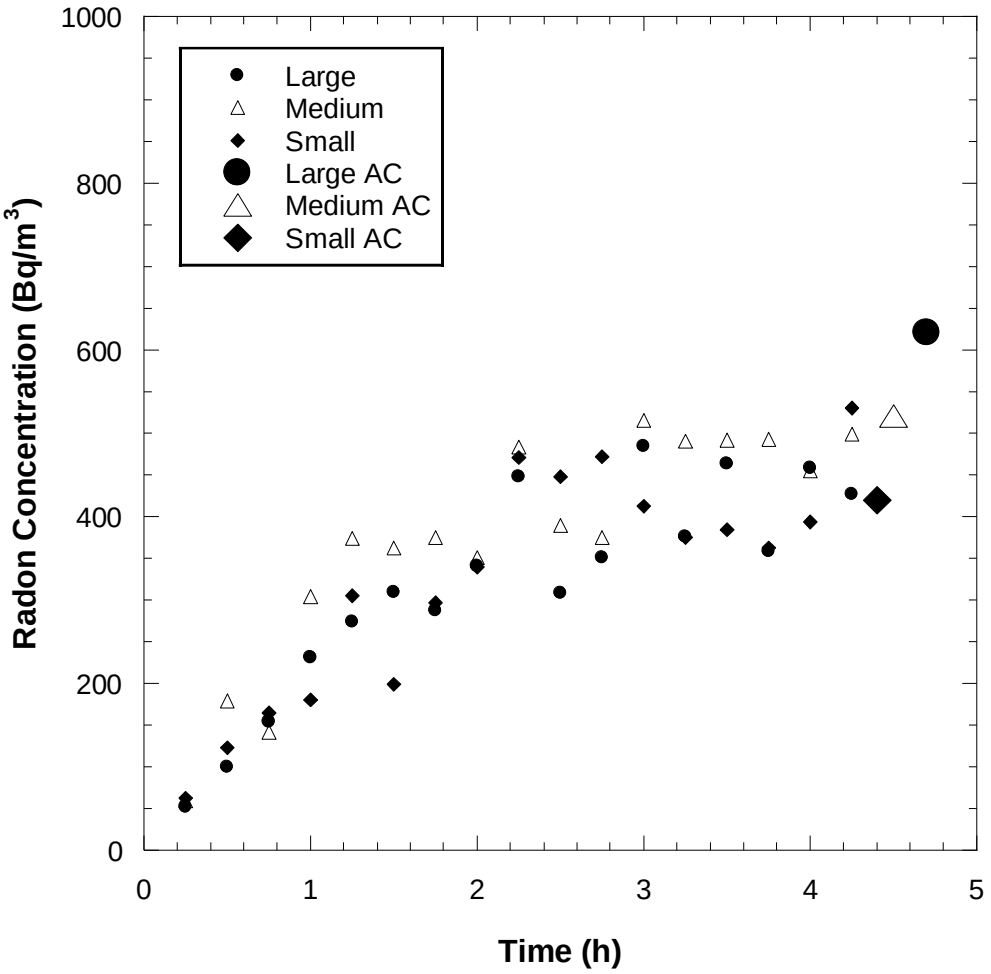

Figure 153 - Radon concentration buildup curves measured at DC-13 at Lakeview, OR.